HYDRAULIC OPTIMISATION OF A POSTULATED SEDIMENT FLUSHING SYSTEM IN LOW-LEVEL DAM OUTLETS

By
Liam van der Spuy

Thesis presented in fulfilment of the requirements for the degree of Master of Engineering in Civil Engineering in the Faculty of Engineering at Stellenbosch University

Supervisor: Prof GR Basson

March 2020

UNIVERSITEIT·STELLENBOSCH·UNIVERSITY
jou kennisvennoot • your knowledge partner

Plagiaatverklaring / Plagiarism *Declaration*

1 Plagiaat is die oorneem en gebruik van die idees, materiaal en ander intellektuele eiendom van ander persone asof dit jou eie werk is.
Plagiarism is the use of ideas, material and other intellectual property of another's work and to present is as my own.

2 Ek erken dat die pleeg van plagiaat 'n strafbare oortreding is aangesien dit 'n vorm van diefstal is.
I agree that plagiarism is a punishable offence because it constitutes theft.

3 Ek verstaan ook dat direkte vertalings plagiaat is.
I also understand that direct translations are plagiarism.

4 Dienooreenkomstig is alle aanhalings en bydraes vanuit enige bron (ingesluit die internet) volledig verwys (erken). Ek erken dat die woordelikse aanhaal van teks sonder aanhalingstekens (selfs al word die bron volledig erken) plagiaat is.
Accordingly all quotations and contributions from any source whatsoever (including the internet) have been cited fully. I understand that the reproduction of text without quotation marks (even when the source is cited) is plagiarism.

5 Ek verklaar dat die werk in hierdie skryfstuk vervat, behalwe waar anders aangedui, my eie oorspronklike werk is en dat ek dit nie vantevore in die geheel of gedeeltelik ingehandig het vir bepunting in hierdie module/werkstuk of 'n ander module/werkstuk nie.
I declare that the work contained in this assignment, except where otherwise stated, is my original work and that I have not previously (in its entirety or in part) submitted it for grading in this module/assignment or another module/assignment.

March 2020

Abstract

Reservoir sedimentation is an ongoing critical concern worldwide with a recorded global average of 33% of reservoir storage capacity already been lost therefrom, which is expected to exceed 50% by 2050 (i.e. not considering new dam projects). Drawdown or pressure flushing at hydropower intakes are common mitigation measures for removing locally deposited sediment from reservoirs. This is periodically necessary to especially keep hydropower intakes free of coarse non-cohesive sediment, as sand fractions will typically damage turbines in hydropower conduits.

The aim of this study was to provide design guidelines for a postulated configuration for a sediment flushing system of a low-level outlet at a dam for control of reservoir sedimentation to protect the hydropower intakes. The postulated design, which comprised of a hybrid low-level outlet conduit and intake structure, was optimised by means of numerical and physical modelling for effectively flushing sediments (i.e. sand, gravel and boulders when the settled sediment delta has reached the dam) during different flood and water level scenarios. The intake structure (a semi-circular low-weir and ogee-type spillway with wing-walls) was designed and positioned in the vicinity of the low-level intake inside of the typical sediment scour cone that forms during pressure flushing. The main aim of the spillway was to produce desirable supercritical flow conditions upstream of the conduit intake, as well as through it. This was necessary to help optimise the flushing of sediments during free-surface flow conditions as well as to prevent deposition of coarse sediment near the outlet gates, thereby preventing closure. The submerged weir was, however, also designed for pressure flushing where the aim was: (1) local sediment removal; and (2) preventing main reservoir sediments from depositing near the outlet gate and hindering gate closure.

For this study, 3D CFD modelling in *ANSYS Fluent v19.1* was used to hydraulically compare four different proposed flushing system designs, from which the best design option could be chosen and further refined. Flow vectors (representing the degree of streamlined flow) and flow depths and velocities (representing the degree of supercritical flow) along the model during free-flow flushing conditions were considered for comparisons. A 1:40 scale physical model of the postulated flushing system design, which evolved from the findings of the numerical model simulations, was built for further testing and refinement. The main aim of the physical model was to test the robustness, reliability and actual flushing capability of the design. The following prototype conditions were considered during hydraulic testing of the physical model: (1) two different upstream sediment bed configurations for both pressure and free-flow flushing (2) four different sediment sizes (d_{eff} = 3.6, 468, 659 and 1532 mm) for both pressure and free-flow flushing; and (3) three different upstream water levels (H_u = 24.16, 29.08 and 34 m), above the conduit inlet invert level, for pressure flushing. Similar testing was also performed in the absence of the intake structure in order to derive comparative results to determine the degree of influence of the postulated structure.

It was found from physical model tests on the numerically optimised design that the postulated intake structure: (1) can fully flush the intake area of the considered sediment groups regarding the different upstream sediment bed configurations during free-flow flushing; (2) does not appear to affect the pressure flushing extent upstream of the intake;

and (3) is crucial during free-flow flushing, where the weir is required to hold back main reservoir sediments from moving towards, or depositing near, the outlet gate operation area.

Opsomming

Damtoeslikking is wêreldwyd 'n kritieke probleem aangesien ongeveer 33% van die totale reservoirkapasiteit reeds verlore is en wat na verwagting teen 2050 tot 50% sal styg (d.w.s. sonder om nuwe damprojekte in ag te neem). In die gevalle waar damtoeslikking ‘n impak het op die inlate van byvoorbeeld hidrokragstasies, word die uitspoel van sediment in die lokale omgewing van die inlate van tyd tot tyd soos nodig gedurende die bedryf daarvan toegepas om die inlate vry te hou van growwe, nie-kohesiewe sediment wat turbines kan beskadig.

Die doel van hierdie studie was derhalwe om riglyne te ontwikkel vir die ontwerp van 'n gepostuleerde konfigurasie vir 'n laevlak dam-uitlaat vir die uitspoel van sediment (op ‘n vlak na aan die rivier bedding en onder die inlaat) van ‘n hidrokragstasie om die inlaat na laasgenoemde vry te hou van sediment wat turbines kan beskadig. Die gepostuleerde ontwerp is geoptimeer deur numeriese en fisiese modellering vir die effektiewe spoel van sediment (nl. sand, gruis en rotse wanneer die gevestigde sediment-delta die dam bereik het) tydens verskillende vloed- en watervlak-scenario's.

Die sediment uitspoel struktuur ('n lae kruin semi-sirkelvormige keerwal met ogee oorloop-profiel en vleuelmure) is ontwerp en geposisioneer op die rivier bedding aan die stroomop kant van ‘n laevlak dam uitlaat in die sedimentuitskuur-keël wat natuurlik tydens drukvloei-spoeling vorm. Die hoofdoel van die keerwal was om in geval van beide drukvloei- en vryvlakvloei-stromingstoestande effektiewe superkritiese vloeitoestande te bewerkstellig in die gebied stroomaf van die keerwal om sedimentasie (wat die werking van sluise kan belemmer) te verhoed.

Die hidrouliese aspekte (vloeisnelhede, vloeilyne en waterdieptes) van die gepostuleerde spoelstelsel is ge-optimeer vir vryvlak-stromingstoestande met behulp van numeriese modellering (*ANSYS Fluent v19.1* 3D CFD-model). Vier parameters is verstel in hierdie numeriese model studie waaruit die mees effetiewe konfigurasie gekies is om verder verfyn te word ten opsigte van sediment vervoer in ‘n 1:40 Froude-skaal fisiese laboratorium model. Verdere doelwitte van die fisiese model was om die robuustheid, betroubaarheid en werklike spoelvermoë van die ontwerp te toets. Die volgende afgeskaalde prototipe-opstellings is getoets in die fisiese model: (1) twee verskillende stroomop sedimentbedkonfigurasies vir druk- en as vryvlakvloei-spoeling (2) vier verskillende sedimentgroottes (d_{eff} = 3.6, 468, 659 en 1532 mm) vir drukvloei- en vryvlakvloei-spoeling; en (3) drie verskillende stroomop watervlakke (H_u = 24.16, 29.08 en 34 m), bo die drumpel van die onderuitlaat, vir die drukvloei-spoeling. Soortgelyke toetse is ook uitgevoer in die afwesigheid van die keerwal vleuel-mure gedeelte van die spoelstelsel ten einde vergelykende resultate te verkry om die invloed van laasgenoemde te bepaal.

Fisiese modeltoetse op die numeries geoptimeerde ontwerp het bevind dat die gepostuleerde spoelstelsel struktuur: (1) bewerkstellig volledige spoeling van die getoetste sedimentgroepe vir die verskillende stroomopstellings van die sediment tydens beide drukvloei- en vryvlakvloei-spoeling; (2) is krities tydens vryvlakvloei-stroming, waar uitskuring nodig is om reservoirsediment te weerhou om naby die uitlaatsluis te deponeer.

Acknowledgements

Firstly, I would like to thank my supervisor, Prof Gerrit Basson, as well as my co-supervisor, Mr Eddie Bosman, for their continued input, support and guidance throughout my studies. Your knowledge and expertise in the field of hydraulic engineering field is highly admired and has significantly contributed towards my understanding and application of hydraulic engineering.

I would like to say a very big thank you to Dr Ousmane Sawadogo for all his help and assistance during the design and simulation phases of my numerical models.

To Mr Johan Nieuwoudt and Mr Illiyaaz Williams, the water laboratory technical staff, thank you very much for your very friendly and eager assistance and support during the construction and testing phases of my physical model.

To the South African Water Research Commission (WRC), thank you very much for providing me with funding to help complete my studies.

To Ms Claudia Mcleod and Mr Ruben Saayman, thank you for your comradery, enthusiasm and contributions during our group work. We made a great team!

To my parents, Kevin and Estelle, thank you so very much for providing me with the opportunity to complete my studies. Your continued love, support and guidance will forever be appreciated. I feel immensely lucky and blessed to have had you two by my side, and for instilling me with the morals, values and work ethic that I possess today.

Lastly, thank you very much to all my friends and loved ones for making this an experience of a lifetime. Your friendship, support and encouragement will always be remembered and appreciated.

Table of Contents

Plagiarism declaration ..... **i**

Abstract ..... **ii**

Opsomming ..... **iv**

Acknowledgements ..... **v**

List of figures ..... **x**

List of tables ..... **xiii**

Nomenclature ..... **xv**

List of abbreviations and acronyms ..... **xxii**

1 Introduction **1**

1.1 Background 1

1.1.1 Sedimentation 1

1.1.2 Low-level outlets 2

1.1.3 Problem statement 3

1.2 Objectives 4

1.3 Thesis outline 5

2 Literature review **6**

2.1 Physical properties of sediment 6

2.1.1 Particle size 6

2.1.2 Particle shape 7

2.1.3 Grading of bed material 8

2.1.4 Particle density and specific gravity 9

2.1.5 Underwater angle of repose 10

2.1.6 Particle settling velocity 10

2.2 Incipient motion of sediment 13

2.2.1 Liu's stream power approach 13

2.2.2 Correction for steep bed slopes 15

2.2.3 Shield's parameter 16

2.3 Sediment transport and deposition 17

2.3.1 River transport 18

2.3.2 Reservoir sediment transport 20

2.3.3 Sediment deposition in reservoirs 22

2.4 Sediment management and control 23

2.4.1 Sediment sluicing 24
2.4.2 Sediment flushing 25
2.4.3 Bypass tunnel flushing designs 29
2.5 Low-level outlets 34
2.5.1 Introduction 34
2.5.2 Types of designs 34
2.5.3 Layout 35
2.5.4 Multiphase flow through conduit 36
2.5.5 Discharge capacities 38
2.5.6 Conduit structure 42
2.5.7 Inlet structure 44
2.5.8 Outlet structure 47
2.5.9 Air vents 48
2.5.10 Hydraulic and structural issues 51
2.5.11 Gates 54
2.5.12 General operation, inspection and maintenance 56
2.5.13 Checking and testing of hydro-mechanical equipment 56

3 Postulated flushing system design guidelines 59
3.1 Layout 59
3.2 Low-level outlet design 60
3.2.1 General conduit structure 60
3.2.2 Conduit shape and dimensions 60
3.2.3 Conduit bed slope 60
3.2.4 Conduit inlet structure 61
3.2.5 Conduit outlet structure 61
3.2.6 Air vent 61
3.3 Design sediment size for flushing 63
3.3.1 Particle size 63
3.3.2 Particle shape 63
3.3.3 Particle density, specific gravity and angle of repose 63
3.3.4 Particle settling velocity 63
3.3.5 Incipient motion 64
3.4 Hydraulic design 65
3.4.1 Design discharge for free-flow flushing 65
3.4.2 Design discharge for pressure flushing 65
3.4.3 Minimum submergence requirement of conduit inlet 66
3.5 Intake structure design 66
3.5.1 Introduction 66
3.5.2 Predicted sediment scour hole geometry 67

3.5.3 Conceptual designs evaluated 69
3.5.4 Upstream approach free-flow conditions 76
3.5.5 Weir crest radius and length 78
3.5.6 Wing-wall orientation and design 79
3.5.7 Weir crest design head 81
3.5.8 General Uncontrolled Ogee spillway profile 83
3.5.9 Added spillway surfaces 84

4 Numerical model and results 86
4.1 Hydraulic calculations 86
4.2 CFD modelling and results 87
4.2.1 3D geometry 87
4.2.2 Meshing 88
4.2.3 Simulation setup 90
4.2.4 Post processing (results) 91
4.3 Final best design option 99
4.3.1 3D geometry 99
4.3.2 Meshing 100
4.3.3 Simulation setup 101
4.3.4 Post processing (results) 101
4.3.5 Summary of final CFD design 103

5 Physical model and results 104
5.1 Introduction 104
5.2 Prototype-model similarity laws 104
5.3 Sediment scaling 105
5.4 Apparatus 105
5.5 Construction methodology 106
5.6 Experimental testing and results 107
5.6.1 Sediment sizing and properties 107
5.6.2 Tested sediment depths 111
5.6.3 Tested pressure flushing water levels 112
5.6.4 Free-flow flushing 113
5.6.5 Pressure flushing 121

6 Summary and Conclusions 130
6.1 Literature study 130
6.2 Numerical model study 131
6.3 Physical model study 132

7 Recommendations 133

8 Bibliography 134

Appendix A: Numerical model and results 141

Appendix B: Physical model and results 167

List of figures

Page

Figure 1.1-1: Mbashe HPP weir (Eastern Cape, South Africa) 3

Figure 2.1-1: Particle sphericity and roundness (Morris and Fan, 1998) 8

Figure 2.1-2: Angle of repose (SANRAL, 2013) 10

Figure 2.1-3: Drag coefficient versus Reynolds number (Concha, 2009) 12

Figure 2.2-1: Criteria for incipient motion (Langmaak, 2013) 14

Figure 2.2-2: Modified Liu diagram (SANRAL, 2013) 15

Figure 2.3-1: River sediment transport (Dey, 2014) 18

Figure 2.3-2: Turbidity current through a reservoir (Morris *et al.*, 2008) 21

Figure 2.3-3: Reservoir sediment deposition profiles (Morris and Fan, 1998) 23

Figure 2.3-4: Reservoir sediment deposition zones (adapted from Morris and Fan, 1998) 23

Figure 2.4-1: Types of sediment management strategies (Morris, 2015) 24

Figure 2.4-2: SST example (Tsengwen Dam in Taiwan) (ICOLD, 2018a) 25

Figure 2.4-3: Common stages of flushing (ICOLD, 2018b) 27

Figure 2.4-4: SBT example (Koshibu Dam in Japan) (ICOLD, 2018a) 30

Figure 2.4-5: Cross-section of typical SBT and SST (ICOLD, 2018a) 30

Figure 2.4-6: Long section of sediment bypass tunnel (ICOLD, 2018c) 30

Figure 2.5-1: Typical low-level outlet profile (adapted from Vischer and Hager, 1998) 34

Figure 2.5-2: Long-section of low-level outlet in Cerro del Águila Dam (adapted from Sayah *et al.*, 2015) 35

Figure 2.5-3: Different zones of highly turbulent flows (Falvey, 1980) 36

Figure 2.5-4: Flow types that cause air demand (Sharma, 1976) 37

Figure 2.5-5: Cd value for submerged and free flow under gate (Lewin, 2001) 42

Figure 2.5-6: Long section of bell-mouth roof design (adapted from IS 9761, 1995) 45

Figure 2.5-7: Plan view of bell-mouth wall design (adapted from IS 9761, 1995) 46

Figure 2.5-8: Definition sketch for submergence (adapted from Knauss, 1987) 47

Figure 2.5-9: Vortex formation (Rindles and Gulliver, 1983) 53

Figure 2.5-10: Typical outlet testing procedures (ICOLD, 2018a) 58

Figure 3.1-1: Conceptual layout of postulated flushing system 59

Figure 3.2-1: Downstream air vent and conduit ceiling layout (adapted from Bosman and Basson, 2012) 62

Figure 3.5-1: Long section of sediment scour cone geometry (adapted from Dreyer, 2018) 68

Figure 3.5-2: Plan view of sediment scour cone geometry (adapted from Dreyer, 2018) 68
Figure 3.5-3: Final conceptual design (free-flow flushing) 69
Figure 3.5-4: Long section of *Design 1* (water profile indicated for free-flow scenario) 71
Figure 3.5-5: Plan view of *Design 1* 72
Figure 3.5-6: Long section of *Design 2* (water profile indicated for free-flow scenario) 74
Figure 3.5-7: Plan view of *Design 2* 75
Figure 3.5-8: Permissible velocities (SANRAL, 2013) 77
Figure 3.5-9: Hu vs $Hsed - up$ to maintain Lco = 12 m 79
Figure 3.5-10: Plan view of basic design CFD geometry 80
Figure 3.5-11: Plan view of final wing-wall design 80
Figure 3.5-12: Discharge coefficients for vertical-faced ogee (USBR, 1987) 82
Figure 3.5-13: Discharge coefficients for other than design head (USBR, 1987) 82
Figure 3.5-14: Top ogee profile having a vertical u/s face (adapted from USBR, 1987) 83
Figure 3.5-15: Bottom ogee profile having a vertical u/s face (USBR, 1987) 83
Figure 3.5-16: Typical ogee spillway structure with various surfaces 85
Figure 3.5-17: Typical long section of deflection surface 85
Figure 4.2-1: Conceptual 3D geometries in *ANSYS SCDM 19.1* (free-flow flushing) 88
Figure 4.2-2: Design 2 (α = 45˚) model mesh and Named Selections 89
Figure 4.2-3: Design 1 (α = 45˚): geometry boundaries 92
Figure 4.2-4: Design 1 (α = 45˚): long section of simulated water flow profile 92
Figure 4.2-5: Design 1 (α = 45˚): plan layout of simulated velocity magnitude vectors 93
Figure 4.2-6: Design 1 (α = 30˚): geometry boundaries 94
Figure 4.2-7: Design 1 (α = 30˚): long section of simulated water flow profile 94
Figure 4.2-8: Design 1 (α = 30˚): plan layout of simulated velocity magnitude vectors 95
Figure 4.2-9: Design 2 (α = 45˚): geometry boundaries 96
Figure 4.2-10: Design 2 (α = 45˚): long section of simulated water flow profile 96
Figure 4.2-11: Design 2 (α = 45˚): plan layout of simulated velocity magnitude vectors 97
Figure 4.2-12: Design 2 (α = 30˚): geometry boundaries 98
Figure 4.2-13: Design 2 (α = 30˚): long section of simulated water flow profile 98
Figure 4.2-14: Design 2 (α = 30˚): plan layout of simulated velocity magnitude vectors 99
Figure 4.3-1: Final design: geometry boundaries 100
Figure 4.3-2: Final design: long section of simulated water flow profile 102
Figure 4.3-3: Final design: plan layout of simulated velocity magnitude vectors 102

Figure 5.5-1: Chosen measuring points along physical model 107

Figure 5.6-1: Settling velocity distribution for different sediment groups 109

Figure 5.6-2: Upstream sediment bed setups for $deff$ = 0.659 m sediment group 112

Figure 5.6-3: Example of fully-flushed downstream river channel 114

Figure 5.6-4: Centreline flow profile of Q = Qe = 119 m³/s along model 115

Figure 5.6-5. Centreline flow profiles of discharges (Qfc) for *sediment depth 1* setup 117

Figure 5.6-6: Initial maximum scour of $deff$ = 1.532 m *sediment depth 1* inside intake area (free-flow flushing) 117

Figure 5.6-7: Enlarged reverse bottom curve radius (R = 4 m) 117

Figure 5.6-8. Final maximum scour of $deff$ = 1.532 m *sediment depth 1* inside intake area (free-flow flushing) 118

Figure 5.6-9. Centreline flow profile of Qfc for $deff$ = 0.004 m *sediment depth 2* 119

Figure 5.6-10. Centreline flow profile of Qfc for $deff$ = 0.468 m *sediment depth 2* 119

Figure 5.6-11. Centreline flow profile of Qfc for $deff$ = 0.659 m *sediment depth 2* 120

Figure 5.6-12. Scour of $deff$ = 0.468 m *sediment depth 2* after free-flow flushing 120

Figure 5.6-13. Scour of $deff$ = 0.659 m *sediment depth 2* after free-flow flushing 121

Figure 5.6-14. Deposition of different boulder groups near outlet gate after free-flow flushing (without intake structure) 121

Figure 5.6-15: Observed scour cone of $deff$ = 0.004 m *sediment depth 2* during pressure flushing 123

Figure 5.6-16: Observed scour profiles of $deff$ = 0.004 m *sediment depth 1* 124

Figure 5.6-17: Observed scour profiles of $deff$ = 0.468 m *sediment depth 1* 125

Figure 5.6-18: Observed scour profiles of $deff$ = 0.659 m *sediment depth 1* 126

Figure 5.6-19: Observed scour profiles of $deff$ = 1.532 m *sediment depth 1* 126

Figure 5.6-20: Observed scour profiles of $deff$ = 0.004 m *sediment depth 2* 127

Figure 5.6-21: Observed scour profiles of $deff$ = 0.468 m *sediment depth 2* 128

Figure 5.6-22: Observed scour profiles of $deff$ = 0.659 m *sediment depth 2* 129

List of tables

Page

Table 2.1-1: Sediment size classes (Simons and Sentürk, 1992) 6

Table 2.1-2: Grading width classes (CIRIA et al., 2007) 8

Table 2.2-1: Proposed Movability numbers 15

Table 2.4-1: Free-flow or drawdown flushing vs pressure flushing 26

Table 2.4-2: Recorded W-D ratios (Basson and Rooseboom, 1999) 28

Table 2.4-3: Sediment bypass tunnel specifications (ICOLD, 2018a) 32

Table 2.5-1: Rectangular-shaped low-level outlets in Chinese HPPs (Guo, 2012) 43

Table 2.5-2: Constants for different bell-mouth inlet conditions (Bratko and Doko, 2013) 45

Table 2.5-3: Comparison of low-level outlet sliding and radial gate 54

Table 2.5-4: Comparison of different low-level outlet gate locations (USACE, 2003) 55

Table 3.5-1: Predicted dimensions of scour cone geometry (Dreyer, 2018) 67

Table 4.1-1: Summary of calculated flow depths and velocities for different designs 87

Table 4.2-1: Summary of Meshing details for initial design models 89

Table 4.2-2: Summary of *Fluent Setup* details for initial design models 90

Table 4.3-1: Summary of Meshing details for final design model 100

Table 4.3-2: Summary of *Fluent Setup* details for final design model 101

Table 4.3-3: Maximum sediment particle sizes transported along design bed surfaces (based on analytical calculations) 103

Table 5.2-1: Froude's Law scalar relationships (Webber, 1971) 105

Table 5.5-1: Elevations of chosen measuring points relative to conduit inlet invert level 107

Table 5.6-1: Bulk particle densities of different sediment groups 108

Table 5.6-2: Settling velocity distribution for different sediment groups 108

Table 5.6-3: Effective particle diameters of different sediment groups 109

Table 5.6-4: Summary of $d50$ = 0.095 mm sediment properties (Dreyer, 2018) 110

Table 5.6-5: Summary of $d50$ = 13.2 mm sediment properties 110

Table 5.6-6: Summary of $d50$ = 19 mm sediment properties 110

Table 5.6-7: Summary of $d50$ = 37.5 mm sediment properties 111

Table 5.6-8: Water levels (relative to IL) and water depths along model for Q = 119 m³/s 115

Table 5.6-9. Critical free-flow flushing results of *sediment depth 1* setup for different sediment group sizes 116

Table 5.6-10. Critical free-flow flushing results of *sediment depth 2* setup for different sediment group sizes 118

Table 5.6-11. Free-flow flushing without intake structure for *sediment depth 2* setup for different sediment group sizes 120

Table 5.6-12: Tailwater levels and depths of pressure flushing discharges for different upstream water levels 123

Table 5.6-13: Required discharges to maintain upstream water levels (without structure) for different upstream water levels 124

Table 5.6-14: Critical pressure flushing results of $deff$ = 0.004 m *sediment depth 1* for different upstream water levels 124

Table 5.6-15: Critical pressure flushing results of $deff$ = 0.468 m *sediment depth 1* for different upstream water levels 125

Table 5.6-16: Critical pressure flushing results of $deff$ = 0.659 m *sediment depth 1* for different upstream water levels 125

Table 5.6-17: Critical pressure flushing results of $deff$ = 1.532 m *sediment depth 1* for different upstream water levels 126

Table 5.6-18: Critical pressure flushing results of $deff$ = 0.004 m *sediment depth 2* for different upstream water levels 127

Table 5.6-19: Critical pressure flushing results of $deff$ = 0.468 m *sediment depth 2* for different upstream water levels 128

Table 5.6-20: Critical pressure flushing results of $deff$ = 0.659 m *sediment depth 2* for different upstream water levels 128

Nomenclature

A	Cross-sectional flow area (m²)
A_a	Cross-sectional area of air vent (m²)
a, b, c	Mutually perpendicular dimensions through sediment particle (a = longest; c = shortest) (m)
α	Angle of wing-wall to the conduit longitudinal centreline (°)
α	Bed slope angle normal to the direction of flow (°)
B	Conduit or channel width (m)
β	Air demand ratio (m²)
β	Bed slope angle in the direction of the flow (°)
b	Gate opening height (m)
b_c	Weir crest length (m)
b_{oc}	Conduit width along centreline (m)
b_{oe}	Conduit width along outside edge (m)
b_u	Upstream design channel width (m)
C	Chezy's roughness coefficient (dimensionless)
C_B	Coefficient for upstream (inlet) control (dimensionless)
C_c	Contraction coefficient (dimensionless)
C_d	Discharge coefficient (dimensionless)
C_d	Drag coefficient (dimensionless)
C_e/C_o	Ratio of coefficients for uncontrolled ogee crests (dimensionless)
C_h	Coefficient for upstream (inlet) control (dimensionless)
C_o	Discharge coefficient for uncontrolled ogee crests (dimensionless)
D	Conduit inlet height (m)
D_{co}	Sediment scour cone depth (m)
d	Height of start of conduit bed slope above conduit inlet invert level (m)

d	Particle diameter or sieve size (m)
d_1	Maximum particle diameter subjected to lifting from the channel bed (m)
d_2	Maximum particle diameter subjected to lifting from the channel side slopes (m)
d_{50}	Particle diameter at which 50% of the sample's mass consists of particles with a diameter less than this value (i.e. median particle diameter) (m)
d_{90}	Particle diameter at which 90% of the sample's mass consists of particles with a diameter less than this value (m)
d_{eff}	Effective particle diameter (m)
d_m	Effective particle diameter (m)
d_{max}	Maximum sediment size to enter the low-level outlet (m)
d_y	Particle diameter at which y% of the sample's mass consists of particles with a diameter less than this value (i.e. intercept for y% of the cumulative mass) (m)
F_r	Froude number (dimensionless)
F_{rc}	Froude number at vena contracta (dimensionless)
g	Gravitational acceleration (= 9.81 m/s²)
g_s^*	Under water weight of specific bed-load transport per unit width (kg/m.s)
H	Upstream energy level, measured relative to centreline of the jet (m)
H_1 and H_2	Upstream and downstream energy levels, measured relative to the inlet invert level (m)
H_{co}	Sediment scour cone height (m)
H_e	Energy head loss from the outlet entrance to the gate section (m)
H_e	Safety design head above the weir crest (m)
H_n	Energy level at point n (m)
H_{sed}	Local design sediment level, measured relative to IL_1 (m)
H_{sed-up}	Upstream sediment level, above the inlet invert level (m)
H_{si}	Conduit inlet submerged water depth, measured relative to the inlet invert level (m)
H_t	Total height of the weir crest above the local NGL (m)

H_u	Upstream reservoir head, above the inlet invert level (m)
H_w	Upstream design water depth, measured relative to IL_1 (m)
h	Depth of contracted jet (m)
h	Depth of water (m)
h	Settling depth in tank (m)
h_{atm}	Atmospheric pressure head (m)
h_c	Flow depth at vena contracta (m)
$h_{f_{1-2}}$	Friction losses between point 1 and 2 (m)
$h_{L_{1-2}}$	Transitional (secondary) losses between point 1 and 2 (m)
h_{min}	Minimum submergence requirement of conduit inlet centreline (m)
h_v	Vapour pressure head (m)
IL	Conduit inlet invert level (m)
IL_1	Conduit inlet invert level of *Design 1* (m)
IL_2	Conduit inlet invert level of *Design 2* (m)
J_s	Riverbed slope (m/m)
J_w	Water surface slope (m/m)
K and n	Empirical coefficients (dimensionless)
K_{in} and K_{out}	Inlet and outlet secondary loss coefficients (dimensionless)
K_x, K_y	Constants for different inlet conditions (dimensionless)
k_α	Ratio of the critical drag force at a given transverse slope to the critical drag force at the normal bed (dimensionless)
k_β	Ratio of the critical drag force at a bed sloped longitudinally to the critical drag force at the horizontal bed (dimensionless)
k_s	Surface roughness coefficient (m)
k_w	Coefficient of roughness of channel sides (dimensionless)
L	Bed length of conduit (m)
L	Hydraulic diameter (m)

L_{1-2}	Horizontal distance between point 1 and 2 (m)
L_{3p}	Horizontal distance between measuring points, p_3 and p_p (m)
L_{co}	Sediment scour cone length (m)
m	Intake bed surface gradient (m/m or °)
m_a	Mass of the saturated surface-dry aggregate (g)
m_b	Mass of the oven-dried aggregate (g)
m_c	Mass of the suspended basket plus aggregate in $25°$ water (g)
m_d	Mass of the suspended empty basket in $25°$ water (g)
n	Manning's roughness coefficient (s/m$^{1/3}$)
θ	Angle of channel side slopes (°)
θ	Angle of weir (°)
θ	Gate lip angle, measured relative to the horizontal axis (°)
$\emptyset$	Underwater angle of repose of the sediment (°)
ϕ	Conduit bed slope (m/m or °)
σ_c	Incipient cavitation index (dimensionless)
P	Weir crest height, measured relative to H_{sed} (m)
P	Wetted flow perimeter (m)
$P_1, P_2, P_3, P_4, P_5, P_6$ and P_7	Chosen measuring points along physical model (dimensionless)
p_1, p_2, p_3, p_p and p_5	Chosen hydraulic control points along model (dimensionless)
ρ	Density of fluid (kg/m³)
ρ_b	Apparent bulk particle density of the aggregate (kg/m³)
ρ_s	Density of sediment (kg/m³)
ρ_w	Density of water (= 1000 kg/m³)
ρ_{wT}	Density of water at the test temperature, T = 25° (kg/m³)
Q	Flow discharge (m³/s)

Q	Water discharge (kg/s)
Q_a	Air flow rate (m³/s)
Q_d	Main river discharge (m³/s)
Q_e	Maximum design discharge for free-flow flushing (m³/s)
Q_{fc}	Critical free-flow discharge to fully flush the intake area (m³/s)
Q_m	Maximum free-flow outlet discharge without flood detention (m³/s)
Q_p	Maximum design discharge for pressure flushing (m³/s)
Q_{pc}	Critical discharge required to maintain the specified upstream water levels during pressure flushing (m³/s)
Q_w	Flow discharge under the gates (m³/s)
R	Hydraulic radius (m)
R	Reverse bottom curve radius (m)
R_c	Weir crest radius (m)
R_e	Reynolds number (dimensionless)
R_e^*	Particle Reynolds number (dimensionless)
r_a	Radius of air vent shaft (m)
SG	Specific gravity of sediment particle (dimensionless)
S_f	Energy slope (m/m)
S_n	Slope of the line connecting the upstream end of the maximum pool level with the low-level outlets (m/m)
S_0	Channel bed slope (m/m)
S_0	Original riverbed slope (m/m)
S_p	Particle shape factor (dimensionless)
S_w	Water surface slope (m/m)
T	Test temperature of fluid (°)
TWL_{max}	Maximum tailwater level during flushing (m)
U_o	Conduit inlet flow velocity (m/s)

μ	Dynamic viscosity (kg/m·s)
V	Water flow velocity (m/s)
$\bar{V}$	Mean fluid velocity (m/s)
V^*	Shear velocity (m/s)
V_c	Flow velocity at vena contracta (m/s)
V_{co}	Sediment scour cone volume (m³)
V_n	Flow velocity at point n (m/s)
V_{ss}	Particle settling velocity (m/s)
$\overline{V_{ss}}$	Effective particle settling velocity (m/s)
V_u	Upstream design flow velocity (m/s)
$\left(\frac{V^*}{V_{ss}}\right)_0$	Movability number for a horizontal bed (dimensionless)
$\left(\frac{V^*}{V_{ss}}\right)_{\beta,\alpha}$	Movability number for any given bed slope (dimensionless)
v	Kinematic viscosity (≈ 1.13 x 10^{-6} m²/s for water at 15°C)
$\bar{v}_1$ and $\bar{v}_2$	Upstream and downstream average flow velocities (m/s)
v_a	Airflow velocity (m/s)
W_{co}	Sediment scour cone width (m)
Ψ_p	Particle sphericity (dimensionless)
w	Gate width (m)
x	Point along axis parallel to conduit centreline (dimensionless)
y	Flow depth (m)
y	Point along axis perpendicular to conduit centreline (dimensionless)
y_1	Upstream water depth, measured relative to the gate invert level (m)
y_3	Water depth downstream of the gate (m)
y_n	Normal flow depth (m)
y_n	Water depth at point n (m)

y_u	Upstream design flow depth, measured relative to H_{sed} (m)
γ_s	Specific gravity of sediment (t/m³)
γ_w	Specific gravity of water (i.e. 1 t/m³)
z_n	Elevation of point n above the inlet invert level (m)

List of abbreviations and acronyms

3D	Three-dimensional
ASCE	American Society of Civil Engineers
CFD	Computational Fluid Dynamics
CFRD	Concrete faced rock-fill dam
HPP	Hydropower plant
ICOLD	International Commission on Large Dams
IL	Invert level
MAR	Mean annual runoff
NGL	Natural ground level
PG	Gravity dam
PVC	Polyvinyl chloride
RCC	Roller compacted concrete dam
SANRAL	South African National Roads Agency Ltd
TWL	Tailwater level
USACE	United States Army Corps of Engineers
USBR	United State Bureau of Reclamation
VA	Arch dam

1 Introduction

1.1 Background

1.1.1 Sedimentation

Reservoir sedimentation occurs when sediment-laden flows are entrained into a reservoir via the upstream river, resulting in sediment deposition and build-up upstream of the dam. This intricate process significantly reduces the live storage capacity of the reservoir, thus limiting water supply (i.e. for agricultural, industrial and potable water usage), water quality, power generation, flood control and ultimately, reservoir sustainability. Rapid sedimentation in reservoirs is known to increase the potential of flooding in upstream areas, as well as abrade hydraulic machinery, damage infrastructure and block and clog hydropower intakes and low-level outlets (Basson and Rooseboom, 1997; Fan and Morris, 1992; Mahmood, 1987). Rapid sedimentation is also known to significantly limit and reduce the sediment load in the downstream river (ICOLD, 2018c). The reduced sediment load ultimately increases the sediment transport capacity of the river which is known to accelerate river bank erosion, abrade the riverbed and potentially undermine existing downstream structures (Morris *et al.*, 2008). As a result of the inadequate amount of fine sediment being released from the dam, fewer associated nutrients are being delivered to downstream ecosystems, as well as less sediment being transported to the coast which ultimately contributes towards coastal erosion (Annandale *et al.*, 2016).

Sedimentation in reservoirs is an ongoing critical concern worldwide with a recorded global average sedimentation rate of 0.8% of the original storage capacity per year (ICOLD Bulletin 147, 2009). The same author reports that South Africa has a recorded average sedimentation rate of 0.37% per year, which is substantially less than the 0.85% per year for the rest of Africa as stated by Basson (2009). According to ICOLD Bulletin 147 (2009), this is due to the fact that only data for “large” dams with a high *capacity to mean annual runoff (MAR) ratio* were considered for calculations. Regardless, an average sedimentation rate of 0.37% per year, together with the fact that large dams in South Africa are typically designed with a dead storage for sedimentation of about 50 years (Basson and Rooseboom, 2007), implies that there are no anticipated short-term sedimentation, storage capacity and/or water supply issues (ICOLD Bulletin 147, 2009). However, even though this rate of 0.37% per year is considered low, Msadala (2009) has found that more than 30% of the original water storage capacity of almost a quarter of South Africa’s large dams has already been lost due to sedimentation. According to ICOLD Bulletin 147 (2009), a global average of 33% of storage capacity of reservoirs has already been lost, and is expected to exceed 50% by 2050 (i.e. not considering new dam projects).

Various sediment management strategies have been implemented worldwide with the aim of limiting reservoir sedimentation (and associated issues) and restoring the effective (live) reservoir storage capacity. Such strategies can be divided into four categories:

a) *Minimising incoming sediment loads* – This is typically achieved through upstream sediment trapping, as well as controlling upstream sediment erosion. The former must be monitored, however, as the formation of an upstream delta increases the risk of

upstream flooding due to backwater. An upstream delta also increases the risk of salinization, soil waterlogging and ecological habitat destruction due to rising groundwater levels (Morris *et al.*, 2008).

b) *Physically removing sediment from the reservoir* – This is typically achieved through drawdown or pressure flushing, dredging and dry mechanical excavation. Dredging and dry mechanical excavation are expensive procedures and should be considered as the last possible solutions (Basson and Rooseboom, 1999). This strategy is typically used in reservoirs with an unsustainable design (i.e. has a design life) (Healy *et al.*, 2014).
c) *Routing sediments through the reservoir* – This is typically achieved through off-stream reservoirs, bypasses, sediment sluicing and venting of turbidity currents. Morris and Fan (1998) recommend this strategy for cases of high sediment loads, preferably in small reservoirs where large flood discharges exceed the storage capacity.
d) *Other* – In situations where versatility is required, the following measures can be implemented: (1) raise the dam wall; (2) reuse storage for a different purpose; or (3) decommission the dam (Morris, 2015).

Sediment management strategies such as flushing, sluicing and bypassing of sediment can result in large quantities of sediment being released downstream of the dam. This can therefore largely impact the downstream river system by causing river channel aggradation and clogging, habitat destruction and flooding (Morris and Fan, 1998). A management strategy therefore needs to be chosen and executed in a manner that aids in reservoir sustainability, but also considers and minimises adverse effects on the downstream environment. Associated operation rules (especially for flushing), which are versatile to site-specific conditions, should also be implemented. The feasibility of a management strategy is also dependant on the economic (e.g. operational costs and potential electricity generation) and water supply requirements of a particular reservoir, as well on the characteristics of the corresponding site, catchment and climate.

1.1.2 Low-level outlets

Low-level dam outlets are hydraulic structures that are essential for dam operation, safety and sustainability. Such structures are commonly used for the emergency release of flood discharge, controlling reservoir water levels, regulating water release downstream of the dam, flushing (i.e. full and partial reservoir drawdown) and sluicing of sediments, preventing sediment from blocking and entering hydropower conduit intakes, and river diversion. According to Morris and Fan (1998), one of the main causes of dam failure is insufficient low-level outlet discharge capacity, even though most dams utilise spillways to safely release excess flow from large floods. Insufficient discharge capacity naturally becomes a serious concern during extreme flood events where high flows and high sediment loads are expected. Reconstruction of low-level outlets is possible but is generally believed to be technically challenging in most cases, as well as unprofitable (Delft Hydraulics, 1992). The location, design capacity and configuration of an outlet is site specific and has to be adapted to specific project restrictions and conditions.

Drawdown or pressure flushing through low-level dam outlets below hydropower intakes are common mitigation measures for removing locally deposited sediment from reservoirs (Basson and Rooseboom, 1999). Drawdown flushing is periodically necessary to especially

keep the hydropower intakes free of non-cohesive sediment, as sand fractions will typically damage turbines in hydropower plants and ultimately reduce power generation output. The low-level intake area also needs to be kept clear of blockage caused by debris and sediment deposition as this could threaten sluice gate operation, prevent drawdown flushing and ultimately result in the uncontrolled emptying of the reservoir.

1.1.3 Problem statement

"Large" dams in South Africa have been found to trap more than 95% of the incoming sediment load (Braune and Looser, 1989). This, together with the typically high evaporation and low precipitation rates in South Africa, implies substantial water conservation and sedimentation issues. Large dams therefore need to be designed so that the storage capacities can contain as much of the mean annual runoff (MAR) as possible in order to achieve over-year storage.

Reservoirs with poor sediment management strategies will likely, at some point, succumb to significant sedimentation upstream of their dam hydropower intakes and low-level outlets. Sedimentation, together with immersed debris, could result in the blockage of the intakes, entrainment into the hydropower conduits, and/or deposition near the sluice gates in the low-level outlets. Such blockage of low-level outlets and other conduits poses a significant safety risk as dam operation is threatened and reservoir drawdown is prevented (Fan, 1985). According to Fan (1985), sedimentation could also weaken the structural stability of the dam due to the chemical reactions within the deposits, as well as the additional exerted pressures which can damage the concrete or surface lining. Significant sedimentation can also adversely affect recreational activities in the reservoir.

In Southern Africa, for example, there have been cases of low-level outlets, usually in the older and more traditional dams, that have never been opened or used. The reason for this is the apprehension that the sluice gates will not be able to be fully closed again once flushing commences due to potential blockage caused by sedimentation in and around the intake area A previous scenario of severe sedimentation upstream of the low-level outlet, in which the outlet gate could not be closed during flushing due to coarse sediment deposition at the gates, is illustrated in Figure 1.1-1. There have also been general cases of lack of maintenance done on mechanical equipment and hydraulic machinery in dams, which have threatened low-level outlet operation reliability.

Figure 1.1-1: Mbashe HPP weir (Eastern Cape, South Africa)

Various international scenarios are known of existing dams where little provision has been made for the flushing of coarse, large-diameter sediments (i.e. gravel and boulders) that occur at the respective dam sites. This lack of provision implies that certain low-level outlet designs may be deficient for such cases, especially during flood events where high sediment concentration is expected. This creates certain apprehension around flushing efficiency, outlet discharge capacity, outlet conduit durability and ultimately dam safety and operation. Boulders can quickly become a notable concern in small reservoirs that fill up quickly with sediment. At larger reservoirs, large-diameter sediments can also accumulate near hydropower intakes once the reservoir has filled with sediment (Basson and Rooseboom, 2007).

It is therefore proposed that new optimised, versatile and robust low-level outlet designs need to be implemented in future dams to ensure suitable dam operation efficiency and sustainability. Furthermore, the potential of low-level outlets to be designed and utilised as a means to regulate the release of flood discharge, either independently or in conjunction with dam spillways, should be further investigated. These designs would then have to sufficiently combat the typical high-risk issues that ultimately arise during flood discharging, such as: (1) cavitation and abrasion damage to the low-level outlet gates and conduit (due to high water velocities and pressures); and (2) blockage of the low-level outlet due to higher sediment and debris concentrations (Amirsayafi, 2015).

1.2 Objectives

The objectives of this study are:

1) Consult literature on hydraulic designs of existing low-level outlet conduits and intakes that have resulted in effective pressure and free-flow flushing (with drawdown) of coarse non-cohesive sediments (i.e. mainly gravel and boulders) during flood events. From this, propose a postulated design for future application. The postulated design must be refined or optimised by means of numerical and physical model studies;
2) Design a semi-circular, ogee-shaped spillway structure (with wing-walls) and position it around the intake area of the low-level outlet and inside of the typical sediment scour hole that forms during pressure flushing. The main aim of the structure is to produce suitable upstream supercritical flow conditions to help optimise the flushing of sediments during free-surface flow or spilling conditions to prevent sediment deposition and blockage at or near the outlet gates. The main aim of the consequent low-weir is during pressure flushing to locally remove and scour sediment, as well as prevent main reservoir sediments from depositing near the outlet gate and hindering gate closure; and
3) Based on numerical and physical model results, propose design guidelines for such a sediment flushing system that ensures effective sediment flushing of the zone at the inlet end of low-level dam outlets to protect hydropower intakes above it against sediment ingress. The guidelines should be versatile to different and varying conditions, such as site location, upstream water levels, downstream tailwater levels, preferred flushing techniques, as well as sediment size and type to be flushed.

1.3 Thesis outline

The format of this thesis study is as follows:

- Section 2: Literature review. This section looks at the important literature needed to understand the physical properties of sediment, as well as the dynamic nature of coarse non-cohesive sediment and how it reacts to fluid forces. The literature provided is also necessary for understanding the different components of low-level outlets, how they operate and how they are designed hydraulically for different flushing scenarios.

- Section 3: Postulated flushing system guidelines. This section justifies the postulated design of an optimised sediment flushing system for a low-level dam intake based on observed literature from Section 2 (*Literature review*). This section systematically summarises relevant literature while discussing the methodology followed in designing a singular: (1) low-level outlet conduit and inlet structure; (2) conduit air vent; and (3) upstream low-weir, ogee spillway structure and associated wing-walls.

- Section 4: Numerical model and results. This section considers hydraulic principles and Computational Fluid Dynamic (CFD) modelling to hydraulically compare four different proposed flushing system designs, from which the best design option can be chosen and further refined in physical modelling.

- Section 5: Physical model and results. This section considers physical modelling of the postulated flushing system design, which evolved from the findings of the numerical model simulations, for further testing and refinement. The main aim of the physical model is to test the robustness, reliability and actual flushing capability of the design.

- Section 6: Conclusions. This section discusses the important findings and conclusions made from the literature, numerical model and physical model studies.

- Section 7: Recommendations. This section provides structural recommendations that are believed to further improve the sediment flushing capability of the postulated sediment flushing system design (for further research).

2 Literature review

The study areas covered in this section include physical properties of sediment, incipient motion of sediment, sediment transport and deposition, sediment management and control, as well as low-level outlet structural design, hydraulic design and operation. The focus is on drawdown and pressure flushing of coarse non-cohesive sediment through low-level outlets.

2.1 Physical properties of sediment

This section investigates the general physical properties of sediment, specifically the sand to boulder classes, with emphasis being placed on gravel and boulders. This section aims to provide a better understanding of the dynamic nature of coarse non-cohesive sediment and how it reacts to fluid forces. The physical properties covered include sediment particle size, shape, density, specific gravity, grading, settling velocity and underwater angle of repose.

2.1.1 Particle size

Particle size is often used to describe a sediment particle for several practical purposes, with the sediment size distribution that forms the reservoir bed and banks being of great importance (Simons and Sentürk, 1992). A general classification of relevant sediment sizes is indicated in Table 2.1-1.

Table 2.1-1: Sediment size classes (Simons and Sentürk, 1992)

Size (mm)	Class
4000 - 2000	Very large boulders
2000 - 1000	Large boulders
1000 -500	Medium boulders
500 - 250	Small boulders
250 - 130	Large cobbles
130 - 64	Small cobbles
64 - 32	Very coarse gravel
32 - 16	Coarse gravel
16 - 8	Medium gravel
8 - 4	Fine gravel
4 - 2	Very fine gravel
2 - 1	Very coarse sand
1 - 1/2	Coarse sand
1/2 - 1/4	Medium sand
1/4 - 1/8	Fine sand
1/8 - 1/16	Very fine sand

Particle size and type determines whether the sediment is either fine (i.e. clays and silts) or coarse (i.e. sand and larger sizes) (Morris and Fan, 1998), as well as either cohesive (i.e. clay particles smaller than 0.002 mm) or non-cohesive (Garcia, 2008). Cohesive sediment is naturally less susceptible to erosion due to resulting flocculation and is therefore harder to predict in terms of erosional and transport behaviour.

According to Simons and Sentürk (1992), the boulder class has received little attention when considering sediment transport problems. The authors state that although it is relatively easy to measure the size of individual particles within this class range, it can be challenging to identify the size distribution of a bed of boulders due to the large volume of the sample and the variety of particle sizes.

Optical methods, sieve analysis, calipers, sedimentation methods and/or photographic methods can be used to measure particle size (Simons and Sentürk, 1992). The particle size distribution is often determined from the results of a sieve analysis which are ultimately plotted as a cumulative frequency distribution curve. According to Langmaak (2013), the median diameter or sieve size, d_{50}, is usually used to express a single particle size, whereas the diameter d_y is rather used to express a sample of particles. The subscript y indicates the percentage of the sample that consists of particles with diameters smaller than d_y or that passes through a sieve size. The median particle diameter (d_{50}) is thus the diameter at which 50% of the sample consists of particles with diameters smaller than this d_{50} value.

2.1.2 Particle shape

Particle shape generally relates to the overall geometric form of the particle, not considering the particle's physical composition or size. Simons and Sentürk (1992) state that the dynamic behaviour of a particle may govern its shape, as it appears that particles of completely different shape, which possess the same density and volume, may have the same behaviour in fluids.

Roundness – defined as the smoothness of a particle's edges and corners – can be used to define a particles shape. According to Simons and Sentürk (1992), *sphericity* – being defined by Wadell (1932) as the ratio of the surface area of a sphere of equal volume to the actual surface area of the particle – is considered as one of the most important shape parameters and is used to describe the relative motion between the falling particle and the fluid. The same authors state that sphericity is dimensionless, appears to decrease with decreasing particle size and depends on mineral composition. As the sphericity of a particle is difficult to measure in a practical sense, it can be related to different particle dimensions which are measured along three mutually perpendicular axes through the particle: the longest dimension, or a-axis; the intermediate dimension, or b-axis; and the shortest dimension, or c-axis (Simons and Sentürk, 1992). Krumbein (1932) suggested the following expression to calculate sphericity:

$$\Psi_p = \sqrt[3]{\left(\frac{b}{a}\right)^2 \cdot \frac{c}{b}} \qquad \textbf{Equation 2-1}$$

Simons and Sentürk (1992) state that a particle's shape factor (S_p) has been found to be the most suitable expression for shape, and is expressed as follows:

$$S_p = \frac{c}{\sqrt{a \cdot b}} \qquad \textbf{Equation 2-2}$$

Long and flat particles are generally considered to be less stable than those with similar dimensions along a, b and c (Langmaak, 2013). The closer a particle's sphericity or shape factor is to 1, the more spherical and round it is in shape. Figure 2.1-1 illustrates the different degrees of particle sphericity and roundness.

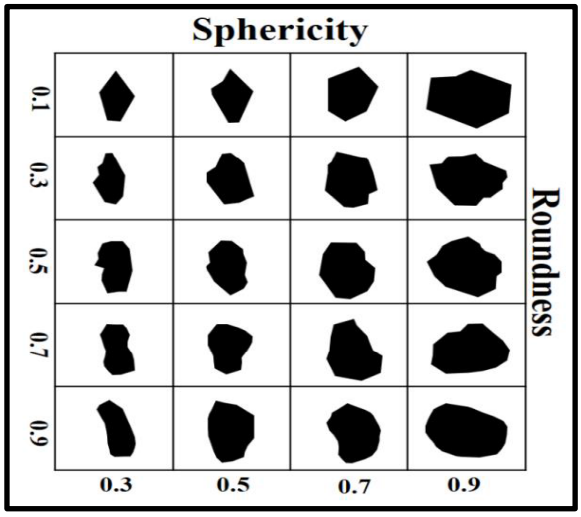

Figure 2.1-1: Particle sphericity and roundness (Morris and Fan, 1998)

2.1.3 Grading of bed material

The grading of bed material is an indication of how well particle size (i.e. larger and smaller rocks) is distributed in the sample. A well-graded sample is characterised by secure interlocking of individual particles with minimal movability (i.e. high internal friction) and does not contain any significant gaps within the grading width (Langmaak, 2013). This results in a stable top layer boulder surface, which is subjected to flow forces. The more gaps that are present in-between the larger particles, in the absence of finer particles that could have been easily eroded away, the less resistance there is to flow forces.

The grading width (i.e. defined by the ratio: d_{85}/d_{15}) is commonly used to give an indication of the required grading (Langmaak, 2013), and is categorised in Table 2.1-2.

Table 2.1-2: Grading width classes (CIRIA et al., 2007)

Grading	d_{85}/d_{15}
Narrow	< 1.5
Wide	1.5 – 2.5
Very wide	2.5 – 5.0

Simons and Sentürk (1992) provide a commonly used grading method, whereby:

- $d_{100} \geq 2 \cdot d_{50}$
- $d_{20} \geq 0.5 \cdot d_{50}$
- $d_{Min} \geq 0.2 \cdot d_{50}$

Langmaak (2013) states that the above guidelines, after being linearly interpolated on a logarithmic scale for d_{85} and d_{15} values, yielded a grading width (d_{85}/d_{15}) of 3.6 (i.e. "very wide" grading) for riprap.

Lastly, Przedwojski *et al*. (1995) propose $\frac{d_{60}}{d_{10}} \geq 2.5$ for riprap with overtopping flow to ensure stability. The same authors alternatively refer to the riprap design guidelines of 1985 by the US Army Corps of Engineers, which has been modified by Langmaak (2013) as follows:

- $1.26 \cdot d_{50} \leq d_{100} \leq 2 \cdot d_{50}$
- $0.74 \cdot d_{50} \leq d_{15} \leq d_{50}$

2.1.4 Particle density and specific gravity

The density of a sediment particle (ρ_s) is dependent on its mineral composition and is expressed as its mass per unit volume. The density of rock generally does not vary significantly for different types of rocks and can therefore be approximated as 2650 kg/m³ (Simons and Sentürk, 1992; CIRIA *et al*., 2007; SANRAL, 2013).

Bulk particle density is used to represent the density of a sample of sediment and considers both the solid particle and the air voids within. The apparent bulk particle density can be calculated according to the procedure specified in SANS 3001-AG23 (2014), and is defined by the following equation:

$$\rho_b = \frac{m_b}{m_a - (m_c - m_d)} \cdot \rho_{wT} \qquad \textbf{Equation 2-3}$$

Where,

ρ_b = Apparent bulk particle density of the aggregate (kg/m³)

m_b = Mass of the oven-dried aggregate (g)

m_d = Mass of the suspended empty basket in 25° water (g)

m_c = Mass of the suspended basket plus aggregate in 25° water (g)

m_a = Mass of the saturated surface-dry aggregate (g)

ρ_{wT} = Density of water at the test temperature, T = 25° (kg/m³)

The specific gravity of a sediment particle (SG) is a dimensionless unit that describes the ratio of the particle density (ρ_s) to the density of water (ρ_w), usually at a temperature of 4°C (Simons and Sentürk, 1992). As the density of water is commonly taken as 1000 kg/m³, the specific gravity of rock can be estimated as 2.65.

A specific gravity value larger than 1 indicates that the object (i.e. sediment particle) is denser than the reference substance (i.e. water in this case), which means that the object will sink in the reference substance.

2.1.5 Underwater angle of repose

The angle of repose (Ø) of a sample of sediment particles is defined as the steepest angle at which a sloping surface formed by the loose material remains stable (i.e. no incipient sliding of sediment). For non-cohesive sediment, the average slope angle of the sides of the sediment scour hole that forms around the low-level intake during pressure flushing is usually equal to the submerged angle of repose of the deposits (Morris and Fan, 1998).

According to Simons and Sentürk (1992), the angle of repose can be determined by placing sediment particles into water with near zero velocity and thereafter measuring the critical toe angle of the submerged cone of uncompacted deposited sediment. Figure 2.1-2 can also be used to read off the angle of repose (referred to as the "Slope angle") for a specific particle angularity and size. Garcia (2008) states the angle of repose is typically 30° for well-sorted sand and typically increases steadily to 40° for gravel.

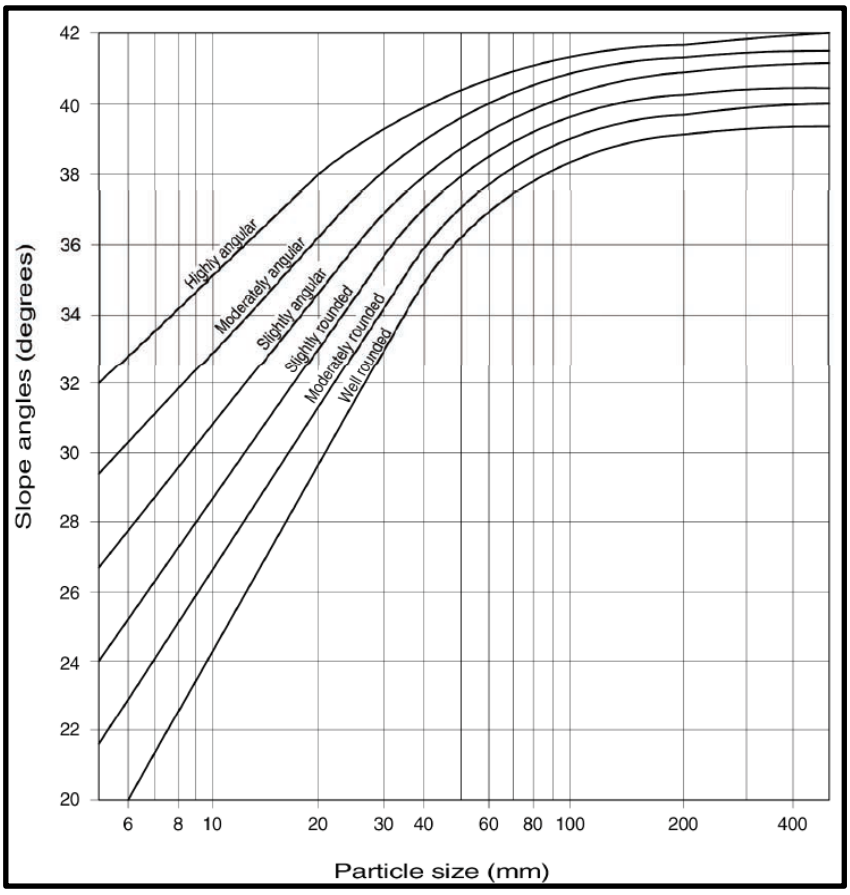

Figure 2.1-2: Angle of repose (SANRAL, 2013)

2.1.6 Particle settling velocity

The settling velocity of a particle is defined as the terminal velocity that is reached by the particle as it falls through a fluid which is in an inactive state. The settling velocity is influenced by a variety of factors, such as the particle's density, size, surface roughness and shape. Most of these factors, however, lose their significance as the particle size increases (Simons and

Sentürk, 1992). Other factors that influence the settling velocity of a particle include the density, temperature, viscosity and salinity of the fluid that it is in (Morris and Fan, 1998).

Simons and Sentürk (1992) implicitly derived an expression for the settling velocity (V_{ss}) of a particle, under the assumption that the considered particle has reached equilibrium and that the Reynolds Number (R_e) is larger than 1000. The expression is as follows:

$$V_{ss} = \sqrt{\frac{4}{3} \cdot \left(\frac{\rho_s - \rho_w}{\rho_w}\right) \cdot \frac{d \cdot g}{C_d}} \qquad \textbf{Equation 2-4}$$

Where,

d = Particle diameter (m)

C_d = Drag coefficient

Figure 2.1-3 can be used to estimate the drag coefficient (C_d) for a specific Reynolds Number (R_e) and for various particle shapes. The Reynolds Number (R_e) can be calculated as follows:

$$R_e = \frac{\rho \cdot \bar{V} \cdot L}{\mu} = \frac{\bar{V} \cdot L}{v} \qquad \textbf{Equation 2-5}$$

Where,

μ = Dynamic viscosity (kg/m·s)

v = Kinematic viscosity (m²/s)

$\bar{V}$ = Mean fluid velocity (m/s)

L = Hydraulic diameter (m), given by the following equation:

$$L = \frac{4 \cdot A}{P} \qquad \textbf{Equation 2-6}$$

Where,

A = Cross-sectional flow area (m²)

P = Wetted flow perimeter (m)

According to Figure 2.1-3, the drag coefficient range becomes $0.4 \leq C_d \leq 2$ for turbulent flow. The lower boundary represents a spherical shape ($S_p = 1$) and the upper boundary represents a non-spherical shape ($S_p \approx 0$). Therefore, for a certain shape factor (S_p) where $0 < S_p < 1$, the drag coefficient (C_d) during turbulent flow is linearly estimated as:

$$C_d = 2 - \left(1.6 \cdot S_p\right) \qquad \textbf{Equation 2-7}$$

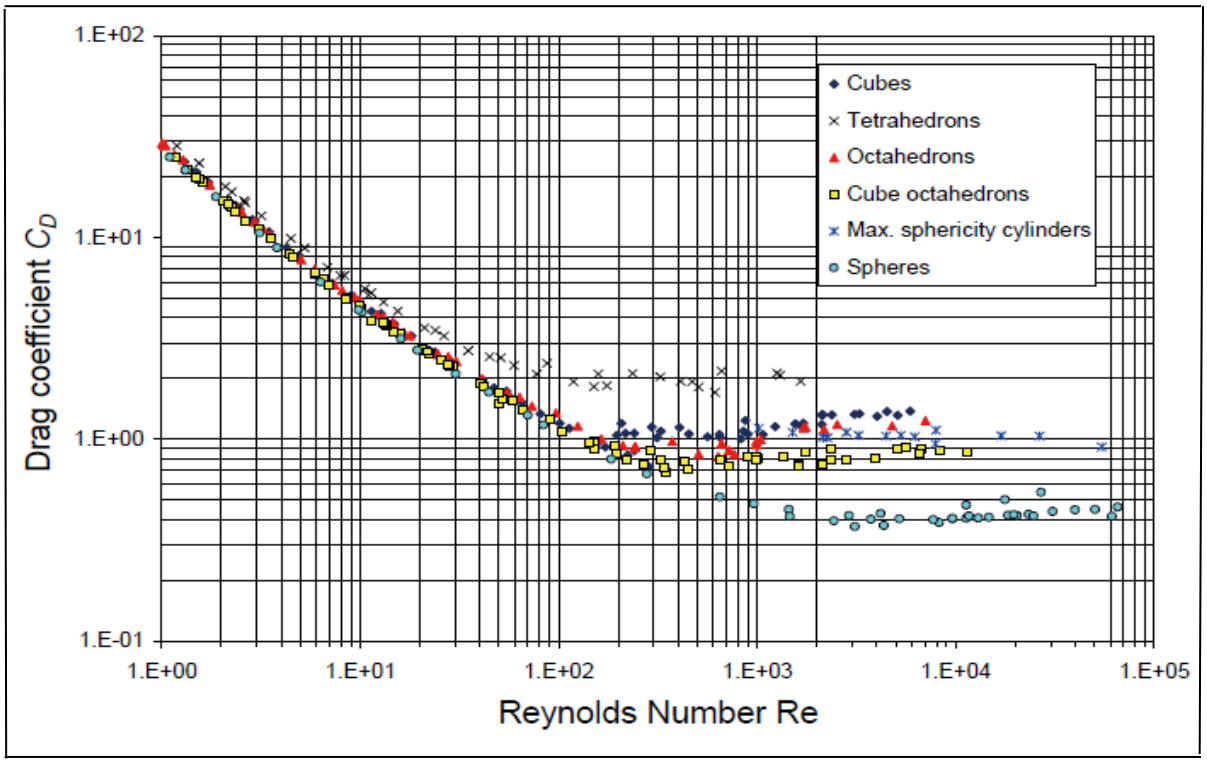

Figure 2.1-3: Drag coefficient versus Reynolds number (Concha, 2009)

Van Rijn (1993) expressed the following settling velocity equations for sediment particles of different particle diameter (d) ranges:

- $d \leq 0.1$ mm (only valid for $R_e \leq 1$)

$$V_{ss} = \frac{1}{18} \cdot \left(\frac{\rho_s - \rho_w}{\rho_w}\right) \cdot \frac{g \cdot d^2}{v} \qquad \textbf{Equation 2-8}$$

- $1 \leq d \leq 0.1$ mm

$$V_{ss} = \frac{10 \cdot v}{d} \cdot \left(\sqrt{1 + \frac{0.01 \cdot \left(\frac{\rho_s - \rho_w}{\rho_w}\right) \cdot g \cdot d^3}{v^2}} - 1\right) \qquad \textbf{Equation 2-9}$$

- $d > 1$ mm

$$V_{ss} = 1.1 \cdot \sqrt{\left(\frac{\rho_s - \rho_w}{\rho_w}\right) \cdot g \cdot d} \qquad \textbf{Equation 2-10}$$

Cheng (1997) derived the following settling velocity formula for individual natural sediment particles exposed to different flow regimes (i.e. $1 \leq R_e \leq 1000$):

$$V_{ss} = \frac{v}{d} \cdot \left(\sqrt{25 + 1.2 \cdot {d_*}^2} - 5 \right)^{1.5} \qquad \textbf{Equation 2-11}$$

Where,

$$d_* = d \cdot \sqrt[3]{\frac{\left(\frac{\rho_S - \rho_W}{\rho_W}\right) \cdot g}{v^2}}$$

Brown and Lawler (2003) examine various settling velocity equations in more detail, but these are not covered in this study.

2.2 Incipient motion of sediment

According to Langmaak (2013), it is agreed upon by various researchers that the initiation of particle motion is caused by complex oscillating eddy currents that exist in the vicinity of the particles. The same author states that the definition of the initiation of motion is very important for the success of laboratory tests and can be better understood and described by considering the hydraulic flow parameters in the particle vicinity.

2.2.1 Liu's stream power approach

Langmaak (2013) considered both the critical flow velocity method as well as Shield's critical shear stress approach for determining the critical condition for incipient motion. The author, however, showed preference towards Liu's stream power approach.

Liu (1957) discovered that a certain relationship exists between the particle Reynolds number (${R_e}^*$) and the Movability number (i.e. the ratio of the shear velocity (V^*) to the settling velocity (V_{ss}) of the particle). The relationship acknowledges the distinction between the way that stream power is transferred, ultimately resulting in the displacement of particles during laminar and turbulent flow. The relationship was studied and applied by different researchers and was used to essentially define and plot their unique criteria for incipient motion, as illustrated in Figure 2.2-1. A modified diagram of Liu's criteria for incipient motion is illustrated in Figure 2.2-2. Table 2.2-1 indicates the different Movability numbers (and corresponding particle Reynolds numbers) proposed by the various authors for turbulent flow conditions. Turbulent flow is of primary interest in this investigation, as ${R_e}^*$ is expected to be much larger than 13 as a result of the large particle size of boulders under consideration.

The particle Reynolds number (${R_e}^*$) is defined by the following equation (Liu, 1957):

$${R_e}^* = \frac{V^* \cdot d}{v} \qquad \textbf{Equation 2-12}$$

Where,

V^* = Shear velocity (m/s), given by the following equation:

$$V^* = \sqrt{g \cdot y \cdot S_f} \qquad \textbf{Equation 2-13}$$

Where,

y = Flow depth (m)

S_f = Energy slope (m/m)

Liu's theory is based on the assumption that the flow under consideration is uniform and homogeneous, indicating that the bed slope (S_o), water surface slope (S_w) and energy slope (S_f) are parallel and equal (Langmaak, 2013). As non-uniform flow is expected in the low-level outlets, this should be kept in mind when applying the method.

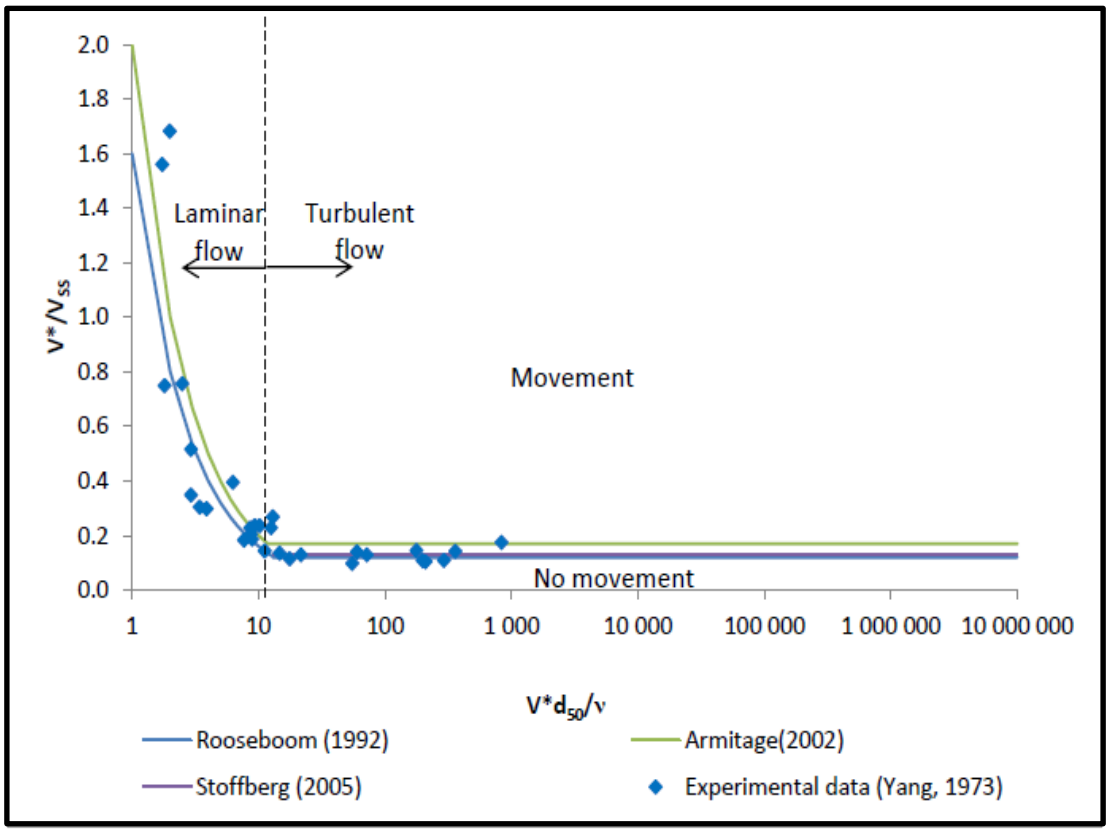

Figure 2.2-1: Criteria for incipient motion (Langmaak, 2013)

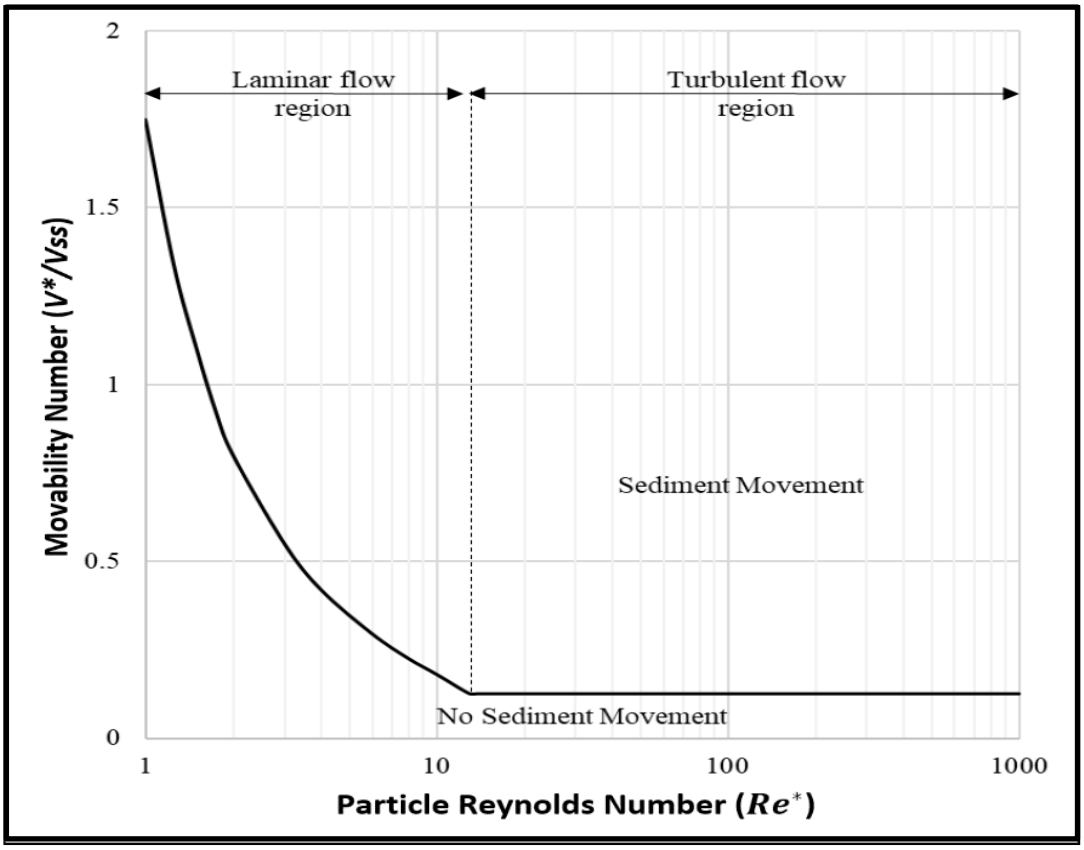

Figure 2.2-2: Modified Liu diagram (SANRAL, 2013)

Table 2.2-1: Proposed Movability numbers

Researcher	Critical Movability Number (V^* / V_{ss})
Rooseboom (1992) (after data from Yang, 1973) SANRAL (2013)	0.12, for R_e^* > 13
Armitage (2002)	0.17, for R_e^* > 11.8
Stoffberg (2005)	0.13, for designing riprap (recommended)

2.2.2 Correction for steep bed slopes

In order to compensate for the effects that steep bed slopes have on the shear stresses and velocities, correction factors need to be considered and implemented.

Armitage (2002), CIRIA, *et al*. (2007) and Stoffberg (2005) have differentiated between two different types of slopes:

1. Horizontal slope (β): It is the downwards angle of the bed in the direction of the flow (unit: degrees).
2. Transverse slope (α): It is the downwards angle of the bed normal to the direction of flow (unit: degrees). When the flow is directed perpendicularly over the side slope, α = 0°; when the flow is directed along the side slope, α = 90°.

The theory behind this discussion only deals with particle stability issues (i.e. the steeper the slope the less stable the particle) due to a change in the gravity force direction, and ignores potential air entrainment in the flow which appears to have a significant effect at slopes steeper than 1:10 (i.e. β > 5.71°) (Langmaak, 2013).

Armitage (2002), Armitage and Rooseboom (2010), CIRIA, *et al*. (2007), Stoffberg (2005) and other researchers defined the correction factors as follows:

$$k_\beta = \frac{\sin(\emptyset - \beta)}{sin(\emptyset)}$$ **Equation 2-14**

$$k_\alpha = \cos(\alpha) \cdot \sqrt{1 - \left(\frac{\tan(\alpha)}{\tan(\emptyset)}\right)^2}$$ **Equation 2-15**

Where,

k_β = Ratio of the critical drag force at a bed sloped longitudinally to the critical drag force at the horizontal bed.

k_α = Ratio of the critical drag force at a given transverse slope to the critical drag force at the normal bed.

$\emptyset$ = Underwater angle of repose of the sediment (°)

The factors k_β and k_α are equal to 1 for a bed that is horizontal in the transverse and longitudinal directions.

According to Armitage and Rooseboom (2010) and Stoffberg (2005), the Movability number for a sloped bed can be defined as follows:

$$\left(\frac{V^*}{V_{ss}}\right)_{\beta,\alpha} = \sqrt{k_\beta \cdot k_\alpha} \cdot \left(\frac{V^*}{V_{ss}}\right)_0$$ **Equation 2-16**

Where,

$\left(\frac{V^*}{V_{ss}}\right)_{\beta,\alpha}$ = Movability number for any given bed slope

$\left(\frac{V^*}{V_{ss}}\right)_0$ = Movability number for a horizontal bed

2.2.3 Shield's parameter

According to SANRAL (2013), the most effective criteria to be used to determine whether non-cohesive sediment particles will be lifted off the bed for a given flow, is the Shield's parameter. The maximum sediment particle diameter (d_1) to be subjected to lifting from the channel bed, as well as the maximum sediment particle diameter (d_2) to be subjected to

lifting from the channel side slopes, for d larger than 6 mm, can be defined according to the following equations (SANRAL, 2013):

$$d_1 \leq 11 \cdot y \cdot S_f \qquad \textbf{Equation 2-17}$$

$$d_2 < \frac{8.3 \cdot y \cdot S_f}{\cos(\theta) \cdot \left[1 - \frac{tan^2(\theta)}{tan^2(\emptyset)}\right]^{0.5}} \qquad \textbf{Equation 2-18}$$

Where,

y = Flow depth in the channel (m)

S_f = Energy slope (m/m)

θ = Angle of channel side slopes (°)

$\emptyset$ = Underwater angle of repose of the sediment (°)

The energy slope is equal to the channel bed slope during uniform flow (i.e. transitional or secondary losses (h_L) are equal to zero). Otherwise, the energy slope ($S_{f_{1-2}}$) between point 1 and point 2 is defined as follows (SANRAL, 2013):

$$S_{f_{1-2}} = \frac{\sum h_{L_{1-2}} + h_{f_{1-2}}}{L_{1-2}} \qquad \textbf{Equation 2-19}$$

Where,

$h_{L_{1-2}}$ = Transitional (secondary) losses between point 1 and 2 (m) (Equation 2-30)

$h_{f_{1-2}}$ = Friction losses between point 1 and 2 (m) (Equation 2-30)

L_{1-2} = Horizontal distance between point 1 and 2 (m)

It must be noted that Shield's equations do not incorporate correction factors for steep bed slopes as recommended for the modified Liu equations in the previous section.

2.3 Sediment transport and deposition

Sediment generally originates upstream of a reservoir as a result of the erosion and weathering of catchment surfaces, as well as of the erosion of riverbed material due to water flow (i.e. flow induced shear stress). Water – usually rainfall that causes sheet erosion (Garcia, 2008) – typically initiates the movement and transport of the loose sediment. According to Mahmood (1987), a significant amount of this displaced loose sediment ends up being deposited in channels, as well as on flood plains and slopes, within the drainage basin. The portion of the loose sediment that does reach the river stream is transported along the river to the entrance of the reservoir, where after the sediment transport capacity in the reservoir is reduced and the sediment load is dependent on the hydraulic conditions in the reservoir

(Basson and Rooseboom, 2007). Sediment can therefore be considered separately when it comes to transport and deposition within a river and within a reservoir.

2.3.1 River transport

The three different zones of sediment particle motion within a river, according to Van Rijn (1993), are illustrated in Figure 2.3-1 and are categorised and discussed below:

1. The **Bed-load** comprises sediment particles that experience a sliding and rolling motion. In this case, the water flow velocity along the riverbed is large enough to result in the incipient motion of the particles, but not large enough to break contact between the particles and the bed.

2. The **Suspended-load** comprises sediment particles that experience a bouncing-type movement (i.e. saltations) along the riverbed. In this case, fast flowing water velocities cause turbulent fluctuations that exert vertical drag and lift forces on the particles. If these forces are larger than the weight of the particles, the particles will be lifted off the riverbed. The period during which the particles remain suspended in the water depends on the strength and frequency of the turbulent fluctuations.

3. The **Wash-load** can be contained within the suspended load, but mainly comprises finer particles (silt and clay) that do not originate from the riverbed, but from the erosion of particles in motion and of land surfaces.

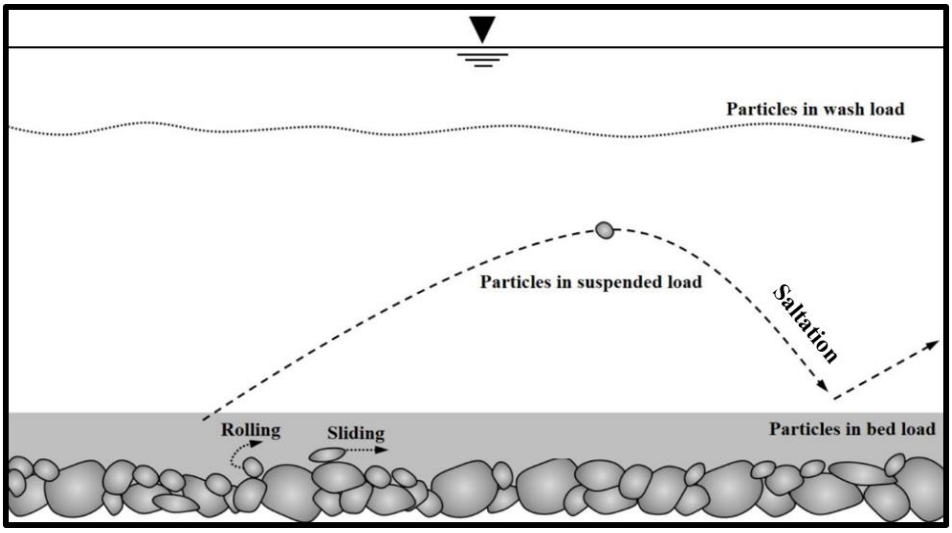

Figure 2.3-1: River sediment transport (Dey, 2014)

Meyer-Peter and Müller (1948) used previous experimental data to derive an empirical law to determine bed-load transport in alluvial rivers for practical (i.e. natural) application. This law was derived from tests that considered slopes from 0.4 to 20%, particle sizes (d and d_m) from 0.4 to 30 mm, water depths (h) from 0.01 to 1.2 m, unit flow discharges from 0.002 to 2 m³/s.m, specific under water gravities ($\gamma_s{}^* = \gamma_s - 1$) from 0.25 to 3.2 tons/m³, and the assumption that the velocity and turbulence distribution is uniform across the whole wetted

cross-section (Meyer-Peter and Müller, 1948). The parameters and formulae needed for calculating the bed-load transport for different conditions, according to the authors, are provided below:

- **Known parameters**:

  Q = Water discharge (kg/s)

  d_m = Effective particle diameter (m)

  d_{90} = Particle diameter at which 90% of the sample's mass is comprised of particles with a diameter less than this value (i.e. intercept for 90% of the cumulative mass) (m)

  B = Width of channel (m)

  k_w = Coefficient of roughness of channel sides

  γ_w = Specific gravity of water (i.e. 1 t/m³)

  γ_s = Specific gravity of sediment (i.e. 2.65 t/m³ for rock)

- **Measured parameters:**

  J_s = Riverbed slope (m/m)

  J_w = Water surface slope (m/m)

  h = Depth of water (m)

  g_s^* = Under water weight of specific bed-load transport per unit width (kg/m.s)

- **Calculated parameters**

  The average flow velocity (V: m/s) in the channel is calculated as:

$$V = \frac{Q}{B \cdot h} \qquad \textbf{Equation 2-20}$$

  The hydraulic radius (R) of free-surface flow is calculated as:

$$R = \frac{B \cdot h}{B + 2h} \qquad \textbf{Equation 2-21}$$

  The energy line slope (J: m/m) is calculated as:

$$J = J_w - \frac{V^2}{g \cdot h} \cdot (J_w - J_s) \qquad \textbf{Equation 2-22}$$

The mean coefficient of roughness (k_m) is calculated as:

$$k_m = \frac{V}{R^{2/3} \cdot J^{1/2}} \quad \textbf{Equation 2-23}$$

The coefficient of roughness of channel bed (k_s) is calculated as:

$$k_s = \frac{k_m \cdot k_w \cdot B^{2/3}}{\left\{B \cdot h^{3/2} + 2 \cdot h \cdot \left(k_w{}^{\frac{3}{2}} - k_m{}^{\frac{3}{2}}\right)\right\}^{2/3}} \quad \textbf{Equation 2-24}$$

The discharge of bed-load transport per unit width (q_s: kg/m.s) is calculated as:

$$q_s = Q \cdot \frac{k_w{}^{3/2}}{2 \cdot h \cdot k_s{}^{3/2} + B \cdot k_w{}^{3/2}} \quad \textbf{Equation 2-25}$$

The coefficient of particle friction with the smooth bed (k_r) in the region of *fully developed turbulence* is calculated as:

$$k_r = \frac{26}{d_{90}{}^{1/6}} \quad \textbf{Equation 2-26}$$

- **Bed-load transport**

The discharge of bed-load transport (Q_s: kg/s) for a bed-load with *uniform grain size and a constant natural specific gravity* is calculated as:

$$Q_s = q_s \cdot B \quad \textbf{Equation 2-27}$$

The discharge of bed-load transport (Q_s: kg/s) for a bed-load with *varied grain size and a constant natural specific gravity* can be implicitly calculated from:

$$\frac{\gamma_w}{\gamma_s - \gamma_w} \cdot \left(\frac{Q_s}{Q}\right)\left(\frac{k_s}{k_r}\right)^{\frac{3}{2}}\left(\frac{h \cdot J}{d_m}\right) = 0.047 + 0.25 \cdot \left(\frac{\gamma_w}{g}\right)^{1/3}\left(\frac{g_s{}^{*2/3}}{d_m}\right)\left(\frac{1}{\gamma_s - \gamma_w}\right) \quad \textbf{Equation 2-28}$$

2.3.2 Reservoir sediment transport

The three different drivers of sediment particle motion within a reservoir, according to Basson and Rooseboom (2007), are categorised and discussed below:

1. **Turbulent suspension** (i.e. similar to that in rivers) occurs when turbulent flow within the reservoir forces sediment particles (i.e. mainly silt, clay and sand) into suspension. The suspended sediment travels through the water column and can partially deposit within the reservoir and/or could partially be transported through the reservoir until it is released downstream (Annandale *et al.*, 2016).

2. **Colloidal suspension** mainly depends on water quality and occurs when electrostatic forces in the water cause fine particles (i.e. 0.001 to 1 µm diameter) to become suspended. Such suspended particles typically only make up about 3% of the total sediment load and typically only occur for sediment concentrations less than 100 ppm.
3. **Density currents** such as interflow, overflow and underflow (i.e. turbidity density currents) occur when suspended sediments in inflowing water create a density difference within the cleaner reservoir water, ultimately producing stratified flow (Chamoun *et al.*, 2016). Turbidity density currents (i.e. underflow) are the most common form of density currents in reservoirs (Mahmood, 1987) and can be illustrated in Figure 2.3-2. These currents, which are known to transport fine to very fine sediment over long distances along the reservoir bed (Annandale *et al.*, 2016), can then be vented through low-level outlets to effectively release accompanying sediment.

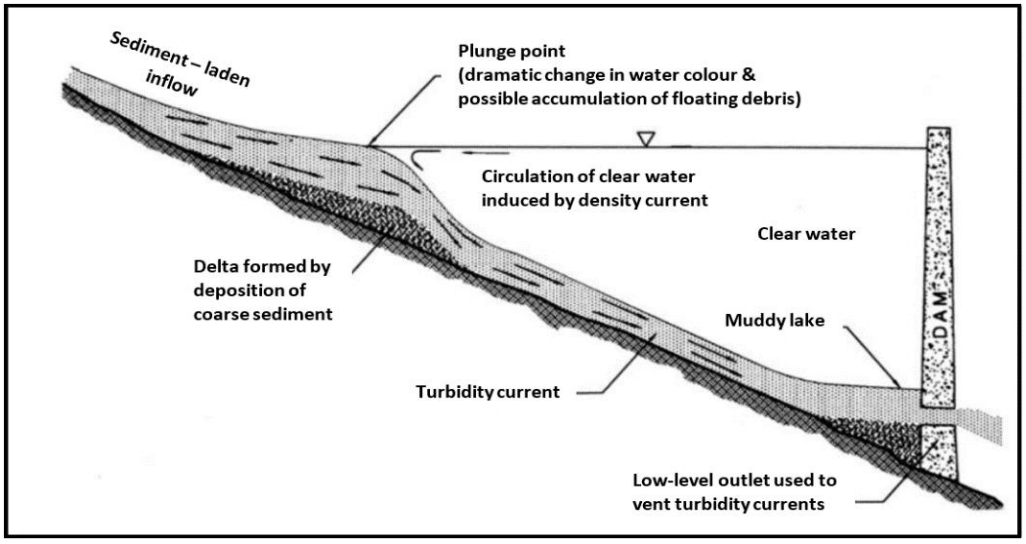

Figure 2.3-2: Turbidity current through a reservoir (Morris *et al.*, 2008)

According to practical observations made in China, Jiang (1980) states that if the following equation holds, the sediment transport capacity of the main reservoir channel will be sufficient to warrant a long-term balance between sediment deposition and erosion.

$$\frac{Q_m}{Q_d} \cdot \frac{S_n}{S_0} \geq 0.5 \qquad \textbf{Equation 2-29}$$

Where,

Q_d = Main river discharge (m³/s)

Q_m = Maximum free-flow outlet discharge without flood detention (m^3/s)

S_0 = Original riverbed slope (m/m)

S_n = Slope of the line connecting the upstream end of the maximum pool level with the low-level outlets (m/m)

2.3.3 Sediment deposition in reservoirs

Once sediment-laden flows from the upstream river enter the reservoir, some of the sediment ends up being transported through the reservoir and released downstream. The rest tends to deposit in the reservoir due to the decrease in flow velocity and increase in flow area (i.e. reduced transport capacity) (Annandale, 2005). According to Dewals *et al.* (2012), a reservoir's trapping efficiency determines the percentage of the inflowing sediment that ends up being deposited or trapped in the reservoir. The same authors state that the trapping efficiency of a reservoir is unique and is influenced by numerous reservoir characteristics (i.e. bed slope, flow, size and shape) and sediment characteristics (i.e. particle shape, size and settling velocity). According to ICOLD Bulletin 147 (2009), a reservoir trap efficiency of nearly 100% has been found to typically exist in large reservoirs, while in smaller reservoirs (i.e. with a low capacity to MAR ratio) a trap efficiency of less than 20% has been found to typically exist.

There are four main longitudinal sediment deposition profiles that typically occur in a reservoir (Figure 2.3-3), each being mainly dependent on density currents, sediment size, reservoir operating procedures and flooding conditions (Annandale *et al.*, 2016). As illustrated in Figure 2.3-4, the delta forms first and can be divided into a *topset bed* (i.e. mainly consisting of bed material and a flatter bed slope than the original riverbed) and a *forset bed* (i.e. mainly consisting of smaller sediment grains and a steeper bed slope) (Fan and Morris, 1992). The *bottomset bed* exists downstream of the delta and is usually comprised of fine sediment deposits which are transported by density currents and/or non-stratified flow (Morris and Fan, 1998). Within the bottomset bed section, muddy lake deposits, which indicate the presence of turbidity currents, can form immediately upstream of the dam (Annandale *et al.*, 2016). Periodic measures such as extreme flooding or pressure flushing can be used to transport the larger sediment that usually deposits in the upstream delta closer to the dam (Morris and Fan, 1998).

Considering any lateral cross-section in a reservoir, it has been found that as sediment begins to deposit and increase in quantity (i.e. from the deepest point, upwards), a near-horizontal sediment surface will eventually form and spread across the submerged floodplains (Dewals *et al*., 2012; Morris and Fan, 1998).

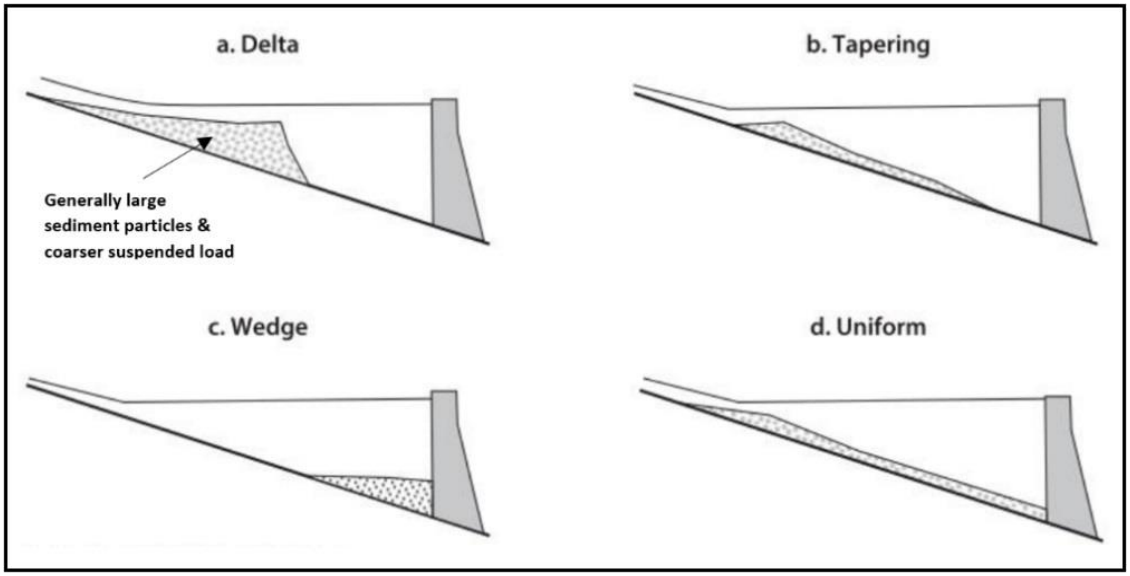

Figure 2.3-3: Reservoir sediment deposition profiles (Morris and Fan, 1998)

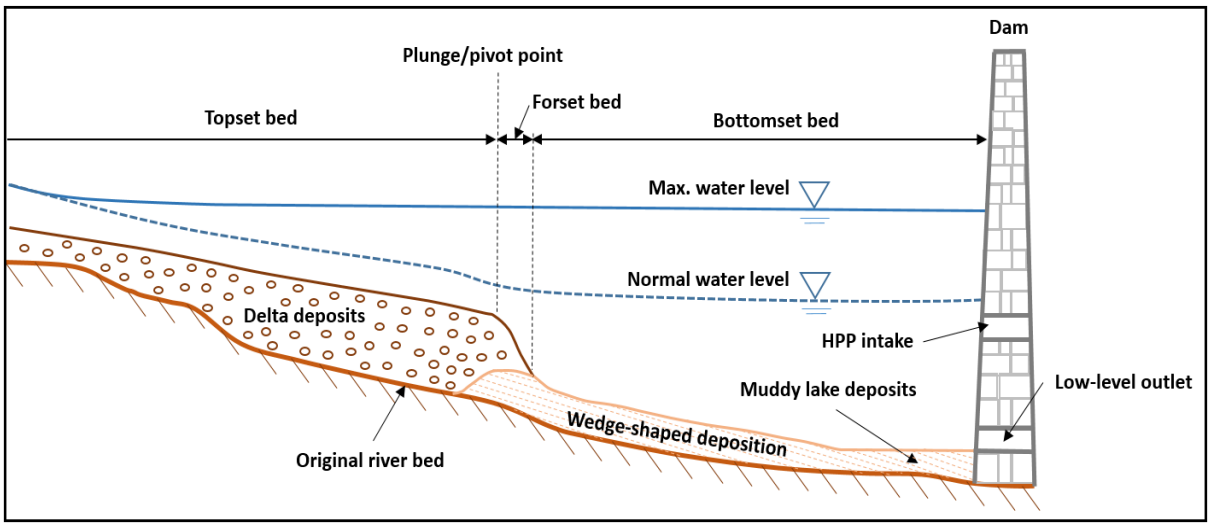

Figure 2.3-4: Reservoir sediment deposition zones (adapted from Morris and Fan, 1998)

2.4 Sediment management and control

This section discusses the sediment management and control measures of particular interest and relevance to this study. Such measures include sediment sluicing, bypassing and flushing (i.e. pressure and free-flow with drawdown). General sediment management strategies in reservoirs, complementing those mentioned in Section 1.1 (*Background*), can be categorised as illustrated in Figure 2.4-1.

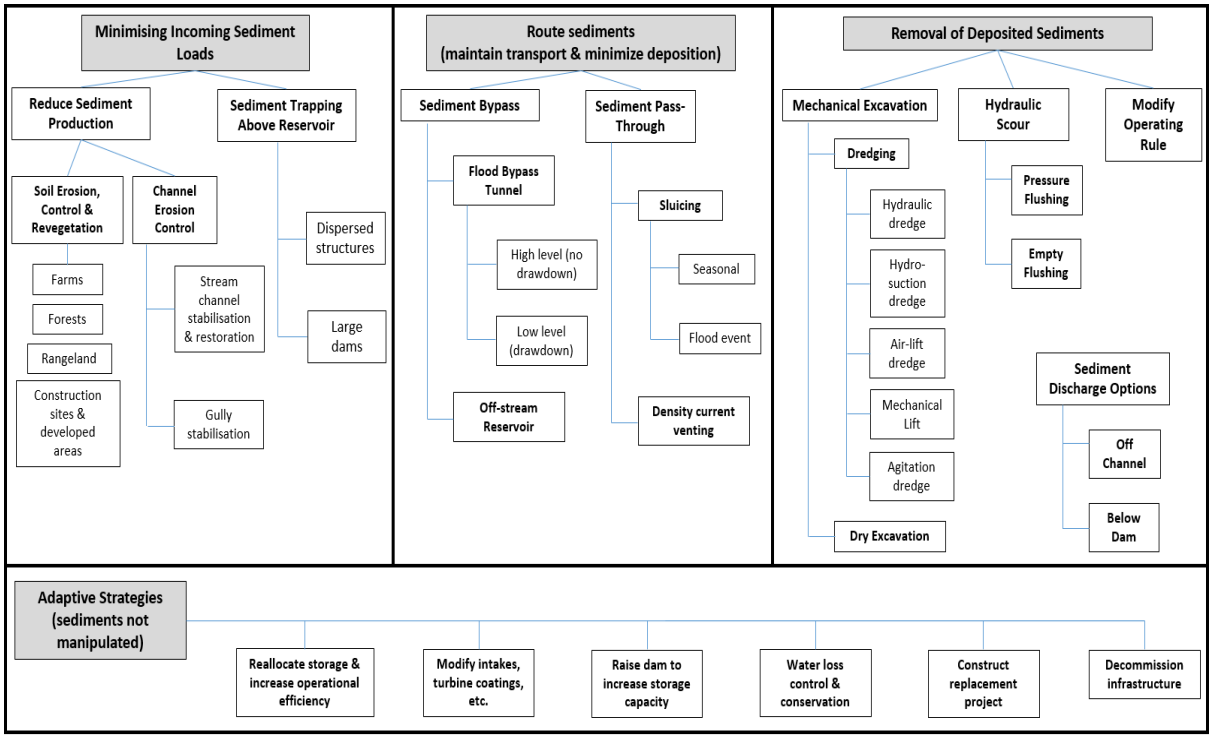

Figure 2.4-1: Types of sediment management strategies (Morris, 2015)

2.4.1 Sediment sluicing

2.4.1.1 Introduction

Sluicing is an operational procedure whereby sediment-laden inflows are passed through a reservoir and are ultimately released through low-level dam outlets before sediment deposition can occur inside of the reservoir. According to Basson and Rooseboom (1997), this process is often carried out during the flood season (especially at the beginning) by operating the reservoir at a lower water level in order to provide sufficient transport capacity (turbulent and colloidal) for releasing the high sediment loads. The same authors state that impoundment (i.e. raising the reservoir water level) should then take place as late as possible towards the end of the flood season when inflow sediment concentrations are low, so that relatively clear water can be stored.

Sluicing is effective for releasing large quantities of highly cohesive sediments that are practically impossible to scour (by flushing) once consolidated in reservoirs (Basson and Rooseboom, 1999). In situations where reservoir drawdown is restricted (e.g. in arid areas), turbidity current venting can be used as an alternative to sluicing (Chamoun *et al.*, 2016). It must be noted, however, that turbidity current venting is relatively less efficient than sluicing and is only effective for very fine sediment particles (i.e. generally less than 30 µm) (Fan and Morris, 1992). A sediment sluicing tunnel (SST) can be used to release already-deposited fine sediment, which exists immediately upstream of the dam structure, downstream of the dam by making use of density current flows (ICOLD, 2018c). A typical SST is illustrated in Figure 2.4-2 and Figure 2.4-5.

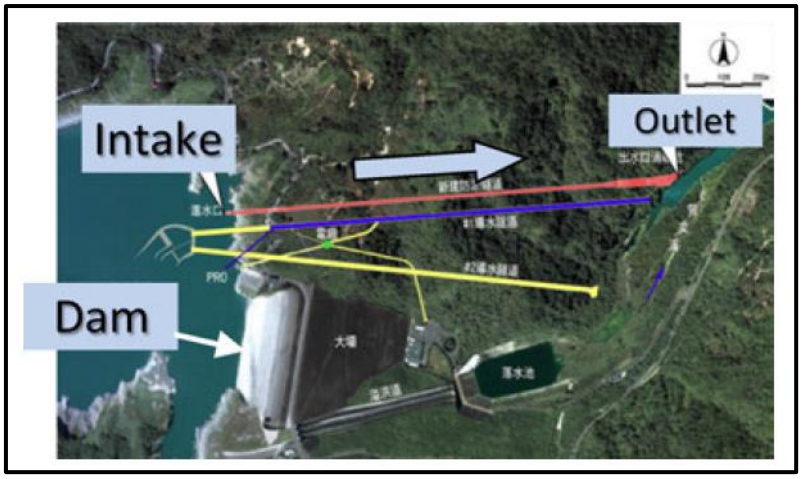

Figure 2.4-2: SST example (Tsengwen Dam in Taiwan) (ICOLD, 2018a)

2.4.1.2 Conditions for sluicing

A few of the conditions and requirements for the use of sluicing, as well as for achieving successful sluicing, as stated by Basson and Rooseboom (1997), are presented below:

- Sufficient excess inflow, and thus a sufficient sediment carrying capacity, must exist in order for sediment to be transported through the reservoir and released.
- Sluicing is usually the most critical sediment release operation and requires strategic operation by well-trained operators.
- A predictable and reliable flow hydrograph at the dam site is necessary to fill the reservoir in time after the sluicing operation.
- Low-level outlets should be located as close to the original river-bed level as possible. They should be designed with a sufficient discharge capacity and in conjunction with hydropower intakes (if present) in order to restrict blockage of the intakes.
- For a narrow reservoir basin configuration (which is preferable), Rooseboom (1992) suggests that inflows up to the 1-in-5-year flood flow rate should be able to pass through the reservoir without significant sediment deposition occurring, while larger flows that deposit sediments should be flushed out during the flood period before consolidation occurs.
- Sluicing is most effective for inflows from rivers transporting suspended sediments.

2.4.2 Sediment flushing

2.4.2.1 Introduction

Sediment flushing is a common operational procedure whereby reservoir drawdown (i.e. either completely or partially lowering the reservoir's water level) is typically used to scour and release already-deposited reservoir sediments through low-level dam outlets. According to ICOLD (2018b), flushing is the only economic approach to sustain long-term storage in reservoirs with extreme sedimentation issues. A comparison of the two types of flushing, namely *pressure* and *free-flow or drawdown* flushing, is presented in Table 2.4-1.

Table 2.4-1: Free-flow or drawdown flushing vs pressure flushing

	Free-flow or drawdown flushing	Pressure flushing
1.	Requires emptying or full drawdown of the reservoir. This operation takes a long period of time and results in large amounts of water being released.	Requires only partial drawdown of the reservoir. The low-level outlet is opened for a short period of time and results in much less water being released.
2.	Sediment is routed or released through the low-level outlet under natural riverine conditions (i.e. free-surface flow).	Sediment is released through the low-level outlet under higher reservoir water level conditions where the low-level outlet intake is submerged.
3.	Can flush large quantities of deposited sediment over a longer period of time (White, 2001).	Only locally deposited sediment is scoured and flushed, with no effect on deposits upstream of the scour cone (Mahmood, 1987).
4.	Is known to effectively restore the live storage capacity in reservoirs (Basson and Rooseboom, 1999).	Effective in keeping the hydropower intakes free of sediment, but ineffective in restoring the live storage capacity in large reservoirs (Morris and Fan, 1998).
5.	Significantly hinders and reduces power generation at HPPs.	Applicable to reservoirs with a small capacity to inflow ratio and where over-year storage is mandatory (Qian, 1982).

During the process of free-flow flushing, a flow channel forms through the reservoir due to the erosion of the deposited sediments. Retrogressive erosion initially occurs and progressive erosion thereafter, with retrogressive erosion usually being the more dominant and more important form of erosion in reservoir desiltation (Basson and Rooseboom, 1999). Sediment entering the reservoir during flushing periods will also be routed through and eventually released (Morris and Fan, 1998). It is common for sluicing and free-flow flushing to be used in combination or alternatively (Basson and Rooseboom, 1999).

During the process of pressure flushing, only the deposited sediment in the vicinity of the low-level outlet intake area is scoured due to the local high approach flow velocities that are created. In a very short period, a stabilised sediment scour (flushing) cone, with a funnel-shaped crater, forms upstream of the low-level outlet opening. After this point, no more sediment will be scoured unless extreme drawdown takes place (Di Silvio, 1990).

In the case of larger diameter sediments (i.e. gravel and boulders), either the flow velocity or discharge can be increased with more drawdown to ensure transportation of the material, and the quantity of transportable material that is released can be increased by extending the duration of routing flows (Morris and Fan, 1998). The largest possible discharge should be used for flushing in order to maximize efficiency (Paul and Dhillon, 1988). Figure 2.4-3 illustrates the three most common stages of flushing.

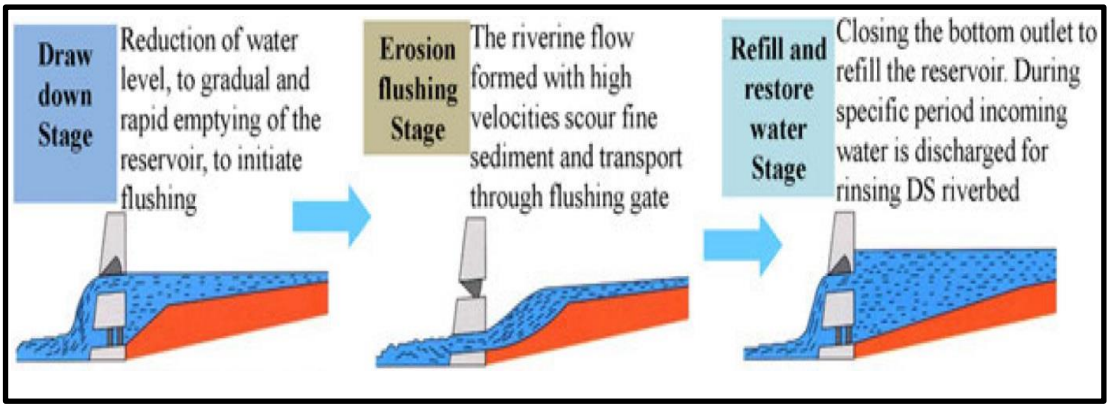

Figure 2.4-3: Common stages of flushing (ICOLD, 2018b)

2.4.2.2 Conditions for flushing

The main conditions and requirements for effective sediment flushing include:

- Narrow reservoirs with a maximum width of 300 m and steep bottom bed slopes of about 2% have resulted in successful sediment flushing in most reservoirs (Singh, 1987).
- A climate with distinct wet and dry seasons is desirable as this allows for flood operation in the early wet season when flows are highly concentrated with sediment, as well as for water storage in the dry season (Basson and Rooseboom, 1999).
- Frequent flushing is required to prevent sediment deposits from consolidating excessively within the reservoir (Delft Hydraulics, 1992). Flushing could vary from at least once every year to once every 3 to 5 years depending on the reservoir conditions (Basson and Rooseboom, 1999). The flushing frequency could lessen for cases where flushing and sluicing operations occur simultaneously (Fan, 1985).
- Drawdown flushing is preferable at reservoirs with a small hydrologic size (a capacity to inflow (C:I) ratio usually less than 0.3) or with a larger hydrologic size that has been reduced in size due to sediment accumulation. These conditions tend to provide enough excess runoff for flushing and allows the reservoir to be refilled quickly if needed (Morris and Fan, 1998).
- In the case of long reservoirs where there are usually low rates of bed change, it is required that drawdown occur for several months in order to successfully complete the flushing process (Basson and Rooseboom, 1999). The same authors state that in order to limit water loss, flushing should be stopped once the outflow sediment concentrations become low.
- According to Morris and Fan (1998), during the flood season it is more effective to implement full-drawdown flushing as larger discharges and higher flow velocities with more erosive energy are available. The same author states that drawdown flushing also allows for flood-borne sediments to be routed through the reservoir, which can take place over periods ranging from days to months.
- In order to maximise the efficiency of sediment flushing, the reservoir must be drawn down to the point where the flow conditions over the sediment deposits replicates that of the original river (i.e. free-surface flow conditions) (White and Bettess, 1984;

Mahmood, 1987). The best starting condition for sediment flushing is therefore an empty reservoir (Basson and Rooseboom, 1999).

- For cases where the localised scour of sediment at low-level outlet intakes is required, flushing without water level drawdown (i.e. free-flow flushing) should be implemented (Basson and Rooseboom, 1999).
- Pressure (i.e. partial drawdown) flushing requires less drawdown but is not commonly used as it is has been found to be less effective (Morris and Fan, 1998).
- Partial drawdown flushing (few hours to days) during single flood events in semi-arid regions is possible if there is excess water available and if the inflow is controlled to ensure that the reservoir is fully filled at the end of the flood (Basson and Rooseboom, 1999). The same authors state that sedimentation will only be limited during impounding during the falling stage of the flood hydrograph for such cases.
- The water-detritus ratio (W-D) (i.e. ratio of volume of water wasted to volume of sediment flushed out) is used as a flushing efficiency indicator and should vary between 20 to 50 according to field data indicated in Table 2.4-2.
- Low-level outlets that are wide and that have flushing gates located as near as possible to the original river-bed level improve flushing conditions (Basson and Rooseboom, 1999).
- Sediment deposition along the main river channel that is caused by flood detention can normally be flushed successfully through large low-level outlets with or without gates during a current or succeeding flood event (Fan, 1985).
- Flushing can be combined with other operations such as dredging to improve efficiency (Basson and Rooseboom, 1999).

Table 2.4-2: Recorded W-D ratios (Basson and Rooseboom, 1999)

Reservoir	Location	Mode of operation	W-D ratio
Grimsel	Switzerland	Bottom outlets, drawdown	16 - 22
Gebiden	Switzerland	Bottom outlets, drawdown	42
Gebiden	Switzerland	Bottom outlets, no drawdown	18
Nebeur	Tunisia	Bottom outlet flushing with drawdown & density current	9
Sefid Rud	Iran	Bottom outlets	13 - 34
Khashm El Girba	Sudan	-	35 - 44
Zemo-Afchar	Russia	-	8 - 83
Guernsey	USA	Overflow spillway	400 - 820
Santo Domingo	Venezuela	Emptying	7 -11
Shuicaozi	China	Overflow spillway	23 - 86
Warsak	Pakistan	Overflow spillway	590

The main constraints and negative impacts of flushing include:

- Flushing operations cannot occur in reservoirs with over-year storage and/or where periodic interruptions in reservoir usage are prohibited (White and Bettess, 1984).
- Flushing operation often results in very high-water losses (especially during reservoir emptying) and should be reconsidered or avoided in semi-arid and arid areas.
- Rapid reservoir drawdown should be avoided as this has been found to sometimes cause sediment slides that can reduce water storage, block the outlets and threaten the safety of particularly earth dams (Basson and Rooseboom, 1999).

- Water level drawdown reduces the potential for hydropower generation and should be monitored for cases where power requirements need to be met.
- Highly concentrated sediment releases during flushing may: (1) aggrade the downstream river channel; (2) threaten the downstream water quality and ecological environment; and (3) abrade the low-level outlets (Basson and Rooseboom, 1999).

2.4.2.3 Drawdown flushing during flood and non-flood season

During the planning phase of the dam, it is recommended that facilities are effectively designed and implemented in order to facilitate the physical removal of floating debris and tree trunks that could result in the blockage of the low-level outlets during free-flow flushing (Fan, 1985). The same author states that before the reservoir is filled, the cutting of deposited trees in the reservoir area and/or the felling of existing trees along the upstream riverbank could take place to minimise the risk of blockage during flushing.

During the initial stage of the flood season (i.e. before the flood peak reaches the reservoir), the low-level outlets should be left open so that the reservoir remains empty and any inflow can be passed through the outlets under free flow conditions (Morris and Fan, 1998). According to Morris and Fan (1998), this procedure is effective in handling additional deposition and flushing previously deposited sediment. The same authors state that the outlets should then be closed towards the end of the flood season to allow for full impoundment of the reservoir for winter irrigation.

Flushing during the non-flood season can also be successful but will require a longer flushing period than flood flushing, as a lower discharge is available. As a result of the limited discharge during the non-flood season and the inability to route flood season inflow through the flushing channel, the rate of sediment (especially coarse) deposition on the floodplain areas is expected to increase (Morris and Fan, 1998).

According to Brandt (2000), in the event that the low-level outlets do become blocked during free-flow flushing, the gates should be closed and the outlets should be flushed again under pressure. Short periods of local scouring at the low-level intake could then take place during pressure flushing to minimise the risk of blockage, especially when the local upstream sediment level reaches a critical depth (Basson and Rooseboom, 1999).

2.4.3 Bypass tunnel flushing designs

2.4.3.1 Introduction

Sediment bypass tunnels (SBTs) are hydraulic structures (i.e. tunnels or open channels) that are used to divert sediment that would enter a reservoir by transporting it around the reservoir and dam structure and then releasing it directly into a downstream river channel. This scenario is illustrated in Figure 2.4-4 and Figure 2.4-5. SBTs to date have been designed and built individually according to the characteristics of a particular dam (ICOLD, 2018a). Figure 2.4-6 illustrates a typical long section of a SBT, the main issues that typically occur within the tunnel itself, as well as the upstream and downstream areas of the SBT.

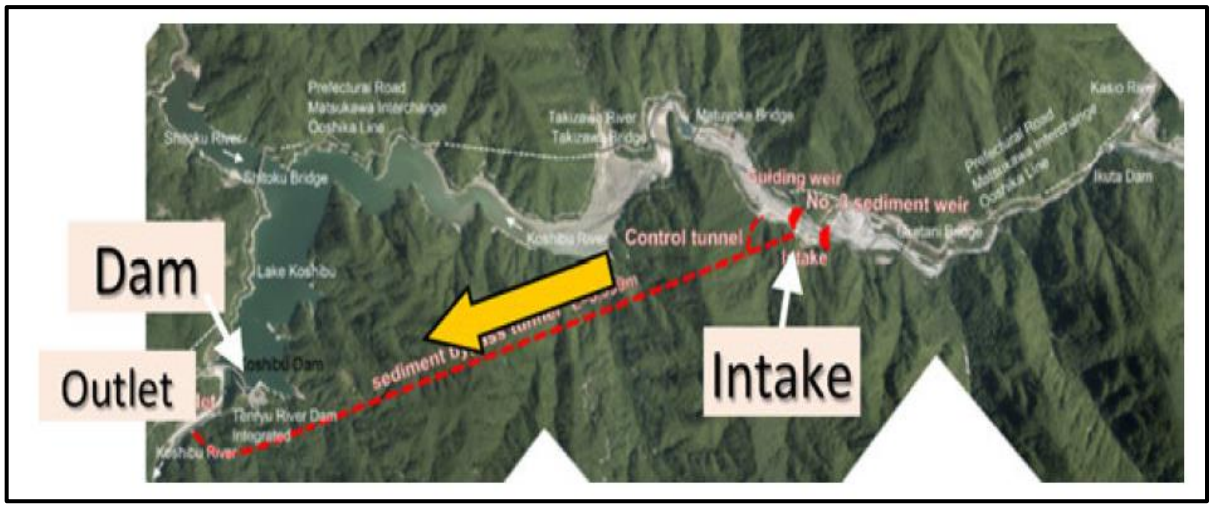

Figure 2.4-4: SBT example (Koshibu Dam in Japan) (ICOLD, 2018a)

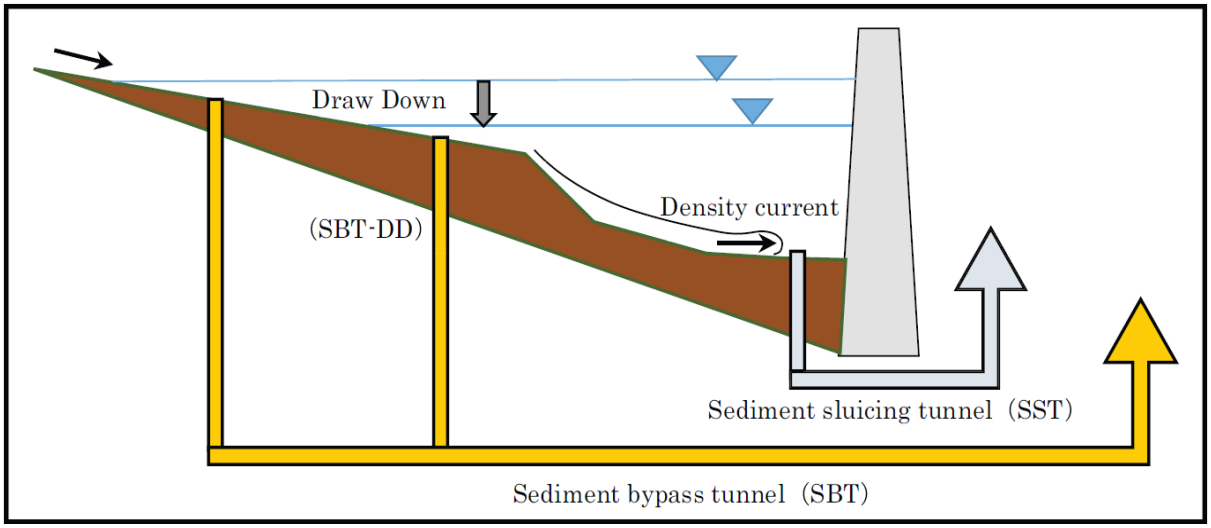

Figure 2.4-5: Cross-section of typical SBT and SST (ICOLD, 2018a)

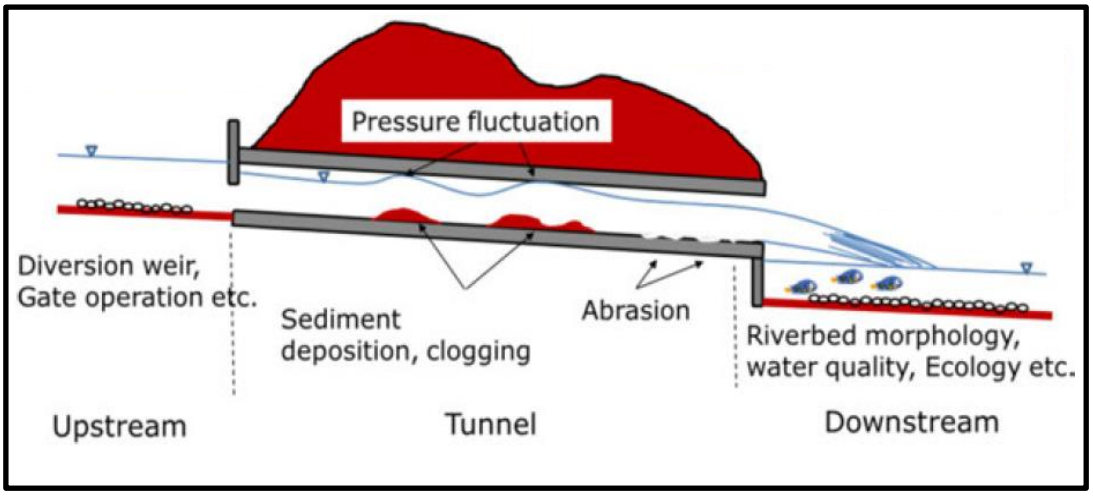

Figure 2.4-6: Long section of sediment bypass tunnel (ICOLD, 2018c)

Sediment bypass tunnels (SBTs) propose various advantages and disadvantages when being implemented as a management procedure to reduce reservoir sedimentation. The fact that SBTs have certain economic, topographical and hydrological limitations has resulted in fairly few of them being constructed globally (ICOLD, 2018c). Nonetheless, SBTs are believed to provide a sustainable remedial approach in reducing sedimentation in reservoirs (Kondolf *et al.*, 2014). Advantageously, SBTs do not involve any form of reservoir drawdown (i.e. evades loss of stored reservoir water); they minimally effect the downstream environment as water inflow can be passed naturally through tunnels during flood events; they can be used to transport all types of sediment; their components can be easily accessed during operation; and they can be constructed and installed at existing dams (ICOLD, 2018c).

2.4.3.2 Typical design specifications of SBTs

Typical countries where sediment bypass tunnels (SBTs) are successfully utilised and maintained include Japan, Taiwan and Switzerland. Table 2.4-3 indicates the main design specifications of existing SBTs in these countries, comparing typical structural designs, design flow velocities and design sediment sizes. ICOLD (2018a) provides additional information on each dam, including dam specifications and other bypass tunnel specifications.

Table 2.4-3: Sediment bypass tunnel specifications (ICOLD, 2018a)

		Bypass tunnel specifications															
Country	Name of Dam	Purpose 1*	Tunnel Specifications					Flow discharge		Design Velocity (m/s)	Operation Frequency (/year)	Intake Specifications			Outlet Energy Dissipator	Target Grain Size (mm)	
			Cross-section shape	Length (m)	Longitudinal slope		Curved section	Design discharge (m^3/s)	Design discharge Return period			Intake Position in Reservoir	Flow Control	Reservoir operation during sediment discharge		dm	d90
					%	m/m											
	Nunobiki-Gohonmatsu	S, W	Hood-type (2.9m x 2.9m)	258	1.3	1/75	No	39	-	-	-	Upstream end	No gate	Keeping water level	No	-	-
	Tachigahata	S, W	-	-	-	-	-	-	-	-	-	Upstream end	-	-	-	-	-
Japan	Miwa	S	Horseshoe (D = 7.8m)	4308	1.0	1/100	Yes	300	1/4.3 year	10.8	1 - 2 times	Mid to upsream end	Gate	Flood control	Yes	Wash load	Wash load
	Asahi	S	Hood-type (3.8m x 3.8m)	2350	2.9	1/35	Yes	140	1/0.5 year	11.4	16 times	Upstream end	Gate	Keeping water level	No	50	300
	Koshibu	S, R	Horseshoe (D = 7.95m)	3999	2.0	1/50	Yes	370	1/6.2 year	15.8	-	Upstream end	Gate	Flood control	Yes	10	70
	Matsukawa	S, R	Hood-type (5.2m x 5.2m)	1417	4.00	1/25	Yes	200	1/25.1 year	15.0	-	Upstream end	Gate	Flood control	Yes	10	60
	Egschi	S	Circle (D = 2.8m)	360	2.60	1/38.5	Yes	50	-	10.0	10 days	Upstream end	Gate	Keeping water level	No	100	300
	Palagnedra	S	Horseshoe (6.2m x 6.1m)	1760	2.00	1/50	Yes	250	-	13.00	2 - 5 days	Upstream end	Gate	Keeping water level	No	74	160
Switzerland	Pfaffensprung	S	Horseshoe (4.7m x 4.8m)	282	3.00	1/33.3	Yes	220	-	14.00	ca. 200 days	Upstream end	Gate	Keeping water level	No	250	2700
	Rempen	S	Horseshoe (3.4m x 3.4m)	450	4.00	1/25	Yes	80	-	12.00	1 - 5 days	Upstream end	Gate	Keeping water level	-	60	200
	Runcahez	S	Hood-type (3.8m x 4.5m)	572	1.40	1/71.4	Yes	110	-	9.00	4 days	Upstream end	Gate	Keeping water level	No	230	500
	Solis	S	Hood-type (4.4m x 4.7m)	968	1.90	1/52.6	Yes	170	1/5 year	11.00	1 - 10 days	Mid stream	Gate	Drawdown	-	60	150
	Shihmen	S	-	-	-	-	-	380	1 - 2/1 year	-	-	Directly upstream of dam	Gate	Flood control	-	0.004 - 0.008	0.05
Taiwan		R, S	Hood-type (8.0m x 9.0m)	3685	2.86	1/34.9	No	600	2 - 2/1 year	10 - 20	-	Mid stream	Gate	Flood control	No	0.04	Density flow
(R.O.C.)	Nanhua	R, S	Horseshoe (9.5m x 9.5m)	1287	1.85	1/54.1	No	1 000	1/5 year	24.50	-	Mid stream	Gate	Flood control	Yes	0.02	Density flow
	Tsengwen	R, S	Horseshoe (9.5m x 9.5m)	1235	5.32	1/18.8	No	995	1/2 - 3 year	18 - 30	-	Directly upstream of dam	Gate	Flood control	Yes	0.005	Density flow

1* Purpose of bypass tunnel (S: sediment discharge; W: water utilization; R: increase release capacity or flood control)

2.4.3.3 Design discharge

ICOLD (2018a) investigated the relationship between the SBT design discharge and other variable factors (i.e. SBT completion year, catchment area and return period) for a variety of cases. From the trends and characteristics obtained, the author concluded that a conservative SBT design discharge can approximately match the dam's 5-year return period flood. However, the individual design approaches and the impact of regional factors (e.g. rainfall patterns) need to be closely considered. The design discharge should also only be set once the sediment discharge form has been considered (ICOLD, 2018a).

2.4.3.4 Tunnel structure

ICOLD (2018a) compared the structural aspects of each tunnel under consideration and concluded that:

- The standard SBT longitudinal slope can be considered to exist between roughly 1 – 5%. However, hydraulic stability, sediment discharge efficiency and sediment abrasion countermeasures need to be considered.

- The standard tunnel diameter can be considered to exist between roughly 3 – 10 m, with the free-flow tunnel design discharge increasing with an increase in tunnel diameter.

- In order to lower the reservoir water level at a time of sediment discharge, as well as to increase the sediment discharge capacity and shorten the tunnel length, the SBT intake can be positioned near the dam structure (such as at the Solis Dam). It is required, however, that a risk assessment of the failure to recover the reservoir water level be carried out.

- A check dam can be utilised upstream of the reservoir to intercept coarse gravel so that the SBT only has to deal with the passing wash load (such as at the Miwa Dam). The SBT intake should then be positioned at a diversion weir downstream of the check dam, which is situated directly below a stockyard. The stockyard is positioned in the reservoir midstream and is used to collect fine sediment that is dredged from the reservoir.

2.4.3.5 Target sediment grain size

ICOLD (2018a) investigated the relationship between the SBT target grain size and design velocity for a variety of cases. From the trends and characteristics obtained, the author concluded that for SBTs which target grain sizes larger than coarse sediment, abrasion resistance along the tunnel's interior must be considered (such as shortening the tunnel length).

2.5 Low-level outlets

2.5.1 Introduction

Low-level outlets are becoming increasingly more vital in terms of contributing towards safe, effective and sustainable dam design. According to Basson and Rooseboom (1997), larger low-level outlets appear to be featuring in modern dams, especially at reservoirs where excess runoff is available. The larger low-level outlets provide a long-term approach towards sedimentation mitigation and reservoir storage preservation. According to Srivastav and Nayak (2015), the construction of low-level outlets, and thus flushing practises, are more common in concrete dams as opposed to earthen dams. This is due to high piping failure and safety risks.

It was concluded by Vischer and Hager (1998) that the successful design of low-level outlets can be achieved through ensuring smooth flow for maximum flow discharge, no leakages, easy access, effective energy dissipation at the outlet structure, a long design life and an economic design.

Due to hydraulic concerns surrounding air entrainment (e.g. via vortex formation at intakes), hydrodynamic forces, vibrations, abrasion, cavitation, energy dissipation and erosion, which usually arise during low-level outlet operation, it is recommended that low-level outlets are not used on a continuous basis for flood discharging (Vischer and Hager, 1998).

2.5.2 Types of designs

A long section of a typical low-level outlet, illustrating its different structural and hydraulic components, is illustrated in Figure 2.5-1.

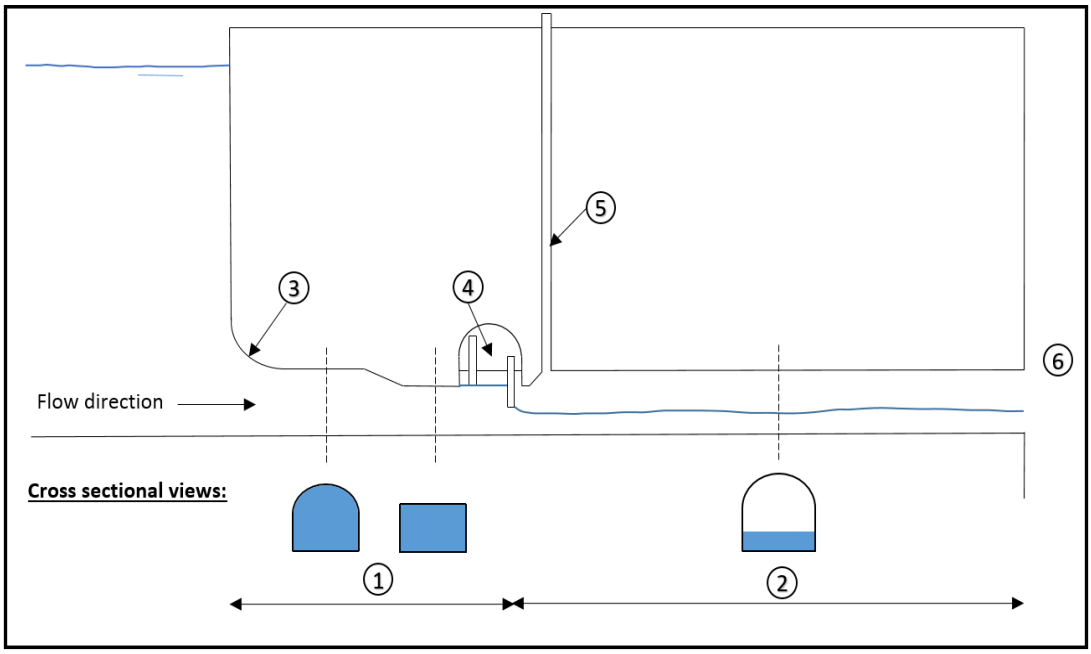

Figure 2.5-1: Typical low-level outlet profile (adapted from Vischer and Hager, 1998)

Referring to Figure 2.5-1, (1) indicates the conduit section upstream of the gates where pressurised (i.e. submerged) flow occurs; (2) indicates the conduit section downstream of the gates where free-surface flow occurs; (3) indicates the conduit inlet which is designed to maximise flow acceleration and streamlined flow conditions into the conduit; (4) indicates the gate chamber (i.e. which houses the gates); (5) indicates the air vent which supplies air flow to alleviate undesirable sub-atmospheric pressures that can form downstream of the gate chamber; and (6) indicates the conduit outlet.

The low-level outlet design illustrated in Figure 2.5-2 implements a syphon upstream of the gate chamber at the conduit inlet. The aim of the syphon is to direct a jet of water at the deposited sediment upstream of the emergency gate to initiate the scouring and flushing process. In the Cerro del Águila Dam, the syphon was able to deliver a 34 m/s water jet at the normal operating level (Sayah *et al.*, 2015). The air vent connected to the gate chamber, the bottom aerator and the conduit outlet provide aeration to the flow downstream of the gate chamber.

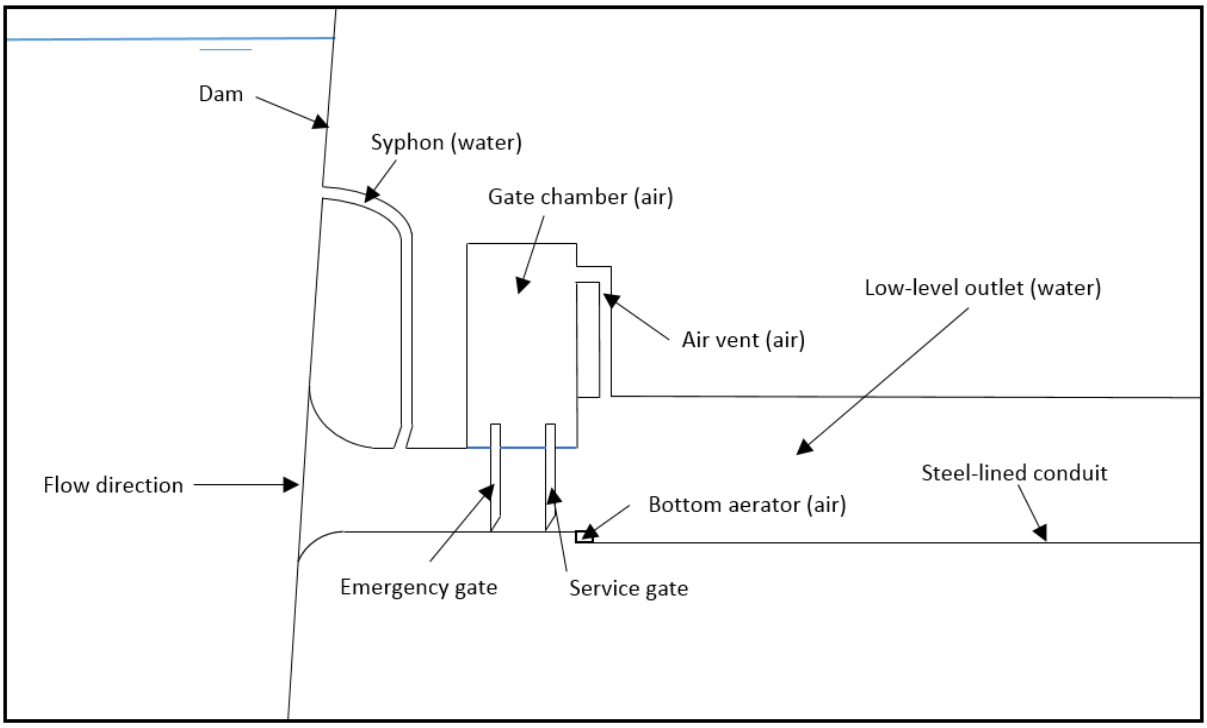

Figure 2.5-2: Long-section of low-level outlet in Cerro del Águila Dam
(adapted from Sayah *et al.*, 2015)

2.5.3 Layout

The intake of a low-level outlet conduit is normally situated inside of the original main river channel at the dam and below the hydropower intakes as recommended by Basson and Rooseboom (1999). In smaller reservoirs, these intakes are usually positioned at a location that limits the amount of sedimentation in front of them (e.g. on the outer, concave bank at a river bend). It is recommended by Morris and Fan (1998) that at least two low-level outlets

should be utilised in order to ensure effective sediment flushing, as well as to ensure reservoir drawdown even if an outlet is blocked or can't be used.

Basson and Rooseboom (1999) state that the most critical layout consideration is the elevation of the low-level outlet. The inlet invert level of the low-level outlet conduit should preferably be at the original riverbed level as this ensures retrogressive erosion of deposited sediment in the reservoir during drawdown flushing (Basson and Rooseboom, 1999; Morris and Fan, 1998). Placing the invert level above the riverbed should be avoided as local sediment build-up (i.e. dead storage) below the invert could occur. The low-level outlets should also be placed sufficiently low enough below the hydropower intakes in order to create local sediment scour zones during flushing that limit sediment entrainment into the intakes. The elevation of the outlets should also be below the contact point of the upper water mass and the sediment laden stream for the venting of density currents (Basson and Rooseboom, 1999).

2.5.4 Multiphase flow through conduit

In a partially-filled low-level outlet conduit (i.e. open channel), water and air flow simultaneously together in a separate and/or mixed state depending on the degree of flow turbulence and pressure. The phase configuration of highly turbulent, free-surface flow is split into four different zones: (1) the upper zone which comprises flying water droplets; (2) the mixing zone which comprises a continuous water surface; (3) the underlying zone which comprises bubbles that are diffused within the water body; and (4) the lower, air free zone (Falvey, 1980). These different zones are illustrated in Figure 2.5-3.

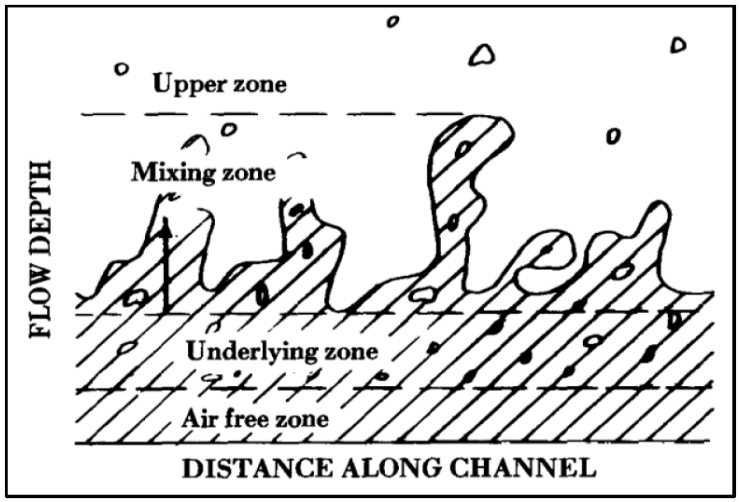

Figure 2.5-3: Different zones of highly turbulent flows (Falvey, 1980)

Considering a conduit with an air vent, the total rate at which air is discharged by the vent is equal to the sum of the rate at which air is entrained into the flow and the rate at which air is being dragged above the flow (i.e. due to air-water shear forces) and released at the conduit outlet. These rates depend on conduit operational procedures, as well as on conduit hydraulic and structural features, and can therefore vary. Sharma (1976) identified six different flow types that cause air demand downstream of a partially closed sluice gate in a conduit without

bottom aerators. These flow types are illustrated in **Error! Reference source not found.** and are described according to Sharma (1976) as follows:

1. ***Spray flow***: This flow typically occurs for relatively small gate openings (i.e. less than 10%) and causes extremely high air entrainment.

2. ***Free flow***: This flow embodies supercritical flow features such as two-phase flow (i.e. air and water) and shockwaves.

3. ***Foamy flow***: This flow typically occurs for non-pressurised, almost full-flowing two-phase flow.

4. ***Hydraulic jump***: This is caused by the transition from pressurised (subcritical) flow to free-surface (supercritical) flow and is followed by free-surface flow as a result of tailwater submergence.

5. ***Hydraulic jump with transition to pressurised tailwater flow***: This tends to represent pipe flow.

6. ***Fully pressurised flow***: This flow typically occurs due to deep tailwater submergence and results in no air demand.

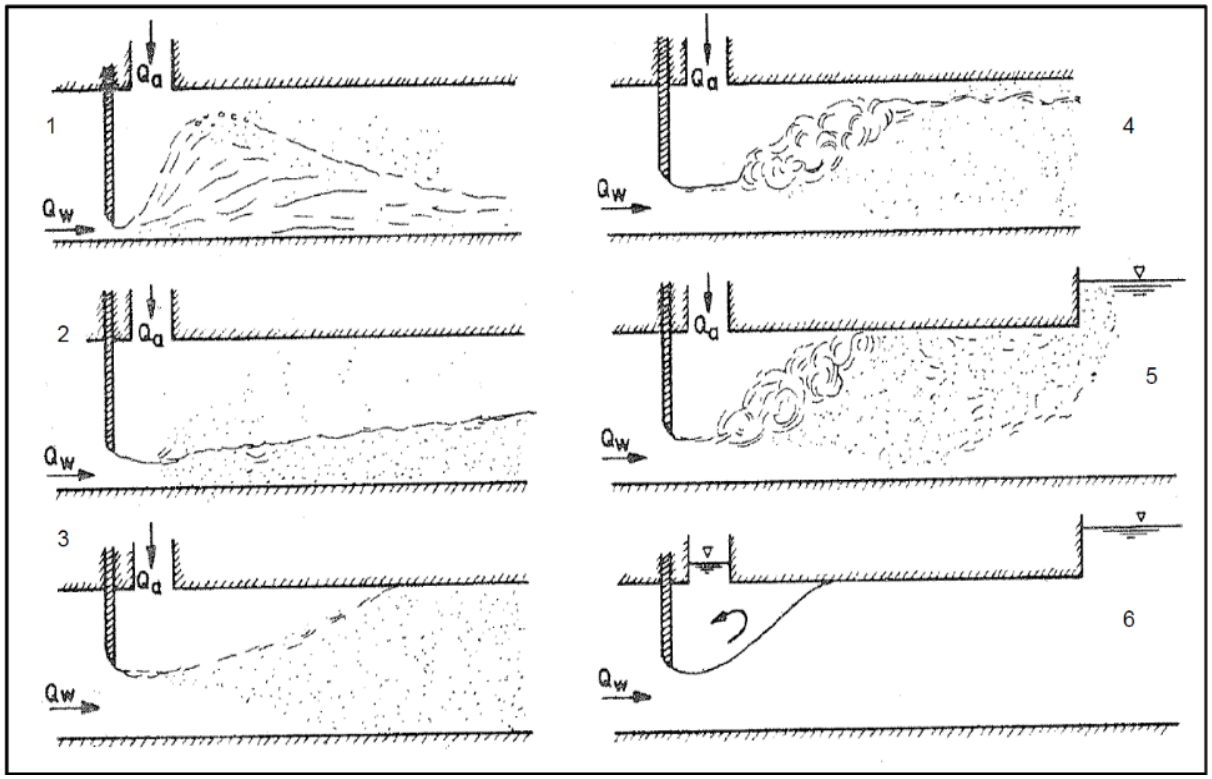

Figure 2.5-4: Flow types that cause air demand (Sharma, 1976)

2.5.5 Discharge capacities

2.5.5.1 General considerations

The outlet design capacity is usually sized so that the backwater level during the highest anticipated flows during flushing operation is minimised (Morris and Fan, 1998). The same authors state that the selection of the outlet design capacity and backwater during the design flow should be determined through modelling.

Basson and Rooseboom (1997) have summarised various rough design guidelines, derived from various authors, regarding general low-level outlet discharge capacities. The design rules include:

- Low level outlets should be designed large enough to be able to handle a 1-in-5 to 1-in-10-year flood, without the flood plains being flooded and with only limited sediment deposition (Rooseboom, 1992). According to Basson and Rooseboom (1997), this would, however, often result in very large and expensive outlet structures.
- Jiang (1980) states that for Chinese reservoirs, the maximum free-flow discharge capacities of the outlets should be greater than half of the bed forming discharge. The bed-forming discharge, which should be determined, regularly complies with a 1-in-5-year flood discharge (Basson and Rooseboom, 1999).
- In Russia, optimal drawdown flushing at three hydro-electric reservoirs was achieved using a discharge capacity of 2 to 4 times the mean annual discharge (Basson and Rooseboom, 1999).
- Pitt and Thompson (1984) have suggested a discharge capacity of at least twice the mean annual discharge.
- Singh (1987) has suggested that in order to reduce coarse sediment deposition, a discharge capacity of 0.3 to 1 times the maximum daily flood inflow would be required.

Each reservoir has its own unique boundary conditions and it is preferable that detailed model tests (by an expert) are carried out. This is necessary to determine the backwater during the design flow, as well as to determine suitable operation rules and outlet discharge capacities to ensure the long-term preservation of the specific reservoir's storage capacities (Basson and Rooseboom, 1999).

2.5.5.2 Inlet and outlet control of conduits

Two types of hydraulic controls can exist in low-level outlet conduits, namely: (1) upstream (inlet) control; and (2) downstream (outlet) control. According to SANRAL (2013), the latter occurs most often and is preferred as it yields the smallest conduit cross-section for a given upstream head, as well as yields higher flow velocities through the conduit which prevent sediment deposition inside. Both controls need to be tested as it is uncertain which one will occur first.

In practise, downstream (outlet) control applies to conduits where pressurised flow occurs along at least a portion of the conduit length during flushing, usually as a results of tailwater effects (SANRAL, 2013). According to SANRAL (2013), the conduit discharge under downstream (outlet) control during flushing can be implicitly calculated for a known upstream

reservoir energy level (H_1), downstream energy level (H_2), conduit dimensions and roughness, from either of the following expressions that represent Bernoulli's Equation:

$$H_1 - H_2 = \frac{K_{in} \cdot \bar{v}_1{}^2}{2 \cdot g} + \frac{K_{out} \cdot \bar{v}_2{}^2}{2 \cdot g} + \frac{\bar{v}^2 \cdot n^2 \cdot L}{R^{\frac{4}{3}}} \quad \textbf{Equation 2-30}$$

$$H_1 - H_2 = \frac{K_{in} \cdot \bar{v}_1{}^2}{2 \cdot g} + \frac{K_{out} \cdot \bar{v}_2{}^2}{2 \cdot g} + \frac{\bar{v}^2 \cdot L}{C^2 \cdot R} \quad \textbf{Equation 2-31}$$

Where,

H_1 and H_2 = Upstream and downstream energy levels, measured relative to the inlet invert level (m) (Equation 2-32)

K_{in} and K_{out} = Inlet and outlet secondary loss coefficients

$\bar{v}_1$ and $\bar{v}_2$ = Upstream and downstream average flow velocities (m/s)

n = Manning's roughness coefficient (0.016 s/m$^{1/3}$ for aged concrete)

L = Bed length of conduit (m)

R = Hydraulic radius (m) ($= A \,/\, P$)

S_0 = Channel bed slope (m/m)

k_s = Surface roughness coefficient (m)

C = Chezy's roughness coefficient ($= 18 \cdot \log\left(\frac{12 \cdot R}{k_s}\right)$)

The energy level (H_n) at point n is defined as follows (SANRAL, 2013):

$$H_n = y_n + \frac{V_n{}^2}{2 \cdot g} + z_n \quad \textbf{Equation 2-32}$$

Where,

y_n = Water depth at point n (m)

V_n = Flow velocity at point n (m/s)

z_n = Elevation of point n above the inlet invert level (m)

In practise, upstream (inlet) control applies to conduits where only free-surface flow occurs along the conduit length during flushing (e.g. orifice flow at the conduit inlet) (SANRAL, 2013). According to SANRAL (2013), the conduit discharge under upstream (inlet) control during flushing, for rectangular-shaped conduits, can be expressed for specific conditions as follows:

For: $0 < \frac{H_1}{D} \leq 1.2$

$$Q = \frac{2}{3} \cdot C_B \cdot B \cdot H_1 \cdot \sqrt{\frac{2}{3} \cdot g \cdot H_1}$$ **Equation 2-33**

For: $\frac{H_1}{D} > 1.2$

$$Q = C_h \cdot B \cdot D \cdot \sqrt{2 \cdot g \cdot (H_1 - C_h \cdot D)}$$ **Equation 2-34**

Where,

Q = Flow discharge (m³/s)

D = Conduit inlet height (m)

B = Conduit inlet width (m)

C_B = 1.0 for rounded inlets (r > 0,1B); 0.9 for square inlets

C_h = 0.8 for rounded inlets; 0.6 for square inlets

2.5.5.3 Normal flow conditions

For normal flow conditions (i.e. uniform flow) inside of a low-level outlet during flushing, Manning's Equation can be used to calculate the flow discharge as follows (SANRAL, 2013):

$$Q = \frac{A^{5/3} \cdot {S_0}^{0.5}}{n \cdot P^{2/3}}$$ **Equation 2-35**

Where,

Q = Flow discharge (m³/s)

A = Cross-sectional flow area (m²) ($A = y_n \cdot B$)

P = Wetted flow perimeter (m) ($P = B + 2 \cdot y_n$ for free-surface flow)

y_n = Normal flow depth (m)

2.5.5.4 Flow under the gates

Gates can be used as a control for regulating flow discharge through the conduit. Either pressurised flow or free-surface flow can occur at partially-closed gates in high-headed low-level outlet conduits (Figure 2.5-1). Free-surface flow usually occurs downstream of the gates and comprises partially-full flow conditions (i.e. the space above the water is filled with air). Pressurised flow usually occurs upstream of the gates and comprises submerged flow conditions.

An unstable hydraulic jump can form downstream of the gates in the conduit due to: (1) large gate openings; and (2) the transition from subcritical pressurised flow (i.e. F_r < 1) to supercritical free surface flow (i.e. F_r > 1) (Naudacher, 1991). The transition must occur exactly behind the gate in order to avoid submergence of the gate chamber (Vischer and Hager, 1998).

According to Vischer and Hager (1998), pressurised flow downstream of the gates should be avoided as much as possible as it increases the risk of vibration and cavitation damage. The same authors state that low-level outlets should therefore always be designed for free-surface flow to reduce possible structural damage.

If a uniform velocity distribution is assumed in the flow jet forming under the vertical sluice gate, then the discharge under a high-head gate may be expressed as follows (Naudacher, 1991):

$$Q = C_c \cdot w \cdot b \cdot \sqrt{2 \cdot g \cdot (H - H_e - C_c \cdot b - h)} \qquad \textbf{Equation 2-36}$$

Where,

Q = Discharge under the gate (m³/s)

C_c = Contraction coefficient (0.6 for outlet orifice with sharp edges and 0.8 for rounded edges (SANRAL, 2013))

w = Gate width (m)

b = Gate opening height (m)

H = Upstream energy level, measured relative to centreline of the jet (m)

H_e = Energy head loss from the outlet entrance to the gate section (m)

h = Depth of contracted jet (m)

A similar formula, known as the submerged flow or orifice equation, to calculate discharge under a gate under free flow conditions is given as follows (Lewin, 2001):

$$Q = C_d \cdot w \cdot b \cdot \sqrt{2 \cdot g \cdot y_1} \qquad \textbf{Equation 2-37}$$

Where,

C_d = Discharge coefficient (dimensionless)

y_1 = Upstream water depth, measured relative to the gate invert level (m)

Figure 2.5-5 provides a graph to determine the C_d value for a specific gate opening height (b), upstream water depth (y_1) and water depth downstream of the gate (y_3).

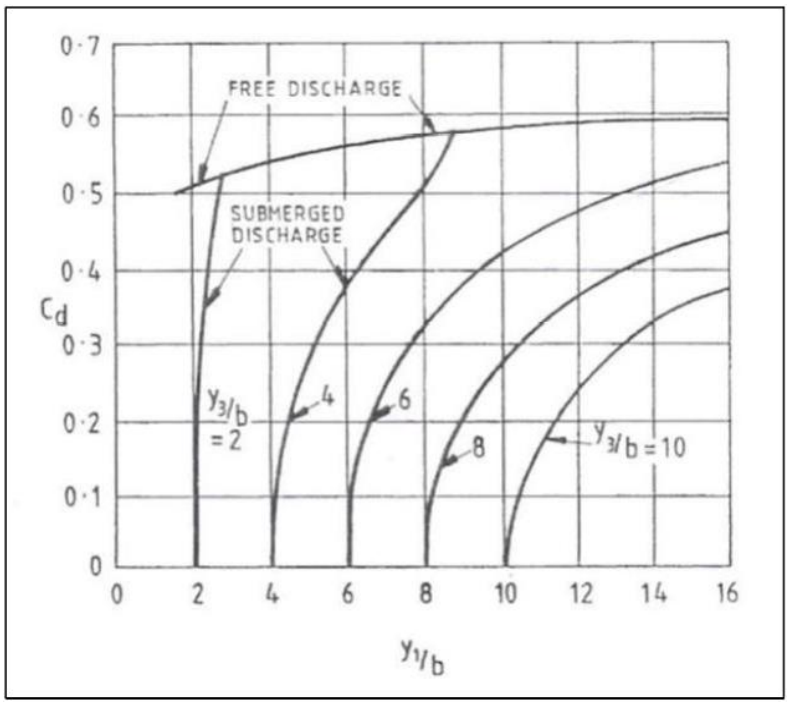

Figure 2.5-5: C_d value for submerged and free flow under gate (Lewin, 2001)

A more conservative approach for calculating the discharge coefficient (C_d) for a specific type of gate is defined as follows (Chadwick *et al.*, 2013):

$$C_d = \frac{C_c}{\sqrt{1 + \frac{C_c \cdot b}{y_1}}} \qquad \textbf{Equation 2-38}$$

According to Chadwick *et al.* (2013), the contraction coefficient (C_c) has been found to equal 0.61 for vertical sluice gates under free-flow conditions where $0 < b \,/ \left(y_1 + \frac{{V_1}^2}{2g}\right) < 0.5$. For underflow radial gates, however, the contraction coefficient (C_c) varies depending on the instantaneous gate lip angle and can be calculated as follows:

$$C_c = 1 - 0.75 \cdot \left(\frac{\theta}{90}\right) + 0.36 \cdot \left(\frac{\theta}{90}\right)^2 \qquad \textbf{Equation 2-39}$$

Where,

θ = Gate lip angle, measured relative to the horizontal axis (°)

2.5.6 Conduit structure

2.5.6.1 Shape

The cross-sectional area of the low-level outlet conduit will be directly proportional to the required outlet discharge capacity, and should also be large enough when compared to the

conduit length, as well as the initial depth of the sediments above the low-level outlet (Basson and Rooseboom, 1999).

After recognising various cases of successful flushing operations in certain countries (such as India, Russia and China), Paul and Dhillon (1988) recommend a low-level outlet with a rectangular cross section and an optimum height of 1.5 to 2.5 m (for fine sediment flushing). The same authors present rough guidelines in their study for determining the optimum outlet size, which involve altering the width of the outlet(s). According to USACE (2003), rectangular shaped conduits are easier to construct (i.e. in terms of entrance, openings, tunnel, etc.) as well as make it easier to install and operate gates and other hydraulic equipment.

Dreyer (2018) investigated and tested various low-level outlet conduit shapes in order to determine what effects they would have on the sediment scour cone geometry that forms immediately upstream of the conduit intake during pressure flushing of hydropower reservoirs. This was done for various scenarios where the upstream sediment level and water depth were varied. The scaled sediment considered was fine, non-cohesive silca sand with an effective diameter of 0.09 mm (Dreyer, 2018). The author found through physical modelling experiments that for an individual low-level outlet, a flat rectangular shape (with a height to width ratio of approximately 1:2) proved to yield the widest, longest and deepest scour cones (i.e. largest volume of sediment flushed) for most scenarios. The author also recommends that for hydropower plants (HPP) that use pressure flushing techniques, a wide low-level outlet design should be used.

China is known for their effective hydropower practises and innovative hydraulic research in discharge structures (Guo, 2012). Considering present day Chinese dams (i.e. younger than 20 years), a trend in the usage of rectangular shaped low-level outlets has been identified. Considering the thirteen major Chinese HPPs indicated in Table 2.5-1, 11 out of 13 utilise more than one low-level outlet and 12 out of 13 utilise upright rectangular-shaped outlets (i.e. width-to-height ratios less than 1). For the eleven dams with more than one low-level outlet (i.e. all upright rectangular-shaped), an average low-level outlet height of about 7 m, width of about 5 m and width-to-height ratio of 0.717 was determined.

Table 2.5-1: Rectangular-shaped low-level outlets in Chinese HPPs (Guo, 2012)

Project Name	Country	Type of dam	Dam Height (m)	Low-level outlets			
				No. of	Width (m)	Height (m)	Width-to-height ratio
Gongboxia	China	CFRD	127	1	7.5	6	1.25
Longyangxia	China	PG/VA	178	1	5	7	0.71
Dongjiang	China	VA	157	2	6	7	0.86
Goupitan	China	VA	225	2	6	7	0.86
Guangzhao	China	RCC	196	2	4	6	0.67
Longtan	China	RCC	216	2	5	8	0.63
Shuibuya	China	CFRD	233	2	4	5	0.8
Dachaoshan	China	RCC	115	3	7.5	10	0.75
Ankang	China	PG	128	4	5	8	0.63
Ertan	China	VA	240	4	3	5	0.6
Wuqiangxi	China	PG	84.5	5	3.5	7	0.5
Xiluodu	China	VA	273	7	5	6	0.83
Three Gorges	China	PG	183	23	7	9	0.78

Note: PG = gravity dam, RCC = roller compacted concrete dam, VA = arch dam, CFRD = concrete faced rockfill dam

2.5.6.2 Orientation and bed slope

The direction of flow through the low-level outlet conduit should change as little as possible, with supercritical flow only being allowed to change direction very gradually unless it converts to subcritical flow (SANRAL, 2013). The same author states that flow velocity should also be altered as little as possible, as flow deceleration could potentially cause sediment deposition, and flow acceleration could potentially cause downstream scour.

According to SANRAL (2013), in order to prevent sediment deposits inside of conduits with flat gradients, it should be ensured that the bed slope is not less than about 1%, and that the flow velocities through the conduit are not less than 1 m/s. The bed slope should, however, be designed as flat as possible in order to avoid the upstream movement of air which can cause possible blowback issues (Falvey, 1980).

2.5.7 Inlet structure

2.5.7.1 Functions and features

According to Kumar and Singal (2013), the main hydraulic functions of the inlet structure of a low-level outlet are to:

1. Minimise head losses during flushing. This can be achieved by implementing a bell-mouth shaped inlet opening to streamline flow into the conduit;
2. Draw the required amount of water at minimum reservoir water level. This is dependent on the size of the inlet and the location of the inlet centreline; and
3. Avoid the formation of local vortices. This is dependent on the size and shape of the inlet as well as the location of the inlet centreline.

According to Amirsayafi (2015), there are also certain geotechnical and structural factors that need to be considered when designing the inlet structure of a low-level outlet. Such factors include:

- Foundation strength (especially for earthquake loads).
- Wear and tear of concrete material (which could weaken the structure) due to aging and exposure to water with an unusual PH.
- Implementing a diver friendly design (e.g. designing an overhead crane).
- Supplying debris control (e.g. trashracks upstream of the inlet opening).
- Taking fatigue and vibration into account when designing the trash rack or trash strut bars.
- Considering a 50% blockage of the trashracks for hydraulic calculations.
- If possible, installing a bulkhead gate, which is used to block flow from entering the conduit in order to allow for inspection of the conduit in emergency situations.

2.5.7.2 Structural design

The curved surface profile of the inlet structure should follow the typically elliptical (i.e. bell-mouth) shape that replicates the natural contraction curve of a jet that is issued from a sharp-edged orifice (IS 9761, 1995). The same author also states that the conduit (i.e. penstock) should be sized to that of the jet at maximum contraction. According to IS 9761 (1995), this

design maximises flow acceleration into the conduit, minimises energy losses at the inlet and successfully streamlines flow into the conduit (i.e. avoids flow separation and the formation of dead zones).

The bell-mouth profile of the inlet roof and wall design recommended by IS 9761 (1995) are illustrated in Figure 2.5-6 and Figure 2.5-7, respectively. Bratko and Doko (2013) also defined an equation for a general bell-mouth shape for different inlet shapes and conditions. This equation was based on laboratory tests and field studies, and is defined as follows:

$$\frac{x^2}{(3 \cdot K_x \cdot D)^2} + \frac{y^2}{(K_y \cdot D)^2} = 1$$ **Equation 2-40**

Where,

x = Point along axis parallel to conduit centreline

y = Point along axis perpendicular to conduit centreline

D = Conduit inlet height (m)

K_x, K_y = Constants for different inlet conditions, indicated in Table 2.5-2.

Table 2.5-2: Constants for different bell-mouth inlet conditions (Bratko and Doko, 2013)

Conditions	K_x	K_y
Circular entrance	0.167	0.15
Rectangular or square entrance	0.33	0.33
Suppressed bottom and side contractions	0.5	0.5
Suppressed one side only, for unsuppressed side	0.33	0.67

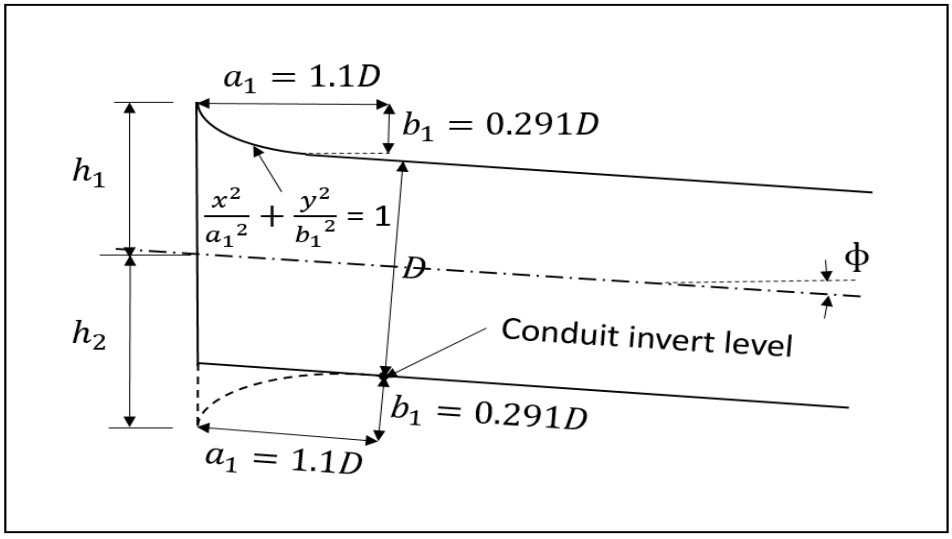

Figure 2.5-6: Long section of bell-mouth roof design (adapted from IS 9761, 1995)

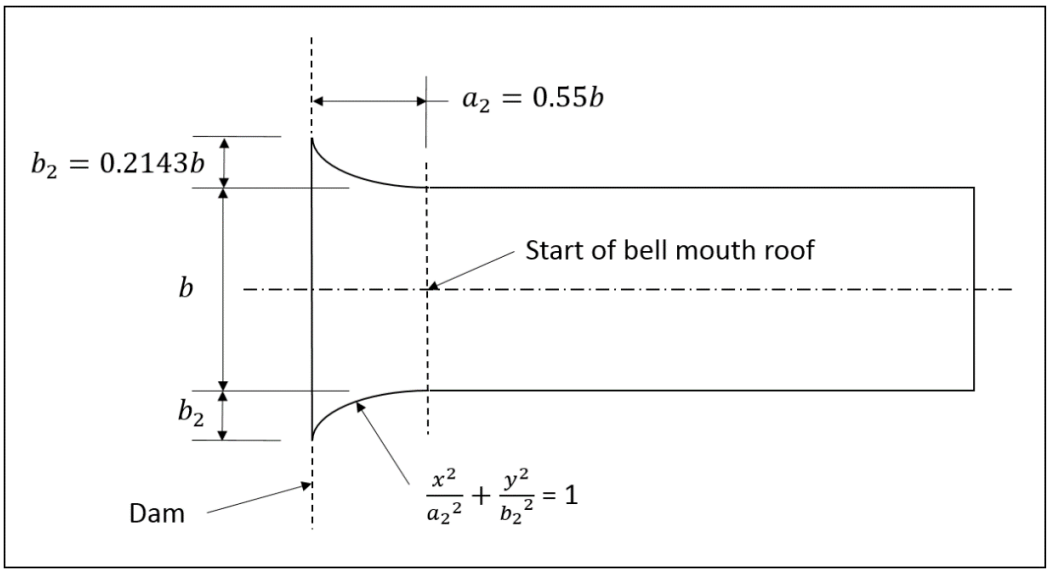

Figure 2.5-7: Plan view of bell-mouth wall design (adapted from IS 9761, 1995)

Considering the dimensions in Figure 2.5-6, the following equations apply (IS 9761, 1995):

$$h_1 = D\left(\sqrt{1.21\tan^2(\phi) + 0.0847} + \frac{1}{2\cos(\phi)} - 1.1\tan(\phi)\right) \quad \textbf{Equation 2-41}$$

$$h_2 = D\left(\frac{0.791}{\cos(\phi)} - 0.077\tan(\phi)\right) \quad \textbf{Equation 2-42}$$

2.5.7.3 Inlet submergence

Various authors (e.g. Knauss, Gordon, Rohan, etc.) have proposed design guidelines and formulae for determining the required submergence of a conduit intake to avoid vortex formation during drawdown pressure flushing. Sarkardeh (2017) compared the results of different submergence formulae in literature to that of corresponding numerical simulations and physical modelling, and found that the equation defined by Knauss (1987) proved to be the most accurate, but required a rational safety factor.

Knauss' equation is valid for median and small size installations (i.e. $F_r \geq 0.33$) and for intakes with symmetric approach flow conditions, but without the use of special devices for vortex suppression (Knauss, 1987). The equation is defined as follows:

$$h_{min} = D \cdot (2 \cdot F_r + 0.5) \quad \textbf{Equation 2-43}$$

Where,

h_{min} = Minimum submergence requirement of conduit inlet centreline (m) (Figure 2.5-8)

D = Conduit inlet height (m)

F_r = Froude Number at inlet, given by the following equation:

$$F_r = \frac{V}{\sqrt{g \cdot y}}$$ **Equation 2-44**

Where,

V = Water velocity at inlet (m/s)

y = Flow depth at inlet (m)

Since these empirical formulae have been defined according to general structural and hydraulic conditions for design purposes, it is necessary to accurately determine the specific submergence requirement (i.e. water level at which vortices begin to form) through physical modelling and associated numerical simulations.

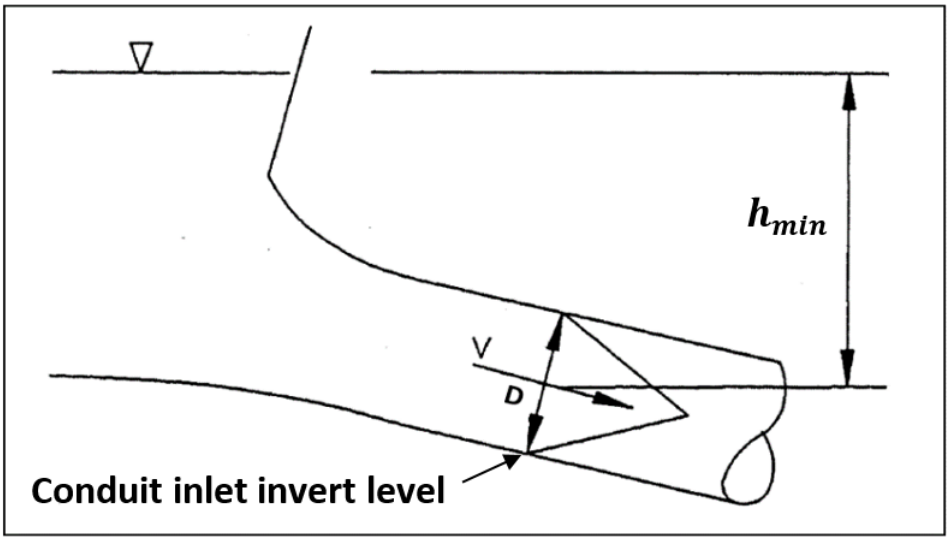

Figure 2.5-8: Definition sketch for submergence (adapted from Knauss, 1987)

2.5.8 Outlet structure

In the case of erosive flows with high velocities, debris and coarse sediment that typically exit the low-level outlet conduit, an energy dissipation structure (e.g. stilling basin) needs to be constructed downstream of the outlet (not looked at in this study). Factors such as the frequency of low-level outlet use, outflow velocity and downstream foundation strength determine the level of necessity for energy dissipation and erosion protection (Amirsayafi, 2015). Inadequate energy dissipation and erosion protection can result in scouring of the downstream side, which could ultimately lead to failure.

Downstream river flow conditions, such as the Manning's roughness coefficient of the riverbed, are variable, unpredictable and significantly influence the structural design of the outlet structure (Amirsayafi, 2015). The same author states that in order to be conservative when designing the outlet structure, a lower range for Manning's coefficient discharge can be

considered and used to calculate the outlet structure apron, whereas an upper range can be considered and used to calculate the elevation of the outlet structure walls to avoid damages and the submergence of the structure.

It is recommended that the outlet structure does not incorporate any mechanism (e.g. a radial gate) that could constrict the air and water flow at the downstream end of the conduit, especially at the soffit of the conduit (Bosman, *et al.*, 2016). The outlet structure should preferably be designed to release the exiting flow in the original direction of the river flow in order to prevent the alteration of the downstream erosion pattern (SANRAL, 2013).

2.5.9 Air vents

Due to the undesirable sub-atmospheric pressures that are created downstream of a partially opened gate where high flow velocities exist (i.e. in a low-level outlet conduit with a relatively high upstream head), an air vent is needed to allow downstream air release to alleviate and stabilise these hydraulic pressures (Sharma, 1976). Such pressures could ultimately result in water hammer problems (Aydin, 2002), as well as cause vibration and cavitation that results in structural damage i.e. to the gates and conduit (Sharma, 1976). Air vents are typically only required in longer conduits where additional aeration is needed.

2.5.9.1 Functions and features

The main functions of air vents, as stated by Erbisti (2004), are:

- They reduce or eliminate sub-atmospheric pressures in the conduit during emergency or partial gate operations;
- They make it possible for air to escape the conduit as the conduit is being filled with water flow; and
- They make draining of the conduit possible.

Due to the fact that the region in the conduit immediately downstream of the gates is where air demand is most critical and can reach a maximum (i.e. when the gates are being operated under the highest reservoir head at some partial opening), air vent outlets are usually constructed around this region (Bosman and Basson, 2012). According to Erbisti (2004), the air vent outlet should be located at most 2 m away (i.e. downstream) from the emergency gate to be most effective. In order to avoid interference with air flow, the air vent inlet must be constructed above the maximum reservoir water level on the dam's downstream face (Bosman and Basson, 2012).

Erbisti (2004) recommends that the air vent shaft must be constructed as straight and uniform as possible, minimising the number of bends and sharp corners as well as avoiding sudden changes in cross-section. According to Bosman and Basson (2012), although it is sometimes easier to mould and construct an air vent with a rectangular or square cross-section, a circular shape is usually considered.

2.5.9.2 Sizing and dimensioning

In order to determine the required sizing of an air vent, the maximum airflow rate in the vent first needs to be calculated. This can be determined once the maximum air demand ratio and corresponding flow discharge under the gates are known.

Lewin (2001) has found that for free-surface flow conditions in a conduit, a maximum air demand ratio exists for very small gate openings (4% to 8%) that result in spray flow, as well as for gate openings between 40% and 70%. According to Sharma (1976), a gate opening of 80% can be assumed to result in the maximum air demand immediately downstream of the gates.

In order to avoid the increase in vacuum formation (i.e. excessive reduction in pressure) behind the gates, the maximum airflow velocity that is entrained into the conduit via the air vent may not exceed 45 m/s (USACE, 1980). The magnitude of the reduced pressure acting downstream of the gates can be estimated once the air vent is dimensioned and the pressure drop (i.e. no more than 1.5 m water head) along the vent is calculated – this is important for analysing imposed loads on structural components (USACE, 1980).

It has been concluded by Bosman and Basson (2012) that the empirical equations that have been defined in literature for estimating air demand in low-level outlets appear to be suitable for simple geometries; in cases of more complex geometries that result in more complex flow patterns, a more profound understanding of air-entrainment behaviour is still required. These empirical equations are therefore generally inaccurate and it is recommended that physical modelling of the gated conduits be done for accurately determining the air demand ratio (β), the cavitation index and pressures along the conduit, the gate rating curve, as well as the flow conditions downstream of the gate (Bosman and Basson, 2012). However, the method used to roughly estimate the expected air demand (i.e. flow rate) and required air vent size for the design specifications of this thesis are described in the following paragraphs.

The airflow rate through the air vent can be calculated implicitly according to the air demand ratio defined by Kalinske and Robertson (1943), as follows:

$$Q_a = \beta \cdot Q_w \qquad \textbf{Equation 2-45}$$

Where,

Q_a = Air flow rate (m³/s)

β = Air demand ratio (m²)

Q_w = Flow discharge under the gates (m³/s)

Once the upstream reservoir water head (H) and gate opening percentage is known or chosen, the water discharge (Q_w) under the gate under free flow conditions can be calculated using the orifice flow equation (Equation 2-37).

The following equation, defined by Erbisti (2004), can be used for calculating the air demand ratio for a specific experimental setup, and is often recommended by most published authors (Bosman and Basson, 2012):

$$\beta = K \cdot (F_{rc} - 1)^n \quad \textbf{Equation 2-46}$$

Where,

K and n = Empirical coefficients

F_{rc} = Froude number at vena contracta, given by the following equation:

$$F_{rc} = \frac{V_c}{\sqrt{g \cdot h_c}} \quad \textbf{Equation 2-47}$$

Where,

V_c = Flow velocity at vena contracta (m/s)

h_c = Flow depth at vena contracta (m)

Bosman and Basson (2012) considered various studies that proposed different equations for calculating the air demand ratio for design purposes. The most conservative formula was found to be that of USACE (1980), which is applicable to conduits in which *no* hydraulic jump forms downstream of the gates. This equation is defined below as:

$$\beta = 0.03 \cdot (F_{rc} - 1)^{1.06} \quad \textbf{Equation 2-48}$$

The alternating equation which is applicable to conduits in which a *hydraulic jump* forms downstream of the gates and fills the conduit, is defined below. This equation is defined by Kalinske and Robertson (1943) and is recommended by USACE (1980) and Sharma (1976).

$$\beta = 0.0066 \cdot (F_{rc} - 1)^{1.4} \quad \textbf{Equation 2-49}$$

Once the air flow rate (Q_a) in the vent has been calculated, the air vent can be dimensioned so that the maximum airflow velocity that is entrained into the conduit via the vent is less than 45 m/s. The cross-sectional area of the air vent can be calculated according to the following equation (SANRAL, 2013):

$$A_a = \frac{Q_a}{v_a} \quad \textbf{Equation 2-50}$$

Where,

A_a = Cross-sectional area of air vent (m²)

v_a = Airflow velocity (m/s)

2.5.10 Hydraulic and structural issues

2.5.10.1 Abrasion

Abrasion occurs inside of low-level outlet conduits when coarse sediment (ranging from sand to boulders) is discharged through and abrades the conduit lining, gates, mechanical equipment, etc. Abrasion-resistant material to cover the inside surfaces of the conduit should therefore be considered, especially when in contact with high sediment loads. The joints of plates, slabs or blocks of abrasion-resistant material (metal, non-metal, natural or artificial), when used, are often the weak areas of abrasion resistance (Basson and Rooseboom, 1999).

Morris and Fan (1998) proclaim that normal concrete has limited abrasion resistance but can be reinforced with various abrasion-resistant materials such as timber, steel (at least 2 cm thick, excluding anchors), dressed stone, a coarse granite aggregate or fibre-reinforced concrete. A medium- to high-strength concrete is therefore typically considered for the lining of the conduit (Boes *et al.*, 2018). Steel linings are commonly applied to surfaces that are susceptible to high flow velocities (and thus high abrasion), such as at the intake area where flow acceleration into the conduit occurs (Dreyer, 2018). Boes *et al.* (2018) recommend that either steel or concrete (cheaper), and preferably not natural stone, should be used for cases where the saltation of large sediment particles is likely.

Wei (1991) concluded that:

- high-strength concrete (60 MPa) is a relatively low-cost abrasive-resistant material
- plain concrete and steel plate have a weak resistance to abrasion
- for plain concrete, steel plate and high-strength concrete, the maximum allowable velocities to evade significant abrasion are 12 m/s, 10 m/s and 25 m/s respectively.
- mortar and epoxy resins proved to yield the best results, but they have limitations for large-scale use due to high costs and strict technological requirements.

Considering sediment bypass tunnels, experimental studies have shown that polymer and steel-fibre concrete provide high abrasion resistance to coarse grain sediment (ICOLD, 2018a). According to ICOLD (2018a), other examples of abrasion countermeasures that have been used in practise include basalt concrete, granite blocks (for reinforcement) and quartzite plates.

2.5.10.2 Cavitation

Cavitation inside low level outlet conduits occurs when areas of negative pressure are formed along the flow stream. This takes place when local pressures decrease and become lower than the vapour pressure as a result of local increase in flow velocity and separation, sudden change in elevation, turbulence and vortices (Amirsayafi, 2015). These negative pressures cause the water to separate into gas and liquid phases which form bubbles that eventually collapse (Morris and Fan, 1998). The dynamic energy released as a result of the cavity collapse is highly erosive and can cause hydraulic structures and equipment to be seriously damaged.

Cavitation commonly occurs at gate slots in conduits, as well as downstream of gate slots, where high flow velocities typically exist. According to Lewin (2001), cavitation occurs when flow velocities reach or surpass 13 to 15 m/s. According to Peterka (1953), cavitation will

conservatively not occur for local air concentrations larger or equal to 8%, even if negative pressures exist.

Morris and Fan (1998) state that cavitation noise can be used as an indicator for possible cavitation damage. Raudkivi (1993) states that flow containing suspended sediments causes more cavitation noise and damage than flow comprising clear water for sediment concentrations of up to 100 g/L, with the maximum effect at about 25 g/L. On the other hand, the degree of cavitation becomes less than clear water flow for sediment concentrations above 100 g/L. According to Koen (2017), cavitation will occur if the operational cavitation index is less than the incipient cavitation index. The incipient cavitation index can be estimated by the equation defined by Khatsuria (2004) as follows:

$$\sigma_c = \frac{h_{atm} - h_v}{\frac{V^2}{2 \cdot g}} \qquad \textbf{Equation 2-51}$$

Where,

σ_c = Incipient cavitation index (dimensionless)

h_v = Vapour pressure head (m)

h_{atm} = Atmospheric pressure head (m)

V = Water flow velocity (m/s)

Various measures have been identified by Chanson (1994) in practise to reduce or prevent the destructive effects of cavitation, such as:

1. Aerating the flow in order to increase the local pressures (e.g. at the pseudo bottom);
2. Directing the cavitation bubbles away from the structural surfaces;
3. Choosing surface materials that increase the allowable tension stresses (e.g. steel fibre concrete); and
4. Decreasing the surface roughness and thus reducing the critical cavitation number.

2.5.10.3 Vortex formation

ASCE (1995) states that vortex formation in reservoirs typically occurs due to insufficient dam intake submergence, abrupt changes in local flow direction and velocity, asymmetrical approach flow conditions, approach flow velocities larger than 0.65 m/s, as well as local flow separation and eddy formation. With regards to pressurised intakes with a low upstream head (i.e. power intakes), vortices have been known to: (1) entrain air into the hydropower conduit and cause cavitation, vibration and unbalanced loads on the turbines; (2) Increase head losses and thus decrease turbine efficiency and conduit discharge capacity; (3) draw floating debris which can cause trash rack blockage; and (4) result in non-uniform flow conditions into and through the conduit (ASCE, 1995). Typical vortex formation is illustrated in Figure 2.5-9.

According to BIS (1995), common anti-vortex devices that are utilised at dams above the intakes include:

a) Perforated breast-walls;
b) Dinorwic louvered type devices; and
c) Vertical and parallel R.C.C. fins.

Figure 2.5-9: Vortex formation (Rindles and Gulliver, 1983)

2.5.10.4 Air blowback

Air blowback is a relatively common phenomenon in which pockets of air are entrained into a low-level outlet conduit from the downstream end and can be violently blown upstream above the free-surface flowing water towards the conduit intake works (Webby, 2003). According to FEMA (2004), air blowback can cause conduits to experience structural damage as well as operational issues. According to Falvey (1980), the conduit slope has the most significant effect on air blowback and blowback issues are usually avoided for slopes less than 0.1. Webby (2003) discusses a model study where air blowback only occurred during low conduit flow rates and could be prevented by installing an air vent. Lowe (1944) discusses a model study where air blowback occurred as a result of the flow being constricted (i.e. submerged) at the outlet due to wave action.

Bosman *et al*. (2016) have proposed the following guidelines for the design of future low-level outlets in order to prevent air blowback through the conduit and in the air vents:

- The conduit bed slope should be designed as flat as possible in order to avoid the upstream movement of air which can cause possible blowback issues (Falvey, 1980).
- Low-level outlets should be designed to ensure free-surface flow under all possible flow conditions over the entire conduit length, and the creation of hydraulic jumps in the conduit should be avoided (USACE, 1997).
- No structure or mechanism should constrict the air and water flow at the downstream end of the conduit (especially at the soffit of the conduit) (Bosman *et al*., 2016).
- The conduit ceiling heights – and not the inverts – should be matched in order to prevent air entrapment that occurs at changes in conduit cross section (USACE, 1997).
- Downstream of the emergency gate, the conduit should be designed as straight and as short as possible (Bosman *et al*., 2016).

- In order to effectively observe detailed flow behaviour and to minimise scale effects, large-scale hydraulic models (i.e. larger than 1:20) should incorporate partially full-flow outlet conduit designs (Speerli, 1999; Bosman and Basson, 2012).
- If a ski-jump is used at the downstream end of the conduit, it's crest height should be low enough to ensure that submergence of the conduit does not occur under low-flow conditions (Bosman *et al*., 2016).
- In the case of radial gate failure while in a partially opened position at the downstream end of the conduit, dangerous air blowback could potentially arise during emergency gate closures due to flow constriction and restriction. A possible solution to avoid this would be to implement a dual radial gate system in which: (1) each gate can handle the full design discharge capacity; and (2) the service gate can be opened fully to allow uncompressed flow before the emergency gate is closed (Bosman *et al*., 2016).

2.5.11 Gates

According to Morris and Fan (1998), low-level outlets usually operate with two gates in series. The downstream (i.e. service) gate is used for normal operations and the upstream gate acts as an emergency gate which can be closed to allow for repair of the service gate. Srivastav and Nayak (2015) state that the spacing between the gates must be large enough to avoid debris build-up and blockage (e.g. trees).

Two important factors to consider when designing and installing gates are the gate type and gate location. Two common types of sluice gates that are used in low-level outlet conduits for discharge control are radial gates and sliding gates. A comparison of these two types of gates are provided in Table 2.5-3. Although Blind (1985) highly recommends that the service and emergency gates should be installed as far upstream as possible in order to minimize the length of the pressurised portion of the conduit, a comparison of different gate locations within the conduit is provided in Table 2.5-4.

Table 2.5-3: Comparison of low-level outlet sliding and radial gate

	Sliding gates	Radial gates
Advantages	• Take up less space, are easier to install and have a smaller impact on dam stability (Rollo *et al.*, 2018). • Suitable for discharge control and preventing siltation (Rollo *et al.*, 2018). • Can effectively avoid pulsation and vibration during partial gate openings when designed and installed correctly (Rollo *et al.*, 2018). • Effective when dealing with smaller discharges as well as reservoir heads larger than 120 m (ICOLD, 2017).	• Do not use guide slots or mechanical equipment in the conduit canal (Morris and Fan, 1998). • Gate seals are protected from sediment loads and thus avoid sediment abrasion. • Recommended for when the discharge through the conduit needs to be controlled by changing the gate opening (Srivastav and Nayak, 2015). • The use of hydraulic actuators to operate the gates allows gates to deal with high

		discharges (Morris and Fan, 1998). • Effective when dealing with reservoir heads less than 120 m (ICOLD, 2017).
Disadvantages	• Require guide slots in the conduit canal which can interfere with uniform flow. • Gate seals are exposed to sediment loads and are thus susceptible to sediment abrasion.	• Take up a large amount of space and are more challenging to install.

Table 2.5-4: Comparison of different low-level outlet gate locations (USACE, 2003)

Position	Description	Advantages	Disadvantages
Upstream end	Gates, bulkheads and/or trash-racks combined into a single structure at the upstream end of the low-level outlet conduit.	• Allows for inspection or maintenance of the entire conduit. • Lower internal hydrostatic pressure in the conduit. • A single structure is more economical.	• Extra cost of extending the structure above the pool level. • Requires an access bridge.
Near to dam axis	Gates positioned in a chamber or shaft in the abutment.	• Provides better seismic protection. • No extra cost of extending the structure above the pool level.	• Separate bulkhead required to drain the upstream end of conduit for maintenance. • Design required to withstand high earth loads in embankment dams. • Conduit upstream of the gate chamber needs to be designed for full internal hydrostatic load.
Downstream end	Gates located at downstream end of the low-level outlet conduit.	• Preferable in special conditions such as high-head projects with short outlet tunnels.	• Maximum internal hydrostatic pressure over the entire conduit. • Requires steel lining inside of the concrete lining for safety. • Less economical. • Upstream bulkhead closure required.

2.5.12 General operation, inspection and maintenance

Amirsayafi (2015) insists that the following factors must be complied with in order to ensure the suitable function of low-level outlets and to help avoid expected operational issues:

- Stilling basins located downstream of the outlets must be cleaned of debris that could cause erosion.
- The sections of the outlet conduit downstream and upstream of the service gates must be sufficiently inspected.
- The intake structure must be cleared of debris that could cause blockage.
- Mechanical equipment and gates must be sufficiently inspected and tested.
- It must be ensured that the air conduit remains unblocked, by sufficiently inspecting the air vents.
- Free-flow in the conduit must exist downstream of the control room and must have a smooth and uniform surface; cavitation can be caused by any alteration due to the high flow velocity.
- Measures to prevent seepage into the embankment should be taken.
- Implementing suitable transitions in the conduit to avoid the separation of flow from the surface, as well as to reduce head loss. An example is the transition from the conduit outlet to the stilling basin.
- It is important to have emergency guard facilities for the service gates.

2.5.13 Checking and testing of hydro-mechanical equipment

It is essential that service (operation) and maintenance (emergency) sluice gates – which are usually located near the intake structure of low-level outlets – can maintain their desired level of functioning and performance, as well as be operated (i.e. open and closed) under all possible circumstances at any given time. This is necessary to ensure reliable outlet functioning and to essentially ensure safe dam operation.

ICOLD (2018a) provides some general recommendations for testing and inspecting the gates over the entire dam operation period, in order to help avoid potential operational failure.

2.5.13.1 Inspection procedures

The inspection procedures regarding the electrical, mechanical and structural features of the low-level outlet, according to ICOLD (2018a), can be classified as follows:

1. *Inspection of the accessible features during normal reservoir operation*: This includes inspecting the equipment, outlet channel (i.e. including the aeration and energy dissipation setup), service gate (i.e. from the downstream end) and valve chamber. This inspection should take place at least once a year – usually during the period of testing of the gates – by the engineer and operator (i.e. who oversee dam safety), as well as periodically by the dam attendant.
2. *Inspection of the section which is normally submerged*: This includes inspecting specific areas of interest such as sedimentation behaviour around the trashracks, gates, intake, intake channel and stoplogs, using either video inspection or divers. This

inspection can take place once the stoplogs have been installed or during reservoir emptying (i.e. flushing), with 10 to 15-year inspection periods usually occurring.

3. *Inspection and maintenance of electrical and mechanical equipment*: This involves disassembling the equipment and occurs at least 40 years after installation depending on the inspection and performance results obtained during testing.
4. *Other*: Inspections should generally be carried out by personnel who know the facilities well. It also wise to utilise checklists during inspections. It is recommended that outside experts should do inspections about every five years.

2.5.13.2 Testing procedures

The testing procedures of the gates recommended by ICOLD (2018a) are illustrated in Figure 2.5-10. The "dry" tests indicate that no water discharge exists, whereas the "wet" test incorporates a water discharge. After the tests have taken place, the gate setup can be restored to the initial condition. Additional information on the testing procedures, as stipulated by ICOLD (2018a), include:

- Gates should be operated by the normal and/or emergency power supply, but should also be able to be operated manually if needed.
- Gate tests should occur at a reservoir level that is as high as possible.
- Gate tests should usually occur once a year.
- Even though most of the wet tests can be controlled to only discharge a small amount of water, it is desirable that the bottom outlet is fully opened and flushed at least once every five to ten years. This should only be allowed if it is ensured that no flooding at the downstream riverbed will occur.
- It is required before each west test to check if there is any human activity along the downstream river that is at risk of being threatened.
- There should also be communication checks between the control centre and the site for bottom outlets that can be operated from remote control centres. Weak points could be identified through system analysis and testing.
- The following important entries should be recorded during tests: (1) date, time and reservoir water level; (2) test procedure; (3) required oil pressure or electricity consumption for starting opening, during opening and for closing of gates; (4) gate operation duration; (5) water discharge quantity or percentage open; and (6) specific observations(e.g. water colour, aeration, noises, vibrations, etc.).
- Tests should generally be carried out by personnel who know the facilities well. It is also advised to utilise checklists during tests.

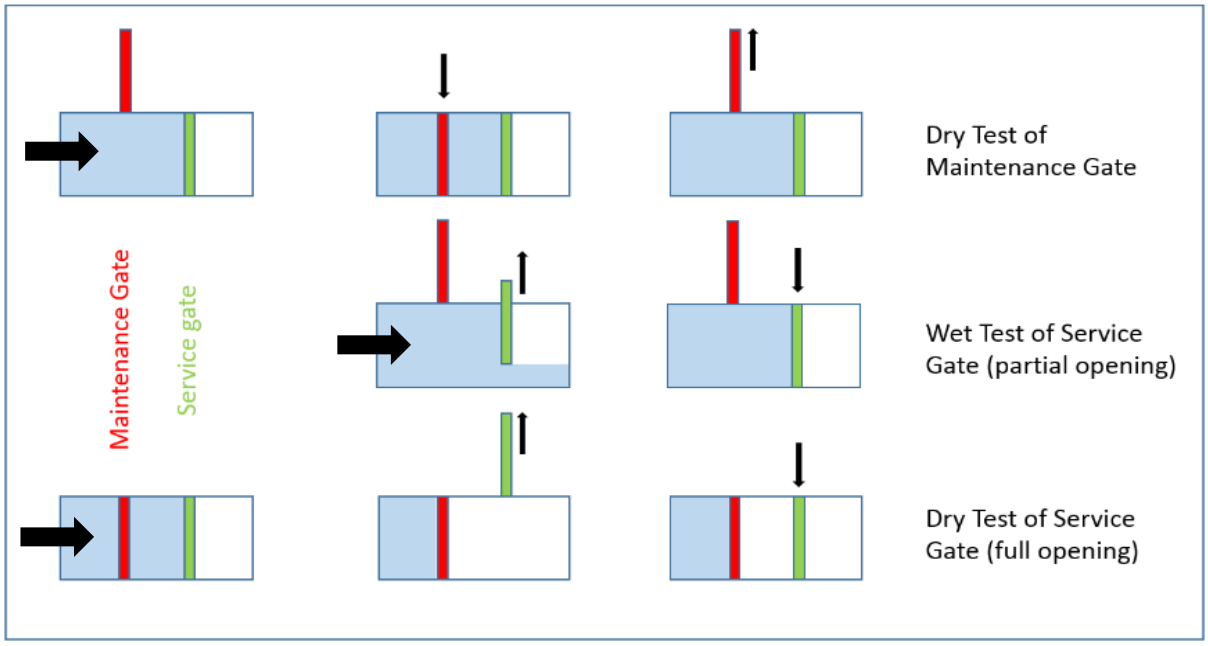

Figure 2.5-10: Typical outlet testing procedures (ICOLD, 2018a)

3 Postulated flushing system design guidelines

This section justifies the postulated design of an optimised sediment flushing system for a low-level dam intake based on observed literature from Section 2 (*Literature review*). This section systematically summarises relevant literature while discussing the methodology followed in designing a singular: (1) low-level outlet conduit and inlet structure; (2) conduit air vent; and (3) upstream low-weir, ogee spillway structure and associated wing-walls.

Two variations of the postulated design were initially considered, followed by two different wing-wall orientations for each. A total of four designs were thus tested and compared numerically (Section 4, *Numerical model and results*), from which a final best design was chosen. The design parameter values presented in this section were calculated according to the chosen final best design. The top and side views of both design variations, together with their respective structural and hydraulic design parameters and chosen hydraulic control points, are illustrated in Section 3.5.3.1 (*Design 1*) and Section 3.5.3.2 (*Design 2*).

3.1 Layout

The intake of the low-level dam outlet was positioned directly below the hydropower intakes. The conduit inlet invert level was designed below the original riverbed level in order to allow for: (1) desirable drawdown flushing (emptying) conditions and retrogressive erosion of locally deposited sediments; (2) faster flow velocities into the conduit to improve free-flow flushing of sediments (discussed later); and (3) the formation of local sediment scour zones during pressure flushing that effectively limit sediment entrainment into the hydropower intakes. The postulated low-weir, spillway structure and wing-walls were positioned upstream of the conduit inlet and inside of the sediment scour hole that typically forms around the low-level intake area during pressure flushing for sediment sizes in the sand regime. A conceptual layout of the postulated flushing system is illustrated in Figure 3.1-1.

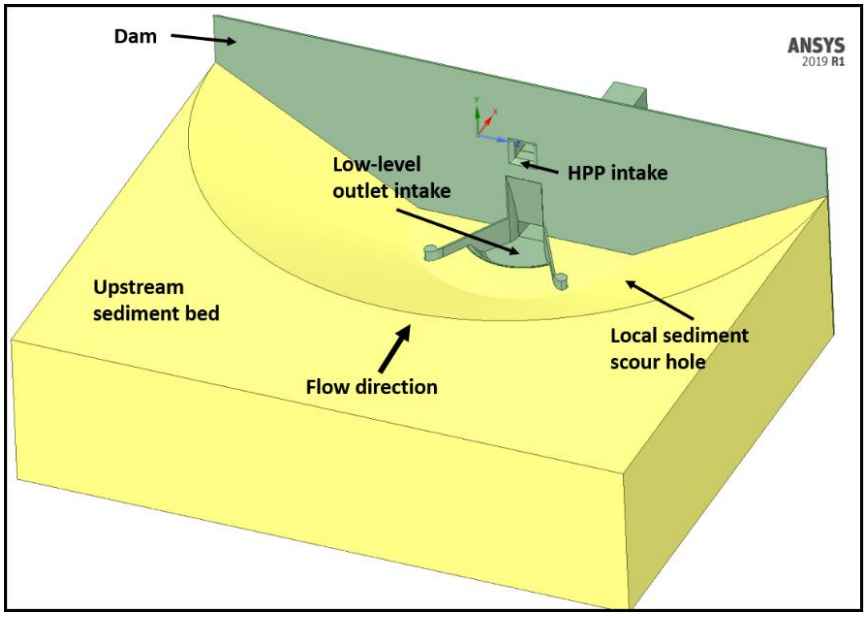

Figure 3.1-1: Conceptual layout of postulated flushing system

3.2 Low-level outlet design

3.2.1 General conduit structure

A gate chamber housing an emergency (upstream) and service (downstream) vertical sluice gate which operate in series, was positioned at the inlet end of the low-level outlet in order to minimise the length of the pressurised portion of the conduit. The conduit was designed to be short after the gate chamber, as well as straight in general to minimise the change in flow direction and velocity during flushing.

The soffit along the pressurised portion of the conduit was designed parallel to the bed slope and tangent to the inlet roof curve in order to help guide or channel streamlined flow into the conduit during full-flow pressure flushing (i.e. sluice gates are 100% open). Thereafter, the soffit level was raised and designed horizontally until the outlet in order to ensure continuous free-surface flow under all possible flow conditions, as well as minimise potential air entrapment and air blowback issues during pressure flushing.

A vertical, circular-shaped air vent through the dam and into the conduit, just downstream of the gates, was installed to aerate critical flow and thus increase local pressures during pressure flushing with partial gate openings. This will prevent consequent issues such as water hammer problems, as well as structural damage due to cavitation and vibration.

3.2.2 Conduit shape and dimensions

A wide, flat-rectangular shaped conduit with a height to width ratio of 1:2 was considered for this study. As stated by the various authors, this specific shape appears to result in the largest volume of sediment being scoured locally upstream during singular operation for most scenarios. It has also been found that rectangular-shaped conduits are typically easier to construct (i.e. in terms of entrance, openings, tunnel, etc.) as well as make it easier to install and operate gates and other hydraulic equipment.

The choice of conduit width (B) and inlet height (D) was influenced by: (1) the structural and economic limitations with regards to installing gates (i.e. service and emergency) inside of the conduit; and (2) the size of sediment and floating debris (e.g. trees, etc.) designed to be flushed through the conduit. Based on these typical conditions and specifications, B = 6 m and D = 3 m was chosen for this study.

3.2.3 Conduit bed slope

A conduit bed slope (ϕ) of 1:12 was chosen for this study, with the choice being influenced by the following factors: (1) SANRAL (2013) recommends ϕ > 1% to avoid general sediment deposition inside the conduit during flushing; (2) the bed slope should be steep enough to facilitate the flushing of the largest design sediment (i.e. gravel and boulders) without deposition; and (3) as the horizontal conduit soffit downstream of the gate chamber will result in an increase in conduit cross-sectional area as one moves downstream, a smaller slope choice is desired. The steeper the bed slope, the larger the opening at the downstream end of the conduit (especially for a very long conduit) – this could become structurally and economically impractical.

Note: Section 3.3 (*Design sediment size for flushing*) was completed to ensure that the chosen conduit dimensions and bed slope were suitable for the theoretical flushing of the chosen design sediments during specific flushing conditions.

3.2.4 Conduit inlet structure

A bell-mouth shaped roof and side-wall entrance was designed and implemented to maximise flow acceleration into the conduit and to minimise inlet energy losses during flushing. The inlet was also designed to streamline flow into the conduit to prevent flow separation. Flow separation could cause cavitation as well as result in the formation of dead zones inside of the conduit in which sediment could deposit.

The design of the roof and side-wall surface profiles were based on that recommended by the Bureau of Indian Standards (IS 9761, 1995) as illustrated in Figure 2.5-6 and Figure 2.5-7.

3.2.5 Conduit outlet structure

An energy dissipation structure (e.g. stilling basin) immediately downstream of the conduit outlet would naturally be required in the case of erosive flows with high velocities that exit the conduit and influence the downstream river conditions. This study does not explicitly focus on the design and implementation of an energy dissipation structure, but in the case of a general stilling basin design, the USBR (1987) guidelines should suffice.

The conduit outlet in this study comprises an upright rectangular shape and avoids any mechanism (e.g. a radial gate) that could constrict the air and water flow at the downstream end of the conduit (especially at the soffit of the conduit). The outlet is also designed to release the exiting flow in the original direction of the river flow in order to prevent the alteration of the downstream erosion pattern.

3.2.6 Air vent

A straight and circular-shaped air vent was designed and installed in the region immediately downstream of the gate chamber. This is where air demand is expected to be most critical and reach a maximum when the gates are being operated during pressure flushing at some partial opening. The orientation, location and shape of the air vent was designed according to the specifications stated in Section 2.5.9.1 (*Functions and features*). The layout of the slanted conduit soffit between the gate chamber and the air vent was designed similarly to that of the Berg River Dam design, as illustrated in Figure 3.2-1. For this study, the air vent outlet was conservatively raised 2 m above the toe of the slanted ceiling surface to provide sufficient space above the water surface for air flow during pressure flushing.

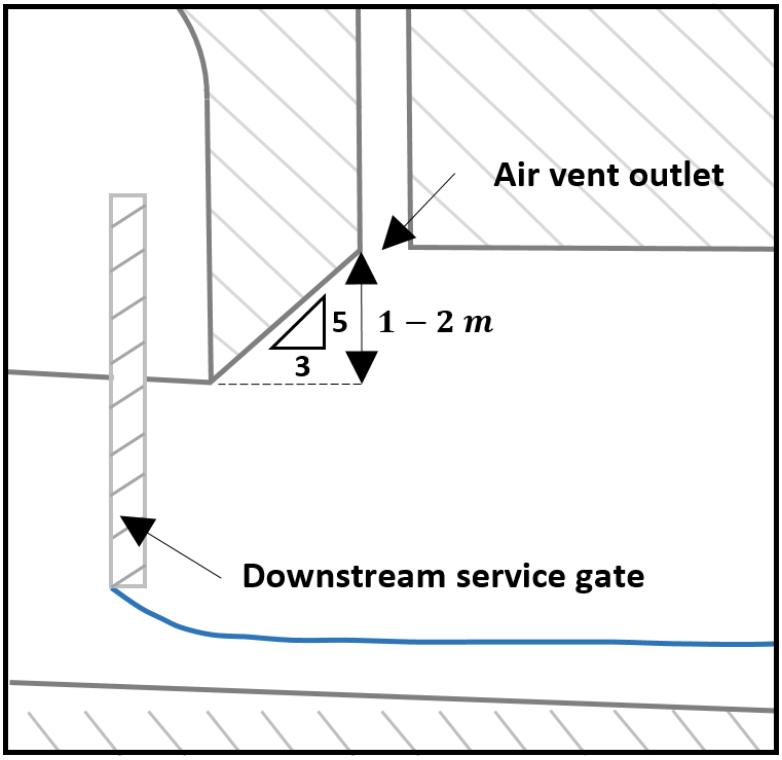

Figure 3.2-1: Downstream air vent and conduit ceiling layout
(adapted from Bosman and Basson, 2012)

The required sizing of the air vent was theoretically determined by first calculating the maximum airflow rate (Q_a) in the vent using the equation defined by Kalinske and Robertson (1943) (Equation 2-45). Once the upstream reservoir head (H) and the gate opening height (b) were known, the discharge under the gates (Q_w) under free-surface flow conditions was calculated using the orifice flow equation (Equation 2-37). The gate opening at which the maximum air demand was expected to occur immediately downstream of the gates was taken as 80% of the full opening (i.e. b = 0.8 × D), as suggested by the Sharma (1976).

The equation defined by USACE (1980) (Equation 2-48) was then used to calculate the air demand ratio (β). Finally, the required radius (r_a) of the air vent shaft was calculated considering the calculated Q_a and limiting the airflow velocity (v_a) in the vent to less than 45 m/s (limitation by USACE, 1980). For this study, the following values were conservatively chosen/calculated: y_1 = 34 m (maximum available head in physical model); b = 2.4 m; w = B = 6 m; C_c = 0.61; C_d = 0.597; Q_w = 222.14 m³/s; h_c = 1.433 m; V_c = 25.828 m/s; F_{rc} = 6.887; β = 0.196; Q_a = 43.64 m³/s; r_a = 0.6 m; v_a = 38.59 m/s.

As these above-mentioned empirical equations are considered generally inaccurate when determining air demand, etc., physical modelling of the gated conduit will have to be executed. This is necessary to verify whether the calculated r_a value is sufficient to limit airflow velocity (v_a) in the vent to less than 45 m/s during pressure flushing at the maximum upstream head (this did not fall under the scope of this study).

3.3 Design sediment size for flushing

This sub-section discusses the systematic procedure for determining the maximum sediment size that can theoretically be transported and flushed through the low-level outlet conduit during optimal flushing conditions. The size will be influenced by the predetermined conduit shape, dimensions and bed slope. Hydraulic testing of the physical model will later be used to verify the actual maximum sediment size that can be flushed.

3.3.1 Particle size

As this study does not consider a site-specific location, it is conservatively assumed that the local upstream reservoir sediment bed is mostly comprised of coarse, non-cohesive fine gravel. It is also conservatively assumed that larger gravel up until the *very large boulders* class can ultimately traverse the reservoir to the low-level outlet intake area upstream of the dam. This would most likely occur during large flood events and towards the end of a reservoir's typical design life (i.e. after about 50 years of operation) once the reservoir has filled up with sediment. Considering a specific reservoir site, the equations defined by Meyer-Peter and Müller (1948) in Section 2.3.1 (*River transport*) would have to consulted to predict the bed-load transport capacity of the alluvial river, as well as the associated sediment size that can be transported by the alluvial river.

The maximum sediment size (d_{max}) that can subsequently enter the low-level outlet is thus limited to the smallest dimension of the conduit inlet structure. For this study, a d_{max} value of 2.5 m was initially assumed, which falls under the *very large boulders* class.

3.3.2 Particle shape

The shape of an individual sediment particle will be expressed by its shape factor as defined by Simons and Sentürk (1992) (Equation 2-2) and as subsequently illustrated in Figure 2.1-1. For this study, a *moderately rounded* (i.e. "spherical") particle shape will be conservatively assumed.

3.3.3 Particle density, specific gravity and angle of repose

As the maximum sediment size (d_{max}) considered for flushing in this study falls under the *boulder* class, the density of rock (ρ_s) of 2650 kg/m³ will be considered for calculations. The specific gravity of rock (SG) will therefore be 2.65, considering ρ_w = 1000 kg/m³.

The underwater angle of repose (∅) of the assumed upstream fine gravel bed, considering an average particle size of 6 mm (Table 2.1-1) and assuming a *moderately rounded* particle shape, was read from Figure 2.1-2 as approximately 23°. The graph also indicates that for any sized boulder that is *moderately rounded,* ∅ will be approximately 40°.

3.3.4 Particle settling velocity

The settling velocity (V_{ss}) equation defined by Simons and Sentürk (1992) (Equation 2-4) will conservatively be used for gravel and boulders as it is eligible for sediment particles with different shapes (i.e. 0.4 < C_d < 2) that have reached equilibrium for R_e > 1000 (assumed).

Equation 2-10 by Van Rijn (1993) will also be considered as it is eligible for sediment particles with a diameter (d) larger or equal to 1 mm, but is expected to be less conservative as it does not take different particle shapes into account. The other equations will not be considered for this section as they correspond to unrelated sediment sizes and flow regimes.

For this study, V_{ss} was calculated as 11.61 m/s according to Equation 2-4, considering a conservative drag coefficient (C_d) of 0.4 for a spherical particle shape (Figure 2.1-3). According to Equation 2-10, V_{ss} was calculated as 7.00 m/s. As Equation 2-4 yields a larger V_{ss} value than Equation 2-10, V_{ss} = 11.61 m/s will conservatively be used in calculations hereafter.

3.3.5 Incipient motion

Conditions for incipient motion of the chosen maximum sediment size (d_{max}) inside of the low-level outlet during flushing will be verified using both Liu's criteria for incipient motion (i.e. modified Liu Diagram) and Shield's parameter. Correction for steep bed slopes must be applied to the former if a steep low-level outlet conduit bed slope is implemented.

The optimal flushing condition for ensuring incipient motion of sediment inside of the low-level outlet will be during full conduit flow during pressure flushing. This corresponds to the flow depth inside of the conduit being equal to the conduit inlet height (D). It is conservatively assumed that normal flow conditions will ultimately occur inside of the conduit, which also implies that the energy slope (S_f) at this point will be equal to the conduit bed slope (ϕ).

For this study, full conduit flow theoretically occurs at a discharge (Q) of 425.6 m³/s according to Manning's Equation (Equation 2-35). This corresponds to a normal flow depth (y_n) of 3 m (equal to D), a cross-sectional flow area (A) of 18 m², a wetted flow perimeter (P) of 12 m and a Manning's roughness coefficient (n) of 0.016 s/m$^{1/3}$ for aged concrete. In order to theoretically achieve this Q value, according to the upstream (inlet) control equation (Equation 2-34), an upstream water level (H_1) of 47 m above the conduit inlet invert level is required during pressure flushing.

3.3.5.1 Modified Liu diagram

For this study, the corresponding shear velocity (V^*) inside of the conduit was calculated as 1.566 m/s according to Equation 2-13. This corresponds to a flow depth (y) of 3 m (equal to y_n) and an energy slope (S_f) of 0.083 m/m (equal to ϕ). The Movability number for a horizontal bed, $(V^*/V_{ss})_0$, was subsequently calculated as 0.135. The particle Reynolds number ($R_e{}^*$) was calculated as $3.46 \cdot 10^6$ according to Equation 2-12.

As a steep conduit bed slope (ϕ) of 4.76° was considered in the longitudinal direction, the corresponding correction factor (k_β) was calculated as 0.898 according to Equation 2-14, provided that $\beta = \phi$ and $\emptyset = 40°$. As the bed slope is horizontal in the traverse direction, $k_\alpha = 1$. The Movability number for the chosen conduit bed slope, $(V^*/V_{ss})_{\beta,\alpha}$, was finally calculated as 0.128 according to Equation 2-15.

According to the modified Liu diagram (Figure 2.2-2), for a Movability number (V^*/V_{ss}) larger than 0.12 and a particle Reynolds number ($R_e{}^*$) larger than 13, it is theoretically implied that

the corresponding design sediment size (i.e. d_{max} = 2.5 m) will not deposit inside of the low-level outlet during optimal flushing conditions.

3.3.5.2 Shield's parameter

According to Shield's parameter (Equation 2-17), the corresponding maximum sediment particle size (d_1) to be subjected to lifting from the conduit bed was theoretically calculated as 2.75 m.

3.3.5.3 Conclusion

Both the calculated maximum design sediment sizes, according to the modified Liu diagram and Shield's parameter, were smaller that the chosen conduit inlet height (D) of 3 m, which implies that it would be possible to flush both sizes. Since the chosen d_{max} value was smaller than the calculated d_1 value, d = 2.5 m will conservatively be considered as the theoretical limiting sediment size for flushing. The actual maximum sediment size for flushing will be verified during hydraulic testing of the physical model.

3.4 Hydraulic design

3.4.1 Design discharge for free-flow flushing

The maximum design discharge (Q_e) for free-flow flushing was initially calculated considering initial submergence of the conduit inlet. An upstream water depth (H_1) equal to that of the conduit inlet height (D) was thus conservatively used in the upstream (inlet) control equation (Equation 2-33), together with the conduit's dimensions and characteristics, to calculate Q_e. This initial, theoretical value of Q_e is required to design the low-weir and ogee spillway structure for subsequent CFD simulations and physical modelling. For this study, Q_e was calculated as 53.15 m³/s.

The value of Q_e must later be refined in CFD simulations and physical modelling as the maximum discharge that can be flushed without causing submergence of the conduit inlet (i.e. water may not touch the conduit inlet soffit). This condition is exclusive to water flowing over the weir crest (i.e. water may not spill over the wing-walls into the intake area). These conditions were addressed in Section 5.6.4.2 (*General results*).

3.4.2 Design discharge for pressure flushing

The maximum design discharge (Q_p) for pressure flushing was initially calculated assuming upstream (inlet) control of the low-level outlet and considering an upstream energy level (H_1) equal to the maximum available upstream head in the reservoir. This condition naturally applies for a fully open conduit where sluice gates are 100% open. For this study, H_1 = 34 m was the maximum available head in the physical model, and Q_p was subsequently calculated as 358.6 m³/s according to Equation 2-34.

The value of Q_p must later be refined in physical modelling as the discharge required to maintain H_1 = 34 m during pressure flushing.

3.4.3 Minimum submergence requirement of conduit inlet

The equation proposed by Knauss (1987) (Equation 2-43) was used to conservatively estimate the required submergence (h_{min}) of the conduit inlet to avoid air-entraining vortex formation during pressure flushing. The conceptual design of the minimum submergence requirement is illustrated in Figure 2.5-8.

The Froude Number parameter required for Equation 2-43 conservatively corresponds to full conduit flow conditions during pressure flushing. As previously calculated in Section 3.3.5 (*Incipient motion*), a discharge (Q) of 425.6 m³/s was required to achieve full conduit flow conditions. The corresponding water velocity (V) at the inlet was calculated as 23.64 m/s. The Froude Number (F_r) at the inlet was subsequently calculated as 4.36 according to Equation 2-44, considering a flow depth (y) of 3 m at the inlet (i.e. equal to D). Finally, h_{min} was calculated as 27.65 m above the conduit inlet centreline (i.e. 29.14 m above the conduit inlet invert level).

Since these empirical equations have been defined according to general structural and hydraulic conditions for design purposes, it is necessary to accurately determine the specific submergence requirement through physical modelling.

3.5 Intake structure design

3.5.1 Introduction

A semi-circular, ogee-shaped spillway structure and associated wing-walls were designed to primarily ensure that the region inside of the low-level outlet where the sluice gates operate is always kept free of sediment deposition and blockage during flushing. The following pointers describe the requirements of the design and implementation thereof:

- For effective location at the dam, the structure and wing-walls will be positioned inside of the sediment scour hole which forms around the low-level intake area during pressure flushing. This location would ideally provide easier access for construction, maintenance and repair (i.e. minimal need for sediment removal), as well as maximise sediment removal during flushing.
- The spillway must be designed to produce suitable supercritical flow conditions upstream of the conduit inlet structure, as well as through it, during free-flow flushing (i.e. after reservoir drawdown). Supercritical flow conditions are especially necessary during lower flows to ideally produce enough force to prevent sediment from depositing in and around the intake area.
- The submerged low-weir is also important for pressure flushing, where the aim is: (1) local sediment removal; and (2) preventing main reservoir sediments from sliding or being transported towards the low level outlet where it could hinder outlet gate closure and thus lead to emptying of the reservoir.
- The associated wing-walls are needed to help streamline the supercritical flow into the low-level outlet during free-flow flushing. It must be ensured that the supercritical flow does not approach the conduit inlet at a wide angle, otherwise a hydraulic jump

could form at the entrance and ultimately result in considerable abrasion, damming and reduction of outlet discharge capacity (SANRAL, 2013).

3.5.2 Predicted sediment scour hole geometry

Dreyer (2018) used physical modelling to derive equations to predict the geometrical dimensions of the sediment scour hole that will typically form during pressure flushing based on different low-level dam outlet conduit shapes, upstream reservoir heads (H_u) and upstream sediment levels (H_{sed-up}). The sediment considered was fine, non-cohesive silica sand with an effective diameter of 0.09 mm. The dimensional equations that are valid for a local upstream fine gravel reservoir bed and a flat-rectangular low-level outlet shape (width-to-height ratio of 2:1) are indicated in Table 3.5-1. The dimensions are illustrated in Figure 3.5-1 and Figure 3.5-2.

Table 3.5-1: Predicted dimensions of scour cone geometry (Dreyer, 2018)

Dimension	Equation	R^2
Length (m) **Equation 3-1**	$L_{co} = H_u \cdot \left[1.2044 \cdot \ln\left(\frac{H_u}{H_u - H_{sed-up}}\right) - 1.6830 \cdot \ln\left(\frac{U_o}{\sqrt{gH_u}}\right) + 0.0755 \cdot \ln\left(\frac{b_{oc} + b_{oe}}{H_u}\right)\right]$	0.998
Width (m) **Equation 3-2**	$W_{co} = H_u \cdot \left[2.4650 \cdot \ln\left(\frac{H_u}{H_u - H_{sed-up}}\right) - 3.5208 \cdot \ln\left(\frac{U_o}{\sqrt{gH_u}}\right) + 0.1607 \cdot \ln\left(\frac{b_{oc} + b_{oe}}{H_u}\right)\right]$	0.998
Height (m) **Equation 3-3**	$H_{co} = H_u \cdot \left[0.7843 \cdot \ln\left(\frac{H_u}{H_u - H_{sed-up}}\right) - 0.7605 \cdot \ln\left(\frac{U_o}{\sqrt{gH_u}}\right) + 0.0306 \cdot \ln\left(\frac{b_{oc} + b_{oe}}{H_u}\right)\right]$	0.998
Depth (m) **Equation 3-4**	$D_{co} = H_u \cdot \left[-0.0179 \cdot \ln\left(\frac{H_u}{H_u - H_{sed-up}}\right) - 0.7628 \cdot \ln\left(\frac{U_o}{\sqrt{gH_u}}\right) + 0.0359 \cdot \ln\left(\frac{b_{oc} + b_{oe}}{H_u}\right)\right]$	0.985
Volume (m^3) **Equation 3-5**	$V_{co} = {H_u}^3 \cdot \left(\frac{L_{co}}{H_u}\right)^{4.1214} \cdot \left(\frac{W_{co}}{H_u}\right)^{-1.2774} \cdot \left(\frac{H_{co}}{H_u}\right)^{0.1575}$	0.999

The parameters in the dimensional equations indicated in Table 3.5-1 are provided below (Dreyer, 2018):

H_u = Upstream reservoir head, above the inlet invert level (m) ($\geq h_{min}$)

H_{sed-up} = Upstream sediment level, above the inlet invert level (m)

U_o = Conduit inlet flow velocity (m/s) (Equation 2-34)

b_{oc} = Conduit width along centreline (m) ($= B$)

b_{oe} = Conduit width along outside edge (m) ($= B$)

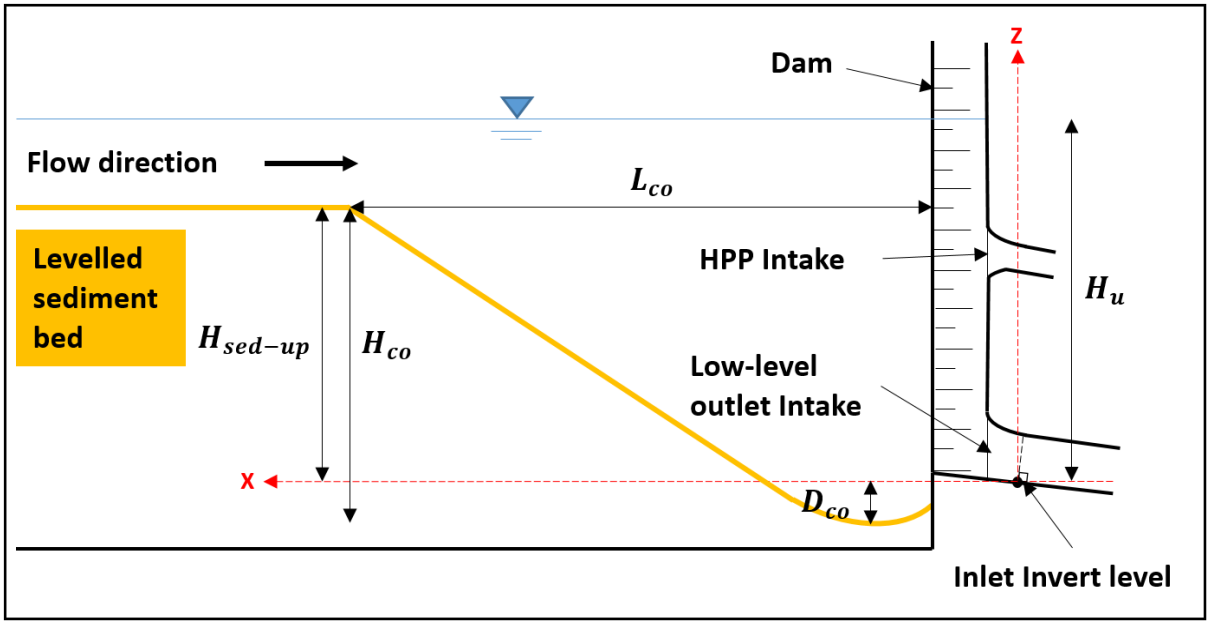

Figure 3.5-1: Long section of sediment scour cone geometry (adapted from Dreyer, 2018)

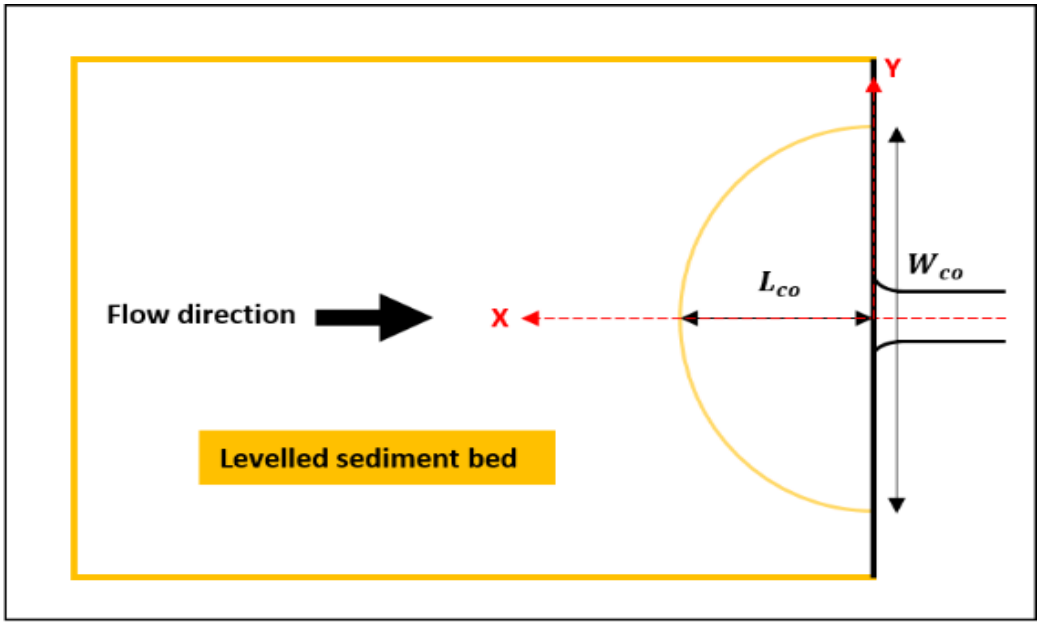

Figure 3.5-2: Plan view of sediment scour cone geometry (adapted from Dreyer, 2018)

3.5.3 Conceptual designs evaluated

This sub-section illustrates and briefly discusses two design options of the low-level outlet conduit, low-weir and ogee spillway structure (with wing-walls) on which model studies were performed. The relevant hydraulic and structural design parameters concerning the low-level outlet conduit have already been discussed in the previous sub-sections, while the remaining design parameters will be discussed and explained hereafter. The final conceptual design, considering free-flow flushing, is illustrated in Figure 3.5-3.

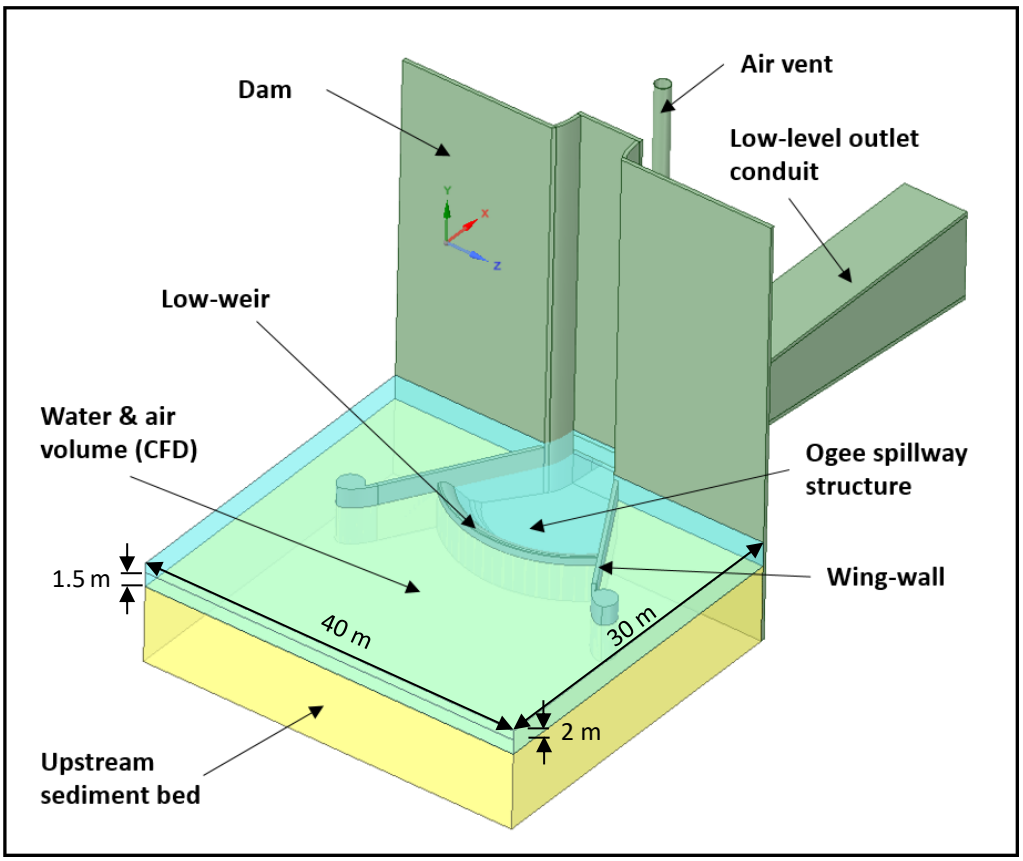

Figure 3.5-3: Final conceptual design (free-flow flushing)

3.5.3.1 Design 1

Design 1 was the initial design whereby the intake bed surface with gradient, m, which originated at the point of intersection between the local NGL and the low-level outlet conduit bed surface with gradient, ϕ, was extended upstream until it intersected the ogee spillway profile. The reverse bottom curve was then implemented between them at the point of intersection. The conduit inlet invert level of this design is referred to as IL_1.

A total of five hydraulic control points was chosen along the longitudinal centreline of the spillway structure and conduit. The first control point (p_1) is located at the weir crest, where critical flow is expected to occur. The second control point (p_2) is located at the downstream edge of the reverse bottom curve. The third control point (p_3) is located at the point of intersection between the intake bed surface and the low-level outlet conduit bed surface. The

fourth control point (p_p) is located at an arbitrary point inside of the conduit, which is downstream of p_3. The horizontal distance (L_{3p}) between p_3 and p_p was manipulated for initial CFD simulations (later) so that only a portion of the conduit was considered – p_p thus, in this case, represented the conduit outlet. The fifth control point (p_5) is located at the actual conduit outlet, which is specified once the actual conduit length has been chosen. Normal flow conditions are expected to occur at this point.

The long section and plan view of *Design 1*, together with the general design parameters and specified hydraulic control points, are illustrated in Figure 3.5-4 and Figure 3.5-5, respectively.

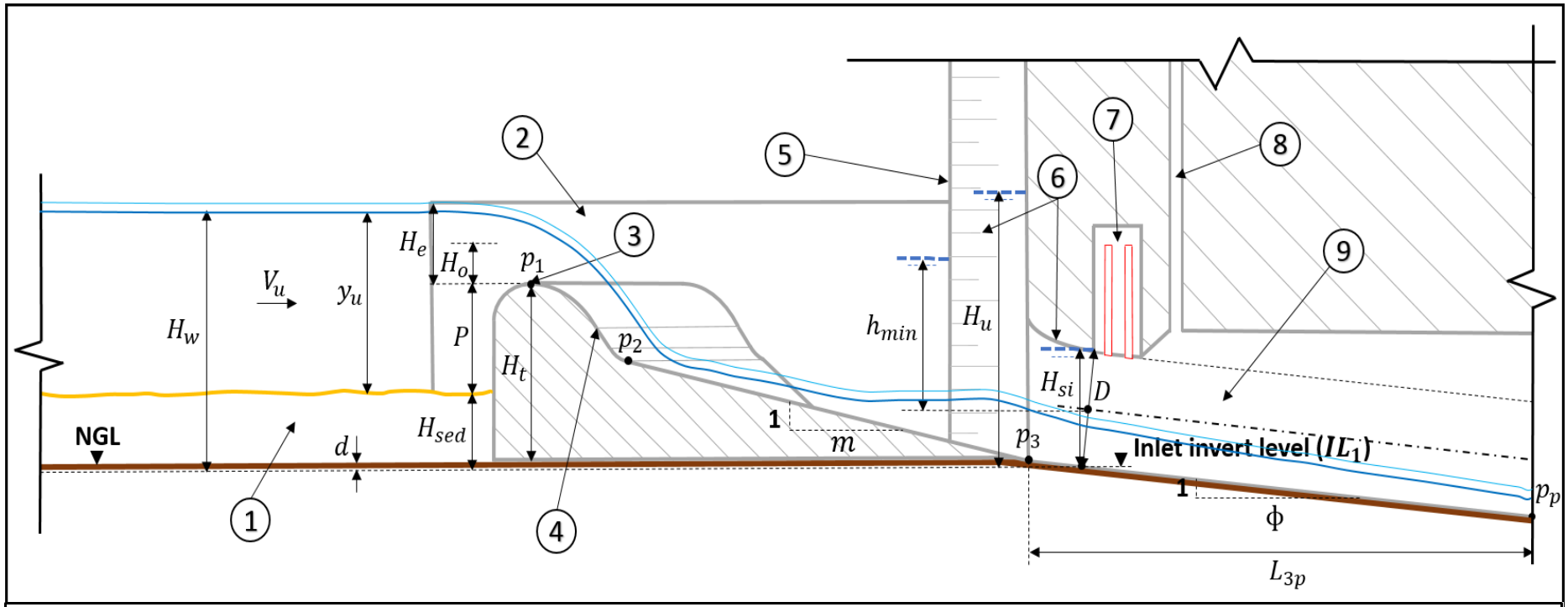

Legend:

(1) Local upstream sediment bed
(2) Wing-wall
(3) Low-weir
(4) Ogee spillway
(5) Dam
(6) Inlet structure
(7) Gate chamber
(8) Air vent
(9) Low-level outlet conduit.

Figure 3.5-4: Long section of *Design 1* (water profile indicated for free-flow scenario)

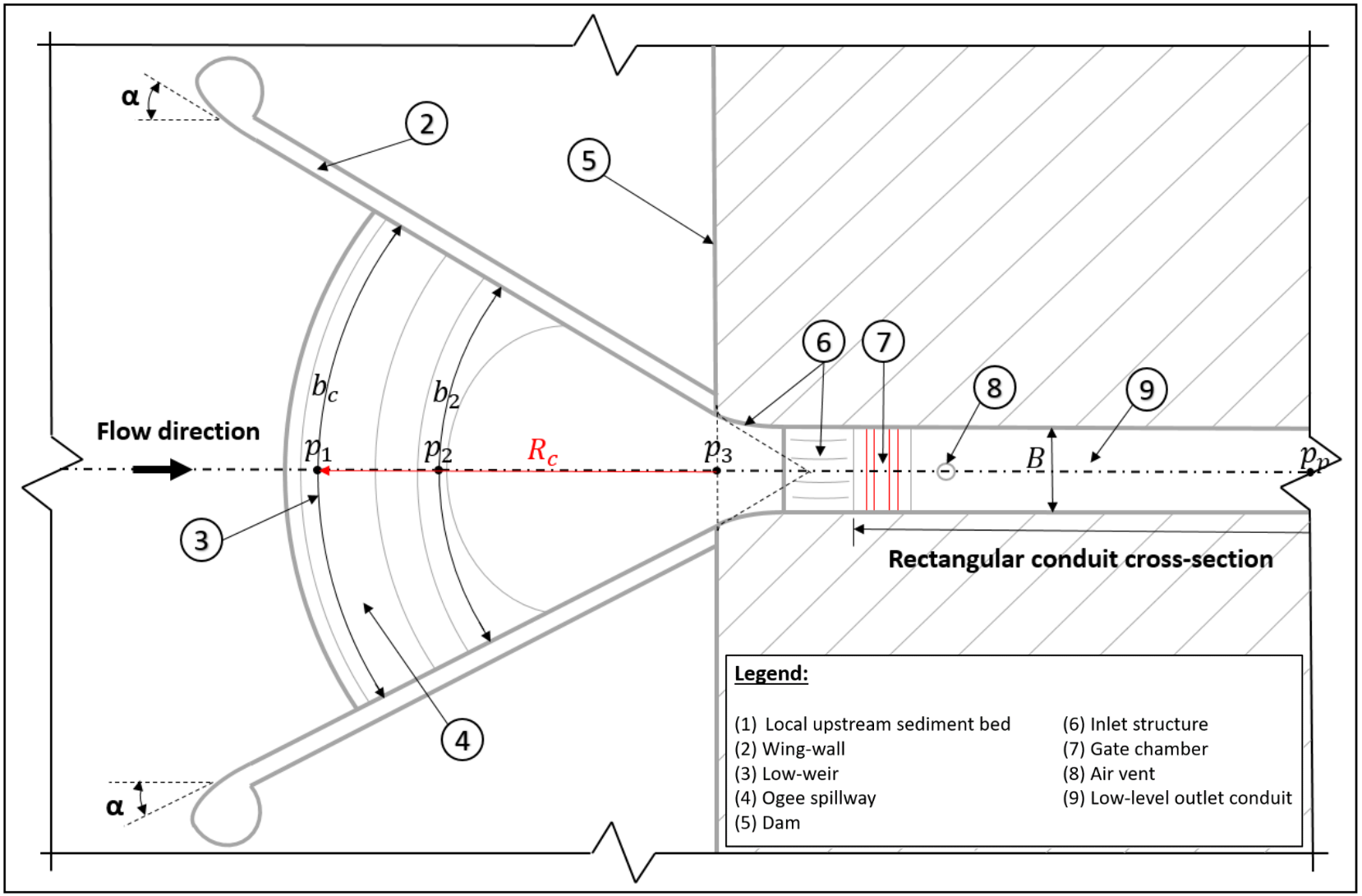

Figure 3.5-5: Plan view of *Design 1*

3.5.3.2 Design 2

Design 2 was a modification of *Design 1*, whereby the original low-level outlet conduit was lowered vertically to the point where the intake bed surface with gradient, m, and the elongated ogee-spillway profile intersected at the local NGL. The reverse bottom curve was then implemented between them at the point of intersection. The conduit inlet invert level of this design is referred to as IL_2.

This design resulted in an elongated ogee spillway profile and thus a lowered elevation of the second control point (p_2) and so forth downstream. According to Bernoulli's Equation (Equation 2-30), this subsequently resulted in faster flow velocities at these points, which was anticipated to ultimately improve free-flow flushing conditions. All conditions and parameter values upstream of weir crest remained the same as in *Design 1*. All five hydraulic control points described in Section 3.5.3.1 (*Design 1*) applied to this design as well.

The long section and plan view of *Design 2*, together with the general design parameters and the specified hydraulic control points, are illustrated in Figure 3.5-6 and Figure 3.5-7, respectively.

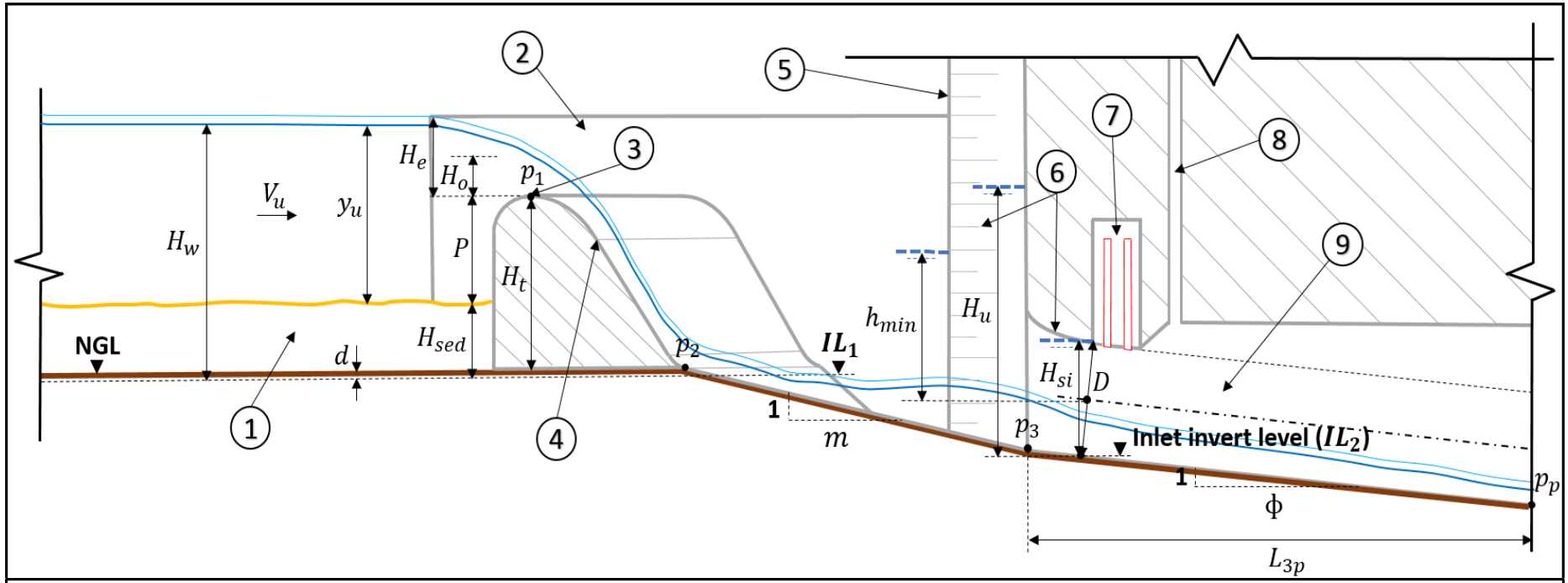

Legend:

(1) Local upstream sediment bed
(2) Wing-wall
(3) Low-weir
(4) Ogee spillway
(5) Dam
(6) Inlet structure
(7) Gate chamber
(8) Air vent
(9) Low-level outlet conduit.

Figure 3.5-6: Long section of *Design 2* (water profile indicated for free-flow scenario)

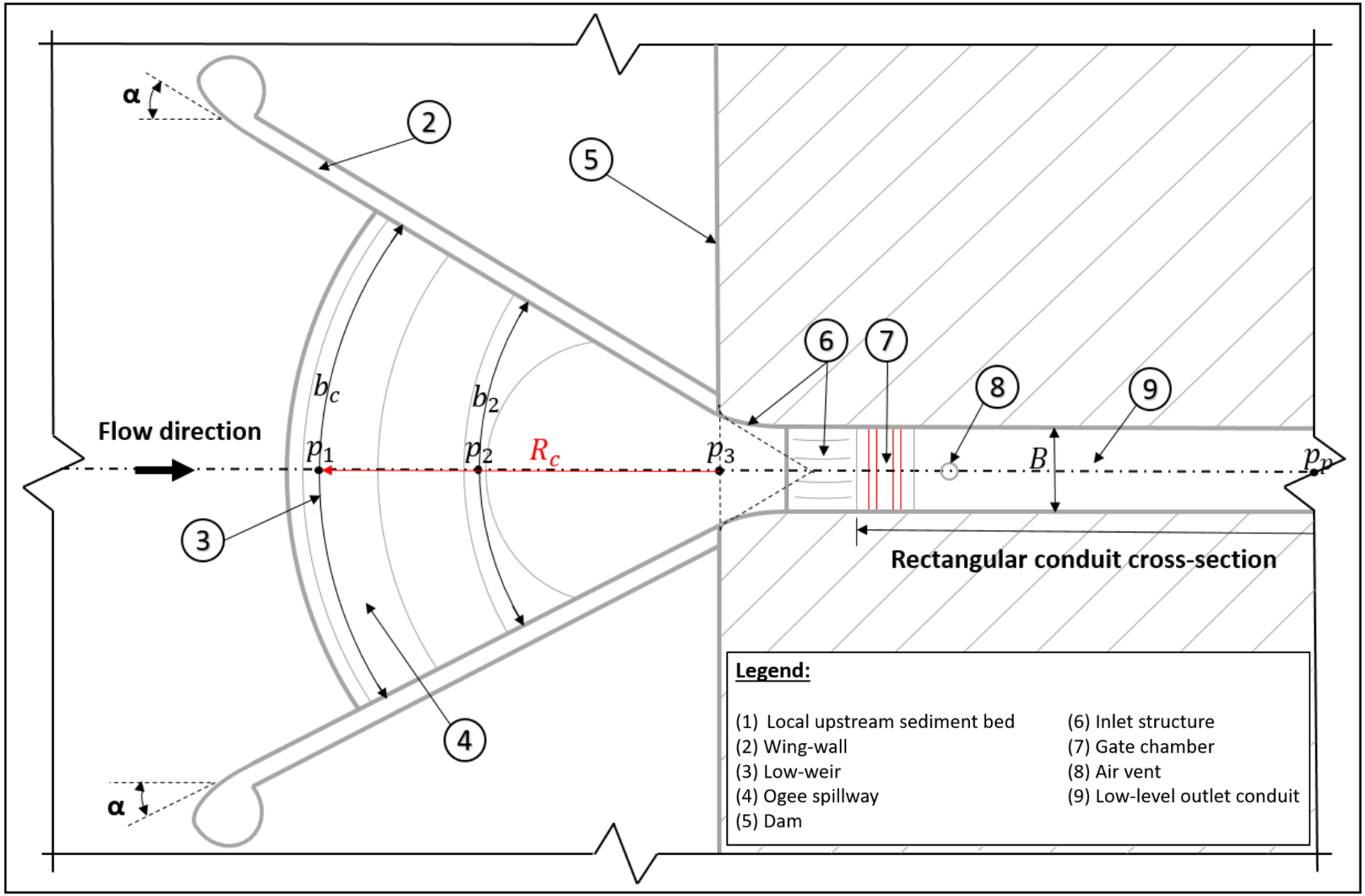

Figure 3.5-7: Plan view of *Design 2*

3.5.4 Upstream approach free-flow conditions

In order to design for conservative approach flow conditions upstream of the weir during free-flow flushing, the upstream water depth was calculated according to the recommended inlet control design ratio of H/D = 1.2 for culverts (SANRAL, 2013). It must be noted that without the influence of the weir upstream of the conduit inlet, this upstream design water depth would result in pressure flushing with minimal inlet energy losses. The upstream design water depth was thus calculated as:

$$H_w = 1.2 \cdot H_{si} \qquad \textbf{Equation 3-6}$$

Where,

H_w = Upstream design water depth, measured relative to IL_1 (m)

H_{si} = Conduit inlet submerged water depth, measured relative to the inlet invert level (m), and defined by the following equation:

$$H_{si} = D \cdot \cos(\phi) \qquad \textbf{Equation 3-7}$$

Where,

D = Conduit inlet height (m)

ϕ = Conduit bed slope (°)

The upstream design flow depth (y_u) and corresponding upstream design flow velocity (V_u), which occur above the sediment bed locally upstream of the weir, were conservatively chosen to ensure a large design head over the weir crest to optimise flushing conditions along the spillway. The chosen y_u and V_u values corresponded to the type of sediment occurring locally upstream (i.e. fine gravel for this study) and were chosen (i.e. read) from Figure 3.5-8.

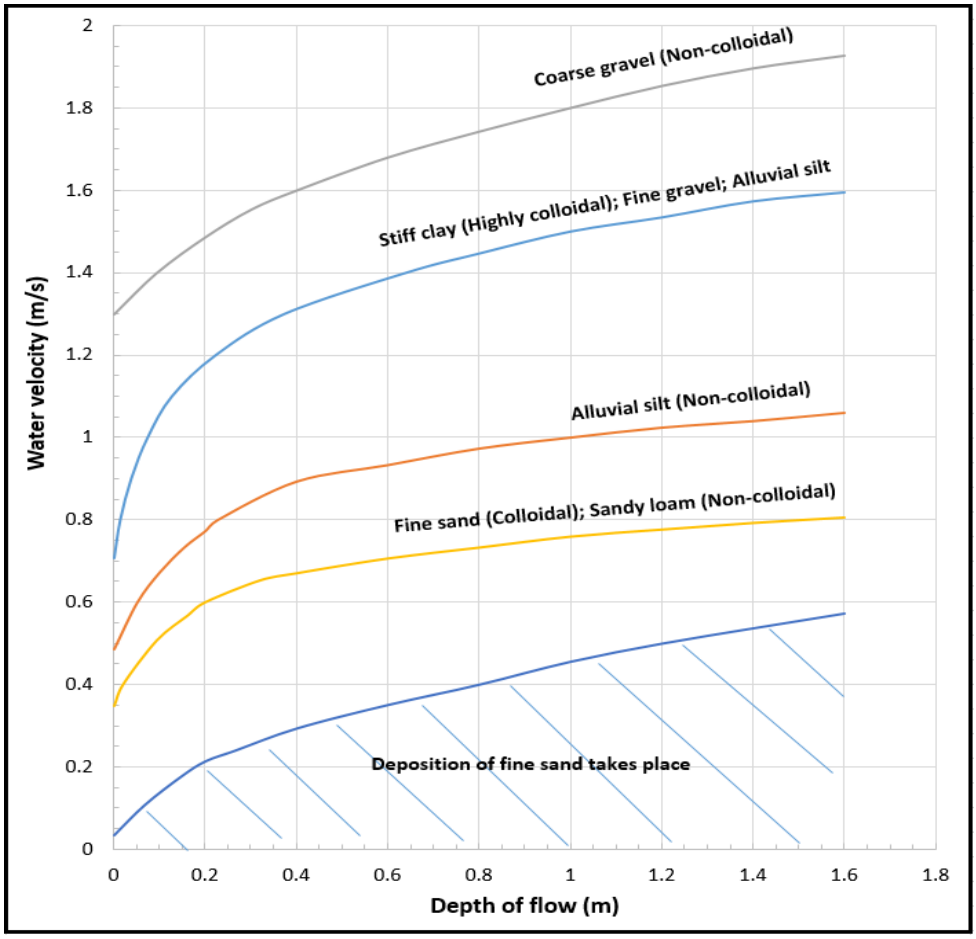

Figure 3.5-8: Permissible velocities (SANRAL, 2013)

The local design sediment depth along the upstream face of the weir was subsequently calculated according to Equation 3-8. It must be noted that hydrodynamic modelling of the movable bed in the reservoir could also be done to evaluate the intake weir design.

$$H_{sed} = H_w - y_u \qquad \textbf{Equation 3-8}$$

Where,

H_{sed} = Local design sediment depth, measured relative to IL_1 (m)

y_u = Upstream design flow depth, measured relative to H_{sed} (m)

For this study, the following values were conservatively chosen or calculated: H_{si} = 2.990 m; H_w = 3.737 m; y_u = 1.600 m (maximum graph value); V_u = 1.595 m/s; H_{sed} = 2.137 m.

3.5.5 Weir crest radius and length

The different factors that influenced the choice of the weir crest radius (R_c) and weir crest length (b_c) (i.e. structural size) are indicated below:

- The chosen R_c value must be larger than half the length of the bell-mouth side-wall intake opening (i.e. $b_2 + b/2$), as illustrated in Figure 2.5-7. For this study, the minimum R_c value was thus calculated as 4.286 m.

- The upstream channel width at which y_u and V_u occur was calculated as follows:

$$b_u = \frac{Q_e}{V_u \cdot y_u} \qquad \textbf{Equation 3-9}$$

  Where,

  b_u = Upstream design channel width (m)

  Q_e = Maximum design discharge for free-flow flushing (m³/s) (Section 3.4.1, *Design discharge for free-flow flushing*)

  This channel width (b_u) naturally forms parallel to the shape of the weir crest (i.e. semi-circular) due to the perpendicular flow direction over the crest, and is constricted by the left and right wing-walls that are to be designed (described in Section 3.5.6, *Wing-wall orientation and design*). Therefore, once the wing-wall orientation had been finalised, a R_c value was chosen that resulted in a corresponding b_c value that was smaller than the calculated b_u value, so that the upstream design conditions could ideally occur. This entire scenario is illustrated in Figure 3.5-10. For this study, b_u was calculated as 20.828 m.

- The chosen R_c value should preferably be smaller than the length (L_{co}) dimension of the existing sediment scour cone around the low-level intake as illustrated in Figure 3.5-1 and Figure 3.5-2. If an R_c value is required which happens to be larger than the existing L_{co} dimension, Equation 3-1 can be used to determine the upstream reservoir head (H_u) needed during pressure flushing to create a scour cone length equal or larger to R_c, considering the available upstream sediment level (H_{sed-up}). A trend line of the relationship between H_u and H_{sed-up} can also be used to predict what conditions are needed to maintain a specific sediment scour cone dimension.

For this study, a R_c value of 12 m was chosen based on the above-mentioned requirements. This, together with the wing-wall orientation design in Section 3.5.6 (*Wing-wall orientation and design*), resulted in a b_c value of 19.400 m. The linear relationship between the specified H_u and required H_{sed-up} to maintain L_{co} = R_c = 12 m is illustrated in Figure 3.5-9.

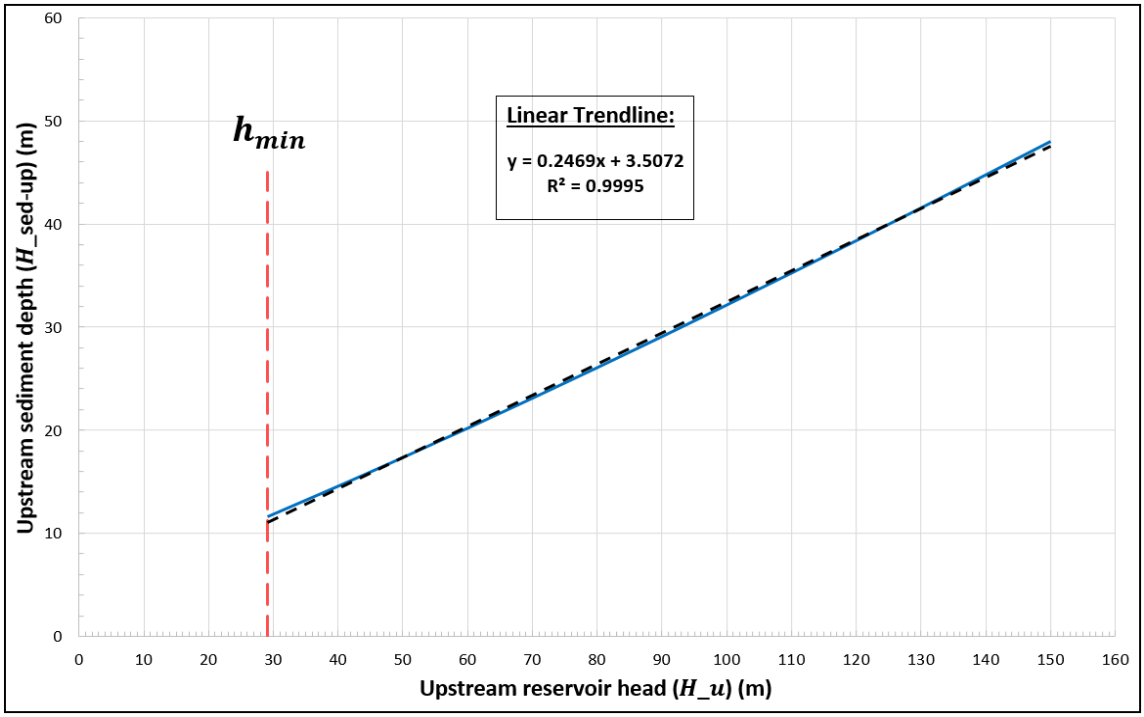

Figure 3.5-9: H_u vs H_{sed-up} to maintain L_{co} = 12 m

3.5.6 Wing-wall orientation and design

The structural design parameters considered in Section 3.2 (*Low-level outlet design*) were used to model the basic geometry of the low-level outlet conduit and inlet structures in *ANSYS SCDM (i.e. SpaceClaim) 19.1*, as illustrated in Figure 3.5-10. Initial CFD simulations of this basic geometry in *ANSYS Fluent 19.1* confirmed the need for wing-walls to successfully streamline flow into the conduit during free-flow flushing conditions. The inside face of each wing-wall was constructed tangent to the corresponding curved bell-mouth side-wall face, as illustrated in Figure 3.5-10.

The angle (α) of the wing-wall to the conduit longitudinal centreline was chosen through trial and error so that suitable resulting b_c and corresponding R_c values were obtained (i.e. according to the requirements specified in Section 3.5.5, *Weir crest radius and length*). More than one value for α yielded suitable b_c and R_c values, with the choice of α influencing: (1) the size and shape of the spillway structure; and (2) the degree of streamlined flow behaviour into the conduit. It is important to reiterate that the size and shape of the intake structure is limited by that of the sediment scour cone. According to the specifications of this study, $30° \leq \alpha \leq 45°$ was the range that was considered for predicted successful resulting structural size and streamlining of flow, as well as yielded suitable b_c and R_c values.

A smaller angle (α) disadvantageously resulted in a longer and narrower spillway structure needing to be constructed in order to achieve the required b_c value, but advantageously improved the acceleration and streamlined behaviour of the flow into the conduit. A larger angle (α) disadvantageously increased the degree of flow separation and damming at the conduit inlet, but advantageously resulted in a shorter and wider spillway structure needing to be constructed in order to achieve the required b_c value. According to numerical (CFD)

results in Section 4 (*Numerical model and results*), a value of α = 30˚ was found to yield the best results in terms of structural and hydraulic requirements.

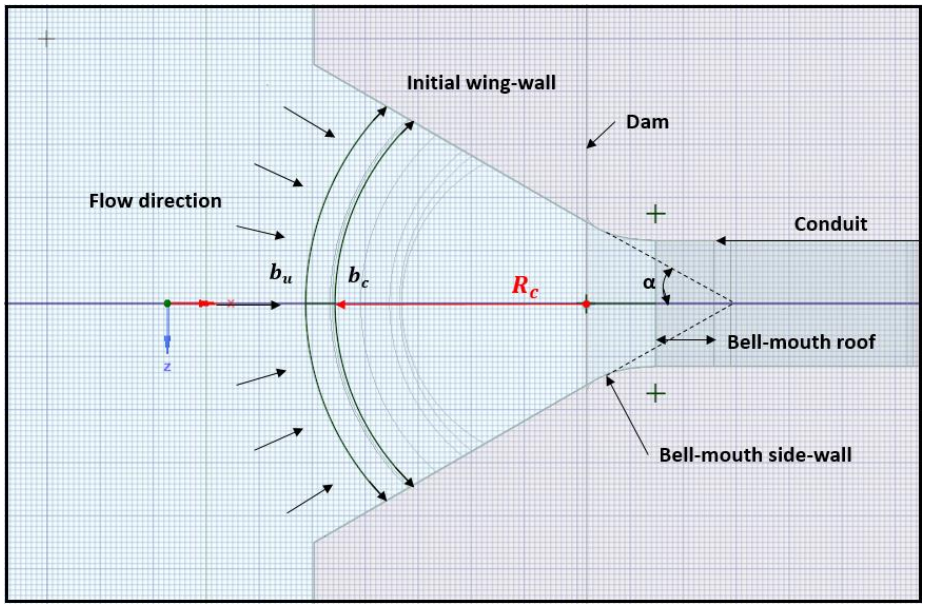

Figure 3.5-10: Plan view of basic design CFD geometry

The finalised structural design of each wing-wall is illustrated in Figure 3.5-11, with the curved intake profile designed similar to that recommended in Section 3.2.4 (*Conduit inlet structure*) for the bell-mouth side-wall. It is recommended that the wall be constructed as narrowly as possible to minimise the volume of sediment that could deposit and silt up along the wall crest. In order to limit structural costs, the wall crest level was designed to match the safety design head (H_e) above the weir crest (Section 3.5.7, *Weir crest design head*), and the upstream face of the wing-walls was extended to the point where the channel width, b_u, could safely occur.

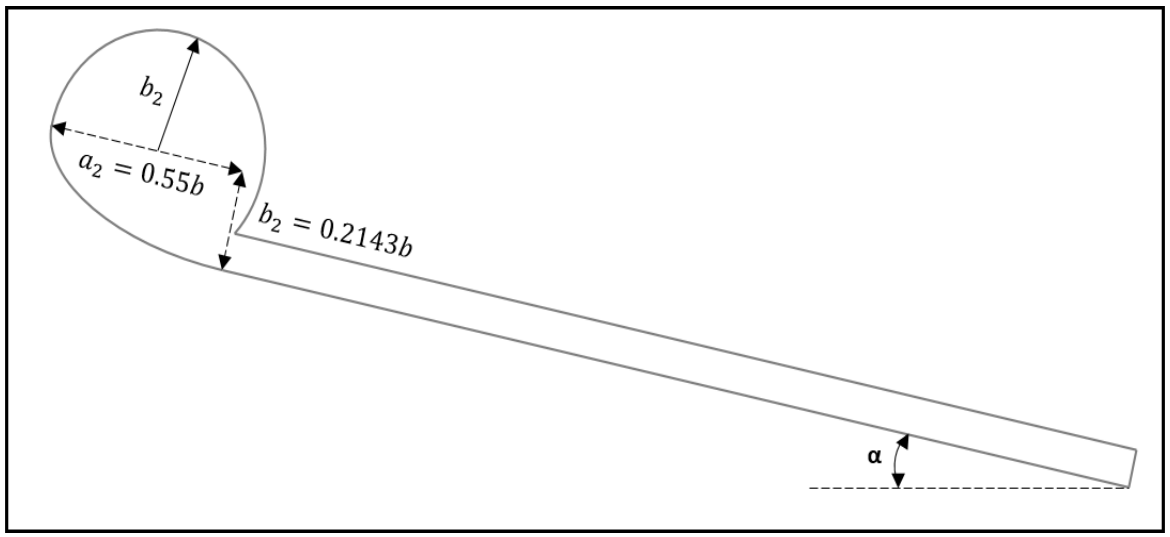

Figure 3.5-11: Plan view of final wing-wall design

3.5.7 Weir crest design head

The safety design head (H_e) above the weir crest was solved implicitly so that the ogee spillway discharge was equal to the maximum design discharge for free-flow flushing (Section 3.4.1, *Design discharge for free-flow flushing*). Therefore, H_e was initially assumed. The design head (H_o) above the weir crest was then calculated considering a conservative H_e/H_o design ratio of 1.33 (USBR, 1987). The weir crest height was calculated as follows:

$$P = H_w + \frac{{V_u}^2}{2 \cdot g} - H_{sed} - H_e \qquad \textbf{Equation 3-10}$$

Where,

P = Weir crest height, measured relative to H_{sed} (m)

H_w = Upstream design water depth, measured relative to IL_1 (m)

H_{sed} = Local design sediment depth, measured relative to IL_1 (m)

V_u = Upstream design flow velocity (m/s)

The height (d) of the start of conduit bed slope (ϕ) (i.e. local NGL) above the conduit inlet invert level was measured from the drawn geometry in *ANSYS SCDM (i.e. SpaceClaim) 19.1*. The total height of the weir crest (H_t) above the local NGL upstream of the dam was then calculated as follows:

$$H_t = P + H_{sed} - d \qquad \textbf{Equation 3-11}$$

The calculated P/H_o ratio was used to read off the corresponding value of the discharge coefficient (C_o) for uncontrolled ogee crests from Figure 3.5-12. The chosen H_e/H_o design ratio was used to read off the corresponding value of the ratio of coefficients (C_e/C_o) for uncontrolled ogee crests from Figure 3.5-13. The correct H_e value was then implicitly solved from the ogee spillway discharge equation (USBR, 1987), as follows:

$$Q_e = \frac{C_e}{C_o} \cdot C_o \cdot b_c \cdot {H_e}^{1.5} \qquad \textbf{Equation 3-12}$$

Where,

Q_e = Maximum design discharge for free-flow flushing (m³/s)

b_c = Weir crest length (m)

It must be noted, however, that the ogee spillway discharge equations apply to straight weirs in plan.

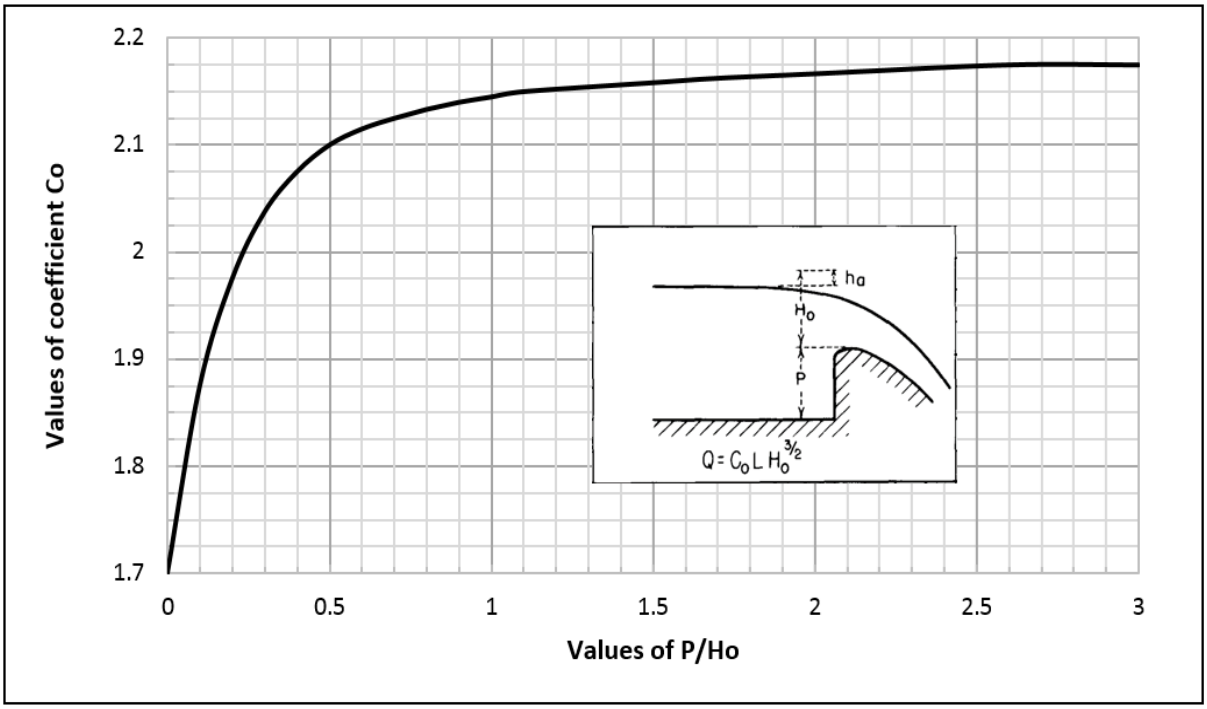

Figure 3.5-12: Discharge coefficients for vertical-faced ogee (USBR, 1987)

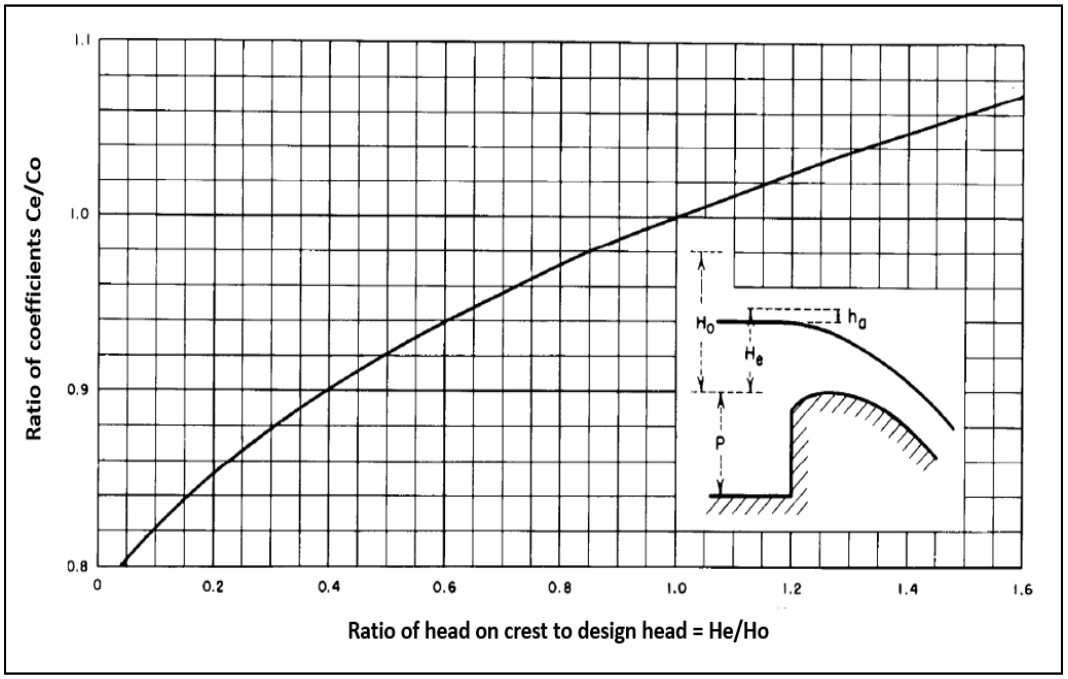

Figure 3.5-13: Discharge coefficients for other than design head (USBR, 1987)

For this study, the following values were measured/calculated/read: H_e = 1.156 m; H_o = 0.869 m; P = 0.574 m; d = 0.212 m; H_t = 2.499 m; P/H_o = 0.660; C_o = 2.120; C_e/C_o = 1.040; Q_e = 53.15 m³/s.

3.5.8 General Uncontrolled Ogee spillway profile

The previously calculated design head (H_o) above the weir crest was used to determine the ogee spillway profile upstream and downstream of the crest. The ogee spillway profile radii are illustrated in Figure 3.5-14, where H_o represents H_d. The curved profile downstream of crest ended once a gradient of 1V:0.8H was reached, after which a tangent surface with the same gradient was extended downwards from this point (USBR, 1987). The downstream reverse bottom curve of the spillway profile is illustrated in Figure 3.5-15.

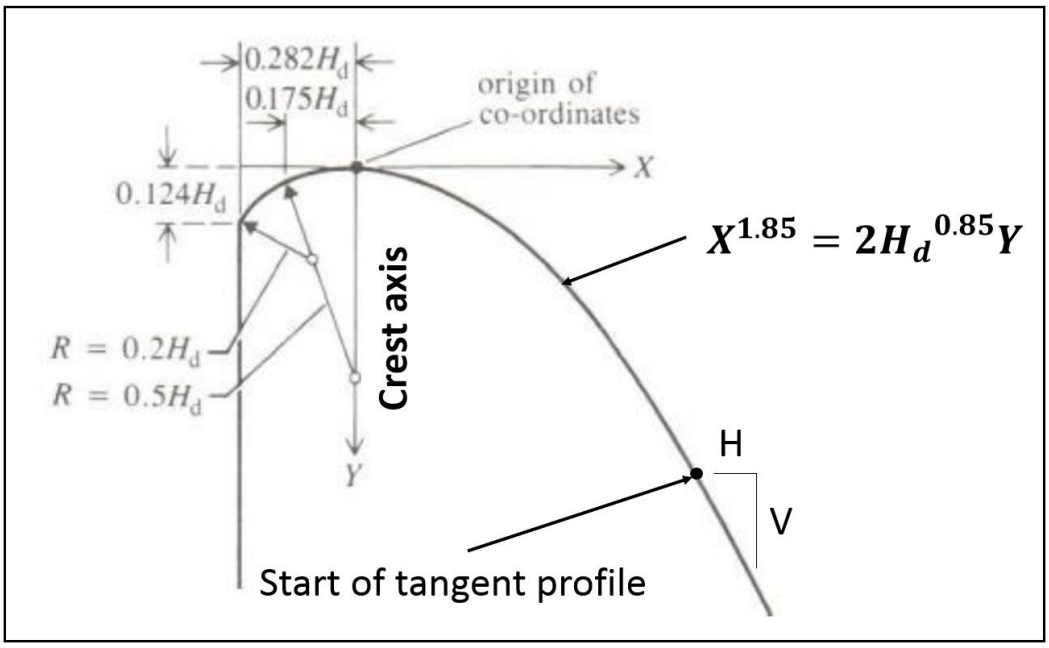

Figure 3.5-14: Top ogee profile having a vertical u/s face (adapted from USBR, 1987)

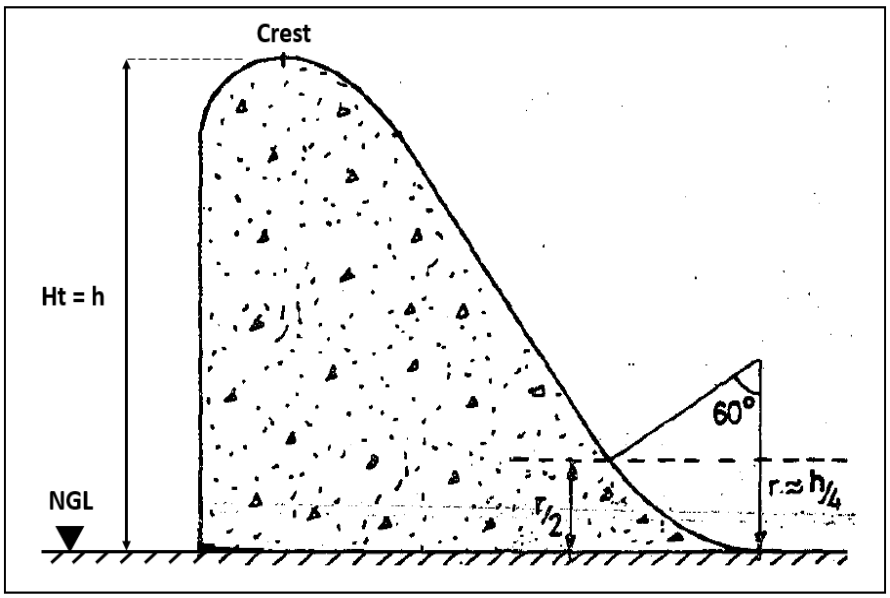

Figure 3.5-15: Bottom ogee profile having a vertical u/s face (USBR, 1987)

3.5.9 Added spillway surfaces

3.5.9.1 Intake bed surface

The *intake bed surface* was designed to extend from the start of the *conduit bed surface* towards the upstream *ogee spillway profile*. A *reverse bottom curve* was implemented between this linear intake bed surface and the linear *tangent surface* of the ogee spillway profile at the point of intersection. These surfaces are illustrated in Figure 3.5-16.

For this study, the intake bed slope (m) was chosen as 1:10, which is relatively steeper than the conduit bed slope (ϕ) of 1:12. This type of transition from a steeper intake bed slope to a more gentle conduit bed slope has shown to typically increase the inlet capacity of long conduits with inlet control (SANRAL, 2013).

High quality CFD modelling of the postulated flushing system design, considering free-flow flushing, should be used to compare Shield's parameter (Equation 2-17) along the intake bed surface and along the conduit bed surface. This comparison is important for predicting whether a certain sediment size that can theoretically be flushed (i.e. transported) along the former can also be theoretically flushed along the latter. Therefore, if the calculated maximum sediment size (d_1) for flushing along the former is smaller or equal to that along the latter, then the ϕ and m pairing is suitable. If this is not the case, m needs to be changed until the condition is achieved. This condition is addressed in Section **Error! Reference source not found.** (***Error! Reference source not found.***).

3.5.9.2 Deflection surface

A uniformly-curved, symmetric deflection surface was designed to fill the gap that existed between the horizontal reverse bottom curve and the intake bed surface. The *Bend* function in *ANSYS SCDM (i.e. SpaceClaim) 19.1* was used to generate the deflection surface between the specified edge boundaries of the design geometry, as illustrated in Figure 3.5-16 and Figure 3.5-17.

The width of the deflection surface along the structural centreline was designed as narrowly as possible to minimise the transition between the reverse bottom curve and the intake bed surface, but large enough to avoid meshing issues at this point in CFD modelling. A width of 0.1 m was found to suffice to meet these requirements and is illustrated in Figure 3.5-16.

The edge boundary of the deflection surface along the inside face of each wing-wall was designed to be relatively steep. This minimised the edge length and subsequently minimised the generated curvature (i.e. deflection) away from the wall. This was anticipated to minimise flow separation and damming along the intake bed surface during free-flow flushing. Through trial and error, it was found that a linear edge at an angle of negative 30° to the horizontal resulted in a suitable generated surface curvature. The long section of the deflection surface (yellow) is illustrated in Figure 3.5-17.

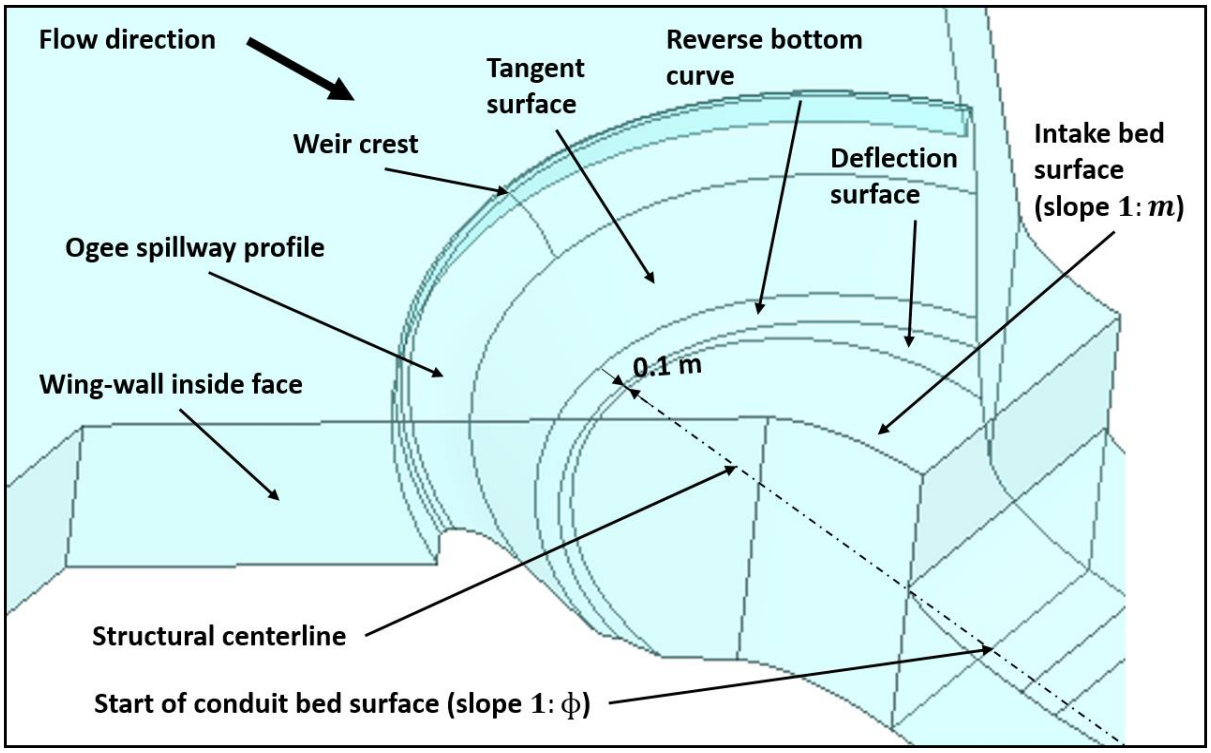

Figure 3.5-16: Typical ogee spillway structure with various surfaces

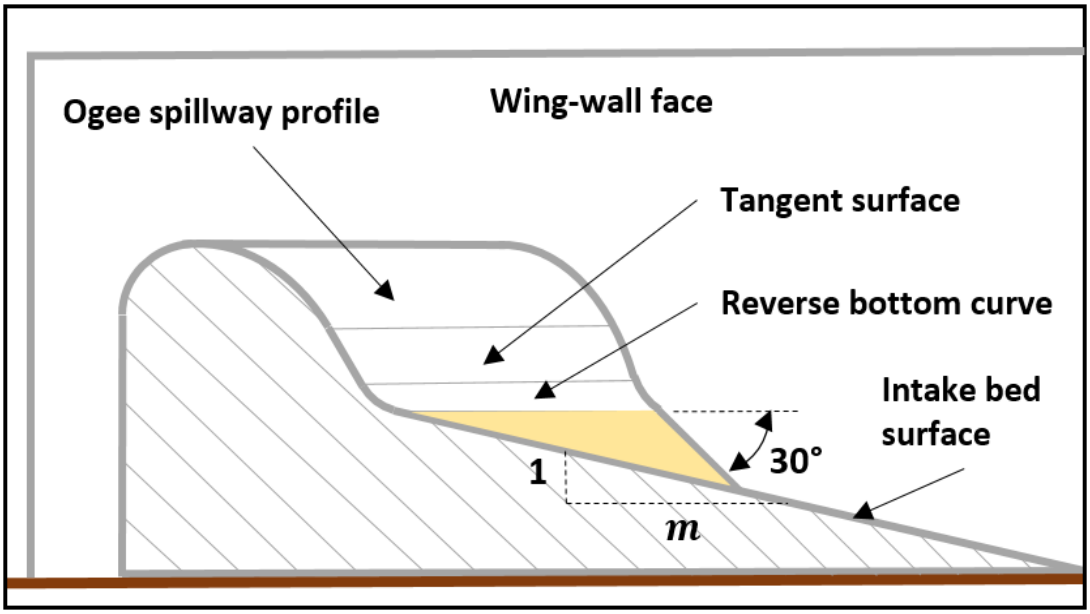

Figure 3.5-17: Typical long section of deflection surface

4 Numerical model and results

This section focuses on numerically comparing the two postulated flushing system design alternatives discussed in Section 3.5.3.1 (*Design 1*) and Section 3.5.3.2 (*Design 2*). For each design, wing-walls with an angle (α) of 30° and 45° to the conduit longitudinal centreline were tested. These two angles correspond to the boundary values of the suitable range of wing-wall angles considered in Section 3.5.6 (*Wing-wall orientation and design*). Therefore, a total of four flushing system designs were ultimately tested and compared numerically using:

(a) Hydraulic calculations: Bernoulli's Equation was used to calculate the theoretical flow depths and flow velocities, corresponding to the maximum design discharge (Q_e) of 53.15 m³/s for free-flow flushing, at the chosen hydraulic control points. This postulated the degree of supercritical flow throughout the design model.

(b) Computational Fluid Dynamic (CFD) simulations: 3D modelling and meshing of the design geometry took place, followed by multiphase (i.e. air and water) CFD simulations incorporating Q_e. The generated CFD results were used to analyse the flow vectors (i.e. degree of streamlined flow), as well as flow depths and velocities (i.e. degree of supercritical flow), at the chosen hydraulic control points.

The above-mentioned numerical results were used to verify the best postulated design option. CFD modelling was then used to further refine the chosen design so that it could ultimately be translated to physical modelling for further testing and refinement.

4.1 Hydraulic calculations

A summary of the calculated flow depth (y) and flow velocity (V) values at the chosen hydraulic control points for each design, considering Bernoulli's Equation (Equation 2-30) and Q = 53.15 m³/s, is tabulated in Table 4.1-1. The calculated Froude number (F_r) at each control point is also indicated, with $F_r > 1$ representing supercritical flow (desired), $F_r < 1$ representing subcritical flow (undesirable) and $F_r = 1$ representing critical flow. The full sequence of calculations used to determine the respective hydraulic design parameters for each design is indicated in the tables of **Appendix A**.

The following must be noted for comparison:

1. Flow depths and velocities at control point, p_1, will differ slightly between using a wing-wall angle (α) of 45° and 30° due to the slight difference in resulting weir crest length values.

2. For each design, p_5 represents the point where normal flow conditions occur.

3. The significant area of comparison is thus between p_1 and p_5.

4. For each design, p_p was chosen to occur 12 m (horizontally) downstream of p_3. This resulted in a long enough conduit section to be able to capture the critical flow behaviour at the inlet during CFD simulations.

Table 4.1-1: Summary of calculated flow depths and velocities for different designs

		Design 1 (α = 45˚)	*Design 1* (α = 30˚)	*Design 2* (α = 45˚)	*Design 2* (α = 30˚)
Hydraulic control point	**Weir crest radius (m)**	8.700	12.000	8.700	12.000
	Weir crest length (m)	19.494	19.400	19.494	19.400
p_1	y_1 (m)	0.912	0.915	0.912	0.915
	V_1 (m/s)	2.991	2.995	2.991	2.995
	F_{r_1}	1.000	1.000	1.000	1.000
p_2	y_2 (m)	0.521	0.523	0.467	0.423
	V_2 (m/s)	6.374	5.855	7.692	7.740
	F_{r_2}	2.818	2.584	3.596	3.800
p_3	y_3 (m)	1.528	1.530	1.241	1.196
	V_3 (m/s)	5.798	5.792	7.137	7.406
	F_{r_3}	1.498	1.495	2.045	2.162
p_p (12 m d/s of p_3)	y_p (m)	1.048	1.048	0.936	0.904
	V_p (m/s)	8.454	8.455	9.467	9.803
	F_{r_p}	2.637	2.637	3.125	3.293
p_5 (normal flow)	y_5 (m)	0.711	0.711	0.711	0.711
	V_5 (m/s)	12.468	12.468	12.468	12.468
	F_{r_5}	4.723	4.723	4.723	4.723

4.2 CFD modelling and results

Computational Fluid Dynamics (CFD) is a form of numerical modelling that can be used to simulate and represent real life physical processes. For this study, it was specifically used to simulate the dynamic behaviour of water and air (i.e. multiphase simulations) when dealing with hydraulic structures. CFD therefore allows for easier and quicker adaptation and refinement of structural and hydrodynamic models, as opposed to in physical modelling. Another benefit of CFD, according to Denys (2019), is that it can be used to explore certain modelling phenomena in more detail as it is able to produce high quality data when dealing with large spatial and temporal scales. It is however important to calibrate the CFD models against physical data (if possible) in order to improve the accuracy and certainty of the numerical results.

4.2.1 3D geometry

The solid 3D geometries of each of the designs were modelled in *ANSYS SCDM (i.e. SpaceClaim) v19.1*. An overall conceptual design of these geometries, considering free-flow flushing, is illustrated in Figure 4.2-1. It must be noted that only the blue 3D geometry labelled "water and air volume" was used for subsequent CFD meshing and multiphase simulations. It must also be noted that an initial, basic wing-wall design was implemented in each design, as the final wing-wall design had not yet been finalised. The final wing-wall design was later implemented in the refined CFD modelling of the final design choice, as illustrated in Figure 3.5-3.

A standardised 36 x 1.5 m *water inlet* was created upstream for each design. A width of 36 m was chosen as it: (1) was wide enough to at least encompass the upstream opening between the wing-walls; (2) appeared to provide a wide enough distribution of inflowing water to emulate realistic approach flow conditions; and (3) minimised the volume of the overall geometry, which subsequently allowed for easier meshing and faster simulation times. A height of 1.5 m was chosen to compensate for the slight increase in flow depth between the wing-walls, due to structural convergence, so that the upstream design flow depth (y_u) of 1.6 m could ideally occur.

A standardised 36 x 2 m *air inlet* was created upstream for each design. A height of 2 m was chosen as it: (1) appeared to result in sufficient air volume above the generated water surface for realistic multiphase simulations; and (2) encompassed a section of the wall above the conduit opening – this provided realistic conditions for airflow simulation into the conduit.

The *water inlet* and *air inlet* faces were designed 15 m upstream of the wing-walls. This appeared to result in a large enough upstream area to realistically emulate approach flow conditions, while sufficiently minimising the volume of the overall geometry.

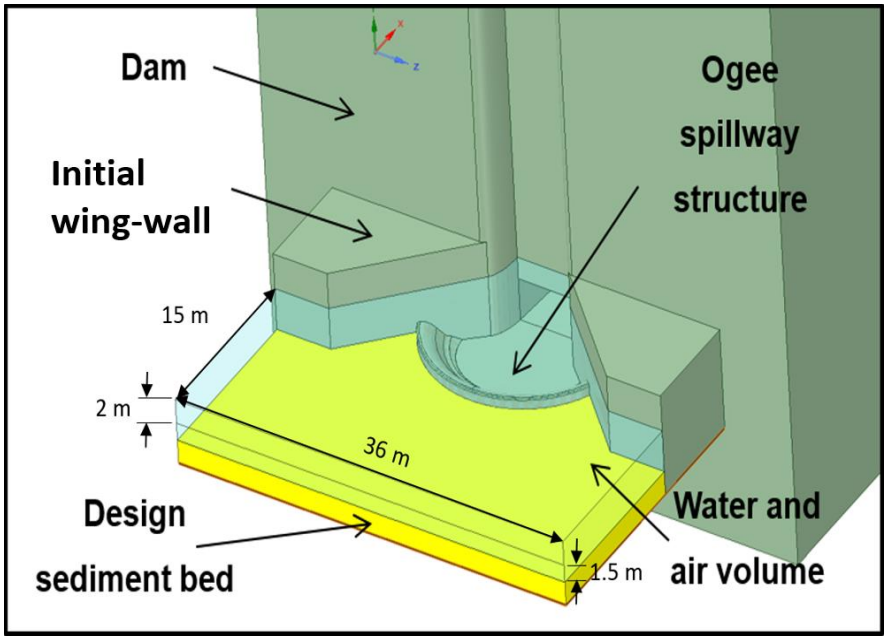

Figure 4.2-1: Conceptual 3D geometries in *ANSYS SCDM 19.1* (free-flow flushing)

4.2.2 Meshing

Meshing of the 3D "Water and air volume" geometry of each design took place in *ANSYS Meshing v19.1*. A summary of the important meshing details and value ranges considered for the design models is indicated in Table 4.2-1. The remaining default settings details were similar to that of the final design model as indicated in Figure A.1 in **Appendix A.6**. An example of a generated model mesh, together with the generically specified *Named Selections*, is illustrated in Figure 4.2-2.

Table 4.2-1: Summary of Meshing details for initial design models

Parameter	Value or option	Comments
Sizing		
Max Element Size (m)	0.35 – 1.28	Smallest allowable size chosen to create finest possible mesh.
Capture Curvature	Yes	Required for models with curved surfaces to improve mesh quality.
Capture Proximity	No	Found to interfere with mesh stability in each model.
Quality		
Mesh Metric	Orthogonal Quality	-
Minimum Orthogonality Quality	0.15 – 0.23	Must be larger than 0.1 for a stable mesh.
Maximum Orthogonality Quality	0.98 – 1.00	The larger the fraction the better the mesh quality.
Average Orthogonality Quality	0.78 – 0.88	The larger the fraction the better the mesh quality (preferably larger than 0.75).
Inflation	None	Found to reduce mesh quality in each model.
Assembly Meshing		
Method	Tetrahedrons	Method found to maximise mesh quality in each model.

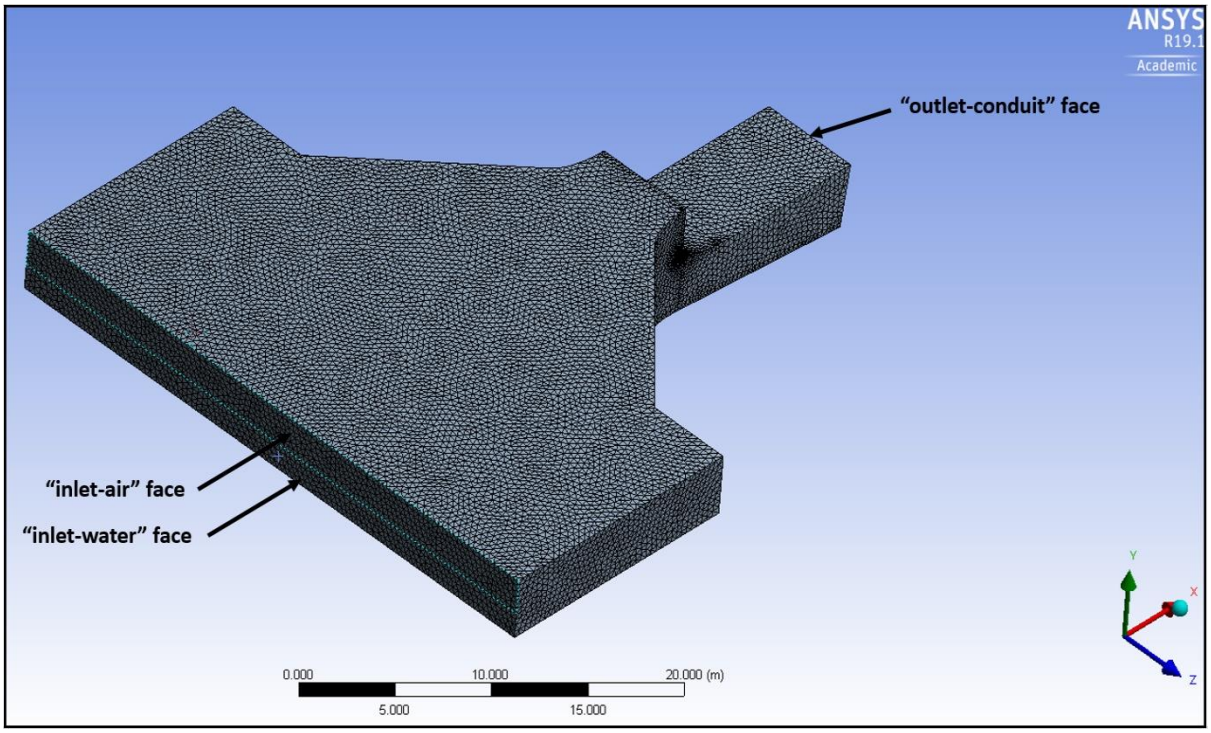

Figure 4.2-2: Design 2 (α = 45˚) model mesh and Named Selections

4.2.3 Simulation setup

CFD simulations of each meshed model were performed in *ANSYS Fluent v19.1*. A summary of the important generic *Fluent Setup* details for each model is indicated in Table 4.2-2. The remaining default settings were similar to that of the final design model as indicated in the figures of **Appendix A.7**.

Table 4.2-2: Summary of *Fluent Setup* details for initial design models

Parameter	Value or option	Comments
Solver		
Time	Steady	-
Type	Pressure-based	-
Models		
Viscous	k-epsilon (2 eqn)	-
Multiphase	Volume of Fluid (VOF)	-
Materials (Phases)		
Fluid	Water-liquid	Primary phase
Fluid	Air	Secondary phase
Zones (Boundaries)		
Name: “inlet-water”		
Type	Velocity inlet	-
Velocity magnitude (m/s)	0.984	Corresponds to $Q = Q_e$ = 53.15 m³/s and A = 36 m x 1.5 m = 54 m².
Specification Method	Intensity and Hydraulic Diameter	-
Turbulence Intensity (%)	5	Default
Hydraulic Diameter (m)	5.538	Corresponds to $H = 4 \cdot A/P$ for open channel (i.e. free-surface) flow
Volume Fraction (air)	0	Only water discharged through boundary
Name: “inlet-air”		
Type	Velocity inlet	-
Velocity magnitude (m/s)	0.001	Realistically emulates zero air inflow
Specification Method	Intensity and Viscosity Ratio	-
Turbulence Intensity (%)	5	Default
Turbulent Viscosity Ratio	10	Default
Volume Fraction (air)	1	Only air discharged through boundary
Name: “outlet-conduit”		
Type	Pressure outlet	-
Gauge Total Pressure (Pascal)	0	Default
Specification Method	Intensity and Viscosity Ratio	-
Turbulence Intensity (%)	5	Default
Turbulent Viscosity Ratio	10	Default
Backflow Volume Fraction (air)	1	Only air pressure at boundary

Name: walls		
Wall Motion	Stationary Wall	Default
Shear Condition	No Slip	Default
Roughness Models	Standard	Default
Roughness Height (m)	10	Default
Roughness Constant	0.5	Default
Solution Methods		
Scheme	Coupled	Default
Spatial Discretisation		
Gradient	Least Squares Cell Based	Default
Pressure	PRESTO!	Default
Momentum	Second Order Upwind	More accurate than First Order Upwind
Volume Fraction	Compressive	Default
Transient Formulation	Pseudo Transient	Default
Solution Controls		
Pseudo Transient Explicit Relaxation Factors	Default	-
Run Calculation		
No. of Iterations	30 000	Required to achieve sufficient model (residual) convergence.

4.2.4 Post processing (results)

4.2.4.1 Design 1 (α = 45˚)

Figure 4.2-3 illustrates the corresponding solid 3D geometry boundaries that were modelled, meshed and simulated. Figure 4.2-4 illustrates the corresponding multiphase *volume fraction contour* results generated by *Fluent 19.1*, along a created longitudinal vertical mid-plane. It must be noted that a volume fraction of 1 (i.e. red) represents water flow, whereas a volume fraction of 0 (i.e. blue) represents air. Figure 4.2-5 illustrates the corresponding water *velocity magnitude vector* results generated by *Fluent 19.1*, along the geometry floor surface.

It is apparent from Figure 4.2-4 that relatively significant flow convergence (i.e. damming) occurred centrally at the conduit inlet. The sharp projection of inflowing water towards the centre, due to the wider 45˚ wing-wall orientation, contributed towards the corresponding increase in flow depth. It is apparent from Figure 4.2-5 that the flow was streamlined around the inlet side-walls and into the conduit, and was characterised by relatively low velocity magnitudes.

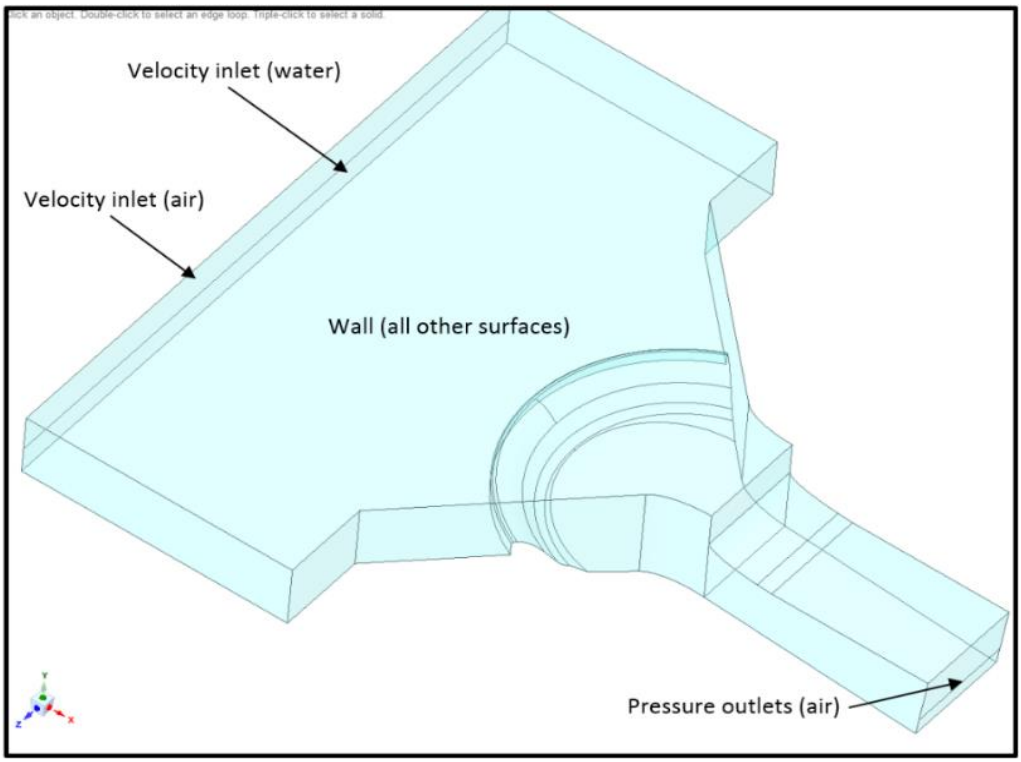

Figure 4.2-3: Design 1 (α = 45˚): geometry boundaries

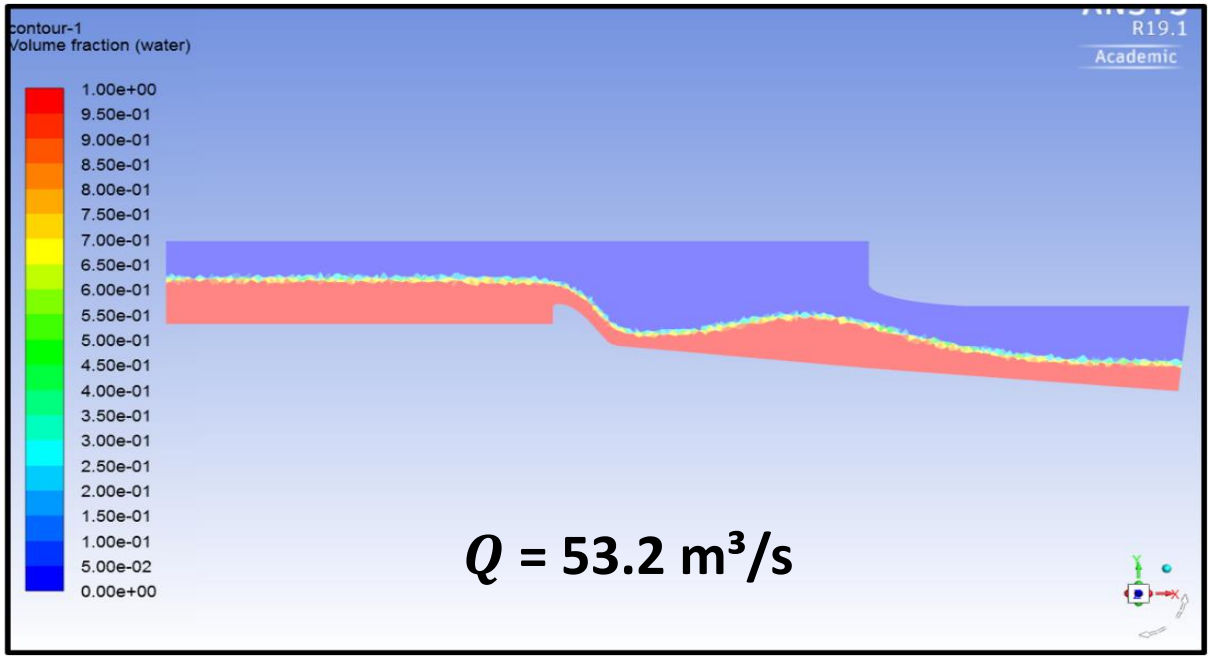

Figure 4.2-4: Design 1 (α = 45˚): long section of simulated water flow profile

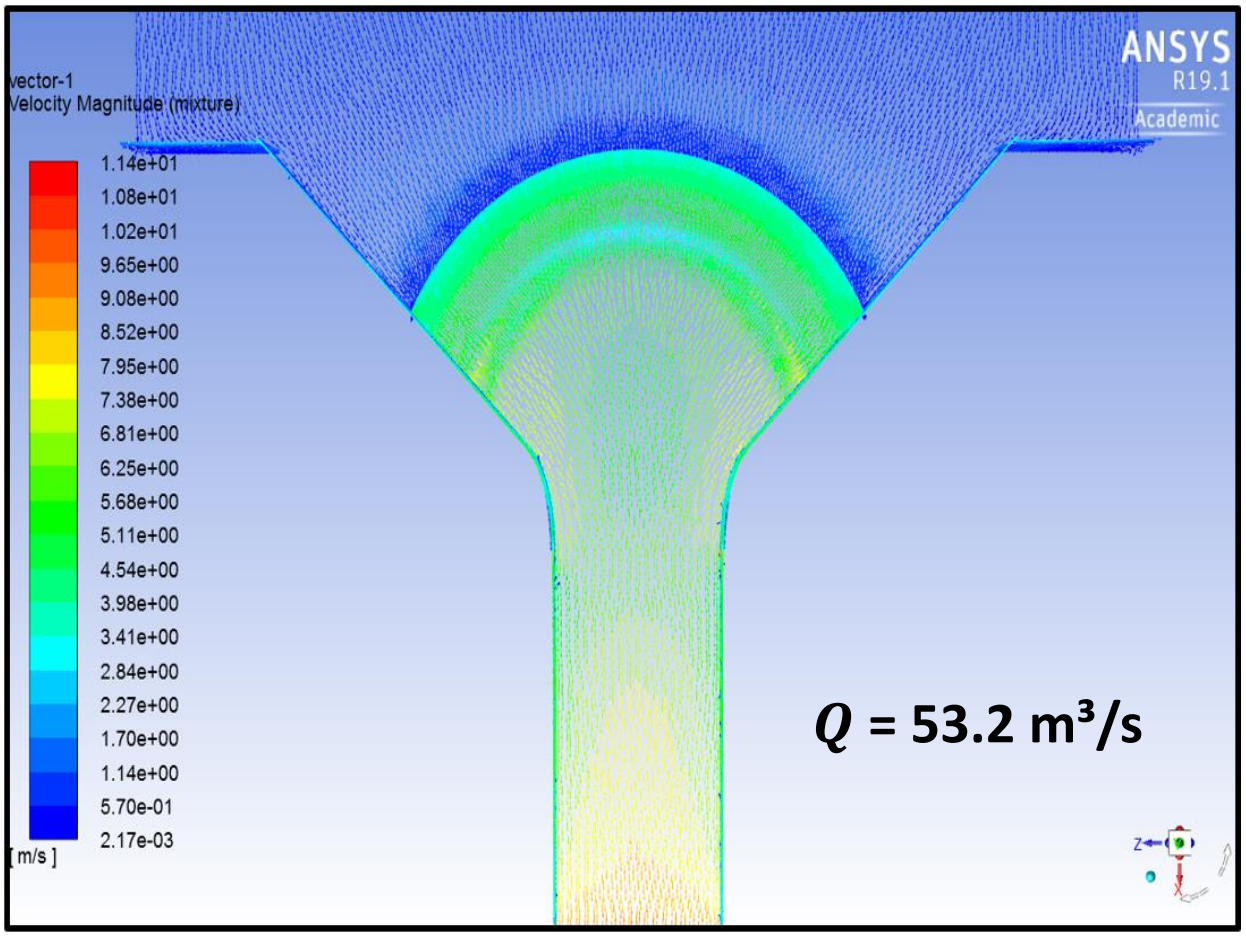

Figure 4.2-5: Design 1 (α = 45˚): plan layout of simulated velocity magnitude vectors

4.2.4.2 Design 1 (α = 30˚)

Figure 4.2-6 illustrates the corresponding solid 3D geometry boundaries that were modelled, meshed and simulated. Figure 4.2-7 illustrates the corresponding multiphase *volume fraction contour* results generated by *Fluent 19.1*, along a created longitudinal vertical mid-plane. It must be noted that a volume fraction of 1 (i.e. red) represents water flow, whereas a volume fraction of 0 (i.e. blue) represents air. Figure 4.2-8 illustrates the corresponding water *velocity magnitude vector* results generated by *Fluent 19.1*, along the geometry floor surface.

It is apparent from Figure 4.2-7 that minor flow convergence (i.e. damming) occurred centrally at the conduit inlet. The gradual projection of inflowing water towards the centre, due to the narrower 30° wing-wall orientation, contributed towards the corresponding increase in flow depth. It is apparent from Figure 4.2-8 that the flow was streamlined around the inlet side-walls and into the conduit, and was characterised by relatively high velocity magnitudes.

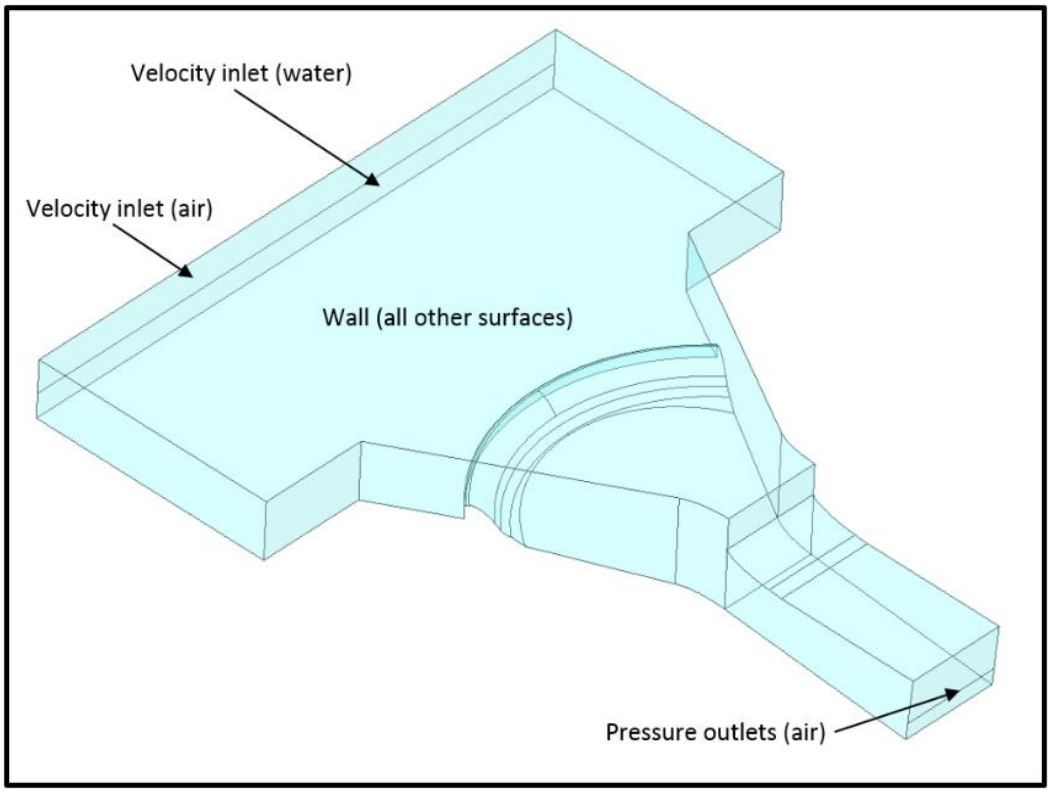

Figure 4.2-6: Design 1 (α = 30˚): geometry boundaries

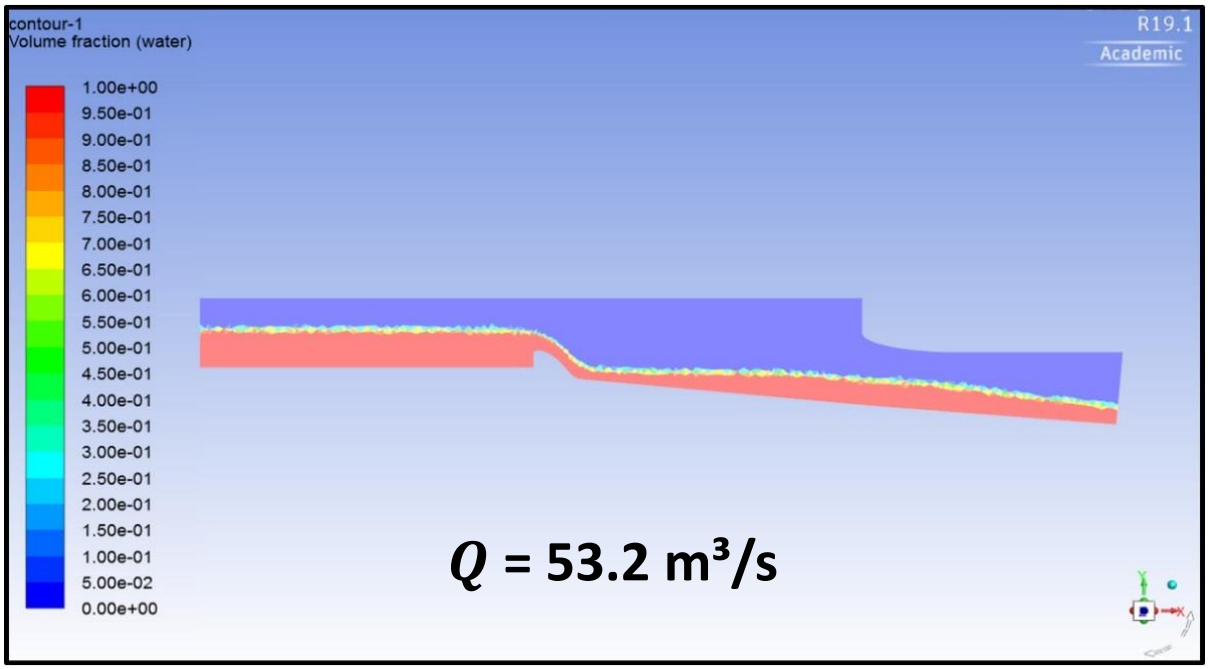

Figure 4.2-7: Design 1 (α = 30˚): long section of simulated water flow profile

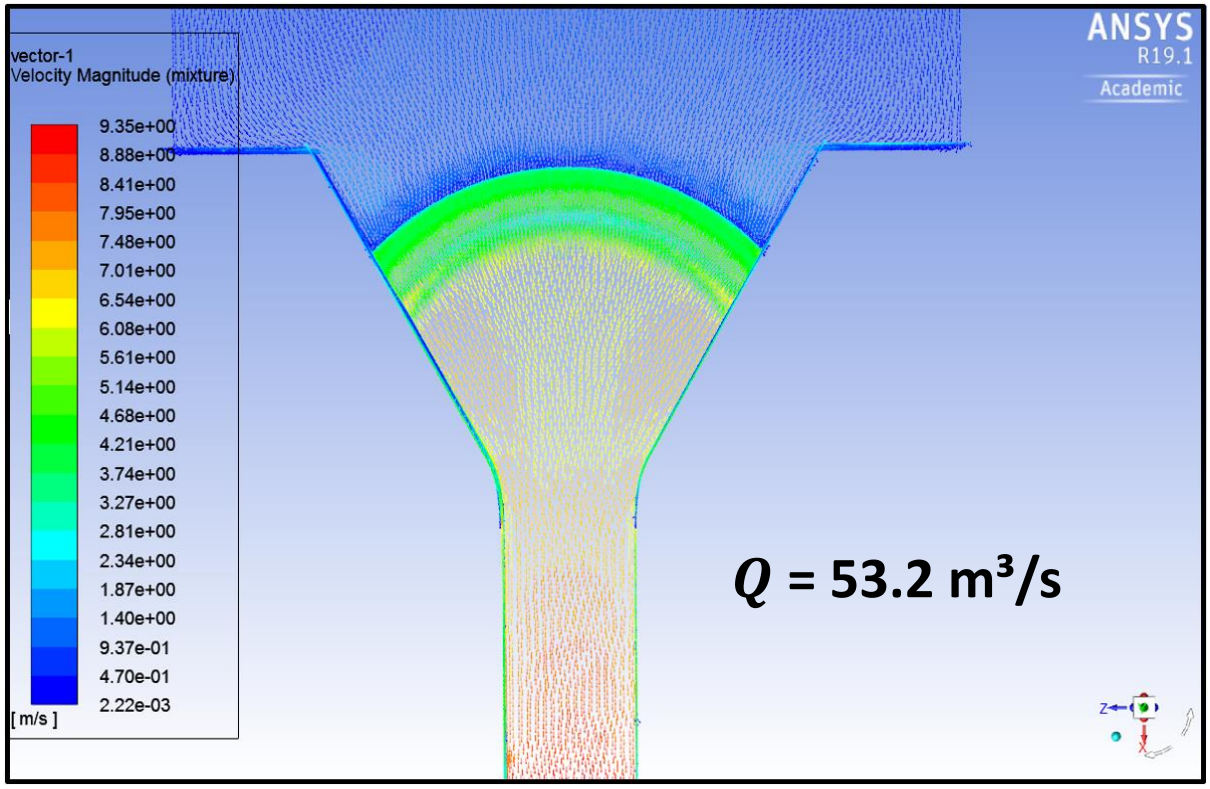

Figure 4.2-8: Design 1 (α = 30˚): plan layout of simulated velocity magnitude vectors

4.2.4.3 Design 2 (α = 45˚)

Figure 4.2-9 illustrates the corresponding solid 3D geometry boundaries that were modelled, meshed and simulated. Figure 4.2-10 illustrates the corresponding multiphase *volume fraction contour* results generated by *Fluent 19.1*, along a created longitudinal vertical mid-plane. It must be noted that a volume fraction of 1 (i.e. red) represents water flow, whereas a volume fraction of 0 (i.e. blue) represents air. Figure 4.2-11 illustrates the corresponding water *velocity magnitude vector* results generated by *Fluent 19.1*, along the geometry floor surface.

It is apparent from Figure 4.2-10 that significant flow convergence (i.e. damming) occurred centrally at the conduit inlet. The sharp projection of faster inflowing water towards the centre, due to the wider 45° wing-wall orientation, contributed towards the corresponding increase in flow depth. It is apparent from Figure 4.2-11 that dead zones (i.e. cavities) developed inside of the conduit where flow velocities were very low. These dead zones increase the risk of sediment deposition which could threaten sluice gate operation.

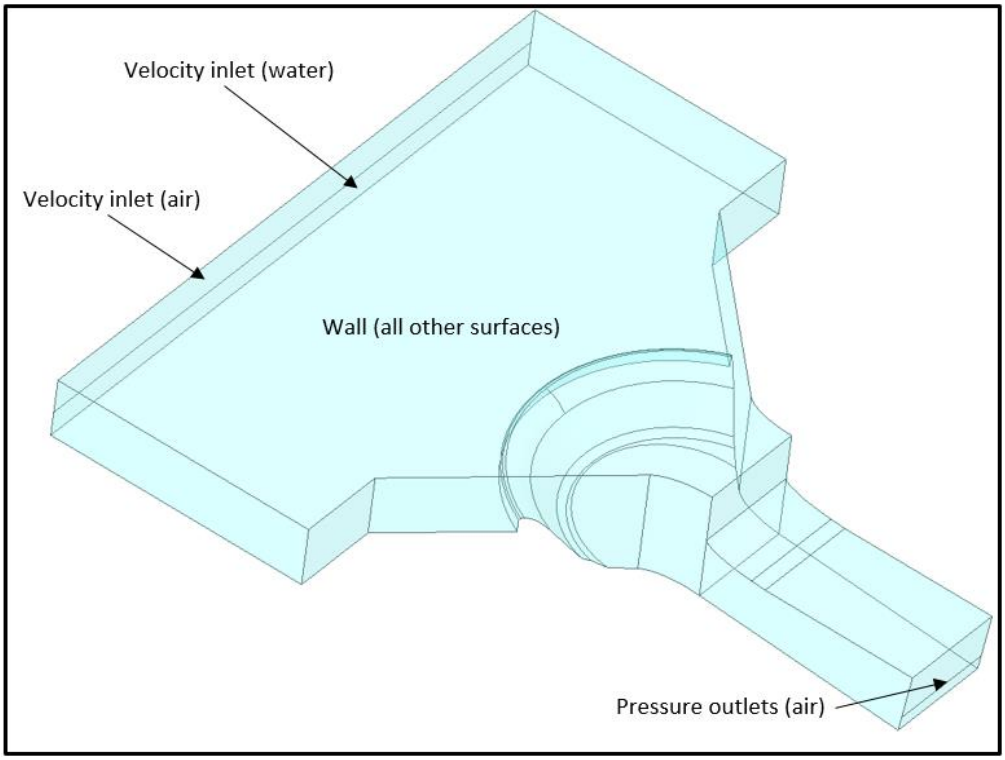

Figure 4.2-9: Design 2 (α = 45˚): geometry boundaries

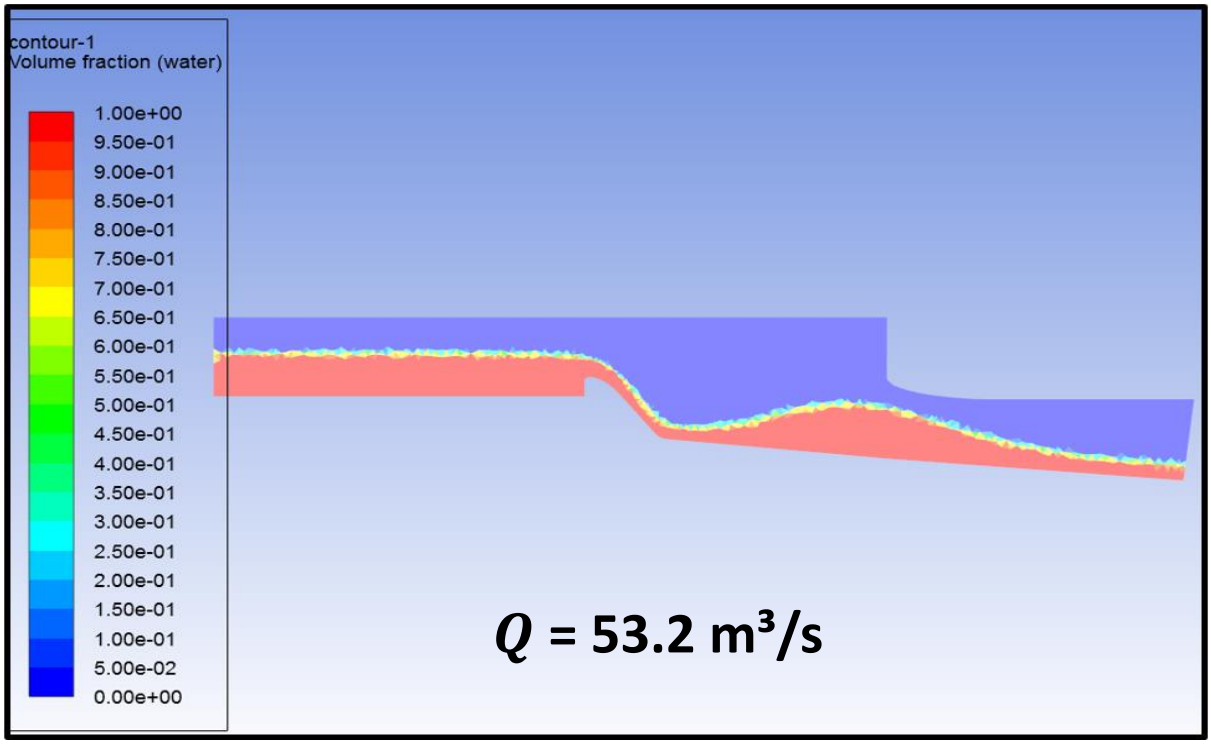

Figure 4.2-10: Design 2 (α = 45˚): long section of simulated water flow profile

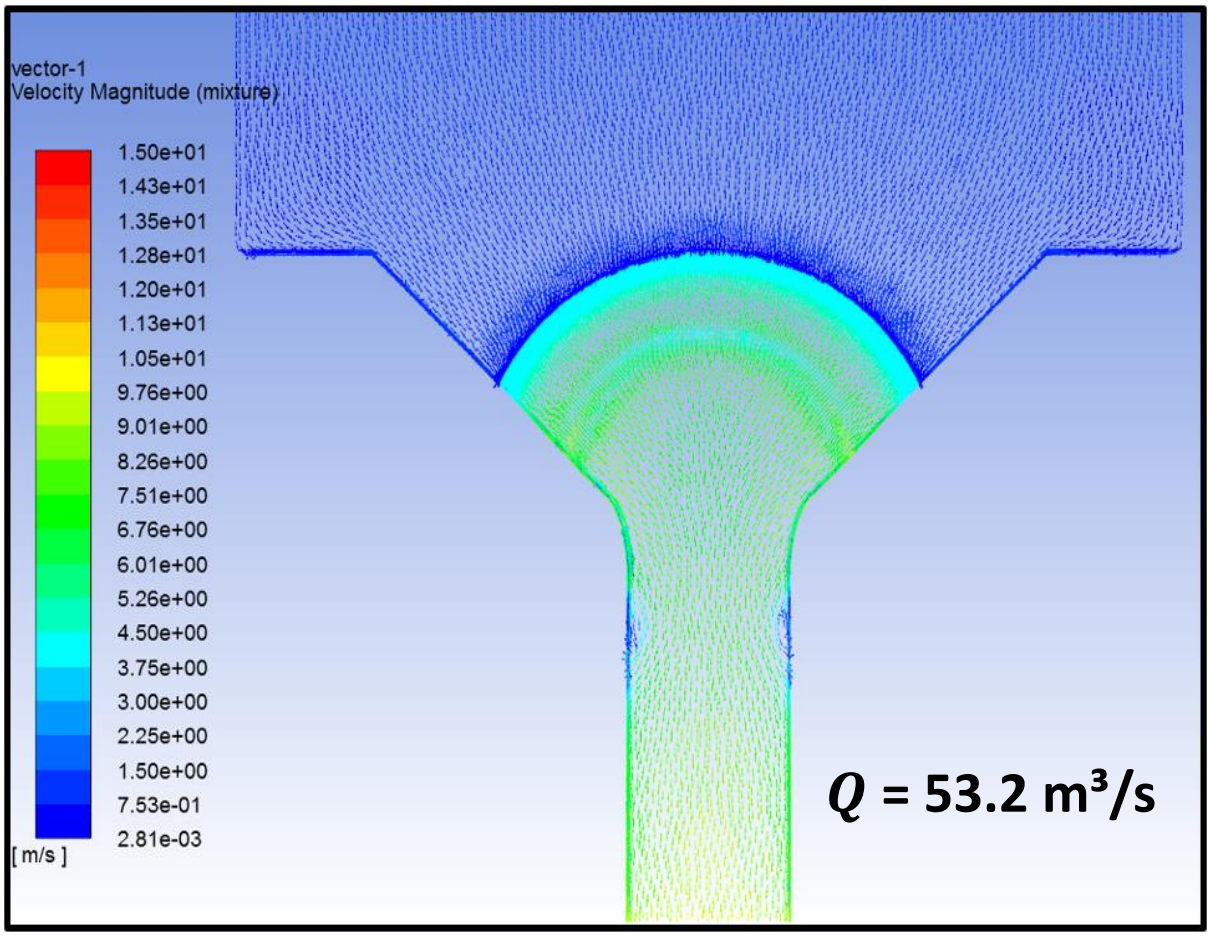

Figure 4.2-11: Design 2 (α = 45˚): plan layout of simulated velocity magnitude vectors

4.2.4.4 Design 2 (α = 30˚)

Figure 4.2-12 illustrates the corresponding solid 3D geometry boundaries that were modelled, meshed and simulated. Figure 4.2-13 illustrates the corresponding multiphase *volume fraction contour* results generated by *Fluent 19.1*, along a created longitudinal vertical mid-plane. It must be noted that a volume fraction of 1 (i.e. red) represents water flow, whereas a volume fraction of 0 (i.e. blue) represents air. Figure 4.2-14 illustrates the corresponding water *velocity magnitude vector* results generated by *Fluent 19.1*, along the geometry floor surface.

It is apparent from Figure 4.2-13 that relatively minor flow convergence (i.e. damming) occurred centrally at the conduit inlet. The gradual projection of faster inflowing water towards the centre, due to the narrower 30° wing-wall orientation, contributed towards the corresponding increase in flow depth. It is apparent from Figure 4.2-14 that the flow was streamlined around the inlet side-walls and into the conduit, and was characterised by high velocity magnitudes.

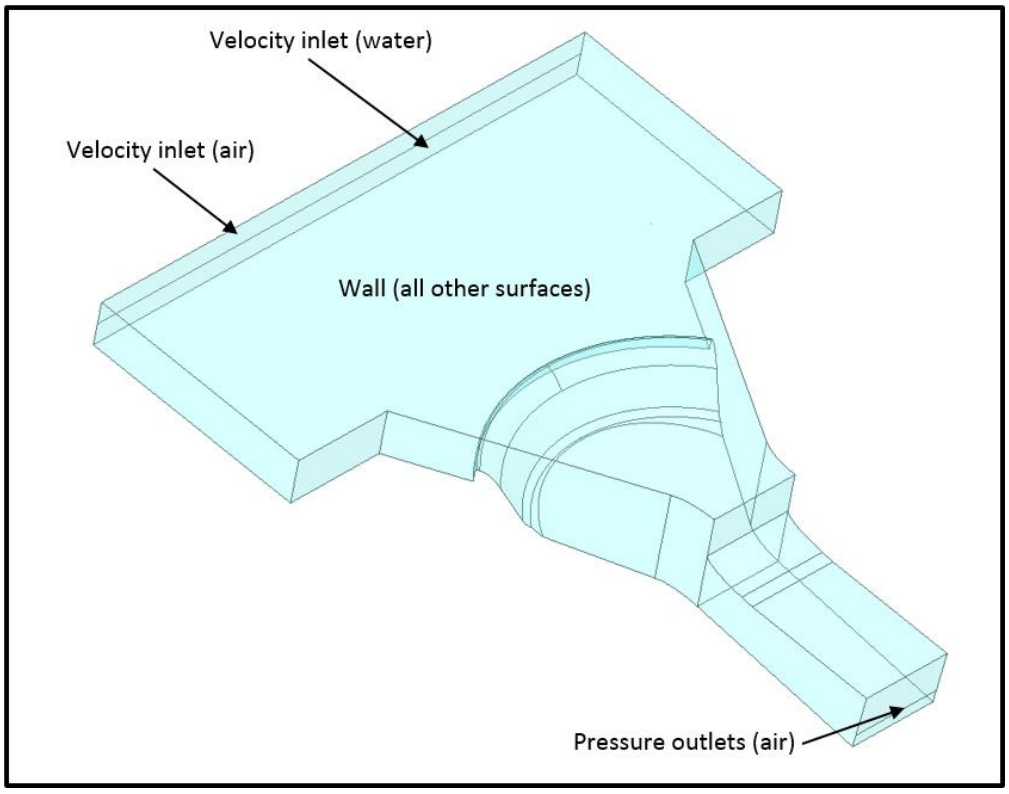

Figure 4.2-12: Design 2 (α = 30˚): geometry boundaries

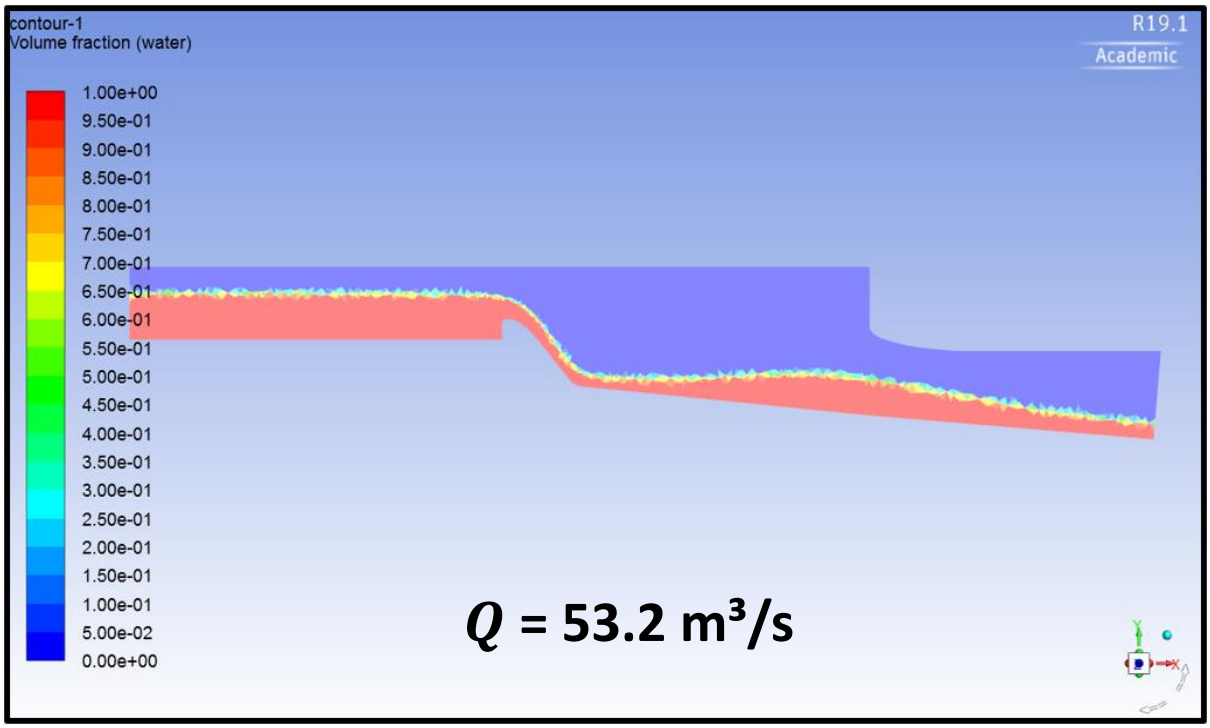

Figure 4.2-13: Design 2 (α = 30˚): long section of simulated water flow profile

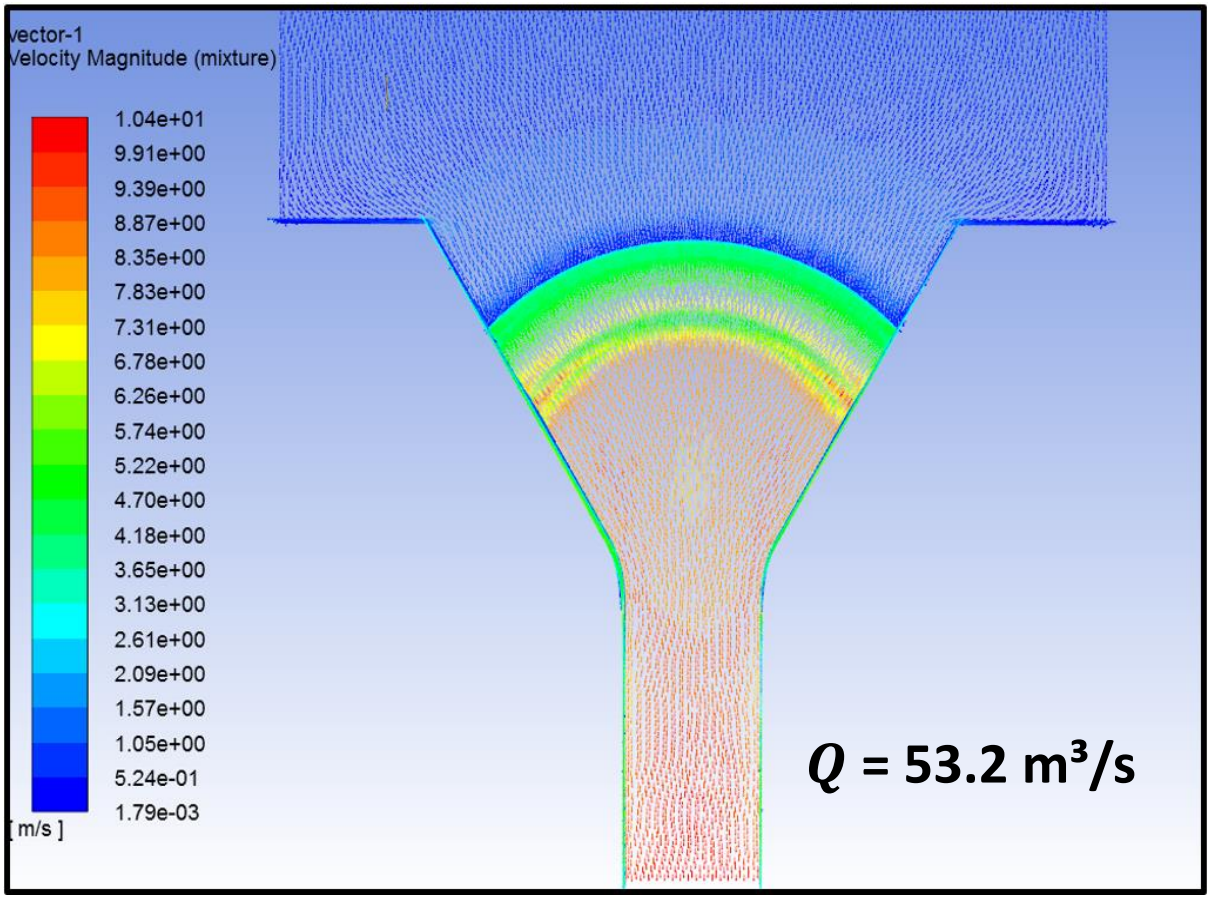

Figure 4.2-14: Design 2 (α = 30˚): plan layout of simulated velocity magnitude vectors

4.3 Final best design option

The hydraulic calculations in Table 4.1-1 suggest that *Design 2 (α = 30˚)* results in the smallest flow depths, highest flow velocities and largest Froude numbers throughout the model, in comparison to the other three designs. It is therefore implied that this design is the best option to maximise supercritical flow behaviour during free-flow flushing.

The numerical CFD simulation results illustrate that *Design 2 (α = 30˚)* produces the fastest streamlined flow throughout the model. This is especially prevalent and critical at the conduit inlet to avoid sediment deposition near the sluice gate area. It must be noted, however, that a slightly larger degree of damming (i.e. flow depth) occurs at the conduit inlet in *Design 2 (α = 30˚)* than in *Design 1 (α = 30˚)*. This is due to the larger inlet energy losses that result from the faster upstream flow velocities in *Design 2*. Regardless, *Design 2 (α = 30˚)* still proves to yield the best overall conditions for supercritical flow behaviour during free-flow flushing.

4.3.1 3D geometry

The refined and finalised version of *Design 2 (α = 30˚)*, implementing the proposed wing-wall design, air vent and calibrated physical model upstream conditions, is illustrated in Figure 3.5-3. Figure 4.3-1 illustrates the corresponding solid 3D geometry boundaries that were modelled, meshed and simulated.

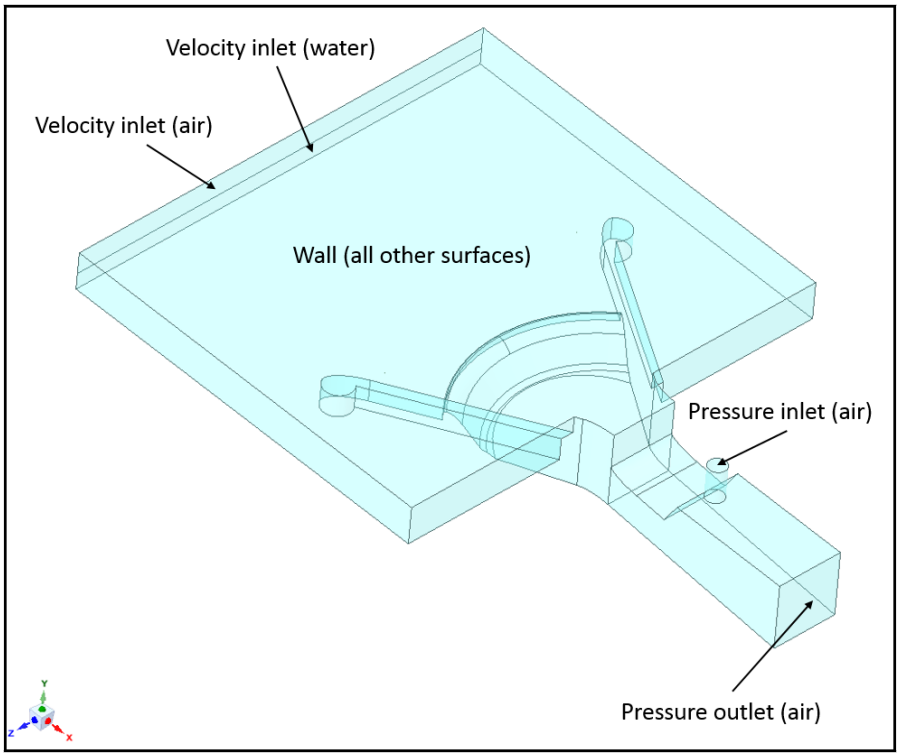

Figure 4.3-1: Final design: geometry boundaries

4.3.2 Meshing

A summary of the important meshing details of the final design model is indicated in Table 4.3-1. The full version of specified meshing details, default settings, inflation mesh details and *Named Selections* are illustrated in the figures of **Appendix A.6**.

Table 4.3-1: Summary of Meshing details for final design model

Parameter	Value or option	Comments
Sizing		
Max Element Size (m)	0.301	Smallest allowable size chosen to create finest possible mesh.
Capture Curvature	Yes	Required for models with curved surfaces to improve mesh quality.
Capture Proximity	Yes	Automatically created finer meshes around regions of complex geometry transition.
Quality		
Mesh Metric	Orthogonal Quality	-
Minimum Orthogonality Quality	0.193	Must be larger than 0.1 for a stable mesh.
Maximum Orthogonality Quality	1	The larger the fraction the better the mesh quality.
Average Orthogonality Quality	0.869	The larger the fraction the better the mesh quality (preferably larger than 0.75).

Inflation	Yes	Manually created finer meshes along specified critical surfaces.
Assembly Meshing		
Method	Tetrahedrons	Method found to maximise mesh quality.

4.3.3 Simulation setup

The full version of the *Fluent Setup* details for the final design model is illustrated in the figures of **Appendix A.7**. A summary of the important *Fluent* Setup details is indicated in Table 4.2-2. In this case, however, the maximum design discharge (Q_e) for free-flow flushing was simulated as 119 m³/s. This value was calibrated from the physical model as the maximum discharge that could be flushed without causing submergence of the conduit inlet. This condition was exclusive to water flowing over the weir crest, resulting in a required wing-wall crest level of 2 m above the weir crest to avoid water spilling over the sides. The only subsequent changes to the *Setup* details in Table 4.2-2 are indicated in Table 4.3-2.

Table 4.3-2: Summary of *Fluent Setup* details for final design model

Parameter	Value or option	Comments
Zones (Boundaries)		
Name: "inlet-water"		
Velocity magnitude (m/s)	1.983	Corresponds to $Q = Q_e$ = 119 m³/s and A = 40 m x 1.5 m = 60 m²
Hydraulic Diameter (m)	5.581	Corresponds to $H = 4 \cdot A/P$ for open channel (i.e. free-surface) flow
Run Calculation		
No. of Iterations	60 000	Required to achieve sufficient model (residual) convergence.

4.3.4 Post processing (results)

Figure 4.3-2 illustrates the corresponding multiphase *volume fraction contour* results generated by *Fluent 19.1*, along a created longitudinal vertical mid-plane. It must be noted that a volume fraction of 1 (i.e. red) represents water flow, whereas a volume fraction of 0 (i.e. blue) represents air. Figure 4.3-3 illustrates the corresponding water *velocity magnitude vector* results generated by *Fluent 19.1*, along the geometry floor surface.

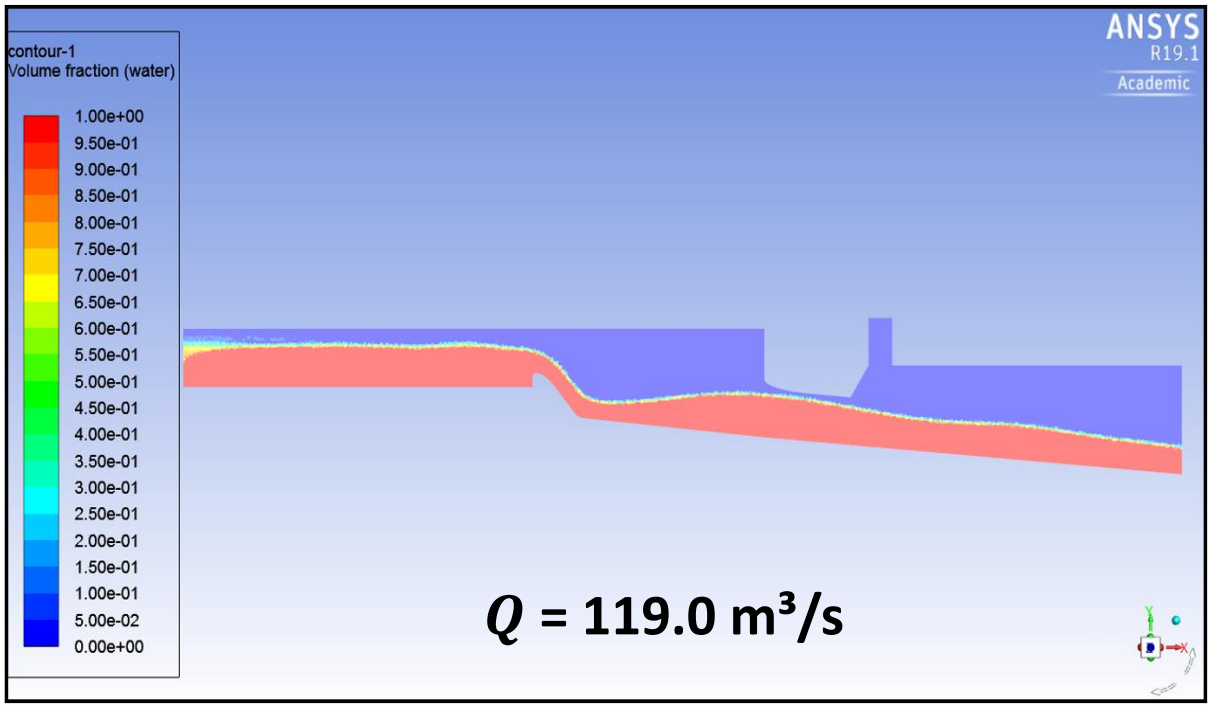

Figure 4.3-2: Final design: long section of simulated water flow profile

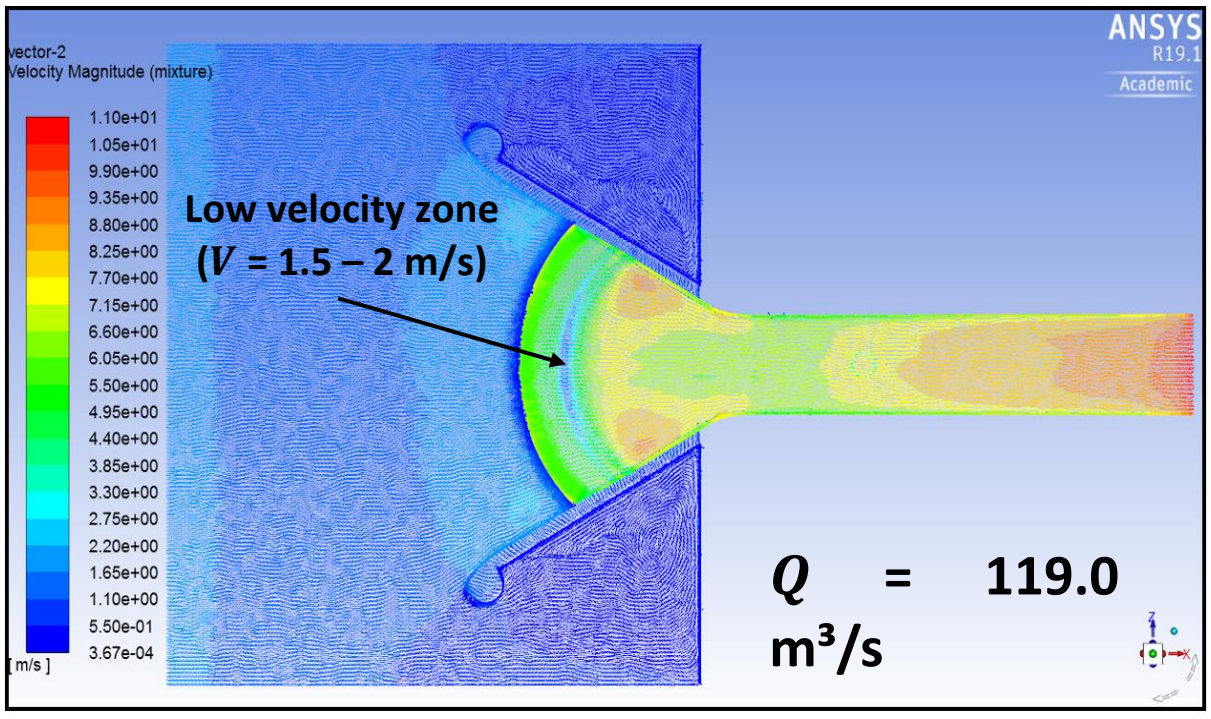

Figure 4.3-3: Final design: plan layout of simulated velocity magnitude vectors

4.3.5 Summary of final CFD design

The following conclusions were drawn from the CFD modelling of the proposed final design:

1. It is visible from Figure 4.3-2 that a flushing discharge (Q) of 119 m³/s results in a water flow profile that marginally avoids contact with the conduit inlet soffit. This therefore reaffirms that the physically determined Q_e = 119 m³/s is accurate. Figure 4.3-3 visually reaffirms the suitable degree of flow acceleration, velocity magnitude and streamlined conditions through the conduit inlet.

2. A section of significantly low-velocity flow vectors (V = 1.5 – 2 m/s) has been generated along the region of the reverse bottom curve. This suggests a possible dead zone location for sediment deposition during flushing, which will need to further be addressed and refined (if necessary) in the physical model.

3. Considering Shield's parameter, the theoretical maximum particle sizes (d_1) to be subjected to lifting from both the intake bed surface and conduit bed surface during free-flow flushing of $Q = Q_e$ = 119 m³/s were conservatively calculated as described in the tables of **Appendix A.8**. A summary of the important design parameter values is indicated in Table 4.3-3.

   According to Table 4.3-3, and based on the requirement check specified in Section 3.5.9.1 (*Intake bed surface*), the transition from the chosen upstream bed slope (m) of 1:10 to the conduit bed slope (ϕ) of 1:12 is theoretically suitable for sediment flushing purposes.

Table 4.3-3: Maximum sediment particle sizes transported along design bed surfaces (based on analytical calculations)

	Intake bed surface (centreline)	Low-level outlet conduit (normal flow conditions)
Energy slope (S_f) (m/m)	0.048	0.083
Average flow depth (y_{avg}) (m)	2.069	1.212
Maximum sediment size subjected to lifting (d_1) (m)	1.098	1.111

5 Physical model and results

5.1 Introduction

A 1:40 scale physical model of the prototype design of the postulated flushing system, which evolved from the findings of the numerical model simulations (Section 4, *Numerical model and results*), was built for further testing and refinement. The model was needed to test the robustness, reliability and actual flushing capability of the design, considering different design sediment sizes, sediment depths and flushing conditions (i.e. pressure flushing and free-flow flushing with drawdown). Relatively coarse sediment was tested due to their presence in run-of-river schemes as well as at larger dams where the reservoir contains a high percentage of sediment.

The horizontal length of the low-level outlet conduit (i.e. from p_3 to p_5) was chosen to be 1.200 m (i.e. 48 m in prototype) in the physical model in order to: (1) keep the conduit relatively short (realistic in concrete dams); and (2) maximise the available head in the model above the conduit inlet invert level for pressure flushing. The entire model was placed in a 1 x 40 x 1.15 m deep laboratory glass flume with a flat bed for hydraulic testing, as illustrated in Figure B.1 in **Appendix B**.

It must be noted that all results in this section are given as prototype values, according to the 1:40 scale. The only model scale values referred to are the median particle diameters (d_{50}) of the different sediment groups considered for flushing tests. After Section 5.6.1 (*Sediment sizing and properties*), the prototype effective particle diameter (d_{eff}) values will be referred to for representation of the respective sediment size groups.

5.2 Prototype-model similarity laws

Various similarity laws exist which can be used to scale geometric (i.e. shape), kinematic (i.e. motion) and dynamic parameters from physical prototype (i.e. full scale) to model scale, and vice versa, with no scale effects occurring (Heller, 2011). Such similarity laws include Euler's Law, Weber's law, Reynold's Law and Froude's Law.

Froude's Law describes the dynamic similarity between physical model and prototype and is solely governed by the force of gravity. The law states that in the case of free-surface flow, flow is acted upon by gravitational and inertial forces in an identical manner in both prototype and scaled model (Webber, 1971). As gravity is the dominant force acting upon the flow in the physical hydraulic model, with free-surface flow always occurring throughout the low-level outlet conduit (i.e. orifice flow during pressure flushing), prototype-model similarity is obtained by Froude's law. The prototype-model scalar relationships of the different parameters according to Froude's Law are indicated in Table 5.2-1.

Table 5.2-1: Froude's Law scalar relationships (Webber, 1971)

Parameter	SI Unit	Natural scale (1: λ)
Geometric		
Length	m	λ
Area	m^2	λ^2
Volume	m^3	λ^3
Kinematic		
Time	s	$\lambda^{1/2}$
Velocity	m/s	$\lambda^{1/2}$
Acceleration	m/s^2	1
Discharge	m^3/s	$\lambda^{5/2}$
Dynamic		
Pressure	P_a	$\rho_r\lambda$
Force	N	$\rho_r\lambda^3$
Energy	J	$\rho_r\lambda^4$
Power	W	$\rho_r\lambda^{7/2}$

**where $\rho_r = \rho_p/\rho_m$ (density of water)*

5.3 Sediment scaling

Rooseboom *et al.* (1983) recommend using the particle settling velocity and the Modified Liu Diagram to represent the hydraulic behaviour (i.e. incipient motion) of sediment particles in scaled physical models with movable beds. Therefore, once the physical settling velocities of a sample of sediment have been determined, the representative sediment size (d) can be implicitly calculated according to settling velocity equations. The remaining parameters for the Modified Liu Diagram can subsequently be calculated.

The dimensions of a sediment particle with a diameter (d) larger than 6 mm can be scaled linearly between prototype and scaled physical model, and vice versa (Liu, 1957).

5.4 Apparatus

The following facilities, equipment and materials were used to construct the model:

- 1 x 40 x 1.15 m deep laboratory glass flume with a smooth and flat bed.
- Flow pipe inlet.
- Flow or volt-meter.
- A 1 x 1 x 0.01 m steel plate that could slot into the flume (i.e. "dam wall").
- Sheets of Perspex (10 mm thick) to construct the regular-shaped model components.
- A low-density, low-cost plastic (e.g. PLA) to be used for 3D printing or CNC cutting the curved model components.
- A 40 mm PVC pipe to be used as the air vent.
- Upstream V-notch weir (90 degrees)
- Dumpy level and vertically-fixed needle.
- Submersible pump (for pumping out water upstream of steel plate).
- Approximately 1 m^3 of each sediment group considered for hydraulic testing.

5.5 Construction methodology

The following steps were followed in the construction of the physical model:

1. Constructed and assembled the physical model components of the low-level outlet conduit, air vent, wing-walls and intake structure according to the CFD design specifications.

2. Inserted the cut-out steel plate into the gate slots inside of the flume. The gate slots were then sealed on both sides of the plate.

3. Installed a 10 mm thick platform (supported by bricks) that was level with the bottom crest of the rectangular hole in the steel plate. This platform extended until 2 m upstream of the steel plate to conservatively allow for sufficient length for approach flow conditions. The platform was sealed along its sides where it made contact with the steel plate and flume inside-walls.

4. Fixed the ogee-spillway and wing-wall model components onto the platform at the correct locations upstream of the steel plate.

5. Fixed, reinforced and sealed the rest of the model components to the downstream face of the steel plate and ogee-spillway component.

6. Surveyed the model with a dumpy level to ensure that: (1) the conduit bed slope (ϕ) was 1:12; (2) the weir crest and wing-wall crests were levelled; (3) the elevation of the weir crest, wing-wall crests and conduit invert levels were correct in relation to each other.

7. Used the vertically-fixed needle, mounted at the top of the flume, to determine the elevations of chosen hydraulic measuring points along the centreline of the model bed surfaces. The conduit inlet invert level was used as the general reference point, with an elevation of 0 m. The longitudinal profile of the physical model showing these chosen measuring points is illustrated in Figure 5.5-1. The respective measuring point elevations, relative to the conduit inlet invert level, are indicated in Table 5.5-1.

8. Once all physical model flushing tests have been completed considering the proposed intake structure (i.e. ogee spillway structure and wing-walls), remove the intake structure and insert a flat upstream bed that is level with the start point of the conduit bed slope (i.e. p_3). This scenario is illustrated in Figure B.2 in **Appendix B**.

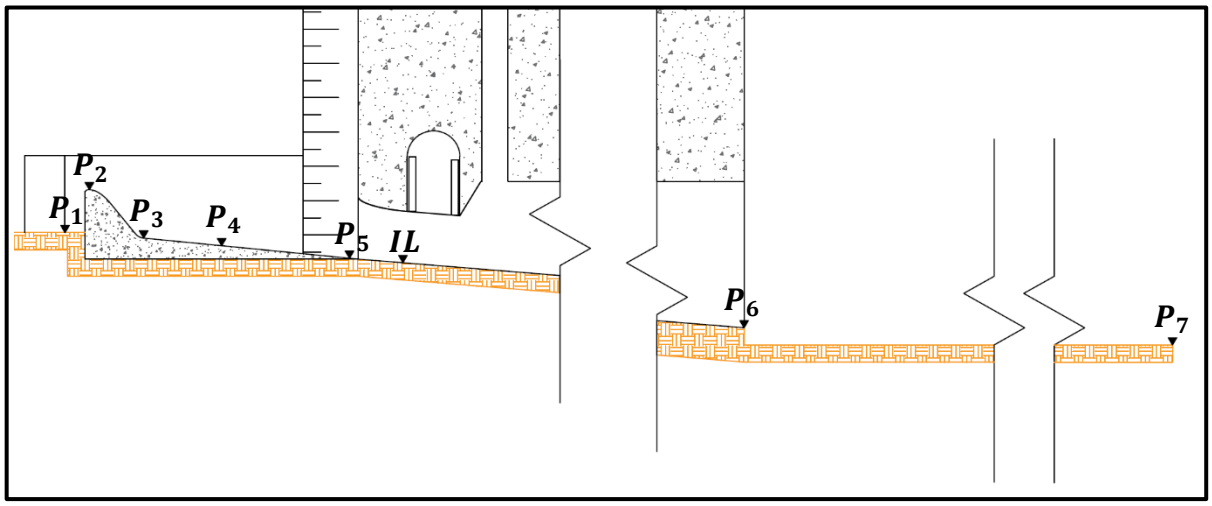

Figure 5.5-1: Chosen measuring points along physical model

Table 5.5-1: Elevations of chosen measuring points relative to conduit inlet invert level

Measuring point	Value	Unit	Location description
P_1	1.781	m	Local NGL upstream of weir
P_2	4.280	m	Weir crest
P_3	1.480	m	Downstream edge of reverse bottom curve
P_4	1.000	m	Centre of intake bed surface
P_5	0.280	m	Immediately upstream of conduit opening
IL	0	m	Conduit inlet invert level
P_6	-3.820	m	Conduit outlet
P_7	-4.820	m	180 m downstream of P_6 (for tailwater levels controlled by downstream sluice gate)

5.6 Experimental testing and results

5.6.1 Sediment sizing and properties

Four different sediment size groups were considered for hydraulic testing in the physical model. These non-cohesive sediments were graded by sieve analysis by the supplier, from whom the respective median particle diameter (d_{50}) values were obtained. The representative particle size (d) of a uniformly graded sediment sample is typically given by the d_{50} value (as for this study). The model d_{50} values that were ultimately used were: (1) 0.095 mm; (2) 13.2 mm (3) 19 mm; and (4) 37.5 mm.

5.6.1.1 Bulk particle density

The calculated bulk particle densities (ρ_b) of the respective sediment groups (according to Equation 2-3), as well as the associated physically-measured parameter values, are indicated in Table 5.6-1. For settling velocity calculations (later), $\rho_s = \rho_b$.

Table 5.6-1: Bulk particle densities of different sediment groups

	d_{50} = 13.2 mm	d_{50} = 19 mm	d_{50} = 37.5 mm
m_b (g)	500.0	503.0	530.8
$(m_c - m_d)$ (g)	316.9	319.2	331.5
m_a (g)	503.4	506.0	531.3
ρ_{wT} (kg/m³)	997.0	997.0	997.0
ρ_b (kg/m³)	2673	2685	2649

5.6.1.2 Particle settling velocity

A sample of 30 sediment particles were considered for laboratory settling velocity tests for each sediment group. The settling velocity tests were conducted as follows:

1. Two different cylindrical tanks were filled with water. The size or height of the tanks was chosen so as to accurately determine the sediment particles terminal velocity i.e. a deeper tank depth for the larger particles. A physical mark was made slightly below the water surface to indicate the point from which the submerged sediment particles would be released. The height between the mark and the tank floor represented the settling depth (h). For the d_{50} = 13.2 mm and d_{50} = 19 mm samples, a 2 m high tank and h = 1.9 m were used. For the d_{50} = 37.5 mm sample, a 5.5 m high tank and h = 5.16 m were used. Since the terminal settling velocity of sediment in water is reached rapidly, the height required for a particle to transition from rest to terminal velocity is relatively small in comparison with the selected tank heights (h) for the above cases.
2. The three mutually perpendicular particle dimensions were measured for each particle in each sample with a calliper.
3. Each particle was subsequently released from rest at the corresponding settling depth (h) and timed with a stopwatch until it hit the tank floor. Sound was used as an indicator to stop timing.
4. The respective physical settling velocities were calculated by dividing the specific settling depth by the corresponding recorded settling times.

All the measured values of the above-mentioned parameters are recorded in the tables of **Appendix B.3**. The resulting settling velocity (V_{ss}) distributions for the different sediment groups are indicated in Table 5.6-2 and illustrated in Figure 5.6-1.

Table 5.6-2: Settling velocity distribution for different sediment groups

	Settling velocity (m/s)		
% passing	d_{50} = 13.2 mm	d_{50} = 19 mm	d_{50} = 37.5 mm
0	0.304	0.363	0.712
10	0.408	0.412	0.760
15	0.419	0.450	0.781
50	0.482	0.526	0.917
85	0.587	0.609	1.037
90	0.606	0.621	1.168
100	0.631	0.655	1.262

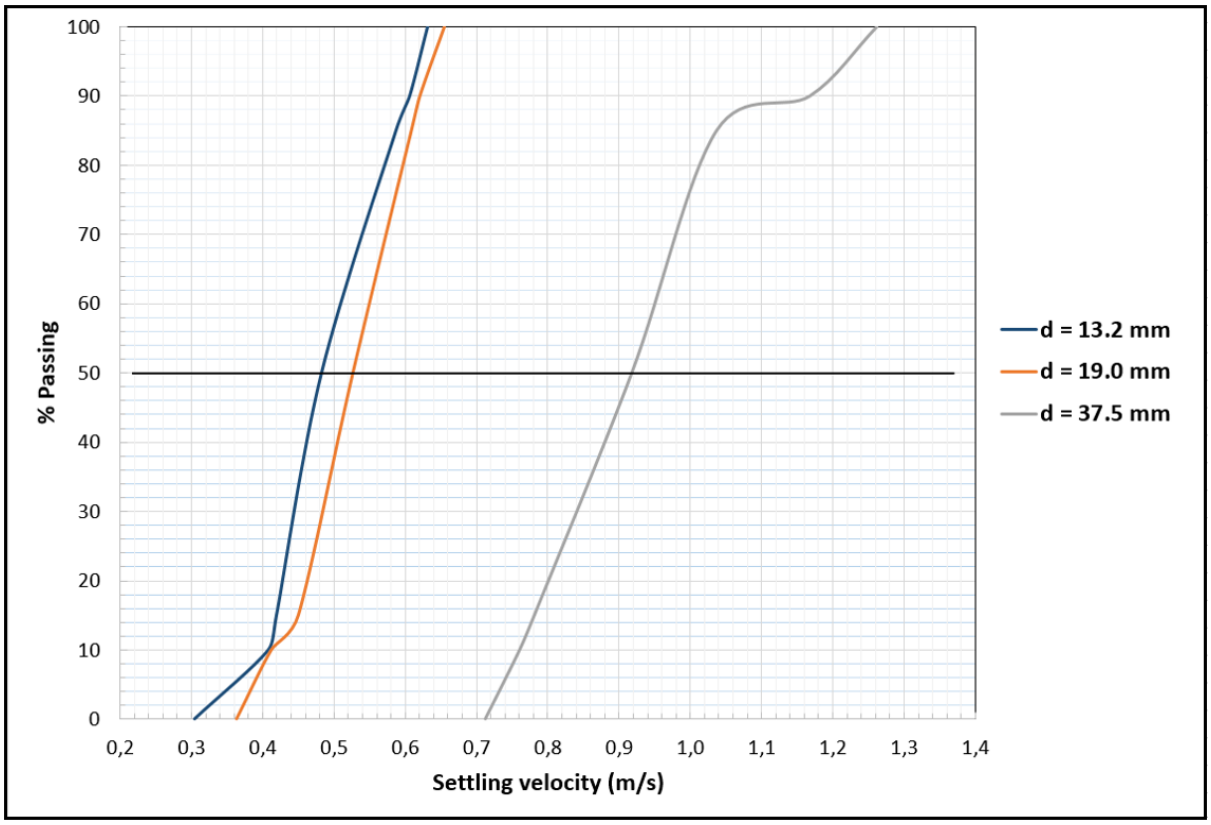

Figure 5.6-1: Settling velocity distribution for different sediment groups

5.6.1.3 Effective particle diameter

The effective particle diameter (d_{eff}) of a sediment group represents the d_{50} value that theoretically corresponds to the measured settling velocities of a sample of sediment. The physically-measured sediment particle dimensions and settling velocities from Section 5.6.1.2 (*Particle settling velocity*) were used to implicitly calculate the respective matching particle diameters (d), as indicated in the tables of **Appendix B.3**. The d_{eff} was then calculated as the median particle diameter (d_{50}) of the sample as indicated in Table 5.6-3.

Table 5.6-3: Effective particle diameters of different sediment groups

	d_{50} = 13.2 mm	d_{50} = 19 mm	d_{50} = 37.5 mm
d_{eff} (mm)	11.70	16.46	38.31

5.6.1.4 Sediment group: d_{50} = 0.095 mm

This physical sediment size and type represents *very fine sand* according to Table 2.1-1, and is the finest non-cohesive sand that can be used for hydraulic testing (Dreyer, 2018). A summary of the calculated sediment properties is indicated in Table 5.6-4.

Table 5.6-4: Summary of d_{50} = 0.095 mm sediment properties (Dreyer, 2018)

Parameter	Unit	Value
Bulk particle density (ρ_b)	kg/m³	1461
Specific gravity (SG)		2.65
Median particle diameter (d_{50})	mm	0.095
Effective particle diameter (d_{eff})	mm	0.090
Effective settling velocity ($\overline{V_{ss}}$)	m/s	0.0065

If the effective diameter (d_{eff}) were to be scaled linearly to prototype size, considering a 1:40 scale, it would represent *very fine gravel* according to Table 2.1-1 (i.e. d_{eff} = 3.6 mm).

5.6.1.5 Sediment group: d_{50} = 13.2 mm

This physical sediment size and type represents *medium gravel* according to Table 2.1-1. A summary of the calculated sediment properties is indicated in Table 5.6-5.

Table 5.6-5: Summary of d_{50} = 13.2 mm sediment properties

Parameter	Unit	Value
Bulk particle density (ρ_b)	kg/m³	2673
Specific gravity (SG)		2.67
Median particle diameter (d_{50})	mm	13.2
Effective particle diameter (d_{eff})	mm	11.7
Effective settling velocity ($\overline{V_{ss}}$)	m/s	0.482

If the effective diameter (d_{eff}) were to be scaled linearly to prototype size, considering a 1:40 scale, it would represent *small boulders* according to Table 2.1-1 (i.e. d_{eff} = 468 mm).

5.6.1.6 Sediment group: d_{50} = 19 mm

This physical sediment size and type represents *coarse gravel* according to Table 2.1-1. A summary of the calculated sediment properties is indicated in Table 5.6-6.

Table 5.6-6: Summary of d_{50} = 19 mm sediment properties

Parameter	Unit	Value
Bulk particle density (ρ_b)	kg/m³	2685
Specific gravity (SG)		2.69
Median particle diameter (d_{50})	mm	19
Effective particle diameter (d_{eff})	mm	16.5
Effective settling velocity ($\overline{V_{ss}}$)	m/s	0.526

If the effective diameter (d_{eff}) were to be scaled linearly to prototype size, considering a 1:40 scale, it would represent *medium boulders* according to Table 2.1-1 (i.e. d_{eff} = 659 mm).

5.6.1.7 Sediment group: d_{50} = 37.5 mm

This physical sediment size and type represents *very coarse gravel* according to Table 2.1-1. A summary of the calculated sediment properties is indicated in Table 5.6-7.

Table 5.6-7: Summary of d_{50} = 37.5 mm sediment properties

Parameter	Unit	Value
Bulk particle density (ρ_b)	kg/m³	2649
Specific gravity (SG)		2.65
Median particle diameter (d_{50})	mm	37.5
Effective particle diameter (d_{eff})	mm	38.3
Effective settling velocity ($\overline{V_{ss}}$)	m/s	0.917

If the effective diameter (d_{eff}) were to be scaled linearly to prototype size, considering a 1:40 scale, it would represent *large boulders* according to Table 2.1-1 (i.e. d_{eff} = 1532 mm).

5.6.2 Tested sediment depths

Two different upstream sediment bed scenarios were considered for hydraulic testing, namely:

1. ***Sediment depth 1***: This scenario involved filling the intake area with an individual sediment group until level with the conduit inlet soffit level. This ultimately avoided blockage of the inlet during flushing with the toe of each sediment bed forming near the inlet invert level at the angle of repose. The sediment bed upstream and adjacent to the intake area always consisted of the d_{eff} = 0.468 m sediment group and was raised until level with the low-weir crest level. This was the smallest sediment size considered for testing that did not scour locally during flushing, thus providing consistent approach flow conditions during different tests. The sediment bed was extended until about 100 m (prototype) upstream of the dam in order to model realistic approach flow conditions during free-flow flushing tests.

2. ***Sediment depth 2*****:** This scenario involved filling the upstream area with an individual sediment group until level with the recommended wing-wall crest level. This level corresponded to slightly more than twice the conduit inlet height (i.e. 6 m) above the inlet invert level. This scenario was applied to all but the d_{eff} = 1.532 m sediment group in order to ultimately avoid blockage of the inlet during flushing, with the toe of each of the respective sediment beds forming near the inlet invert level at the angle of repose. Each respective sediment bed was extended until about 100 m (prototype) upstream of the dam in order to model realistic approach flow conditions during free-flow flushing tests.

Typical layouts of the two sediment bed configurations are illustrated in Figure 5.6-2. The respective sediment bed setups for the different sediment groups are illustrated in the figures of Section B.4 in **Appendix B**.

Figure 5.6-2: Upstream sediment bed setups for d_{eff} = 0.659 m sediment group

5.6.3 Tested pressure flushing water levels

Three different upstream water levels (H_u) were considered for pressure flushing testing, namely:

1. ***Water level 1:*** This represents the lowest chosen water level and related to the physically identified minimum submergence requirement (h_{min}) to avoid the formation of vortices during pressure flushing in the physical model. This value was identified as 24.16 m above the conduit inlet invert level (compared to 29.14 m calculated in Section 3.4.3, *Minimum submergence requirement of conduit inlet*).

2. ***Water level 2:*** This represents the intermediate water level between *water level 1* and *water level 3*. This value was calculated as 29.08 m above the conduit inlet invert level.

3. ***Water level 3:*** This represents the maximum available head that could be achieved in the physical model. This value was identified as 34 m above the conduit inlet invert level.

The above-mentioned water level scenarios in the physical model are illustrated in Figure B.5 in **Appendix B.4**.

5.6.4 Free-flow flushing

5.6.4.1 Test procedure

Firstly, it was necessary to physically determine the maximum discharge (Q_e) that could flush without submerging the conduit inlet. This was done by incrementally increasing the flow until just before water made contact with the conduit inlet soffit. It was necessary to simultaneously raise the wing-wall crest level to prevent water from spilling over the sides during flushing, as illustrated in Figure B.3 in **Appendix B**. Overflow was found to disrupt the supercritical flow along the spillway, causing the inlet to submerge for lower flows, therefore minimising the free-flow discharge capacity. The maximum discharge (Q_e) was determined in the presence of an upstream sediment bed that was level with the weir crest (i.e. P = 0 m). This naturally maximised the design head above the weir crest and consequently minimised the discharge required to submerge the inlet, which was more conservative to design for. The determined Q_e value was therefore the limit for free-flow flushing, after which pressure flushing began to occur.

For each subsequent free-flow flushing test considering sediment flushing, the following systematic approach was followed:

1. For the dry setup, fill and level the intake and local upstream area with the respective sediment group according to either *sediment depth 1* or *sediment depth 2*.

2. Ensure that the sluice gate at the downstream end of the flume is fully open (i.e. there must be no downstream tailwater effects).

3. Starting at 0 m³/s, increase the approach flow discharge in small increments until the intake area is fully flushed of sediment. Use the upstream V-notch weir and adjusted needle to identify once the flow has stabilised for each increment, as well as to verify the critical discharge (Q_{fc}) to fully flush the intake area. The V-notch weir equation according to Chadwick *et al*. (2013) is defined as follows:

$$Q = C_d \cdot \left(\frac{8}{15}\right) \cdot \sqrt{2g} \cdot \tan\left(\frac{\theta}{2}\right) \cdot {h_1}^{5/2} \qquad \textbf{Equation 5-1}$$

Where,

Q = Flow discharge (m³/s)

C_d = Discharge coefficient (0.59 for θ = 90°)

θ = Angle of weir (°)

θ = Upstream water depth above weir crest (m) (≥ 0.05 m for accuracy)

It must be noted that if there is a difference in discharge value between the volt or flow meter reading and the calculated flow discharge (Equation 5-1), then the volt or flow meter needs to be calibrated accordingly. This is especially necessary for pressure

flushing testing (later), as the V-notch becomes impractical when submerged by tail waters.

4. Ensure that this critical discharge (Q_{fc}) is also able to subsequently fully flush the low-level outlet conduit and local downstream river channel of the sediment. If this is not the case, continue incrementally increasing the flow discharge until it occurs – this will then be the new critical discharge (Q_{fc}). An example of a fully-flushed downstream river channel is illustrated in Figure 5.6-3.

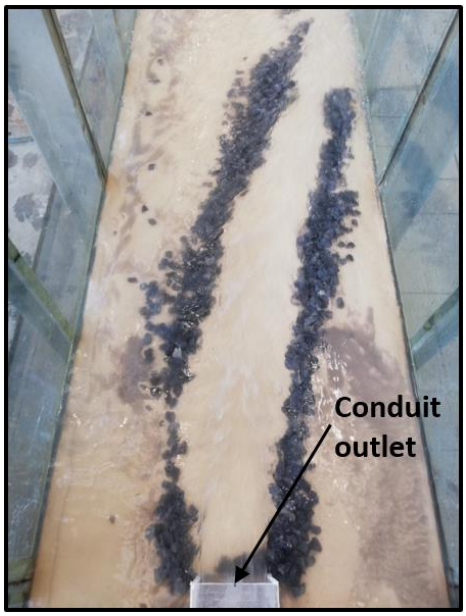

Figure 5.6-3: Example of fully-flushed downstream river channel

5. Incrementally raise the downstream tailwater level, by adjusting the downstream sluice gate, until a hydraulic jump forms inside of the conduit.

6. Turn off the flow, drain the upstream portion of the flume and repeat the dry setup (Step 1).

7. Turn on the flow at the correct critical discharge (Q_{fc}) and ensure that the flow stabilises before any flushing occurs. Once flushing commences, time how long it takes for the intake area to be fully flushed of sediment.

8. Lower the downstream tailwater level in small increments until the low-level outlet conduit and local downstream river channel is fully flushed of sediment. This represents the maximum tailwater level (TWL_{max}) for free-flow flushing.

9. Use the dumpy level or needle to measure the water levels at the predetermined measuring points along the centreline of the model (Figure 5.5-1). Ensure that deposited sediment does not influence the tailwater level reading downstream of the outlet.

10. Repeat Step 2 and re-measure the tailwater levels at the conduit outlet and downstream of the outlet where uniform flow occurs. Ensure that deposited sediment does not influence the tailwater level reading downstream of the outlet.

5.6.4.2 General results

The maximum discharge (Q_e) that could flush without submerging the conduit inlet was physically determined as 119 m³/s. This was reaffirmed by CFD simulations of the corresponding design model as illustrated in Figure 4.3-2. An associated wing-will crest height of 2 m above the weir crest level was found to conservatively avoid water spilling over the sides during the free-flow flushing of Q_e. The flow profile water levels of Q_e were measured at the chosen measuring points (Figure 5.5-1) along the model. The elevations of these water levels, relative to the conduit inlet invert level (IL), and the corresponding flow depths are indicated in Table 5.6-8. The corresponding centreline flow profile of Q_e along the model is illustrated in Figure 5.6-4.

Table 5.6-8: Water levels (relative to IL) and water depths along model for Q = 119 m³/s

Measuring point	Water level (m)	Flow depth (m)
P_1	6.280	2.000
P_2	5.540	1.260
P_3	2.880	1.400
P_4	2.400	1.400
P_5	3.280	3.000
P_6	-2.280	1.540
P_7	-3.040	1.780

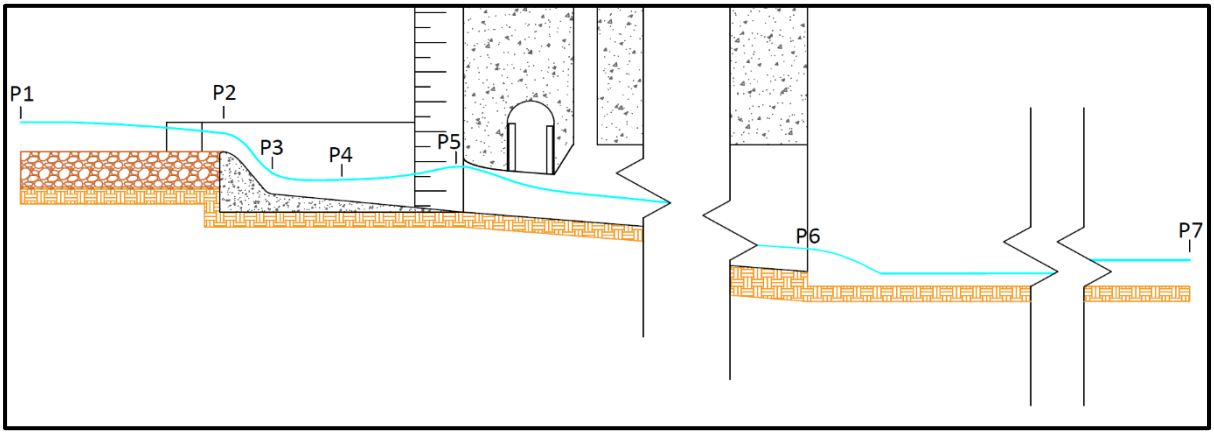

Figure 5.6-4: Centreline flow profile of Q = Q_e = 119 m³/s along model

5.6.4.3 *Sediment depth 1* results

The critical results obtained from the free-flow flushing tests of the four different sediment groups, according to the setup of *sediment depth 1* (Section 5.6.2, *Tested sediment depths*), are indicated in Table 5.6-9. These results correspond to the test procedure requirements

specified in Section 5.6.4.1 (*Test procedure*). The matching centreline flow profile of each discharge (Q_{fc}) along the model is illustrated in Figure 5.6-5.

It must be noted that no singular free-flow discharge (Q_{fc}) was able to fully flush the intake area of the d_{eff} = 1.532 m sediment group. The maximum volume of scour that could be obtained from steadily increasing the discharge from 0 m³/s until the conduit inlet became submerged is illustrated in Figure 5.6-6. As a plausible solution to this issue, the radius of the reverse bottom curve at the downstream end of the ogee-spillway profile was increased to 4 m – this value is typically recommended for roller buckets downstream of weirs with alluvial beds (Basson, 2019). This increase in radius (Figure 5.6-7) was anticipated to minimise the risk of sediment deposition along this region as a result of the smoother and steeper transition from ogee spillway to intake bed surface. This simultaneously addressed the concern of the apparent dead-zone location as observed from CFD results (Figure 4.3-3).

The test to determine Q_{fc} for the d_{eff} = 1.532 m sediment group was repeated thereafter. It was eventually found through trial and error that if the flow was incremented to 99 m³/s and then lowered to 72 m³/s once sediment scouring had stabilised, almost all of the boulders were flushed out of the conduit intake, as illustrated in Figure 5.6-8. It made sense that a continuously increasing discharge would at some point submerge the non-scoured boulders in the intake area before they could all flush out. This submergence resulted in slower water velocities being directed over the deposited sediment, not having any flushing effect. By then decreasing the discharge, the flow ultimately became supercritical again and reinitiated flushing of a portion of the remaining sediments nearer to the inlet. This entire process would have to be iterated until all the sediment is incrementally flushed out of the intake area.

Table 5.6-9. Critical free-flow flushing results of *sediment depth 1* setup for different sediment group sizes

Sediment group size (d_{eff}) (m)	**0.004**	**0.468**	**0.659**	**1.532**
Minimum discharge to fully flush model (Q_{fc}) (m³/s)	8.3	39.8	71.9	-
Time taken to fully flush intake area (min)	28.5	9.5	10.0	-
Measuring point	**Flow depths (m)**			
P_1	0.440	1.000	1.440	-
P_2	0.090	0.430	0.650	-
P_3	0.100	0.480	0.720	-
P_4	0.160	0.640	0.920	-
P_5	0.720	1.640	1.920	-
P_6	0.180	0.740	0.900	-
P_6 (TWL_{max})	0.180	0.820	1.100	-
P_7	0.740	1.180	1.380	-
P_7 (TWL_{max})	0.740	1.700	2.180	-
Measuring point	**Water levels (relative to IL) (m)**			
P_1	4.720	5.280	5.720	-
P_2	4.370	4.710	4.930	-
P_3	1.580	1.960	2.200	-
P_4	1.160	1.640	1.920	-
P_5	1.000	1.920	2.200	-

P_6	-3.640	-3.080	-2.920	-
$P_6\ (TWL_{max})$	-3.640	-3.000	-2.720	-
P_7	-4.080	-3.640	-3.440	-
$P_7\ (TWL_{max})$	-4.080	-3.120	-2.640	-

**where " — "= did not fully flush*

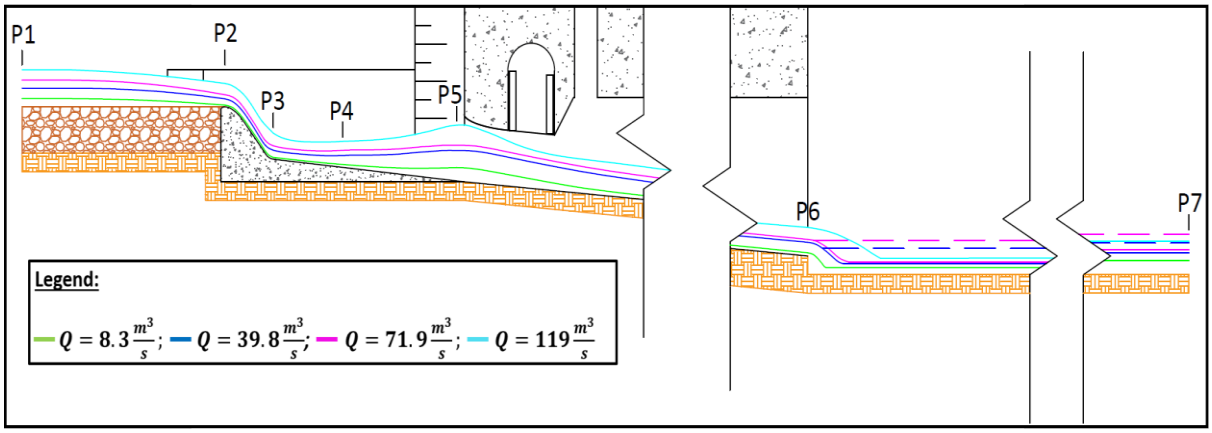

Figure 5.6-5. Centreline flow profiles of discharges (Q_{fc}) for *sediment depth 1* setup

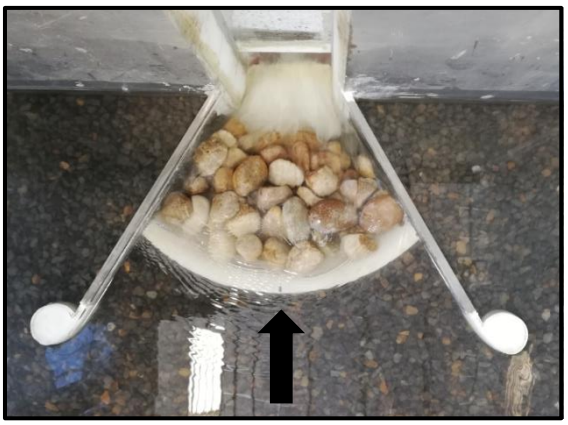

Figure 5.6-6: Initial maximum scour of d_{eff} = 1.532 m *sediment depth 1* inside intake area (free-flow flushing)

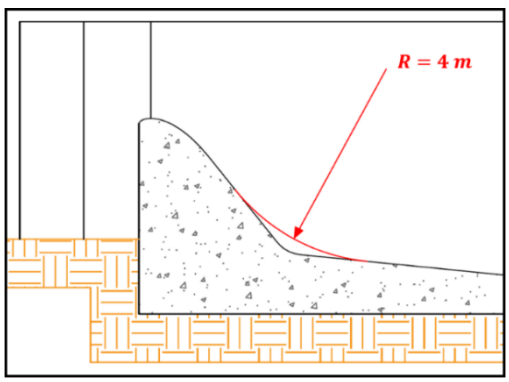

Figure 5.6-7: Enlarged reverse bottom curve radius (R = 4 m)

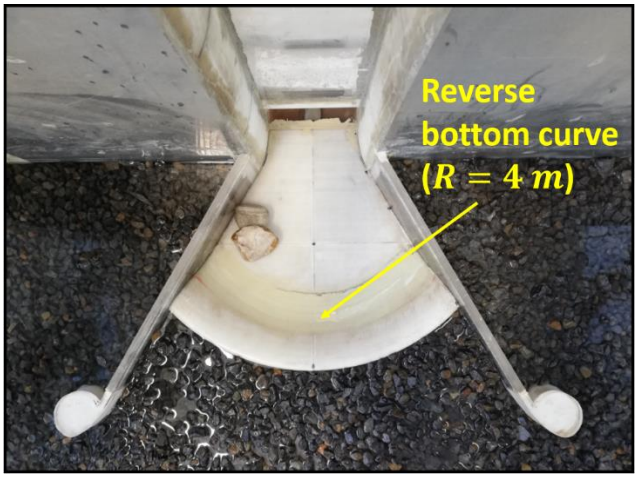

Figure 5.6-8. Final maximum scour of d_{eff} = 1.532 m *sediment depth 1* inside intake area (free-flow flushing)

5.6.4.4 *Sediment depth 2* results

The critical results obtained from the free-flow flushing tests of the four different sediment groups, according to the setup of *sediment depth 2* (Section 5.6.2, *Tested sediment depths*), are indicated in Table 5.6-10. These results correspond to the test procedure requirements specified in Section 5.6.4.1 (*Test procedure*). The matching centreline flow profiles of the discharge (Q_{fc}) along the model are illustrated in Figure 5.6-9, Figure 5.6-10 and Figure 5.6-11.

It must be noted that no singular free-flow discharge (Q_{fc}) was able to fully flush the intake area of the d_{eff} = 0.659 m sediment group. It was eventually found through trial and error that if the flow was incremented to 99 m³/s and then lowered to 66 m³/s once sediment scouring had stabilised, the intake area became fully flushed. The reasoning/theory behind this is the same as stated in Section 5.6.4.3 (*Sediment depth 1 results*). A minimum discharge of 158.4 m³/s was subsequently required to fully flush the downstream river channel of the large sediment load.

Table 5.6-10. Critical free-flow flushing results of *sediment depth 2* setup for different sediment group sizes

Sediment group size (d_{eff}) (m)	**0.004**	**0.468**	**0.659**	**1.532**
Minimum discharge to fully flush model (Q_{fc}) (m³/s)	28.0	78.0	158.4	N/A
Time taken to fully flush intake area (min)	6.9	20.0	14.7	N/A
Measuring point	**Flow depths (m)**			
P_1	0.800	1.400	-	N/A
P_2	0.520	0.760	-	N/A
P_3	0.280	0.960	-	N/A
P_4	0.640	1.360	-	N/A
P_5	1.360	2.240	-	N/A
P_6	0.620	1.100	2.180	N/A
P_6 (TWL_{max})	0.620	1.100	2.180	N/A
P_7	1.060	1.500	2.260	N/A

$P_7\ (TWL_{max})$	1.980	2.340	2.260	N/A
Measuring point	**Water levels (relative to IL) (m)**			
P_1	5.080	7.680	-	N/A
P_2	4.800	5.040	-	N/A
P_3	1.760	2.440	-	N/A
P_4	1.640	2.360	-	N/A
P_5	1.640	2.520	-	N/A
P_6	-3.200	-2.720	-1.640	N/A
$P_6\ (TWL_{max})$	-3.200	-2.720	-1.640	N/A
P_7	-3.760	-3.320	-2.560	N/A
$P_7\ (TWL_{max})$	-2.840	-2.480	-2.560	N/A

**where "N/A" = did not test; " – " = submerged flow*

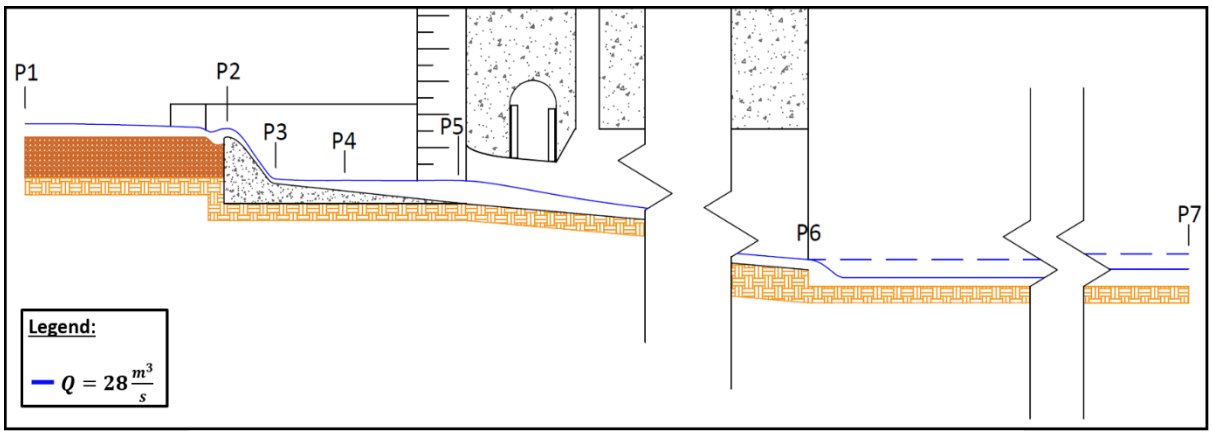

Figure 5.6-9. Centreline flow profile of Q_{fc} for d_{eff} = 0.004 m *sediment depth 2*

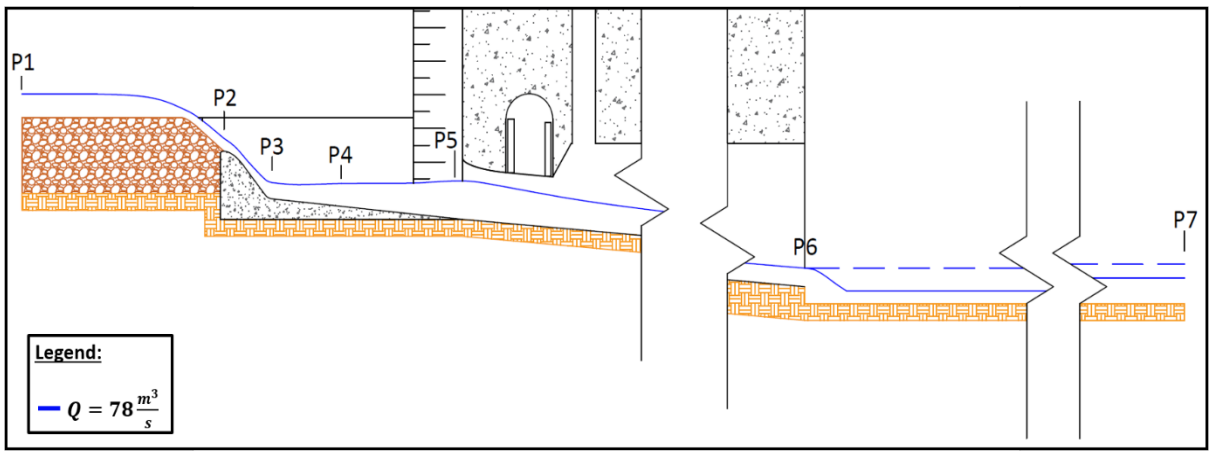

Figure 5.6-10. Centreline flow profile of Q_{fc} for d_{eff} = 0.468 m *sediment depth 2*

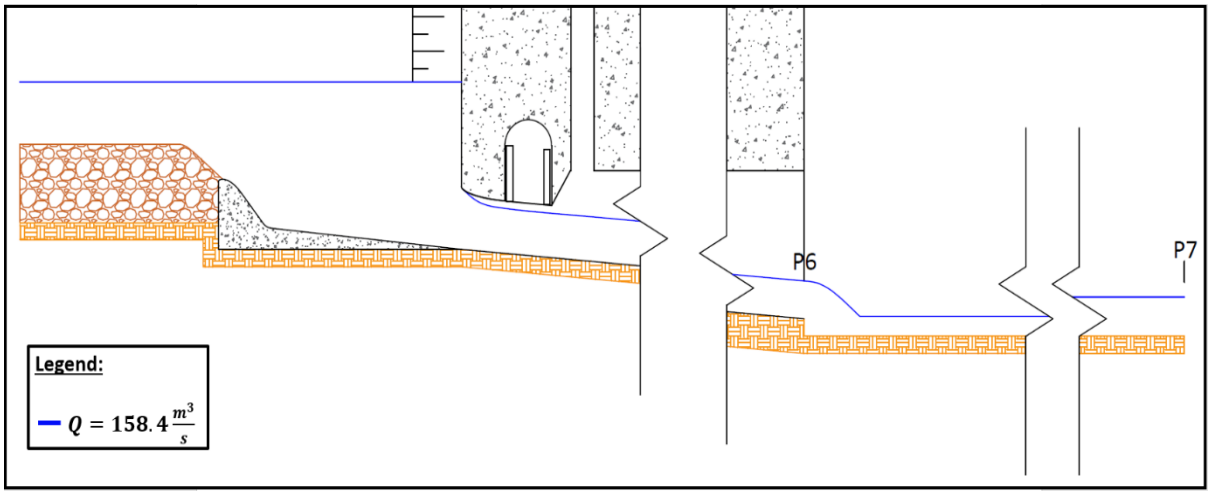

Figure 5.6-11. Centreline flow profile of Q_{fc} for d_{eff} = 0.659 m *sediment depth 2*

The free-flow flushing tests considering the d_{eff} = 0.468 m and 0.659 m sediment groups were repeated in the absence of the intake structure (i.e. ogee-spillway structure and wing-walls). These were considered the most critical for analysis of the influence of the intake structure during free-flow flushing conditions. The corresponding test details are indicated in Table 5.6-11. A comparison of the scouring of the d_{eff} = 0.468 m and 0.659 m *sediment depth 2* setups, with and without the intake structure, after free-flow flushing are indicated in Figure 5.6-12 and Figure 5.6-13, respectively. The corresponding regions of critical sediment deposition are illustrated in Figure 5.6-14.

Table 5.6-11. Free-flow flushing without intake structure for *sediment depth 2* setup for different sediment group sizes

Sediment group size (d_{eff}) (m)	**0.004**	**0.468**	**0.659**	**1.532**
Free-flow discharge (Q_f) (m³/s)	N/A	78.0	99.0	N/A
Time taken to fully flush intake area (min)	N/A	94.9	19.0	N/A

Figure 5.6-12. Scour of d_{eff} = 0.468 m *sediment depth 2* after free-flow flushing

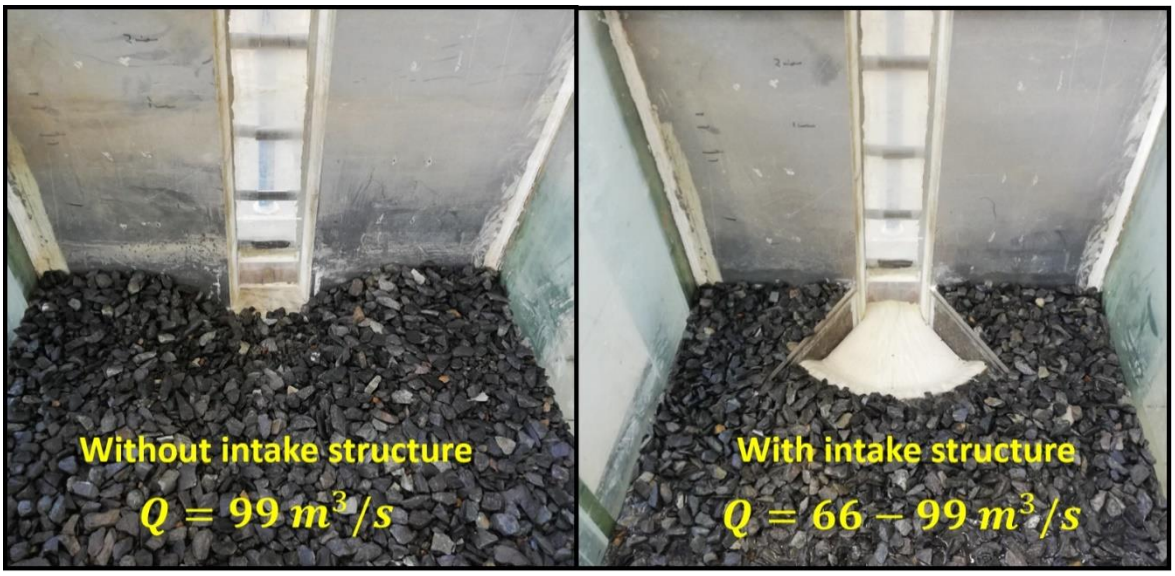

Figure 5.6-13. Scour of d_{eff} = 0.659 m *sediment depth 2* after free-flow flushing

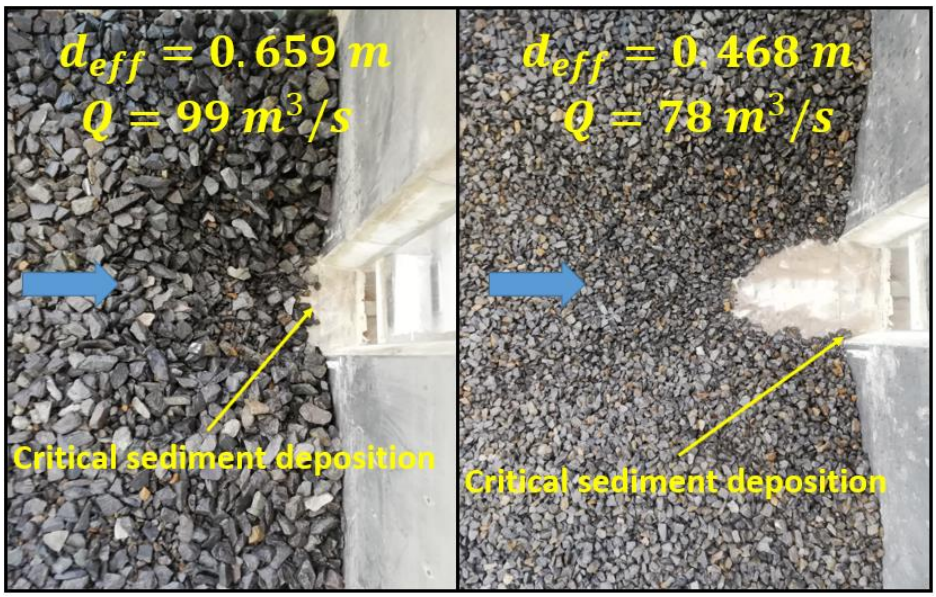

Figure 5.6-14. Deposition of different boulder groups near outlet gate after free-flow flushing (without intake structure)

5.6.5 Pressure flushing

5.6.5.1 Test procedure

Firstly, it was necessary to physically determine the discharges required to maintain the three upstream water levels (Section 5.6.3, *Tested pressure flushing water levels*) during pressure flushing. This was done by impounding the upstream portion of the flume and incrementally changing the discharge until each water level remained stable at the corresponding desired level for a couple of minutes. The vertically-fixed needle and marker were used to identify

and indicate the locations of the desired levels, above the conduit inlet invert level, on the steel plate (i.e. dam).

For each subsequent pressure flushing test considering sediment flushing, the following systematic approach was followed:

1. For the dry setup, fill and level the intake and local upstream area with the respective sediment according to *sediment depth 1* or *sediment depth 2*.

2. Ensure that the sluice gate at the downstream end of the flume is fully open (i.e. there must be no downstream tailwater effects).

3. Slowly impound the upstream portion of the flume until the sediment is submerged, after which increase the discharge to the predetermined discharge required to maintain the respective water level during pressure flushing.

4. Just before the water level reaches the desired level, start to slowly open the low-level outlet sluice gate. Aim to take at least 30 seconds to fully raise the gate (i.e. to achieve a fully open conduit) and to coincide the water level with the desired level at this point in time. Take note of how long it took to fully raise the gate.

5. Time how long it takes for equilibrium to be reached where sediment stops flushing out of the conduit (i.e. clear flow).

6. Measure the tailwater levels at the conduit outlet (i.e. P_6) and at the chosen measuring point downstream of the outlet (i.e. P_7), using a dumpy level or needle.

7. Incrementally raise the downstream tailwater level until just before the soffit of the conduit outlet becomes submerged – this represents the maximum tailwater level (TWL_{max}) for pressure flushing. Repeat Step 6.

8. Turn off the flow, drain the upstream portion of the flume and repeat the dry setup (Step 1).

9. Repeat Step 3 and 4 for *water level 1*. This is a surety test to confirm that the maximum downstream tailwater level has no effect on the flushing of the sediment during pressure flushing at the lowest upstream water level (i.e. worst case scenario). If this is the case, it will evidently remain true for flushing with higher upstream water levels. If this is not the case, re-determine the maximum tailwater level to allow for complete and unhindered flushing, and repeat Step 6.

10. Once equilibrium has been reached and no further sediment is being flushed out of the conduit, lower the low-level outlet sluice gate until fully closed and turn off the flow immediately.

11. Use a submersible pump to slowly drain the upstream portion of the flume until empty so as to not affect the upstream sediment deposition patterns.

12. Take note of the quantity of sediment flushed (i.e. scoured) and measure the dimensions of the sediment scour cone. The critical dimension is the distance of the toe of the sediment scour cone inside the intake bed surface from the conduit inlet invert level. An example of this scenario is illustrated in Figure 5.6-15.

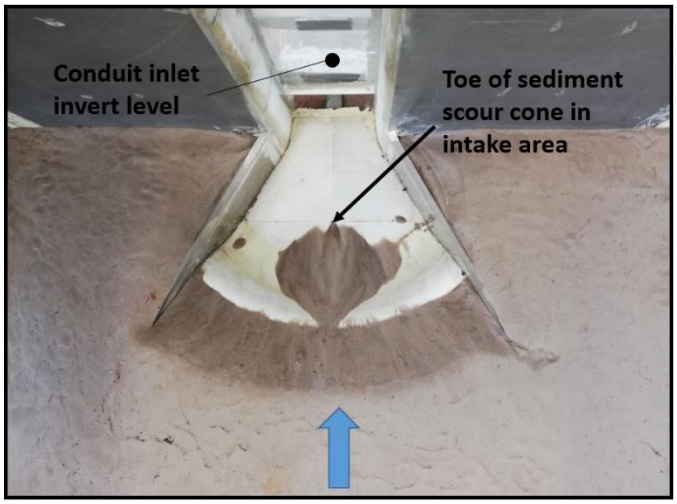

Figure 5.6-15: Observed scour cone of d_{eff} = 0.004 m *sediment depth 2* during pressure flushing

5.6.5.2 General results

The discharge (Q) values required to maintain the upstream water levels (H_u) considered for pressure flushing testing were determined in the physical model as indicated in Table 5.6-12. The natural flow profile tailwater levels of each discharge were measured at the downstream measuring points (i.e. P_6 and P_7). The elevations of these tailwater levels, relative to the conduit inlet invert level (IL), and the corresponding flow depths are indicated in Table 5.6-12. The associated maximum tailwater levels (TWL_{max}) to just avoid submergence of the conduit outlet soffit during flushing were also determined and are indicated in Table 5.6-12.

Table 5.6-12: Tailwater levels and depths of pressure flushing discharges for different upstream water levels

Upstream water levels (H_u) (m)	**24.16**	**29.08**	**34.00**
Measured discharge to maintain H_u (Q) (m³/s)	296.4	329.3	368.8
Measuring point	Flow depths (m)		
P_6	2.220	2.380	2.500
P_6 (TWL_{max})	7.900	8.140	8.260
P_7	2.180	2.060	1.900
P_7 (TWL_{max})	10.140	10.780	11.060
Measuring point	Water levels (relative to IL) (m)		
P_6	-1.600	-1.440	-1.320
P_6 (TWL_{max})	4.080	4.320	4.440
P_7	-2.640	-2.760	-2.880
P_7 (TWL_{max})	5.320	5.960	6.240

For comparison, the discharge (Q) values required to maintain the upstream water levels (H_u) were also determined in the absence of the intake structure (i.e. ogee-spillway structure and wing-walls) from the physical model as indicated in Table 5.6-13.

Table 5.6-13: Required discharges to maintain upstream water levels (without structure) for different upstream water levels

Upstream water levels (H_u) (m)	24.16	29.08	34.00
Measured discharge to maintain H_u (Q) (m³/s)	303.0	355.6	388.5

It must be noted that the results indicated in Table 5.6-12 remained constant for all subsequent corresponding sediment pressure flushing tests. It was also identified from practice that the respective maximum tailwater levels (TWL_{max}) had no influence on the deposition and flushing of sediments at or downstream of the conduit outlet.

5.6.5.3 *Sediment depth 1* results

The critical results obtained from the pressure flushing tests of the d_{eff} = 0.004 m sediment group, according to the setup of *sediment depth 1* (Section 5.6.2, *Tested sediment depths*), are indicated in Table 5.6-14. These results correspond to the test procedure requirements specified in Section 5.6.5.1 (*Test procedure*). The corresponding longitudinal scour profiles of the sediment bed inside of the intake area are illustrated in Figure 5.6-16.

Table 5.6-14: Critical pressure flushing results of d_{eff} = 0.004 m *sediment depth 1* for different upstream water levels

Upstream water levels (H_u) (m)	24.16	29.08	34.00
Time taken to fully open sluice gate (min)	2.1	4.5	4.0
Time taken to flush intake area (min)	7.9	12.1	11.0
Horizontal distance of scoured sediment bed toe from conduit inlet invert level (m)	9.56	10.45	11.06

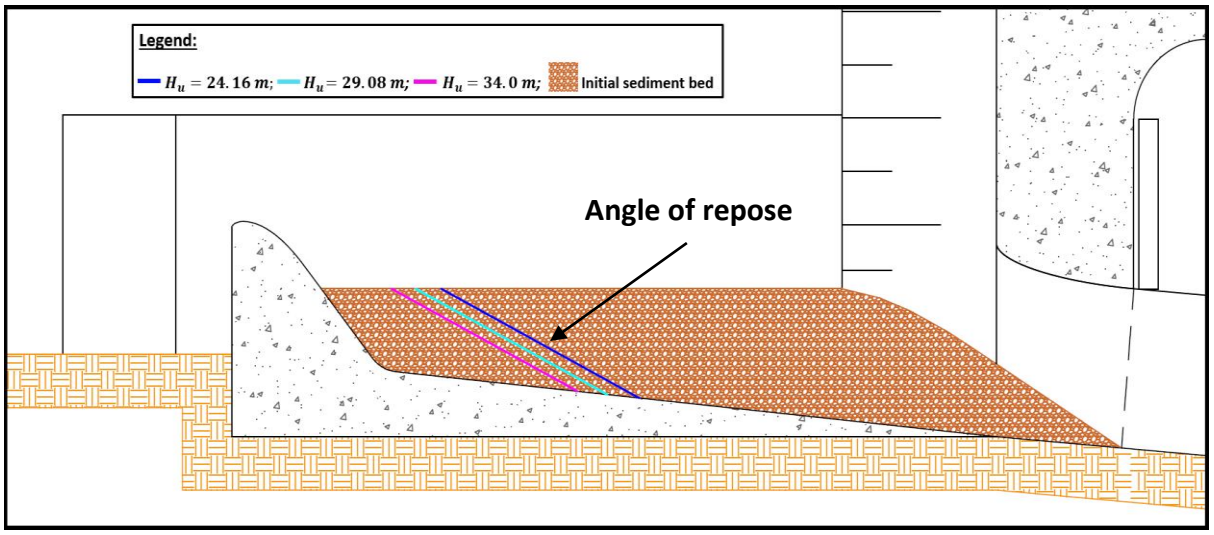

Figure 5.6-16: Observed scour profiles of d_{eff} = 0.004 m *sediment depth 1*

The critical results obtained from the pressure flushing tests of the d_{eff} = 0.468 m sediment group, according to the setup of *sediment depth 1* (Section 5.6.2, *Tested sediment depths*), are indicated in Table 5.6-15. These results correspond to the test procedure requirements specified in Section 5.6.5.1 (*Test procedure*). The corresponding longitudinal scour profiles of the sediment bed inside of the intake area are illustrated in Figure 5.6-17.

Table 5.6-15: Critical pressure flushing results of d_{eff} = 0.468 m *sediment depth 1* for different upstream water levels

Upstream water levels (H_u) (m)	24.16	29.08	34.00
Time taken to fully open sluice gate (min)	3.7	3.2	4.2
Time taken to flush intake area (min)	3.7	3.4	4.0
Horizontal distance of scoured sediment bed toe from conduit inlet invert level (m)	8.87	9.86	10.33

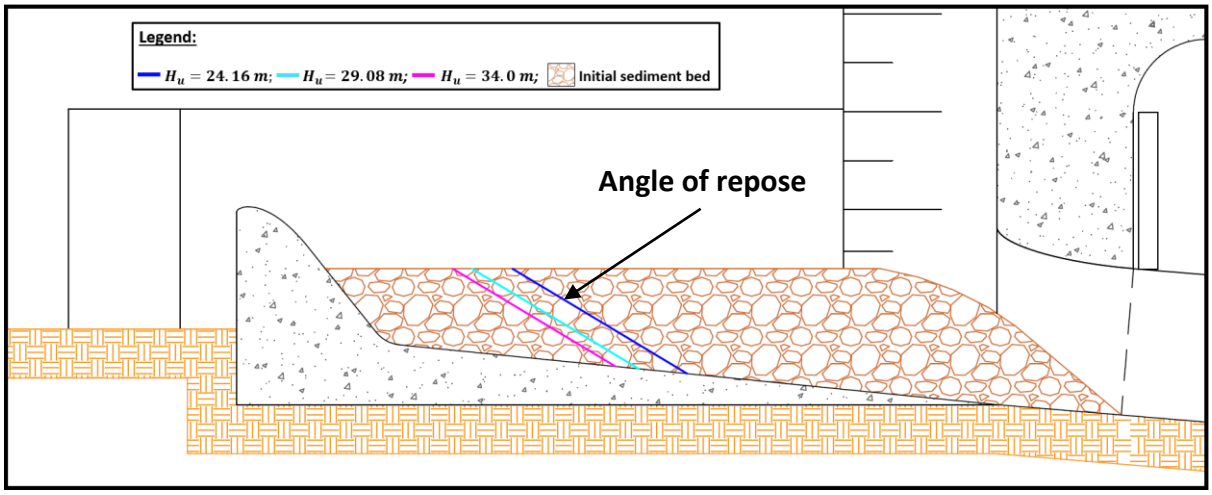

Figure 5.6-17: Observed scour profiles of d_{eff} = 0.468 m *sediment depth 1*

The critical results obtained from the pressure flushing tests of the d_{eff} = 0.659 m sediment group, according to the setup of *sediment depth 1* (Section 5.6.2, *Tested sediment depths*), are indicated in Table 5.6-16. These results correspond to the test procedure requirements specified in Section 5.6.5.1 (*Test procedure*). The corresponding longitudinal scour profiles of the sediment bed inside of the intake area are illustrated in Figure 5.6-18.

Table 5.6-16: Critical pressure flushing results of d_{eff} = 0.659 m *sediment depth 1* for different upstream water levels

Upstream water levels (H_u) (m)	24.16	29.08	34.00
Time taken to fully open sluice gate (min)	3.1	4.0	2.6
Time taken to flush intake area (min)	2.6	3.9	2.7
Horizontal distance of scoured sediment bed toe from conduit inlet invert level (m)	8.72	10.0	10.48

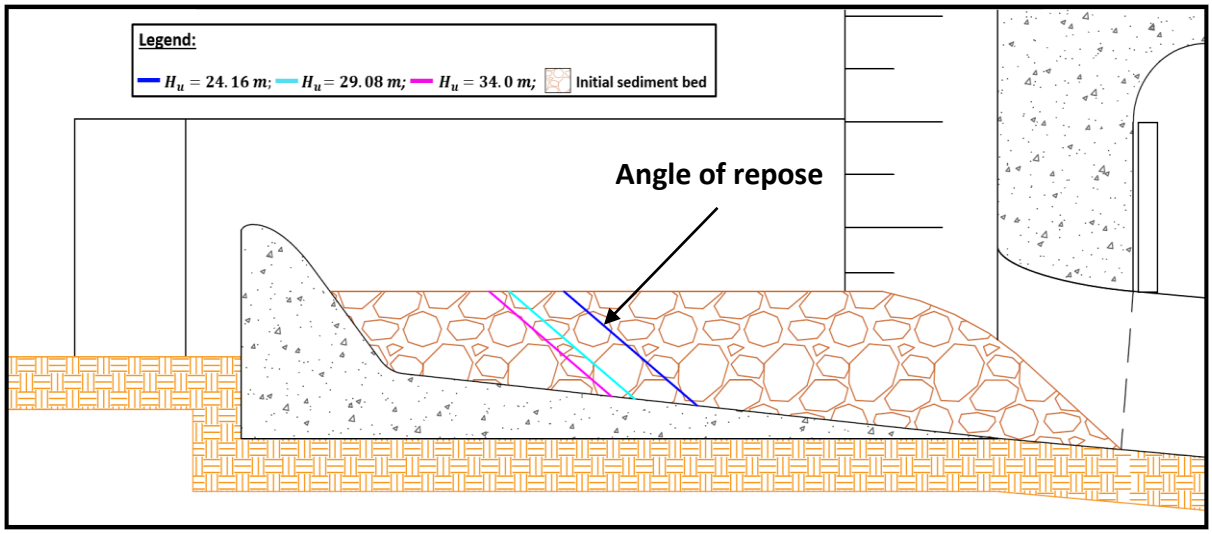

Figure 5.6-18: Observed scour profiles of d_{eff} = 0.659 m *sediment depth 1*

The critical results obtained from the pressure flushing tests of the d_{eff} = 1.532 m sediment group, according to the setup of *sediment depth 1* (Section 5.6.2, *Tested sediment depths*), are indicated in Table 5.6-17. These results correspond to the test procedure requirements specified in Section 5.6.5.1 (*Test procedure*). The corresponding longitudinal scour profiles of the sediment bed inside of the intake area are illustrated in Figure 5.6-19.

Table 5.6-17: Critical pressure flushing results of d_{eff} = 1.532 m *sediment depth 1* for different upstream water levels

Upstream water levels (H_u) (m)	24.16	29.08	34.00
Time taken to fully open sluice gate (min)	3.7	2.1	1.6
Time taken to flush intake area (min)	0.4	0.5	0.9
Horizontal distance of scoured sediment bed toe from conduit inlet invert level (m)	10.29	10.41	10.90

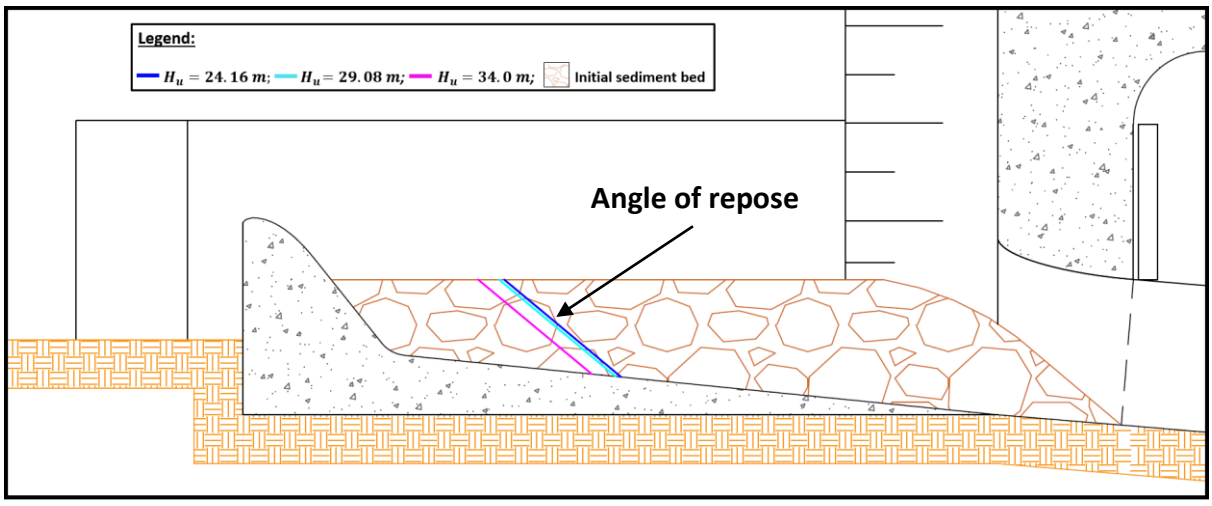

Figure 5.6-19: Observed scour profiles of d_{eff} = 1.532 m *sediment depth 1*

5.6.5.4 *Sediment depth 2* results

The pressure flushing tests considering the upstream water level, H_{u1} = 24.16 m, were repeated in the absence of the intake structure (i.e. ogee-spillway structure and wing-walls). These were considered the most critical for analysis of the influence of the intake structure during pressure flushing conditions. The notation for this group of tests will be "ws" (without structure) in the subsequent tables of results and figures of observed sediment scour profiles. Physical model images of the resulting scour cones of the respective sediment groups during pressure flushing at H_{u1} (without intake structure) are illustrated in the figures of Section B.5 in **Appendix B**.

The critical results obtained from the pressure flushing tests of the d_{eff} = 0.004 m sediment group, according to the setup of *sediment depth 2* (Section 5.6.2, *Tested sediment depths*), are indicated in Table 5.6-18. These results correspond to the test procedure requirements specified in Section 5.6.5.1 (*Test procedure*). The corresponding longitudinal scour profiles of the sediment bed inside of the intake area are illustrated in Figure 5.6-20.

Table 5.6-18: Critical pressure flushing results of d_{eff} = 0.004 m *sediment depth 2* for different upstream water levels

Upstream water levels (H_u) (m)	24.16	24.16 (ws)	29.08	34.00
Time taken to fully open sluice gate (min)	2.3	2.7	2.5	3.0
Time taken to flush intake area (min)	10.5	22.1	16.9	15.6
Horizontal distance of scoured sediment bed toe from conduit inlet invert level (m)	10.31	8.88	10.82	11.18

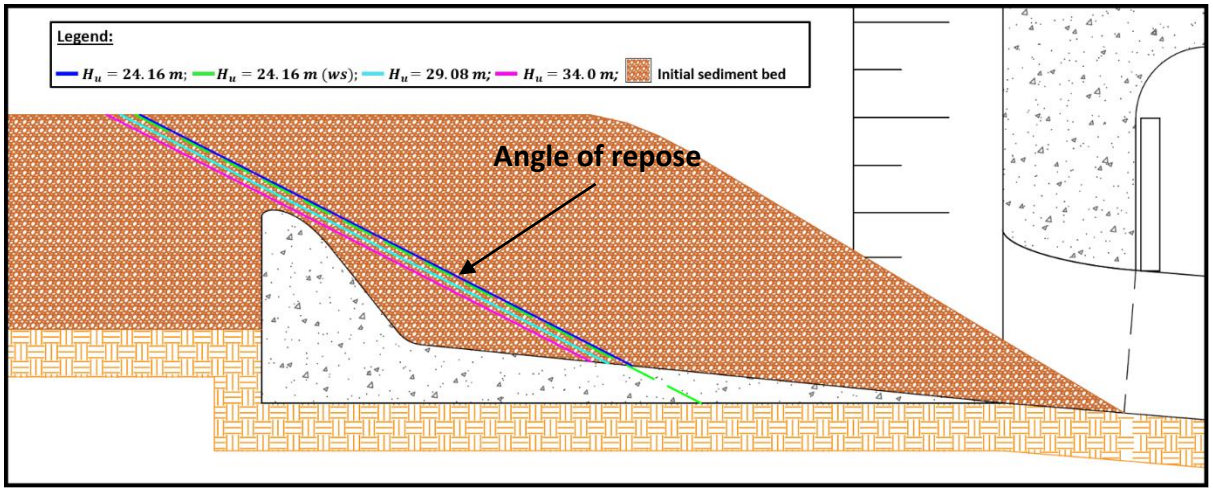

Figure 5.6-20: Observed scour profiles of d_{eff} = 0.004 m *sediment depth 2*

The critical results obtained from the pressure flushing tests of the d_{eff} = 0.468 m sediment group, according to the setup of *sediment depth 1* (Section 5.6.2, *Tested sediment depths*), are indicated in Table 5.6-19. These results correspond to the test procedure requirements specified in Section 5.6.5.1 (*Test procedure*). The corresponding longitudinal scour profiles of the sediment bed inside of the intake area are illustrated in Figure 5.6-21.

Table 5.6-19: Critical pressure flushing results of d_{eff} = 0.468 m *sediment depth 2* for different upstream water levels

Upstream water levels (H_u) (m)	24.16	24.16 (ws)	29.08	34.00
Time taken to fully open sluice gate (min)	3.0	2.1	3.8	3.7
Time taken to flush intake area (min)	3.6	2.4	4.0	3.9
Horizontal distance of scoured sediment bed toe from conduit inlet invert level (m)	10.32	9.28	10.95	11.25

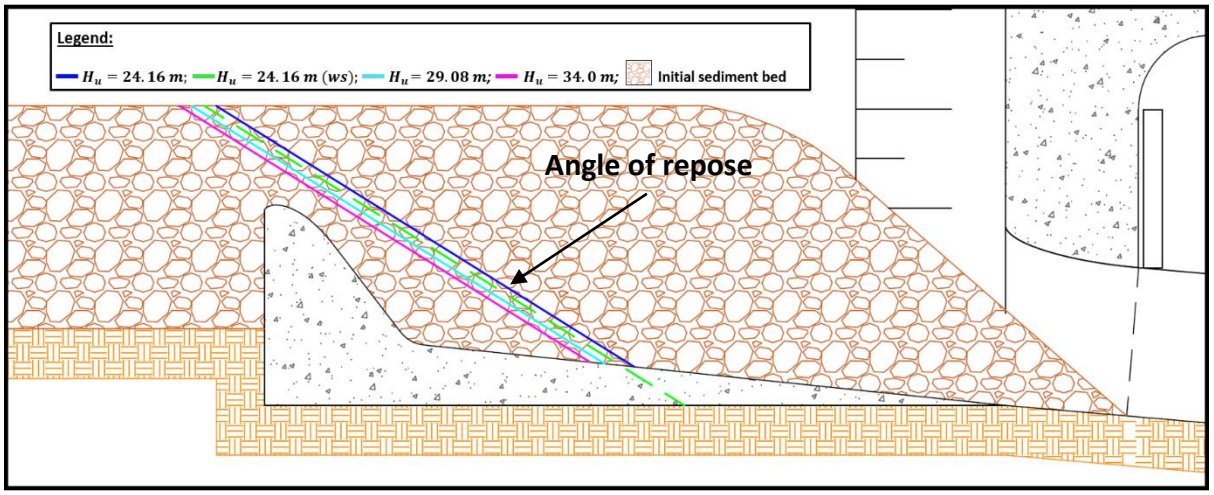

Figure 5.6-21: Observed scour profiles of d_{eff} = 0.468 m *sediment depth 2*

The critical results obtained from the pressure flushing tests of the d_{eff} = 0.659 m sediment group, according to the setup of *sediment depth 1* (Section 5.6.2, *Tested sediment depths*), are indicated in Table 5.6-20. These results correspond to the test procedure requirements specified in Section 5.6.5.1 (*Test procedure*). The corresponding longitudinal scour profiles of the sediment bed inside of the intake area are illustrated in Figure 5.6-22.

Table 5.6-20: Critical pressure flushing results of d_{eff} = 0.659 m *sediment depth 2* for different upstream water levels

Upstream water levels (H_u) (m)	24.16	24.16 (ws)	29.08	34.00
Time taken to fully open sluice gate (min)	1.4	1.9	3.8	1.7
Time taken to flush intake area (min)	1.4	1.9	2.7	1.7
Horizontal distance of scoured sediment bed toe from conduit inlet invert level (m)	10.21	8.88	11.20	11.47

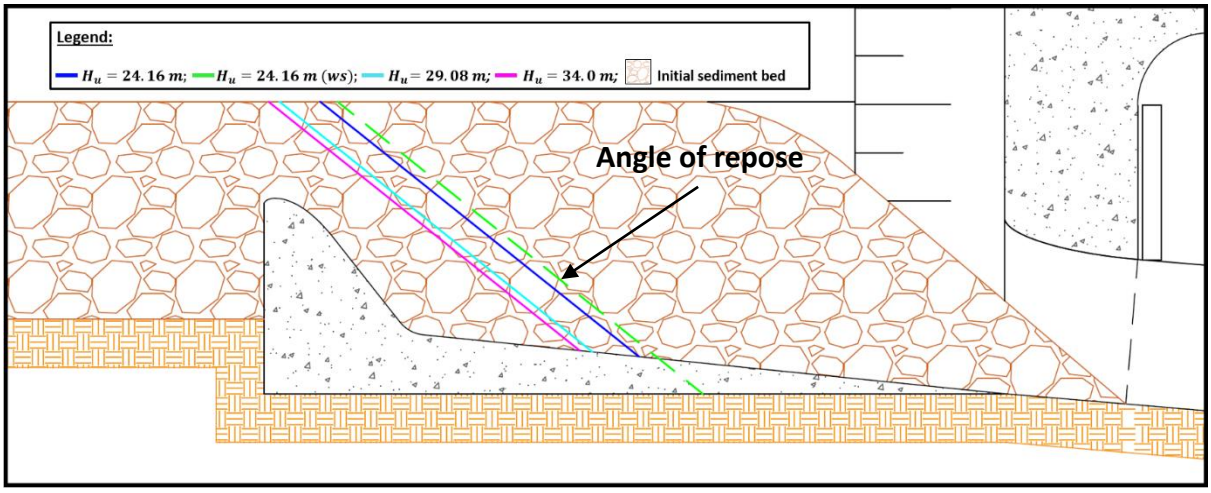

Figure 5.6-22: Observed scour profiles of d_{eff} = 0.659 m *sediment depth 2*

6 Summary and Conclusions

The hydraulic design requirements of low-level outlets at dams located underneath HPP intakes were investigated in this study. The purpose was to improve the understanding of sediment movement near the intakes and thus to prevent non-cohesive sediments entering the turbines. This was achieved through the pressure flushing and/or free-flow water level drawdown flushing (if sufficient excess flow is available) of sediments. An example of an operational risk with a low-level outlet was identified based on the Mbashe River HPP case study in South Africa. In this case study, the low-level outlet gate could not be closed again after free flow sediment flushing due to sediment at the gate. A postulated intake structure at the low-level outlet, designed to keep coarse sediments upstream of the weir after free-flow flushing, was therefore investigated further in this study. The intake structure comprises of a low-weir, wing-walls and ogee spillway structure with steep slopes.

The postulated sediment flushing system (i.e. low-level outlet and intake structure) was optimised and refined by means of numerical (CFD) and physical modelling for effectively flushing sediments (i.e. sand, gravel and boulders when the delta has reached the dam) for different flood and water level scenarios. The following prototype conditions were considered during hydraulic testing of the physical model: (1) two different upstream sediment bed configurations for both pressure and free-flow flushing; (2) four different sediment sizes (d_{eff} = 3.6, 468, 659 and 1532 mm) for both pressure and free-flow flushing; and (3) three different upstream water levels (H_u = 24.16, 29.08 and 34 m), above the conduit inlet invert level, for pressure flushing. Similar testing was also performed in the absence of the intake structure in order to derive comparative results to determine the degree of influence of the structure. The important findings from the literature study, numerical (CFD) model and physical model are provided in the following sections.

6.1 Literature study

The most critical information from literature that complements the objectives of this study is concluded as follows:

1. Drawdown or pressure flushing through low-level dam outlets below hydropower intakes are common mitigation measures for removing locally deposited sediment from reservoirs. Pressure flushing is only effective in scouring and flushing sediment immediately upstream of the low-level intakes, with no effects on deposits upstream of the scour cone. On the contrary, free-flow (drawdown) flushing is known to flush large quantities of deposited sediment over a longer period and can effectively restore the live storage capacity in reservoirs. In arid and semi-arid areas, free-flow flushing with drawdown should only be used if sufficient excess water is available.
2. It is critical to ensure that flushing is able to: (1) keep the hydropower intakes free of non-cohesive sediment, as sand fractions will typically damage turbines in hydropower plants; and (2) keep the area around the low-level outlet gates free of sediment deposition and blockage which could hinder gate operation and ultimately result in the uncontrolled emptying of the reservoir.
3. Boulders can quickly become a notable concern in small reservoirs that fill up quickly with sediment. At larger reservoirs, large-diameter sediments can also accumulate

near hydropower intakes once the reservoir has filled with sediment. Low-level outlets therefore need to be designed to effectively withstand and flush gravel and boulders which can easily block the intakes.

4. Dreyer (2018) derived pressure flushing sediment cone dimensions (considering fine, non-cohesive silica sand) for different low-level outlet shapes from physical model tests considering. His results agreed with those of previous authors, that for singular implementation, a wide and flat-rectangular-shaped inlet (height-to-width ratio of 1:2) generally yields the widest, longest and deepest scour cones (i.e. largest volume of sediment flushed).

6.2 Numerical model study

Three-dimensional (3D), multiphase Computational fluid dynamics (CFD) modelling in *ANSYS Fluent v19.1* was used to hydraulically compare four different configurations of the postulated flushing system during free-flow flushing. This comprised two design options (Section 3.5.3, *Conceptual designs evaluated*) and two wing-wall angles (i.e. α = 30° and α = 45°). A comparison of generated flow vectors (i.e. degree of streamlined flow), as well as of flow depths and velocities (i.e. degree of supercritical flow), along the model were used to choose the best design alternative. The following important findings were obtained from this study:

1. A wing-wall angle (α) of 30° was found to: (1) better streamline flow into the low-level outlet conduit; (2) result in less damming at the centre of the conduit inlet; and (3) result in faster flow acceleration into the conduit.
2. *Design 2* naturally resulted in faster flow velocities upstream of the conduit inlet. This design option, combined with α = 30°, proved to yield the best overall results with regards to structural and hydraulic requirements.
3. CFD simulations of the final design model verified the maximum discharge (Q_e) for free-flow flushing to be 119 m³/s, as initially determined in the physical model. Both scenarios required a wing-wall crest level of 2 m above the weir crest to simultaneously prevent water from spilling over the sides into the intake area.
4. CFD simulations of the final design model verified the suitability of the chosen transition in bed slope from that of the intake bed (i.e. 1:10) to that of the conduit bed (i.e. 1:12).
5. CFD simulations of the final design model illustrated the formation of a strip of significantly low-velocity flow vectors along the region of the reverse bottom curve. This issue was later addressed in the physical model by increasing the radius of the reverse bottom curve to 4 m, which showed to comparatively reduce sediment deposition in this region during flushing.

6.3 Physical model study

A 1:40 scale physical model of the postulated flushing system design, which evolved from the findings of the numerical model simulations, was built for further testing and refinement. The main aim of the physical model was to test the robustness, reliability and actual flushing capability of the design. The following important findings were obtained from this study:

1. The postulated sediment flushing system is able to fully flush the intake area of sand, gravel and boulders up to about 1.5 m in diameter, during free-flow flushing considering specific discharges.
2. Even though the region near the outlet gate operation area was always kept free of sediment deposition following flushing, the only concern was the inability to scour *all* the sediment in the intake structure for all sizes during pressure flushing.
3. The difference in sediment scour cone profile during pressure flushing appeared minimal with and without the intake structure. This therefore implies that the intake structure does not affect the pressure flushing extent upstream of the intake.
4. The intake structure was found to be crucial during free-flow flushing, where the weir was required to hold back main reservoir sediments from moving towards, or depositing near, the outlet gate operation area.

7 Recommendations

To further improve the sediment flushing capability of the postulated sediment flushing system, the following structural changes are recommended for future research:

1. Ensure that the radius centre of the semi-circular weir occurs at the apparent intersection of where the two wing-wall tangent lines would meet. This will ensure that the weir connects perpendicularly to the wing-wall faces. This will positively result in a shortened weir crest length (R_c) as well as better streamline the flow along the wing-walls and into the conduit.
2. Further increase the reverse bottom curve radius downstream of the ogee-spillway profile to minimise the risk of sediment deposition along this region during flushing.
3. Consider combining the reverse bottom curve and *deflection surface* to create a smoother and more uniform transition from ogee spillway profile to intake bed surface. This is anticipated to minimise flow turbulence and diversion along this region, as well as maximise along flow acceleration into the intake area, along.
4. Increase the bed slope (m) of the intake bed surface to larger than 1:10. This will improve conditions for especially flushing large-diameter sediments (i.e. boulders) during lower flows.
5. Place the weir closer to the low-level outlet in order to minimise the sediment deposition zone inside of the intake area during pressure flushing.

8 Bibliography

Amirsayafi, P. (2015) 'Measures for Success in Dam Bottom Outlet Design', *GSTF Journal of Engineering Technology (JET)*, 3(3), pp. 111–117. doi: 10.7603/s40.

Annandale, G. W. (2005) 'Reservoir Sedimentation', in Anderson, M. G. (ed.) *Encyclopedia of Hydrological Sciences*. John Wiley & Sons, Ltd.

Annandale, G. W., Morris, G. L. and Karki, P. (2016) *Extending the Life of Reservoirs : Sustainable Sediment Management for Dams and Run-of-River Hydropower*. Washington, DC: World Bank Group.

Armitage, N. P. (2002) *A unit stream power model for the prediction of local scour in rivers*. Stellenbosch University.

Armitagte, N. P. and Rooseboom, A. (2010) 'The link between movability number and incipient motion in river sediments', *Water SA*, 36(1), pp. 89–96.

ASCE (1995) *Guidelines for Design of Intakes for Hydroelectric Plants*.

Aydin, I. (2002) 'Air demand behind high head gates during emergency closure', *Journal Hydraulics Division*, 40(1).

Basson, G. R. (2009) *Management of siltation in existing and new reservoirs. General Report Q. 89*. Brasilia, Brazil.

Basson, G. R. (2019) *Guidelines for the design of river abstraction works - Volume I (WRC project K5/2750)*. Pretoria: SA Water Research Commission (WRC).

Basson, G. R. and Rooseboom, A. (1999) *Dealing with reservoir sedimentation: Guidelines and case studies*. ICOLD bulletin 115.

Basson, G. R. and Rooseboom, A. (2007) *Mathematical modelling of sediment transport and deposition in reservoirs*. ICOLD.

Blind, H. (1985) 'Design Criteria for Reservoir Bottom Outlets.', *International Water Power and Dam Construction*, 37(7), pp. 30–32.

Boes, R. M. *et al.* (2018) 'Sediment Bypass Tunnels: Swiss Experience With Bypass Efficiency and Abrasion-Resistant Invert Materials', in *ICOLD 26th International Congress on Large Dams 4-6 July, Vienna, Austria*, pp. 625–638.

Bosman, A., Basson, G. R. and Bosman, D. E. (2016) 'Hydraulic model study of the blowback behaviour of the bottom outlet of the Berg River Dam, South Africa', *Journal of the South African Institution of Civil Engineering*, 58(1), pp. 43–52. doi: 10.17159/2309-8775/2016/v58n1a5.

Bosman, E. and Basson, G. R. (2012) *Hydraulic Model Testing of the Outlet Works of the Berg River Dam - Volume I: Physical modelling (WRC project K5/1914)*. Pretoria: SA Water Research

Commission (WRC).

Brandt, S. A. (2000) *Reservoir Desiltation By Means of Hydraulic Flushing: Sedimentological and Geomorphological Effects in Reservoirs and Downstream Reaches As Illustrated by the Cachí Reservoir and the Reventazón River, Costa Rica. Ph.D. Thesis*. University of Copenhagen.

Bratko, D. and Doko, A. (2013) 'Water intake structures for hydropower', in *2nd International Balkans Conference on Challenges of Civil Engineering, BCCCE*, pp. 23–25.

Braune, E. and Looser, U. (1989) 'Cost impacts of sediments in South African rivers', in *Sediment and the Environment (Proceedings of the Baltimore Symposium, May 1989)*. 184th edn. IAHS Publications, pp. 131–143.

Brown, P. P. and Lawler, D. F. (2003) 'Sphere Drag and Settling Velocity Revisited', *Journal of Environmental Engineering*, 129(3), pp. 222–231.

Chadwick, A., Morfett, J. and Borthwick, M. (2013) *Hydraulics in Civil and Environmental Engineering*. 5th edn. CRC Press.

Chamoun, S., De Cesare, G. and Schleiss, A. J. (2016) 'Managing reservoir sedimentation by venting turbidity currents: A review', *International Journal of Sediment Research*. Elsevier, 31(3), pp. 195–204. doi: 10.1016/j.ijsrc.2016.06.001.

Chanson, H. (1994) 'Aeration and deaeration at bottom aeration devices on spillways', *Canadian Journal of Civil Engineering*, 21(3), pp. 404–409.

Cheng, N. S. (1997) *Simplified Settling Velocity Formula for Sediment Particle*, *Journal of Hydraulic Engineering-ASCE*.

CIRIA, CUR and CETMEF (2007) *The rock manual : the use of rock in hydraulic engineering*. 2nd edn. London: CIRIA.

Concha, F. (2009) 'Settling velocities of particulate systems', *KONA Powder and Particle Journal*, 27(0), pp. 18–37.

Delft Hydraulics (1992) *The Control of Reservoir Sedimentation – A Literature Review*. Delft.

Denys, F. (2019) *Investigation into Flow-induced Vibrations of Piano Key Weirs*. University of Stellenbosch.

Dewals, B. *et al.* (2012) 'Long-term sediment management for sustainable hydropower', in Sayigh, A. (ed.) *Comprehensive Renewable Energy*. 6th edn. Oxford: Elsevier, pp. 355–376.

Dey, S. (2014) 'Bed-Load Transport', in *Fluvial Hydrodynamics*. 1st edn. Berlin, Heidelberg: Springer-Verlag, pp. 261–326.

Dreyer, J. S. (2018) *Investigating the Shape and Layout of Low-Level Outlets for Pressure Flushing of Sediments in HPP Reservoirs*. University of Stellenbosch.

Erbisti, P. (2004) *Design of Hydraulic Gates*. 1st edn. Lisse, Netherlands: Swets & Zeitlinger B.

V.

Falvey, H. T. (1980) *Air-Water Flow in Hydraulic Structures*. Engineering Monograph No 41. Denver,CO: Water and Power Resources Service.

Fan, J. (1985) 'Methods of preserving reservoir capacity', in Bruk, S. (ed.) *Methods of computing sedimentation in lakes and reservoirs*. Paris: UNESCO, pp. 65–164.

Fan, J. and Morris, G. L. (1992) 'Reservoir Sedimentation I: Delta and Density Current Deposits', *Journal of Hydraulic Engineering*, 118(3), pp. 354–369.

FEMA (2004) *The National Dam Safety Program: Outlet Works*. Denver, CO: Federal Emergency Management Agency.

Garcia, M. H. (2008) *Sedimentation Engineering Processes, Measurements, Modeling and Practice*. Edited by M. H. Garcia. Virginia: American Society of Civil Engineers.

Guo, J. (2012) 'Recent achievements in hydraulic research in China', *Comprehensive Renewable Energy*, 6, pp. 485–505. doi: 10.1016/B978-0-08-087872-0.00603-X.

Healy, K. M. *et al.* (2014) *State of the practice of sediment management in reservoirs: Minimizing sedimentation and removing deposits*.

Heller, V. (2011) 'Scale effects in physical hydraulic engineering models', *Journal of Hydraulic Research*, 49(3), pp. 293–306.

ICOLD (2017) *Technical Advancements in Spillway Design - Progress and Innovations from 1985 to 2015. Prepared by ICOLD Technical Committee on Hydraulics for Dams*. ICOLD.

ICOLD (2018a) 'Case analysis of sediment bypass tunnels (Switzerland, Taiwan, Japan) (Q.100 – R.22)', in *Twenty-Sixth International Congress on Large Dams*. 1st edn. Vienna: CRC Press, pp. 351–366.

ICOLD (2018b) 'Checking and testing hydro-mechanical equipment', in *Dam surveillance guide, Bulletin 158*. Leiden: CRC Press/Balkema, pp. 43–47.

ICOLD (2018c) *General Reports of Questions of Congress: Q100*.

ICOLD Bulletin 147 (2009) *Sedimentation and Sustainable Use of Reservoirs and River Systems*.

IS 9761 (1995) *Hydropower Intakes - Criteria for Hydraulic Design*. 1st edn. Bureau of Indian Standards.

Jiang, N. (1980) 'Some investigation of reservoir sedimentation on a heavily silt laden stream', *Journal of Sediment Research*, (1), p. 100–110 (in Chinese).

Kalinske, A. A. and Robertson, J. M. (1943) 'Entrainment of Air in Flowing Water: A Symposium: Closed Conduit Flow', *Transactions of the American Society of Civil Engineers*, 108(1), pp. 1435–1447.

Khatsuria, R. M. (2004) 'Spillways, Energy Dissipators, and Spillway Gates', in Khatsuria, R. M. (ed.) *Hydraulics of Spillways and Energy Dissipators*. 1st edn. Boca Raton: CRC Press, pp. 1099–1154.

Knauss, J. (1987) 'Prediction of Critical Submergence', in Knauss, J. (ed.) *Swirling Flow Problems at Intakes*. 1st edn. Rotterdam: IAHR, Balkema.

Koen, J. (2017) *Artificial aeration on stepped spillways with piers and flares to mitigate cavitation damage*. University of Stellenbosch.

Kondolf, G. *et al.* (2014) 'Sustainable sediment management in reservoirs and regulated rivers: Experiences from five continents', *Earth's Future*, 2, pp. 256–280.

Krumbein, W. C. (1932) 'A history of the principles and methods of mechanical analysis', *Journal of Sedimentary Petrology*, 2(2), pp. 89–124.

Kumar, A. and Singal, S. K. (2013) *STANDARDS/MANUALS/ GUIDELINES FOR SMALL HYDRO DEVELOPMENT, A.A. Balkema, Rotterdam, Brookfield*.

Langmaak, K. R. (2013) *Incipient Motion of Riprap on Steep Slopes*. Stellenbosch University. doi: 10.1061/(ASCE)HY.1943-7900.0001016.

Lewin, J. (2001) *Hydraulic gates and valves in free surface flow and submerged outlets*. 2nd edn. London: Jack Lewin and Thomas Telford Limited.

Liu, H. K. (1957) 'Mechanics of sediment-ripple formation', *Journal of the Hydraulics Division*, 83(2), pp. 1–23.

Lowe, F. C. (1944) *Hydraulic Model Studies for the Glory-hole Spillways at Owyhee Dam and Gibson Dam*. Denver, Colorado.

Mahmood, K. (1987) *Reservoir sedimentation: impact, extent, and mitigation (Report no. WTP71)*. 1st edn. Washington, D.C.: The World Bank.

Meyer-Peter, E. and Müller, R. (1948) 'Formulas for Bed-Load Transport, Proceedings, 2nd Congress', *International Association of Hydraulic Research*. Stockholm, pp. 39–64.

Morris, G., Annandale, G. and Hotchkiss, R. (2008) 'Reservoir sedimentation', in Garcia, M. (ed.) *Sedimentation Engineering: Processes, Measurements and Practice*. Reston, VA: American Society of Civil Engineers (ASCE), pp. 579–612.

Morris, G. L. (2015) 'Management alternatives to combat reservoir sedimentation', in Boes, R. M. (ed.) *Proc. First International Workshop on Sediment Bypass Tunnels, VAW-Mitteilungen 232*. VAW,ETH Zurich, Switzerland, pp. 181–192.

Morris, G. L. and Fan, J. (1998) *Reservoir Sedimentation Handbook*. 1st edn. New York: McGraw-Hill Book Co.

Msadala, V. P. (2009) *Sediment Yield Prediction Based on Analytical Methods and Mathematical Modelling*. University of Stellenbosch.

Naudacher, E. (1991) *Hydrodynamic Forces*. Rotterdam: A.A.Balkema.

Paul, T. C. and Dhillon, G. S. (no date) 'Sluice dimensioning for desilting reservoirs', *International Water Power and Dam Construction*, 40(5), pp. 40–44.

Peterka, A. J. (1953) 'The effect of entrained air on cavitation pitting', in *Proceedings: Minnesota International Hydraulic Convention*. ASCE, pp. 507–518.

Pitt, J. D. and Thompson, G. (1984) 'The impact of sedimentation on reservoir life', in Walling, D. E., Foster, S. S. D., and Wurzel, P. (eds) *Challenges in African Hydrology and Water Resources: proceedings of the Harare Symposium*. Harare: IAHS Publications, no. 144, pp. 541–548.

Przedwojski, B., Blazejewski, R. and Pilarczyk, K. W. (1995) *River training techniques : Fundamentals, design and applications*. Rotterdam: A.A. Balkema.

Qian, N. (1982) 'Reservoir sedimentation and slope stability; technical and environmental effects', *Fourth International Congress on Large Dams, Rio de Janeiro, Brazil*, 3, pp. 639–690.

Raudkivi, A. J. (1993) *Sedimentation: Exclusion and Removal of Sediment from Diverted Water*. 6th edn. Rotterdam: A.A. Balkema.

Van Rijn, L. C. (1993) *Principles of sediment transport in rivers, estuaries and coastal seas*. Amsterdam: Aqua Publications.

Rindles, A. J. and Gulliver, J. s. (1983) *An Experimental Study of Critical Submergence to Avoid Free-Surface Vortices at Vertical Intakes (Report No. 224)*. St Paul, Minnesota.

Rollo, C. *et al.* (2018) 'Sedimentation Management of Cerro Del Aguila Reservoir in Peru: A "Mobile Dam" for a Highly Erosive Andean Watershed', in *ICOLD 26th International Congress on Large Dams 4-6 July, Vienna, Austria*, pp. 262–278.

Rooseboom, A. *et al.* (1983) *National Transport Commission Road Drainage Manual*. 2nd edn. Pretoria: SANRAL.

Rooseboom, A. (1992) *Sediment transport in rivers and reservoirs - A Southern African Perspective*. Pretoria.

SANRAL (2013) *Drainage Manual*. 6th edn. Pretoria: The South African National Road Agency.

SANS 3001-AG23 (2014) *Civil engineering test methods, Part AG23: Particle and relative densities of aggregates*. 1.1. Pretoria: SABS Standards Division.

Sarkardeh, H. (2017) 'Minimum Reservoir Water Level in Hydropower Dams', *Chinese Journal of Mechanical Engineering (English Edition)*, 30(4), pp. 1017–1024.

Sayah, S. M. *et al.* (2015) *Design and erection of the 6 bottom outlets of Cerro del Águila dam for flood routing during construction and future sediment flushing*.

Sharma, H. (1976) 'Air-Entrainment in High Head Gated Condiuts', *Journal of the Hydraulics*

Division, 102(11), pp. 1629–1646.

Di Silvio, G. (1990) 'Modeling desiltation of reservoirs by bottom-outlet flushing', in Shen, H. W. (ed.) *Movable bed physical models*. Dordrecht: Kluwer Academic Publishers, pp. 159–171.

Simons, D. B. and Sentürk, F. (1992) *Sediment transport technology : Water and sediment dynamics*. Littleton, Colorado, USA: Water Resources Publications.

Singh, K. P. (1987) 'Lake sedimentation reduction techniques', *Public Works PUWOAH*, 118(9).

Speerli, J. (1999) *Air entrainment of free-surface tunnel flow*. Switzerland: Swiss Federal Institute of Technology.

Srivastav, A. and Nayak, A. (2015) 'Bottom Outlet of Koldam HEPP – Scheme, Challenges and Performance – A Case Study', in *Global Energy Technology Summit*.

Stoffberg, F. W. (2005) *Evaluation of incipient motion criteria for rock in reno mattresses and rip rap*. Stellenbosch University.

USACE (1980) *Hydraulic Design of Reservoir Outlet Structues (EM 1110-2-1602)*. Washington, DC: United States Army Corps of Engineers.

USACE (1997) *Engineering and design – Tunnels and shafts in rock (EM 1110-2-2901)*. Washington, DC: United States Army Corps of Engineers.

USACE (2003) *Engineering and Design: Structural Design and Evaluation of Outlet Works (EM 1110-2-2400)*. Washington, DC: United States Army Corps of Engineers.

USBR (1987) *Design of Small Dams*. 3rd edn. Water Resources Technical Publication.

Vischer, D. L. and Hager, W. H. (1998) *Dam Hydraulics*. 1st edn. West Sussex: John Wiley and Sons Ltd.

Wadell, H. (1932) 'Volume, Shape, and Roundness of Rock Particles', *Journal of Geology*, 40(5), pp. 443–451.

Webber, N. B. (1971) 'Hydraulic Models', in *Fluid Mechanics for Civil Engineers*. 1st edn. London: Chapman and Hall Ltd., pp. 297–304.

Webby, M. G. (2003) *Investigation of Blowback Incidents at Rangipo Power Station*. Wellington, New Zealand.

Wei, Y. (1991) 'Abrasion of the bottom outlets and its repair in Sanmenxia project', *International Journal of Sediment Reseach*, 6(2).

White, R. (2001) *Evacuation of sediments from reservoirs*. London: Thomas Telford publishing. doi: 10.1680/eosfr.29538.

White, W. R. and Bettess, R. (1984) 'The feasibility of flushing sediments through reservoirs', in *Challenges in African Hydrology and Water Resources (Proceedings of the Harare*

Symposium, July 1984). 144th edn. Wallingford, Oxfordshire: International Association of Hydrological Sciences, pp. 577–587.

Yang, C. T. (1973) 'Incipient motion and sediment transport', *Journal of the Hydraulics Division*, 99(10), pp. 1679–1704.

Zhang, R. and Qian, N. (1985) *Reservoir Sedimentation*.

Appendix A Numerical model and results

A.1 General hydraulic parameter calculations

Table A.1: General calculated upstream hydraulic design parameters

Parameter	Equation	Value	Unit	Comments
Upstream initial conduit submerged water level (H_{si})	$H_{si} = D \cdot cos(\phi)$	2.990	*m*	Measured relative to the conduit invert level; $\phi = 0.083\ m/m$ or $\phi = 4.764°$
Upstream design water depth (H_w)	$H_w = 1.2 \cdot H_{si}$	3.737	*m*	Measured relative to IL_1
Upstream design approach flow depth (y_u)		1.600	*m*	Chosen; Measured relative to H_{sed}
Upstream design approach flow velocity (V_u)	Figure 3.5-8	1.595	*m/s*	Corresponds to y_u; Occurs above H_{sed}
Local upstream design sediment level (H_{sed})	$H_{sed} = H_w - y_u$	2.137	*m*	Measured relative to IL_1
Upstream design energy level (H_u)	$H_u = H_w + \frac{{V_u}^2}{2g}$	3.867	*m*	Measured relative to IL_1
Froude number (F_{r_u})	$F_{r_u} = \frac{V_u}{\sqrt{g y_u}}$	0.403		Subcritical flow as $F_r < 1$
Upstream channel width (b_u)	$b_u = \frac{Q_e}{y_u \cdot V_u}$	20.828	*m*	Occurs upstream of weir crest where approach flow conditions occur; $Q_e = 53.153\ m^3/s$.

A.2 Hydraulic calculations: *Design 1* (α = 45°)

Table A.2: Ogee spillway parameters

Parameter	Equation	Value	Unit	Comments
Weir crest radius (R_c)		8.700	*m*	Chosen
Weir crest length (b_c)		19.494	*m*	Measured from drawn geometry in CFD; Influenced by R_c and α, with $b_c < b_u$.
Safety design head (H_e)		1.152	*m*	Solved so $Q = Q_e$
Design head (H_o)	$H_o = H_e/1.33$	0.866	*m*	Recommended design ratio from USBR (1987)
Weir crest height (P)	$P = H_w + \frac{{V_u}^2}{2 \cdot g} - H_{sed} - H_e$	0.578	*m*	Measured relative to H_{sed}

Total weir crest height (H_t)	$H_t = P + H_{sed} - d$	2.503	*m*	Measured relative to local NGL; d = height between local NGL and $IL_1 = 0.212\ m$
Discharge Coefficient (C_o)	Figure 3.5-12	2.121		Corresponds to $\frac{P}{H_0} = 0.667$
Ratio of coefficients (C_e/C_o)	Figure 3.5-13	1.040		Corresponds to $\frac{H_e}{H_0} = 1.33$
Discharge (Q)	$Q = \frac{C_e}{C_o} \cdot C_o \cdot b_c \cdot {H_e}^{1.5}$	53.153	*m³/s*	Uncontrolled ogee spillway equation (USBR, 1987)

Table A.3: Flow depths and velocities at chosen hydraulic control points

Parameter	Equation	Value	Unit	Comments
Control point: p_1				**Location: along weir crest**
Flow depth (y_1)	$y_1 = \left(\frac{{Q_e}^2}{g \cdot {b_c}^2}\right)^{1/3}$	0.912	*m*	Assumed critical flow above weir crest
Flow area (A_1)	$A_1 = y_1 \cdot b_c$	17.773	*m²*	
Wetted flow perimeter (P_1)	$P_1 = b_c + 2 \cdot y_1$	21.317	*m*	
Flow velocity (V_1)	$V_1 = \frac{Q_e}{A_1}$	2.991	*m/s*	
Froude number (F_{r_1})	$F_{r_1} = \frac{V_1}{\sqrt{g \cdot y_1}}$	1.000		Critical flow as $F_r = 1$
Energy level (H_1)	$H_1 = y_1 + \frac{{V_1}^2}{2 \cdot g} + H_t + d$	4.083	*m*	Measured relative to IL_1
Control point: p_2				**Location: downstream edge of reverse bottom curve**
Arc length width (b_2)		15.995	*m*	Measured from drawn geometry in CFD
Elevation above IL_1 (z_2)		1.183	*m*	Measured from drawn geometry in CFD
Surface length between p_1 and p_2 (L_{1-2})		3.024	*m*	Measured from drawn geometry in CFD
Flow depth (y_2)		0.521	*m*	Solved so $H_2 = H_1$
Flow area (A_2)	$A_2 = y_2 \cdot b_2$	8.339	*m²*	
Wetted flow perimeter (P_2)	$P_2 = b_2 + 2 \cdot y_2$	17.038	*m*	
Flow velocity (V_2)	$V_2 = \frac{Q_e}{A_2}$	6.364	*m/s*	
Froude number (F_{r_2})	$F_{r_2} = \frac{V_2}{\sqrt{g \cdot y_2}}$	2.818		Supercritical flow as $F_r > 1$
Average hydraulic radius (R_{avg})	$R_{avg} = \frac{(A_1 + A_2)}{(P_1 + P_2)}$	0.681	*m*	

Average flow velocity (V_{avg})	$V_{avg} = (V_1 + V_2)/2$	4.682	*m/s*	
Transition loss between p_1 and p_2 ($h_{L_{1-2}}$)	$h_{L_{1-2}} = \frac{k \cdot {V_{avg}}^2}{2 \cdot g}$	0.279	*m*	$k = 0.25$ for converging section (SANRAL, 2013)
Friction loss between p_1 and p_2 ($h_{f_{1-2}}$)	$h_{f_{1-2}} = \frac{{V_{avg}}^2 \cdot n^2 \cdot L_{1-2}}{(R_{avg})^{4/3}}$	0.028	*m*	$n = 0.016$
Energy slope between p_1 and p_2 (Sf_{1-2})	$Sf_{1-2} = \frac{\sum h_{L_{1-2}} + h_{f_{1-2}}}{L_{1-2}}$	0.102	*m/m*	
Energy level (H_2)	$H_2 = y_2 + \frac{{V_2}^2}{2 \cdot g} + z_2 + h_{L_{1-2}} + h_{f_{1-2}}$	4.083	*m*	Measured relative to IL_1
Control point: p_3				**Location: start of conduit bed slope**
Conduit width (b_3)		6.000	*m*	$b_3 = B$
Elevation above IL_1 (z_3)		0.212	*m*	Measured from drawn geometry in CFD
Surface length between p_2 and p_3 (L_{2-3})		9.757	*m*	Measured from drawn geometry in CFD
Flow depth (y_3)		1.528	*m*	Solved so $H_3 = H_1$
Flow area (A_3)	$A_3 = y_3 \cdot b_3$	9.168	*m²*	
Wetted flow perimeter (P_3)	$P_3 = b_3 + 2 \cdot y_3$	9.056	*m*	
Flow velocity (V_3)	$V_3 = \frac{Q_e}{A_3}$	5.798	*m/s*	
Froude number (F_{r_3})	$F_{r_3} = \frac{V_3}{\sqrt{g \cdot y_3}}$	1.497		Supercritical flow as $F_r > 1$
Average hydraulic radius (R_{avg})	$R_{avg} = \frac{(A_2 + A_3)}{(P_2 + P_3)}$	0.671	*m*	
Average flow velocity (V_{avg})	$V_{avg} = (V_2 + V_3)/2$	6.086	*m/s*	
Transition loss between p_2 and p_3 ($h_{L_{2-3}}$)	$h_{L_{2-3}} = \frac{k \cdot {V_{avg}}^2}{2 \cdot g}$	0.472	*m*	$k = 0.25$ for converging section (SANRAL, 2013)
Friction loss between p_2 and p_3 ($h_{f_{2-3}}$)	$h_{f_{2-3}} = \frac{{V_{avg}}^2 \cdot n^2 \cdot L_{2-3}}{(R_{avg})^{4/3}}$	0.158	*m*	$n = 0.016$
Energy slope between p_2 and p_3 (Sf_{2-3})	$Sf_{2-3} = \frac{\sum h_{L_{2-3}} + h_{f_{2-3}}}{L_{2-3}}$	0.065	*m/m*	

Energy level (H_3)	$H_3 = y_3 + \frac{{V_3}^2}{2 \cdot g} + z_3 + h_{L_{2-3}} + h_{f_{2-3}}$	4.083	*m*	Measured relative to IL_1
Control point: p_p				**Location: $12\ m$ downstream of p_3**
Conduit width (b_p)		6.000	*m*	$b_p = B$
Elevation above IL_1 (z_p)		-0.788	*m*	Measured from drawn geometry in CFD
Surface length between p_3 and p_p (L_{3-p})		12.042	*m*	Measured from drawn geometry in CFD
Flow depth (y_p)		1.048	*m*	Solved so $H_3 = H_1$
Flow area (A_p)	$A_p = y_p \cdot b_p$	6.287	*m²*	
Wetted flow perimeter (P_p)	$P_p = b_p + 2 \cdot y_p$	8.096	*m*	
Flow velocity (V_p)	$V_p = \frac{Q_e}{A_p}$	8.454	*m/s*	
Froude number (F_{r_p})	$F_{r_p} = \frac{V_p}{\sqrt{g \cdot y_p}}$	2.637		Supercritical flow as $F_r > 1$
Average hydraulic radius (R_{avg})	$R_{avg} = \frac{(A_3 + A_p)}{(P_3 + P_p)}$	0.901	*m*	
Average flow velocity (V_{avg})	$V_{avg} = (V_3 + V_p)/2$	7.126	*m/s*	
Transition loss between p_3 and p_p ($h_{L_{3-p}}$)	$h_{L_{3-p}} = \frac{k \cdot {V_{avg}}^2}{2 \cdot g}$	0	*m*	$k = 0$ for no change in cross-section (SANRAL, 2013)
Friction loss between p_3 and p_p ($h_{f_{3-p}}$)	$h_{f_{3-p}} = \frac{{V_{avg}}^2 \cdot n^2 \cdot L_{3-p}}{(R_{avg})^{4/3}}$	0.180	*m*	$n = 0.016$
Energy slope between p_3 and p_p (Sf_{3-p})	$Sf_{2-3} = \frac{\sum h_{L_{3-p}} + h_{f_{3-p}}}{L_{3-p}}$	0.015	*m/m*	
Energy level (H_3)	$H_3 = y_3 + \frac{{V_3}^2}{2 \cdot g} + z_3 + h_{L_{3-p}} + h_{f_{3-p}}$	4.083	*m*	Measured relative to IL_1
Control point: p_5				**Location: conduit outlet**
Conduit width (b_5)		6.000	*m*	$b_5 = B$
Flow depth (y_5)		0.717	*m*	Assumed normal flow; Solved so $Q = Q_e$
Flow area (A_5)	$A_5 = y_5 \cdot b_5$	4.263	*m²*	
Wetted flow perimeter (P_5)	$P_5 = b_5 + 2 \cdot y_5$	7.421	*m*	

Discharge (Q)	$Q = \frac{{A_5}^{5/3}\Phi^{0.5}}{n{P_5}^{2/3}}$	53.153	*m³/s*	Manning's Equation; $n = 0.016$
Flow velocity (V_5)	$V_5 = \frac{Q}{A_5}$	12.468	*m/s*	
Froude number (F_{r_5})	$F_{r_5} = \frac{V_5}{\sqrt{g \cdot y_5}}$	4.723		Supercritical flow as $F_r > 1$
Energy slope (Sf_5)		0.083	*m/m*	$Sf_5 = \Phi$ (normal flow)

A.3 Hydraulic calculations: *Design 1* (α = 30°)

Table A.4: Ogee spillway parameters

Parameter	Equation	Value	Unit	Comments
Weir crest radius (R_c)		12.000	*m*	Chosen
Weir crest length (b_c)		19.400	*m*	Measured from drawn geometry in CFD; Influenced by R_c and α, with $b_c < b_u$.
Safety design head (H_e)		1.156	*m*	Solved so $Q = Q_e$
Design head (H_o)	$H_o = H_e/1.33$	0.869	*m*	Recommended design ratio from USBR (1987)
Weir crest height (P)	$P = H_w + \frac{{V_u}^2}{2 \cdot g} - H_{sed} - H_e$	0.574	*m*	Measured relative to H_{sed}
Total weir crest height (H_t)	$H_t = P + H_{sed} - d$	2.499	*m*	Measured relative to local NGL; d = height between local NGL and $IL_1 = 0.212\ m$
Discharge Coefficient (C_o)	Figure 3.5-12	2.120		Corresponds to $\frac{P}{H_0} = 0.660$
Ratio of coefficients (C_e/C_o)	Figure 3.5-13	1.040		Corresponds to $\frac{H_e}{H_0} = 1.33$
Discharge (Q)	$Q = \frac{C_e}{C_o} \cdot C_o \cdot b_c \cdot {H_e}^{1.5}$	53.153	*m³/s*	Uncontrolled ogee spillway equation (USBR, 1987)

Table A.5: Flow depths and velocities at chosen hydraulic control points

Parameter	Equation	Value	Unit	Comments
Control point: p_1				**Location: along weir crest**
Flow depth (y_1)	$y_1 = \left(\frac{{Q_e}^2}{g \cdot {b_c}^2}\right)^{1/3}$	0.915	*m*	Assumed critical flow above weir crest
Flow area (A_1)	$A_1 = y_1 \cdot b_c$	17.745	*m²*	
Wetted flow perimeter (P_1)	$P_1 = b_c + 2 \cdot y_1$	21.230	*m*	

Flow velocity (V_1)	$V_1 = \frac{Q_e}{A_1}$	2.995	*m/s*	
Froude number (F_{r_1})	$F_{r_1} = \frac{V_1}{\sqrt{g \cdot y_1}}$	1.000		Critical flow as $F_r = 1$
Energy level (H_1)	$H_1 = y_1 + \frac{{V_1}^2}{2 \cdot g} + H_t + d$	4.083	*m*	Measured relative to IL_1
Control point: p_2				**Location: downstream edge of reverse bottom curve**
Arc length width (b_2)		17.345	*m*	Measured from drawn geometry in CFD
Elevation above IL_1 (z_2)		1.541	*m*	Measured from drawn geometry in CFD
Surface length between p_1 and p_2 (L_{1-2})		2.563	*m*	Measured from drawn geometry in CFD
Flow depth (y_2)		0.523	*m*	Solved so $H_2 = H_1$
Flow area (A_2)	$A_2 = y_2 \cdot b_2$	9.079	*m²*	
Wetted flow perimeter (P_2)	$P_2 = b_2 + 2 \cdot y_2$	18.391	*m*	
Flow velocity (V_2)	$V_2 = \frac{Q_e}{A_2}$	5.855	*m/s*	
Froude number (F_{r_2})	$F_{r_2} = \frac{V_2}{\sqrt{g \cdot y_2}}$	2.584		Supercritical flow as $F_r > 1$
Average hydraulic radius (R_{avg})	$R_{avg} = \frac{(A_1 + A_2)}{(P_1 + P_2)}$	0.677	*m*	
Average flow velocity (V_{avg})	$V_{avg} = (V_1 + V_2)/2$	4.425	*m/s*	
Transition loss between p_1 and p_2 ($h_{L_{1-2}}$)	$h_{L_{1-2}} = \frac{k \cdot {V_{avg}}^2}{2 \cdot g}$	0.249	*m*	$k = 0.25$ for converging section (SANRAL, 2013)
Friction loss between p_1 and p_2 ($h_{f_{1-2}}$)	$h_{f_{1-2}} = \frac{{V_{avg}}^2 \cdot n^2 \cdot L_{1-2}}{(R_{avg})^{4/3}}$	0.022	*m*	$n = 0.016$
Energy slope between p_1 and p_2 (Sf_{1-2})	$Sf_{1-2} = \frac{\sum h_{L_{1-2}} + h_{f_{1-2}}}{L_{1-2}}$	0.106	*m/m*	
Energy level (H_2)	$H_2 = y_2 + \frac{{V_2}^2}{2 \cdot g} + z_2 + h_{L_{1-2}} + h_{f_{1-2}}$	4.083	*m*	Measured relative to IL_1
Control point: p_3				**Location: start of conduit bed slope**
Conduit width (b_3)		6.000	*m*	$b_3 = B$
Elevation above IL_1 (z_3)		0.212	*m*	Measured from drawn geometry in CFD

Surface length between p_2 and p_3 (L_{2-3})		13.362	*m*	Measured from drawn geometry in CFD
Flow depth (y_3)		1.530	*m*	Solved so $H_3 = H_1$
Flow area (A_3)	$A_3 = y_3 \cdot b_3$	9.178	*m²*	
Wetted flow perimeter (P_3)	$P_3 = b_3 + 2 \cdot y_3$	9.059	*m*	
Flow velocity (V_3)	$V_3 = \frac{Q_e}{A_3}$	5.792	*m/s*	
Froude number (F_{r_3})	$F_{r_3} = \frac{V_3}{\sqrt{g \cdot y_3}}$	1.495		Supercritical flow as $F_r > 1$
Average hydraulic radius (R_{avg})	$R_{avg} = \frac{(A_2 + A_3)}{(P_2 + P_3)}$	0.665	*m*	
Average flow velocity (V_{avg})	$V_{avg} = (V_2 + V_3)/2$	5.823	*m/s*	
Transition loss between p_2 and p_3 ($h_{L_{2-3}}$)	$h_{L_{2-3}} = \frac{k \cdot {V_{avg}}^2}{2 \cdot g}$	0.432	*m*	$k = 0.25$ for converging section (SANRAL, 2013)
Friction loss between p_2 and p_3 ($h_{f_{2-3}}$)	$h_{f_{2-3}} = \frac{{V_{avg}}^2 \cdot n^2 \cdot L_{2-3}}{(R_{avg})^{4/3}}$	0.200	*m*	$n = 0.016$
Energy slope between p_2 and p_3 (Sf_{2-3})	$Sf_{2-3} = \frac{\sum h_{L_{2-3}} + h_{f_{2-3}}}{L_{2-3}}$	0.047	*m/m*	
Energy level (H_3)	$H_3 = y_3 + \frac{{V_3}^2}{2 \cdot g} + z_3 + h_{L_{2-3}} + h_{f_{2-3}}$	4.083	*m*	Measured relative to IL_1
Control point: p_p				**Location: $12\ m$ downstream of p_3**
Conduit width (b_p)		6.000	*m*	$b_p = B$
Elevation above IL_1 (z_p)		-0.788	*m*	Measured from drawn geometry in CFD
Surface length between p_3 and p_p (L_{3-p})		12.042	*m*	Measured from drawn geometry in CFD
Flow depth (y_p)		1.048	*m*	Solved so $H_3 = H_1$
Flow area (A_p)	$A_p = y_p \cdot b_p$	6.287	*m²*	
Wetted flow perimeter (P_p)	$P_p = b_p + 2 \cdot y_p$	8.096	*m*	
Flow velocity (V_p)	$V_p = \frac{Q_e}{A_p}$	8.455	*m/s*	
Froude number (F_{r_p})	$F_{r_p} = \frac{V_p}{\sqrt{g \cdot y_p}}$	2.637		Supercritical flow as $F_r > 1$

Average hydraulic radius (R_{avg})	$R_{avg} = \frac{(A_3 + A_p)}{(P_3 + P_p)}$	0.901	*m*	
Average flow velocity (V_{avg})	$V_{avg} = (V_3 + V_p)/2$	7.123	*m/s*	
Transition loss between p_3 and p_p ($h_{L_{3-p}}$)	$h_{L_{3-p}} = \frac{k \cdot {V_{avg}}^2}{2 \cdot g}$	0	*m*	$k = 0$ for no change in cross-section (SANRAL, 2013)
Friction loss between p_3 and p_p ($h_{f_{3-p}}$)	$h_{f_{3-p}} = \frac{{V_{avg}}^2 \cdot n^2 \cdot L_{3-p}}{(R_{avg})^{4/3}}$	0.180	*m*	$n = 0.016$
Energy slope between p_3 and p_p (Sf_{3-p})	$Sf_{2-3} = \frac{\sum h_{L_{3-p}} + h_{f_{3-p}}}{L_{3-p}}$	0.015	*m/m*	
Energy level (H_3)	$H_3 = y_3 + \frac{{V_3}^2}{2 \cdot g} + z_3 + h_{L_{3-p}} + h_{f_{3-p}}$	4.083	*m*	Measured relative to IL_1
Control point: p_5				**Location: conduit outlet**
Conduit width (b_5)		6.000	*m*	$b_5 = B$
Flow depth (y_5)		0.717	*m*	Assumed normal flow; Solved so $Q = Q_e$
Flow area (A_5)	$A_5 = y_5 \cdot b_5$	4.263	*m²*	
Wetted flow perimeter (P_5)	$P_5 = b_5 + 2 \cdot y_5$	7.421	*m*	
Discharge (Q)	$Q = \frac{{A_5}^{5/3} \Phi^{0.5}}{n {P_5}^{2/3}}$	53.153	*m³/s*	Manning's Equation; $n = 0.016$
Flow velocity (V_5)	$V_5 = \frac{Q}{A_5}$	12.468	*m/s*	
Froude number (F_{r_5})	$F_{r_5} = \frac{V_5}{\sqrt{g \cdot y_5}}$	4.723		Supercritical flow as $F_r > 1$
Energy slope (Sf_5)		0.083	*m/m*	$Sf_5 = \Phi$ (normal flow)

A.4 Hydraulic calculations: *Design 2* (α = 45°)

Table A.6: Ogee spillway parameters

Parameter	Equation	Value	Unit	Comments
Weir crest radius (R_c)		8.700	*m*	Chosen
Weir crest length (b_c)		19.494	*m*	Measured from drawn geometry in CFD; Influenced by R_c and α, with $b_c < b_u$.
Safety design head (H_e)		1.152	*m*	Solved so $Q = Q_e$

Design head (H_o)	$H_o = H_e/1.33$	0.866	*m*	Recommended design ratio from USBR (1987)
Weir crest height (P)	$P = H_w + \frac{{V_u}^2}{2 \cdot g} - H_{sed} - H_e$	0.578	*m*	Measured relative to H_{sed}
Total weir crest height (H_t)	$H_t = P + H_{sed} - d$	2.503	*m*	Measured relative to local NGL; d = height between local NGL and $IL_1 = 0.212\ m$
Discharge Coefficient (C_o)	Figure 3.5-12	2.121		Corresponds to $\frac{P}{H_0} = 0.667$
Ratio of coefficients (C_e/C_o)	Figure 3.5-13	1.040		Corresponds to $\frac{H_e}{H_0} = 1.33$
Discharge (Q)	$Q = \frac{C_e}{C_o} \cdot C_o \cdot b_c \cdot {H_e}^{1.5}$	53.153	*m³/s*	Uncontrolled ogee spillway equation (USBR, 1987)

Table A.7: Flow depths and velocities at chosen hydraulic control points

Parameter	Equation	Value	Unit	Comments
Control point: p_1				**Location: along weir crest**
Flow depth (y_1)	$y_1 = \left(\frac{{Q_e}^2}{g \cdot {b_c}^2}\right)^{1/3}$	0.912	*m*	Assumed critical flow above weir crest
Flow area (A_1)	$A_1 = y_1 \cdot b_c$	17.773	*m²*	
Wetted flow perimeter (P_1)	$P_1 = b_c + 2 \cdot y_1$	21.317	*m*	
Flow velocity (V_1)	$V_1 = \frac{Q_e}{A_1}$	2.991	*m/s*	
Froude number (F_{r_1})	$F_{r_1} = \frac{V_1}{\sqrt{g \cdot y_1}}$	1.000		Critical flow as $F_r = 1$
Energy level (H_1)	$H_1 = y_1 + \frac{{V_1}^2}{2 \cdot g} + H_t + d$	4.083	*m*	Measured relative to IL_1
Control point: p_2				**Location: downstream edge of reverse bottom curve**
Arc length width (b_2)		14.811	*m*	Measured from drawn geometry in CFD
Elevation above IL_1 (z_2)		0.183	*m*	Measured from drawn geometry in CFD
Surface length between p_1 and p_2 (L_{1-2})		4.305	*m*	Measured from drawn geometry in CFD
Flow depth (y_2)		0.467	*m*	Solved so $H_2 = H_1$
Flow area (A_2)	$A_2 = y_2 \cdot b_2$	6.910	*m²*	
Wetted flow perimeter (P_2)	$P_2 = b_2 + 2 \cdot y_2$	15.744	*m*	
Flow velocity (V_2)	$V_2 = \frac{Q_e}{A_2}$	7.692	*m/s*	

Froude number (F_{r_2})	$F_{r_2} = \frac{V_2}{\sqrt{g \cdot y_2}}$	3.596		Supercritical flow as $F_r > 1$
Average hydraulic radius (R_{avg})	$R_{avg} = \frac{(A_1 + A_2)}{(P_1 + P_2)}$	0.666	*m*	
Average flow velocity (V_{avg})	$V_{avg} = (V_1 + V_2)/2$	5.341	*m/s*	
Transition loss between p_1 and p_2 ($h_{L_{1-2}}$)	$h_{L_{1-2}} = \frac{k \cdot {V_{avg}}^2}{2 \cdot g}$	0.364	*m*	$k = 0.25$ for converging section (SANRAL, 2013)
Friction loss between p_1 and p_2 ($h_{f_{1-2}}$)	$h_{f_{1-2}} = \frac{{V_{avg}}^2 \cdot n^2 \cdot L_{1-2}}{(R_{avg})^{4/3}}$	0.054	*m*	$n = 0.016$
Energy slope between p_1 and p_2 (Sf_{1-2})	$Sf_{1-2} = \frac{\sum h_{L_{1-2}} + h_{f_{1-2}}}{L_{1-2}}$	0.097	*m/m*	
Energy level (H_2)	$H_2 = y_2 + \frac{{V_2}^2}{2 \cdot g} + z_2 + h_{L_{1-2}} + h_{f_{1-2}}$	4.083	*m*	Measured relative to IL_1
Control point: p_3				**Location: start of conduit bed slope**
Conduit width (b_3)		6.000	*m*	$b_3 = B$
Elevation above IL_1 (z_3)		-0.708	*m*	Measured from drawn geometry in CFD
Surface length between p_2 and p_3 (L_{2-3})		8.953	*m*	Measured from drawn geometry in CFD
Flow depth (y_3)		1.241	*m*	Solved so $H_3 = H_1$
Flow area (A_3)	$A_3 = y_3 \cdot b_3$	7.448	*m²*	
Wetted flow perimeter (P_3)	$P_3 = b_3 + 2 \cdot y_3$	8.483	*m*	
Flow velocity (V_3)	$V_3 = \frac{Q_e}{A_3}$	7.137	*m/s*	
Froude number (F_{r_3})	$F_{r_3} = \frac{V_3}{\sqrt{g \cdot y_3}}$	2.045		Supercritical flow as $F_r > 1$
Average hydraulic radius (R_{avg})	$R_{avg} = \frac{(A_2 + A_3)}{(P_2 + P_3)}$	0.593	*m*	
Average flow velocity (V_{avg})	$V_{avg} = (V_2 + V_3)/2$	7.414	*m/s*	
Transition loss between p_2 and p_3 ($h_{L_{2-3}}$)	$h_{L_{2-3}} = \frac{k \cdot {V_{avg}}^2}{2 \cdot g}$	0.700	*m*	$k = 0.25$ for converging section (SANRAL, 2013)
Friction loss between p_2 and p_3 ($h_{f_{2-3}}$)	$h_{f_{2-3}} = \frac{{V_{avg}}^2 \cdot n^2 \cdot L_{2-3}}{(R_{avg})^{4/3}}$	0.253	*m*	$n = 0.016$

Energy slope between p_2 and p_3 (Sf_{2-3})	$Sf_{2-3} = \frac{\sum h_{L_{2-3}} + h_{f_{2-3}}}{L_{2-3}}$	0.107	*m/m*	
Energy level (H_3)	$H_3 = y_3 + \frac{{V_3}^2}{2 \cdot g} + z_3 + h_{L_{2-3}} + h_{f_{2-3}}$	4.083	*m*	Measured relative to IL_1
Control point: p_p				**Location: $12\ m$ downstream of p_3**
Conduit width (b_p)		6.000	*m*	$b_p = B$
Elevation above IL_1 (z_p)		-1.708	*m*	Measured from drawn geometry in CFD
Surface length between p_3 and p_p (L_{3-p})		12.042	*m*	Measured from drawn geometry in CFD
Flow depth (y_p)		0.936	*m*	Solved so $H_3 = H_1$
Flow area (A_p)	$A_p = y_p \cdot b_p$	5.614	*m²*	
Wetted flow perimeter (P_p)	$P_p = b_p + 2 \cdot y_p$	7.871	*m*	
Flow velocity (V_p)	$V_p = \frac{Q_e}{A_p}$	9.467	*m/s*	
Froude number (F_{r_p})	$F_{r_p} = \frac{V_p}{\sqrt{g \cdot y_p}}$	3.125		Supercritical flow as $F_r > 1$
Average hydraulic radius (R_{avg})	$R_{avg} = \frac{(A_3 + A_p)}{(P_3 + P_p)}$	0.799	*m*	
Average flow velocity (V_{avg})	$V_{avg} = (V_3 + V_p)/2$	8.302	*m/s*	
Transition loss between p_3 and p_p ($h_{L_{3-p}}$)	$h_{L_{3-p}} = \frac{k \cdot {V_{avg}}^2}{2 \cdot g}$	0	*m*	$k = 0$ for no change in cross-section (SANRAL, 2013)
Friction loss between p_3 and p_p ($h_{f_{3-p}}$)	$h_{f_{3-p}} = \frac{{V_{avg}}^2 \cdot n^2 \cdot L_{3-p}}{\left(R_{avg}\right)^{4/3}}$	0.287	*m*	$n = 0.016$
Energy slope between p_3 and p_p (Sf_{3-p})	$Sf_{2-3} = \frac{\sum h_{L_{3-p}} + h_{f_{3-p}}}{L_{3-p}}$	0.024	*m/m*	
Energy level (H_3)	$H_3 = y_3 + \frac{{V_3}^2}{2 \cdot g} + z_3 + h_{L_{3-p}} + h_{f_{3-p}}$	4.083	*m*	Measured relative to IL_1
Control point: p_5				**Location: conduit outlet**
Conduit width (b_5)		6.000	*m*	$b_5 = B$

Flow depth (y_5)		0.717	*m*	Assumed normal flow; Solved so $Q = Q_e$
Flow area (A_5)	$A_5 = y_5 \cdot b_5$	4.263	*m²*	
Wetted flow perimeter (P_5)	$P_5 = b_5 + 2 \cdot y_5$	7.421	*m*	
Discharge (Q)	$Q = \frac{{A_5}^{5/3} \Phi^{0.5}}{n {P_5}^{2/3}}$	53.153	*m³/s*	Manning's Equation; $n = 0.016$
Flow velocity (V_5)	$V_5 = \frac{Q}{A_5}$	12.468	*m/s*	
Froude number (F_{r_5})	$F_{r_5} = \frac{V_5}{\sqrt{g \cdot y_5}}$	4.723		Supercritical flow as $F_r > 1$
Energy slope (Sf_5)		0.083	*m/m*	$Sf_5 = \Phi$ (normal flow)

A.5 Hydraulic calculations: *Design 2* (α = 30°)

Table A.8: Ogee spillway parameters

Parameter	Equation	Value	Unit	Comments
Weir crest radius (R_c)		12.000	*m*	Chosen
Weir crest length (b_c)		19.400	*m*	Measured from drawn geometry in CFD; Influenced by R_c and α, with $b_c < b_u$.
Safety design head (H_e)		1.156	*m*	Solved so $Q = Q_e$
Design head (H_o)	$H_o = H_e / 1.33$	0.869	*m*	Recommended design ratio from USBR (1987)
Weir crest height (P)	$P = H_w + \frac{{V_u}^2}{2 \cdot g} - H_{sed} - H_e$	0.574	*m*	Measured relative to H_{sed}
Total weir crest height (H_t)	$H_t = P + H_{sed} - d$	2.499	*m*	Measured relative to local NGL; d = height between local NGL and $IL_1 = 0.212\ m$
Discharge Coefficient (C_o)	Figure 3.5-12	2.120		Corresponds to $\frac{P}{H_0} = 0.660$
Ratio of coefficients (C_e/C_o)	Figure 3.5-13	1.040		Corresponds to $\frac{H_e}{H_0} = 1.33$
Discharge (Q)	$Q = \frac{C_e}{C_o} \cdot C_o \cdot b_c \cdot {H_e}^{1.5}$	53.153	*m³/s*	Uncontrolled ogee spillway equation (USBR, 1987)

Table A.9: Flow depths and velocities at chosen hydraulic control points

Parameter	Equation	Value	Unit	Comments
Control point: p_1				**Location: along weir crest**

Flow depth (y_1)	$y_1 = \left(\frac{{Q_e}^2}{g \cdot {b_c}^2}\right)^{1/3}$	0.915	*m*	Assumed critical flow above weir crest
Flow area (A_1)	$A_1 = y_1 \cdot b_c$	17.745	*m²*	
Wetted flow perimeter (P_1)	$P_1 = b_c + 2 \cdot y_1$	21.230	*m*	
Flow velocity (V_1)	$V_1 = \frac{Q_e}{A_1}$	2.995	*m/s*	
Froude number (F_{r_1})	$F_{r_1} = \frac{V_1}{\sqrt{g \cdot y_1}}$	1.000		Critical flow as $F_r = 1$
Energy level (H_1)	$H_1 = y_1 + \frac{{V_1}^2}{2 \cdot g} + H_t + d$	4.083	*m*	Measured relative to IL_1
Control point: p_2				**Location: downstream edge of reverse bottom curve**
Arc length width (b_2)		16.244	*m*	Measured from drawn geometry in CFD
Elevation above IL_1 (z_2)		0.183	*m*	Measured from drawn geometry in CFD
Surface length between p_1 and p_2 (L_{1-2})		4.303	*m*	Measured from drawn geometry in CFD
Flow depth (y_2)		0.423	*m*	Solved so $H_2 = H_1$
Flow area (A_2)	$A_2 = y_2 \cdot b_2$	6.868	*m²*	
Wetted flow perimeter (P_2)	$P_2 = b_2 + 2 \cdot y_2$	17.089	*m*	
Flow velocity (V_2)	$V_2 = \frac{Q_e}{A_2}$	7.740	*m/s*	
Froude number (F_{r_2})	$F_{r_2} = \frac{V_2}{\sqrt{g \cdot y_2}}$	3.800		Supercritical flow as $F_r > 1$
Average hydraulic radius (R_{avg})	$R_{avg} = \frac{(A_1 + A_2)}{(P_1 + P_2)}$	0.642	*m*	
Average flow velocity (V_{avg})	$V_{avg} = (V_1 + V_2)/2$	5.368	*m/s*	
Transition loss between p_1 and p_2 ($h_{L_{1-2}}$)	$h_{L_{1-2}} = \frac{k \cdot {V_{avg}}^2}{2 \cdot g}$	0.367	*m*	$k = 0.25$ for converging section (SANRAL, 2013)
Friction loss between p_1 and p_2 ($h_{f_{1-2}}$)	$h_{f_{1-2}} = \frac{{V_{avg}}^2 \cdot n^2 \cdot L_{1-2}}{(R_{avg})^{4/3}}$	0.057	*m*	$n = 0.016$
Energy slope between p_1 and p_2 (Sf_{1-2})	$Sf_{1-2} = \frac{\sum h_{L_{1-2}} + h_{f_{1-2}}}{L_{1-2}}$	0.099	*m/m*	
Energy level (H_2)	$H_2 = y_2 + \frac{{V_2}^2}{2 \cdot g} + z_2 + h_{L_{1-2}} + h_{f_{1-2}}$	4.083	*m*	Measured relative to IL_1

Control point: p_3				**Location: start of conduit bed slope**
Conduit width (b_3)		6.000	*m*	$b_3 = B$
Elevation above IL_1 (z_3)		-1.038	*m*	Measured from drawn geometry in CFD
Surface length between p_2 and p_3 (L_{2-3})		12.270	*m*	Measured from drawn geometry in CFD
Flow depth (y_3)		1.196	*m*	Solved so $H_3 = H_1$
Flow area (A_3)	$A_3 = y_3 \cdot b_3$	7.177	*m²*	
Wetted flow perimeter (P_3)	$P_3 = b_3 + 2 \cdot y_3$	8.392	*m*	
Flow velocity (V_3)	$V_3 = \frac{Q_e}{A_3}$	7.406	*m/s*	
Froude number (F_{r_3})	$F_{r_3} = \frac{V_3}{\sqrt{g \cdot y_3}}$	2.162		Supercritical flow as $F_r > 1$
Average hydraulic radius (R_{avg})	$R_{avg} = \frac{(A_2 + A_3)}{(P_2 + P_3)}$	0.551	*m*	
Average flow velocity (V_{avg})	$V_{avg} = (V_2 + V_3)/2$	7.573	*m/s*	
Transition loss between p_2 and p_3 ($h_{L_{2-3}}$)	$h_{L_{2-3}} = \frac{k \cdot {V_{avg}}^2}{2 \cdot g}$	0.731	*m*	$k = 0.25$ for converging section (SANRAL, 2013)
Friction loss between p_2 and p_3 ($h_{f_{2-3}}$)	$h_{f_{2-3}} = \frac{{V_{avg}}^2 \cdot n^2 \cdot L_{2-3}}{(R_{avg})^{4/3}}$	0.399	*m*	$n = 0.016$
Energy slope between p_2 and p_3 (Sf_{2-3})	$Sf_{2-3} = \frac{\sum h_{L_{2-3}} + h_{f_{2-3}}}{L_{2-3}}$	0.092	*m/m*	
Energy level (H_3)	$H_3 = y_3 + \frac{{V_3}^2}{2 \cdot g} + z_3 + h_{L_{2-3}} + h_{f_{2-3}}$	4.083	*m*	Measured relative to IL_1
Control point: p_p				**Location: $12\ m$ downstream of p_3**
Conduit width (b_p)		6.000	*m*	$b_p = B$
Elevation above IL_1 (z_p)		-2.038	*m*	Measured from drawn geometry in CFD
Surface length between p_3 and p_p (L_{3-p})		12.042	*m*	Measured from drawn geometry in CFD
Flow depth (y_p)		0.904	*m*	Solved so $H_3 = H_1$
Flow area (A_p)	$A_p = y_p \cdot b_p$	5.422	*m²*	
Wetted flow perimeter (P_p)	$P_p = b_p + 2 \cdot y_p$	7.807	*m*	
Flow velocity (V_p)	$V_p = \frac{Q_e}{A_p}$	9.803	*m/s*	

Froude number (F_{r_p})	$F_{r_p} = \frac{V_p}{\sqrt{g \cdot y_p}}$	3.293		Supercritical flow as $F_r > 1$
Average hydraulic radius (R_{avg})	$R_{avg} = \frac{(A_3 + A_p)}{(P_3 + P_p)}$	0.778	*m*	
Average flow velocity (V_{avg})	$V_{avg} = (V_3 + V_p)/2$	8.605	*m/s*	
Transition loss between p_3 and p_p ($h_{L_{3-p}}$)	$h_{L_{3-p}} = \frac{k \cdot {V_{avg}}^2}{2 \cdot g}$	0	*m*	$k = 0$ for no change in cross-section (SANRAL, 2013)
Friction loss between p_3 and p_p ($h_{f_{3-p}}$)	$h_{f_{3-p}} = \frac{{V_{avg}}^2 \cdot n^2 \cdot L_{3-p}}{(R_{avg})^{4/3}}$	0.319	*m*	$n = 0.016$
Energy slope between p_3 and p_p (Sf_{3-p})	$Sf_{2-3} = \frac{\sum h_{L_{3-p}} + h_{f_{3-p}}}{L_{3-p}}$	0.027	*m/m*	
Energy level (H_3)	$H_3 = y_3 + \frac{{V_3}^2}{2 \cdot g} + z_3 + h_{L_{3-p}} + h_{f_{3-p}}$	4.083	*m*	Measured relative to IL_1
Control point: p_5				**Location: conduit outlet**
Conduit width (b_5)		6.000	*m*	$b_5 = B$
Flow depth (y_5)		0.717	*m*	Assumed normal flow; Solved so $Q = Q_e$
Flow area (A_5)	$A_5 = y_5 \cdot b_5$	4.263	*m²*	
Wetted flow perimeter (P_5)	$P_5 = b_5 + 2 \cdot y_5$	7.421	*m*	
Discharge (Q)	$Q = \frac{{A_5}^{5/3} \Phi^{0.5}}{n {P_5}^{2/3}}$	53.153	*m³/s*	Manning's Equation; $n = 0.016$
Flow velocity (V_5)	$V_5 = \frac{Q}{A_5}$	12.468	*m/s*	
Froude number (F_{r_5})	$F_{r_5} = \frac{V_5}{\sqrt{g \cdot y_5}}$	4.723		Supercritical flow as $F_r > 1$
Energy slope (Sf_5)		0.083	*m/m*	$Sf_5 = \Phi$ (normal flow)

A.6 ANSYS Fluent Meshing (final design)

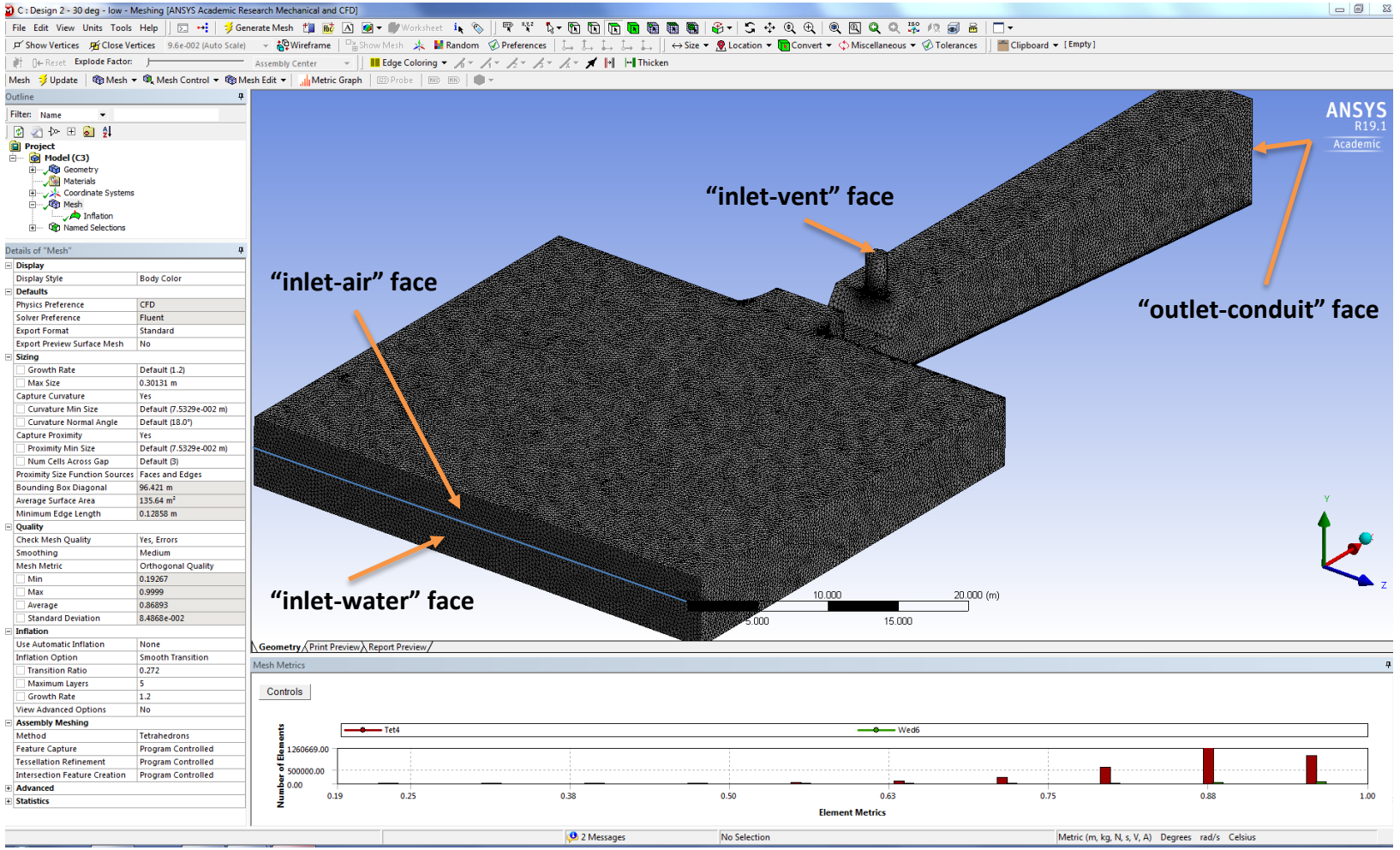

Figure A.1: Meshing and named section details

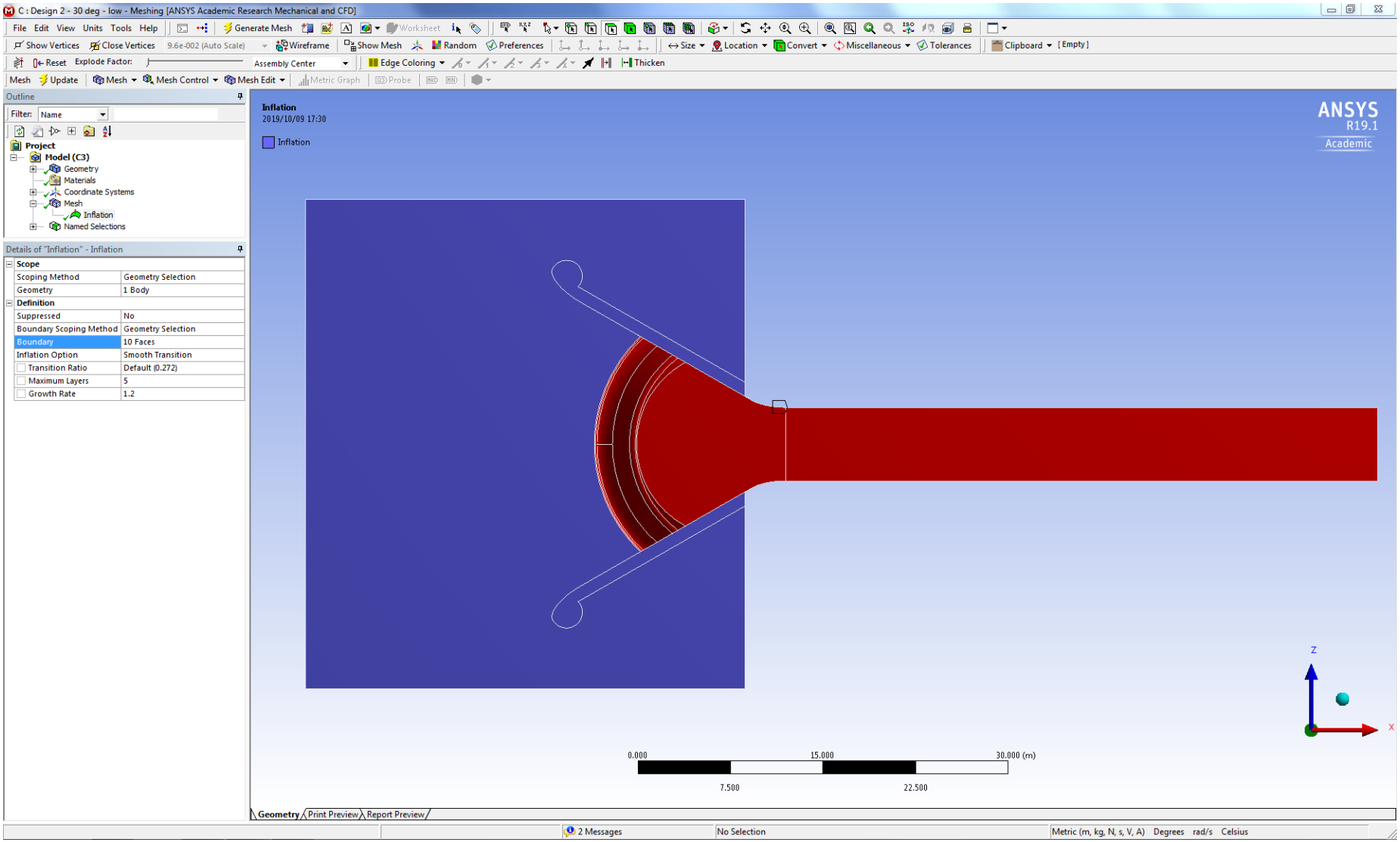

Figure A.2: Mesh Inflation details

A.7 ANSYS Fluent Setup (final design)

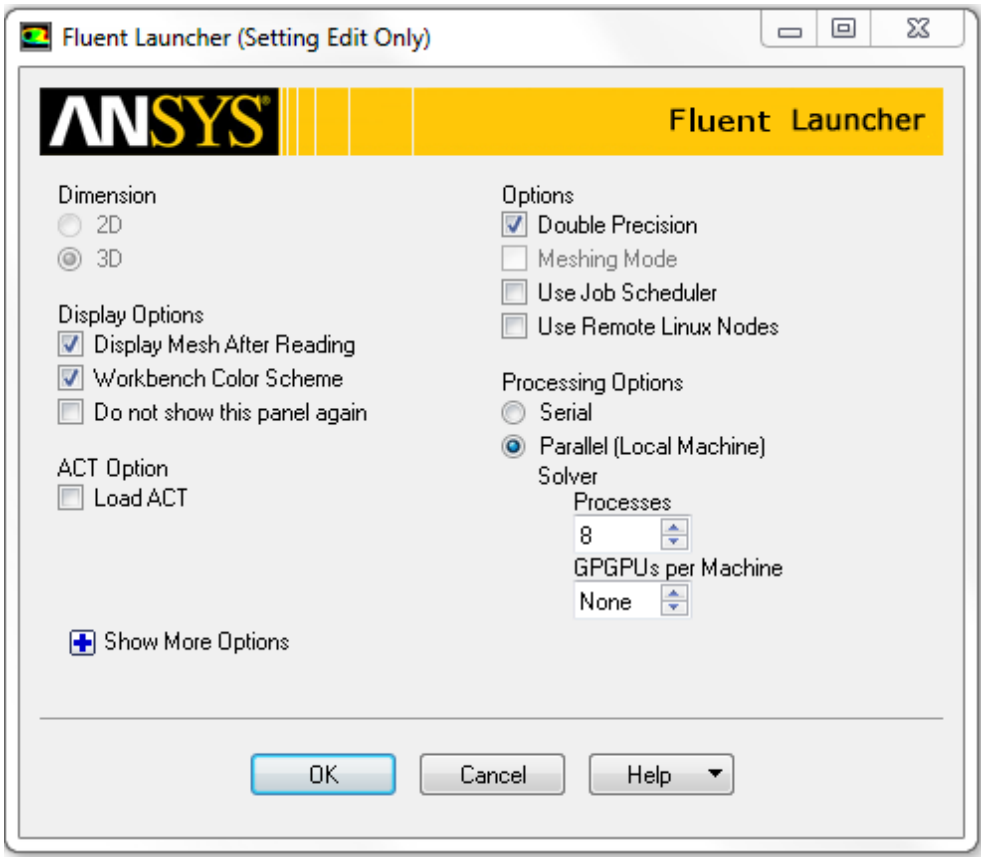

Figure A.3: Fluent Launcher details

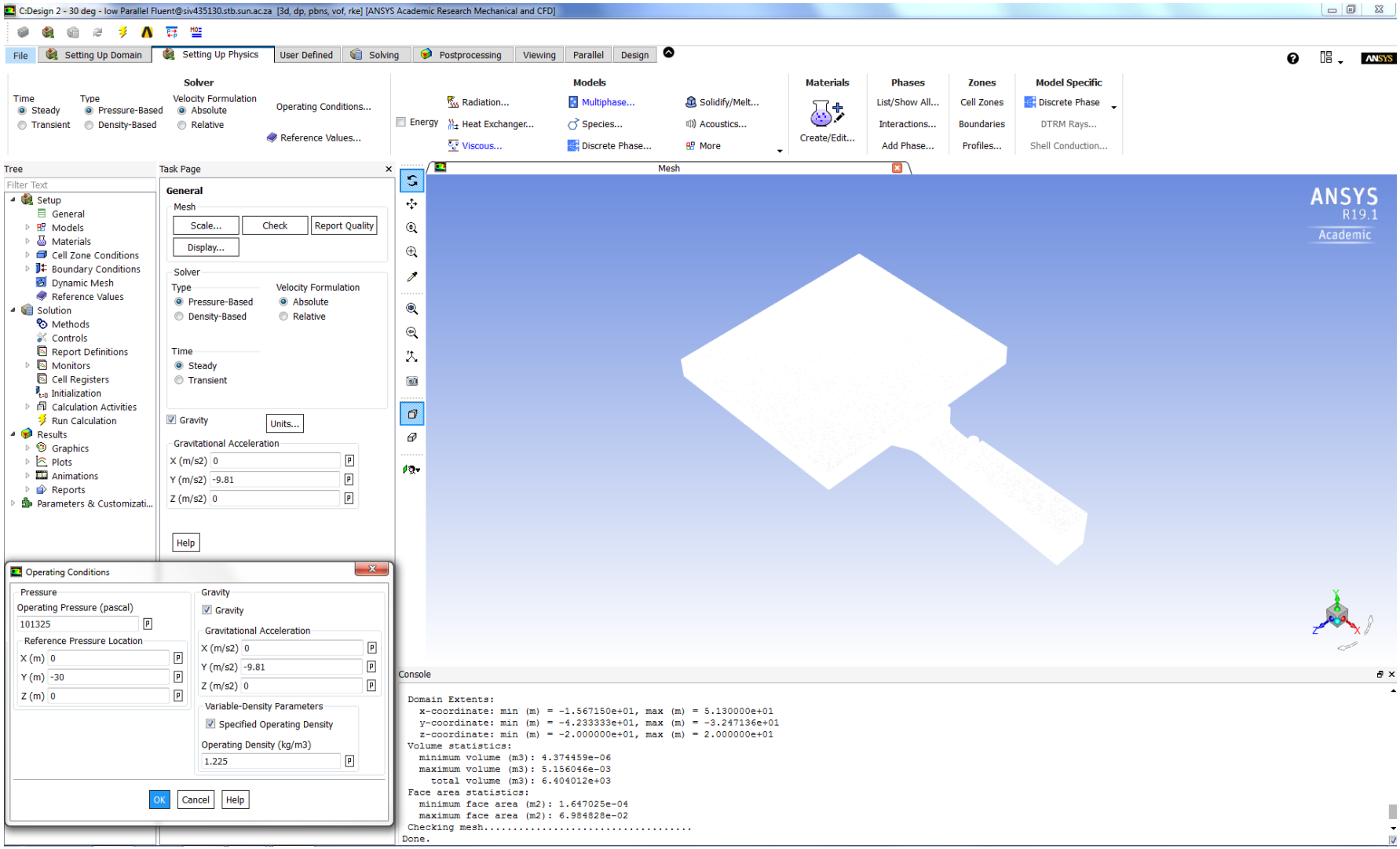

Figure A.4: Setting Up Physics: Operating Conditions details

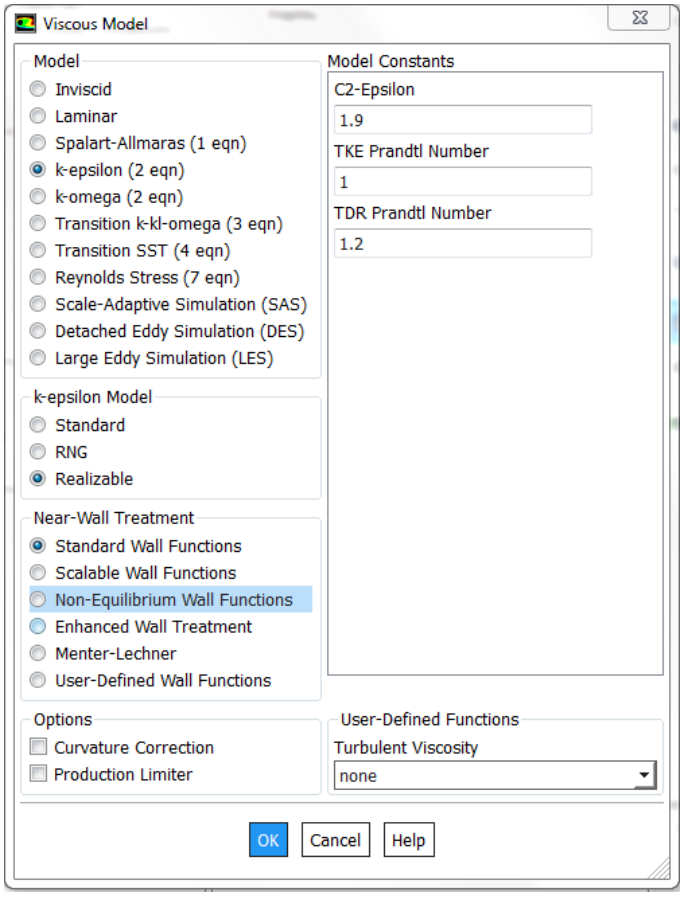

Figure A.5: Setting Up Physics: Viscous Model details

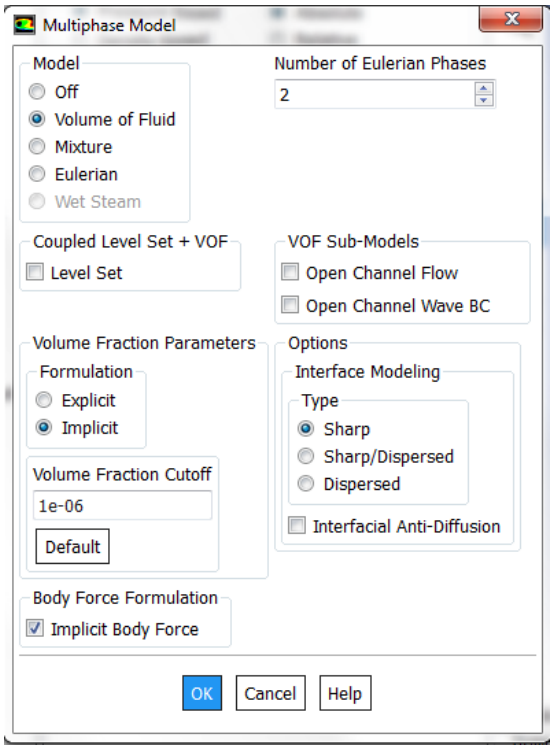

Figure A.6: Setting Up Physics: Multiphase Model details

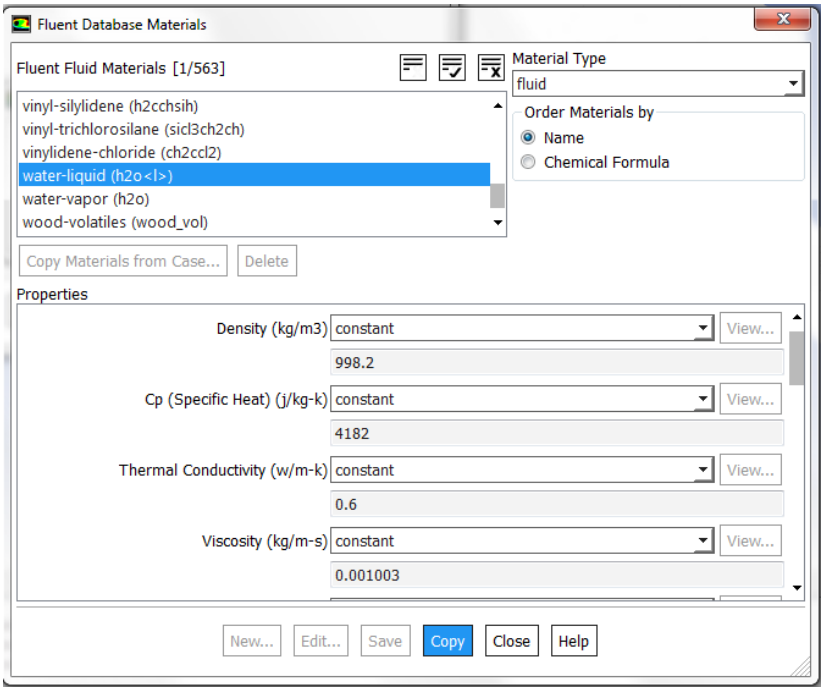

Figure A.7: Setting Up Physics: Materials details

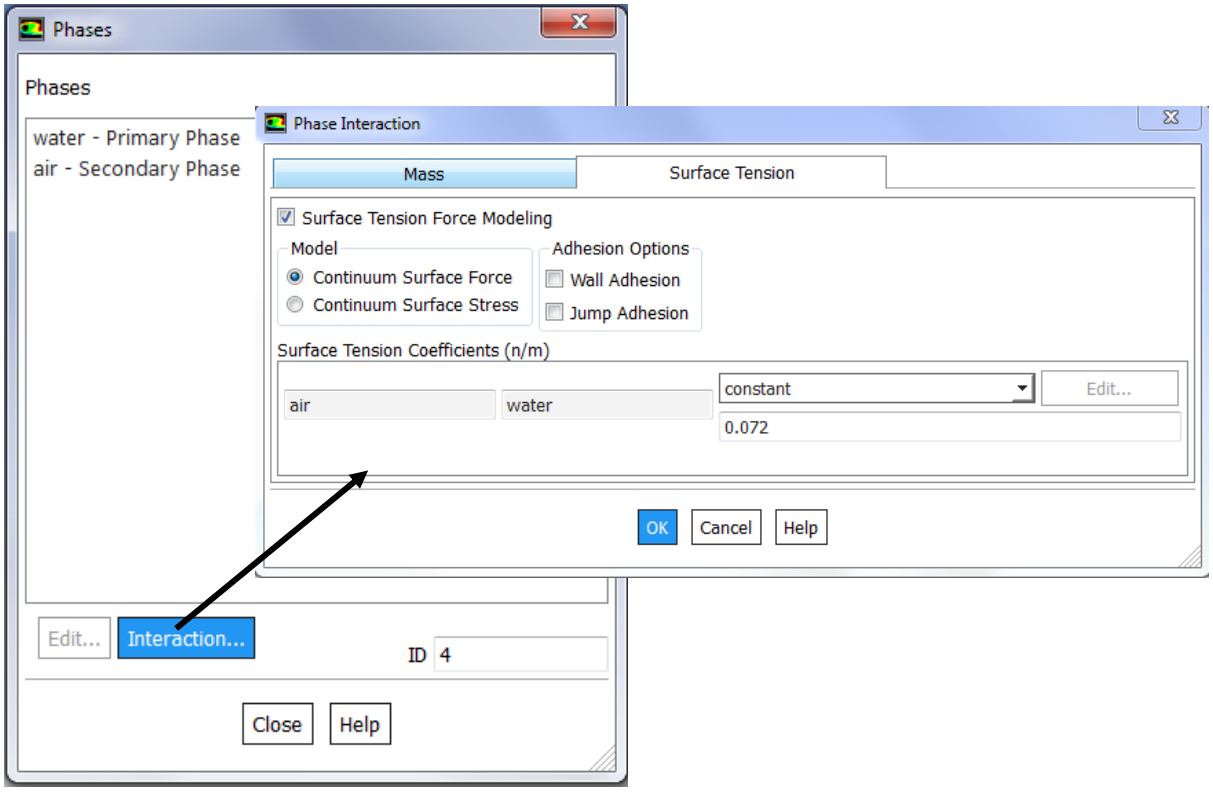

Figure A.8: Setting Up Physics: Phases and Phase Interaction details

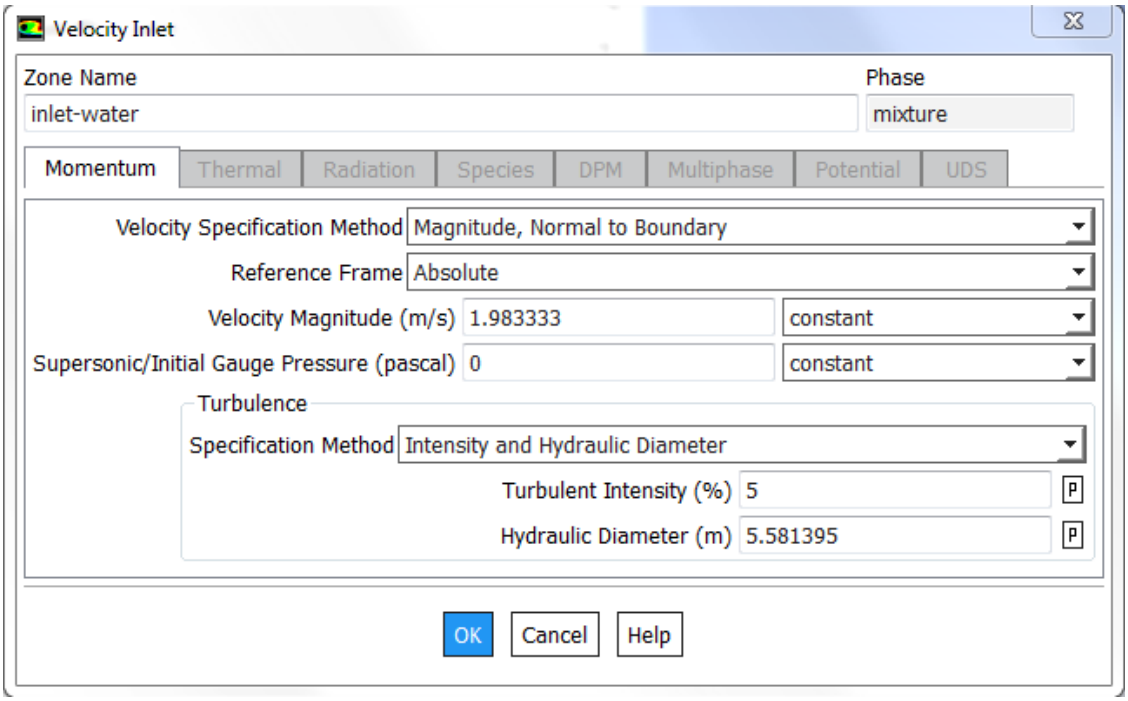

Figure A.9: Setting Up Physics: Boundary Zone: *water inlet* details (air *Volume fraction* = 0)

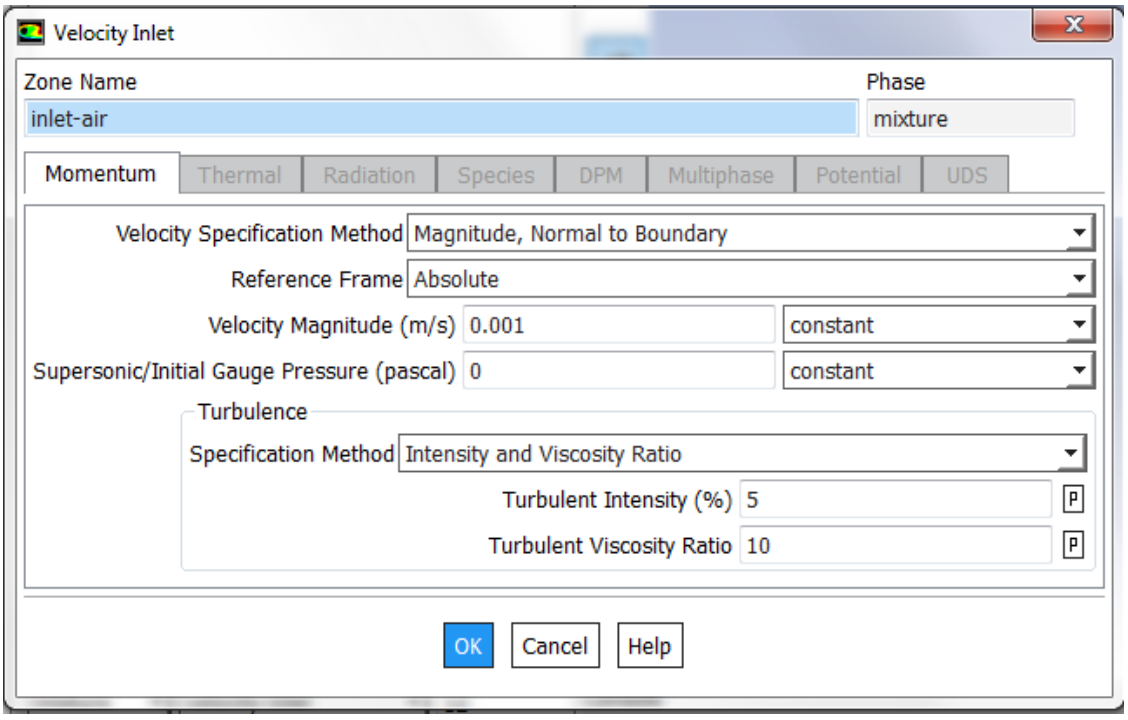

Figure A.10: Setting Up Physics: Boundary Zone: *air inlet* details (air *Volume fraction* = 1)

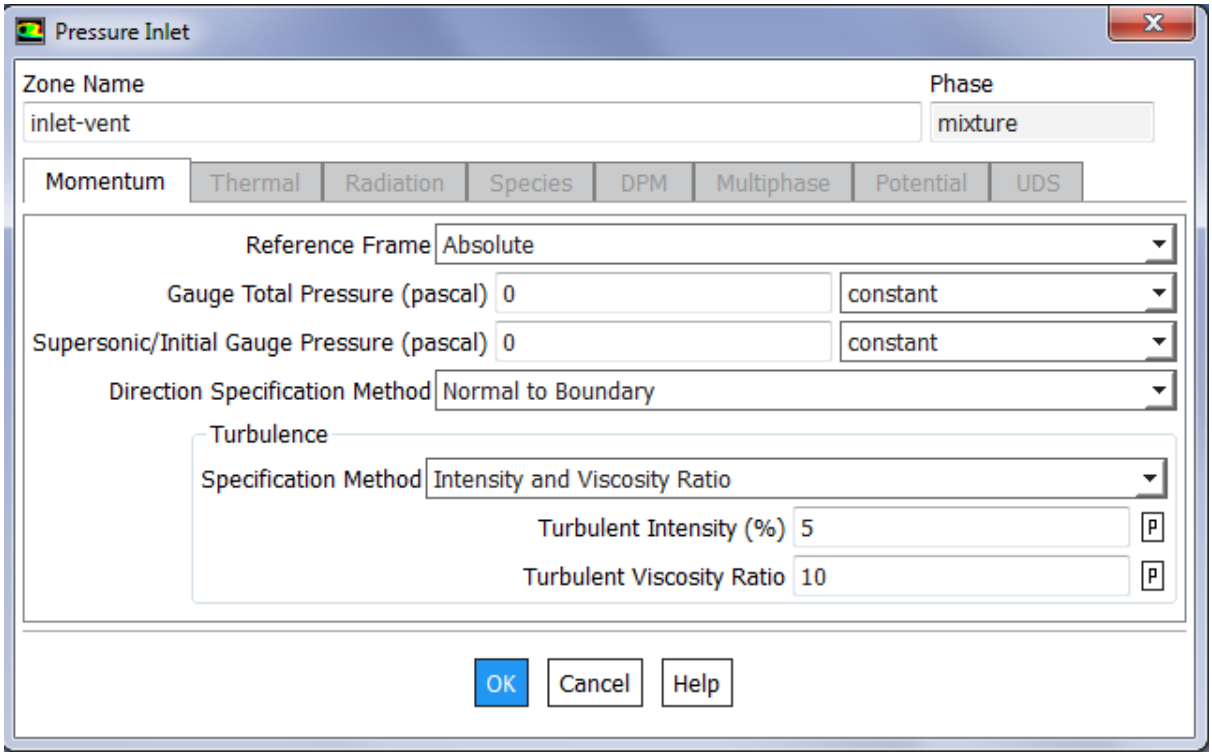

Figure A.11: Setting Up Physics: Boundary Zone: *air vent inlet* details (air *Backflow volume fraction* = 1)

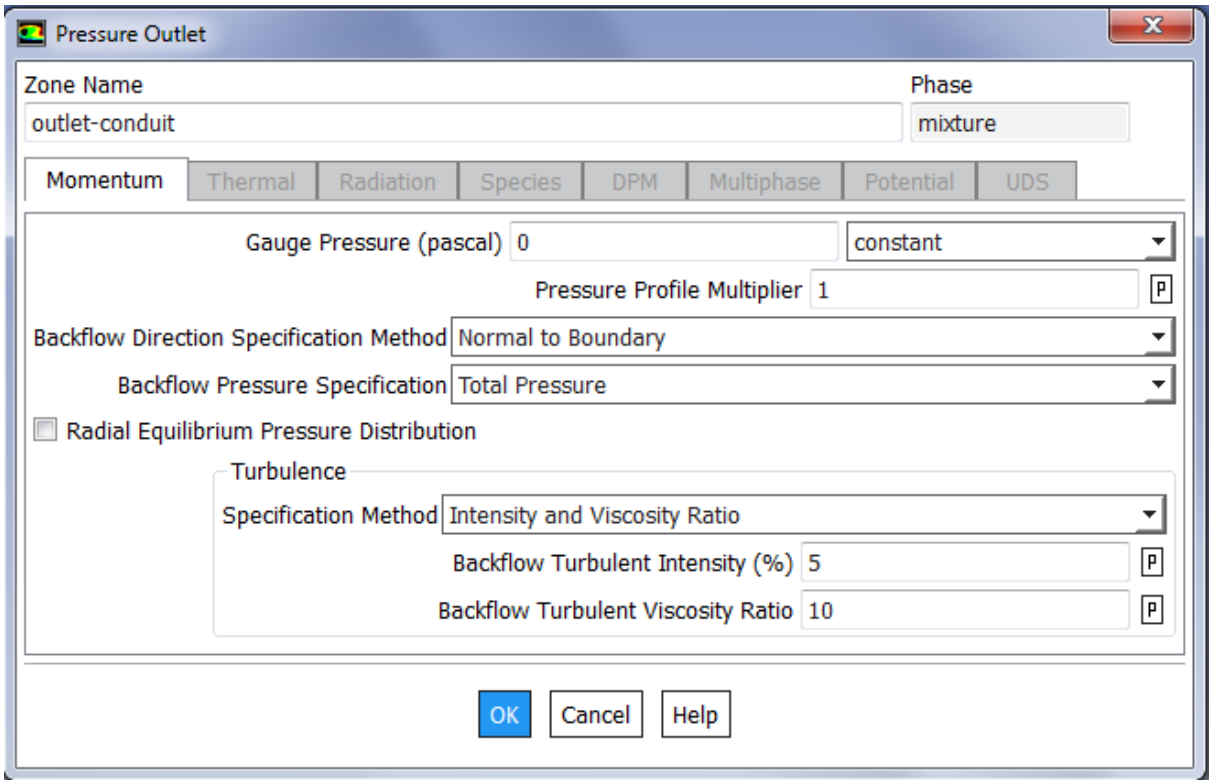

Figure A.12: Setting Up Physics: Boundary Zone: *conduit outlet* details (air *Backflow volume fraction* = 1)

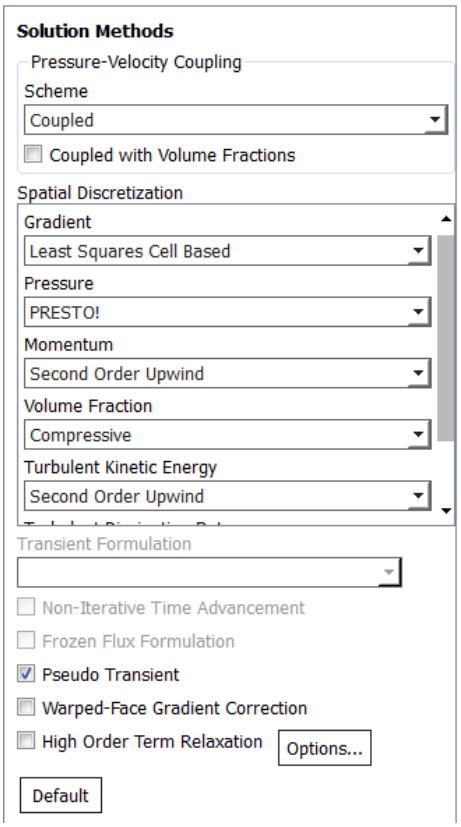

Figure A.13: Solving: Solution Methods details

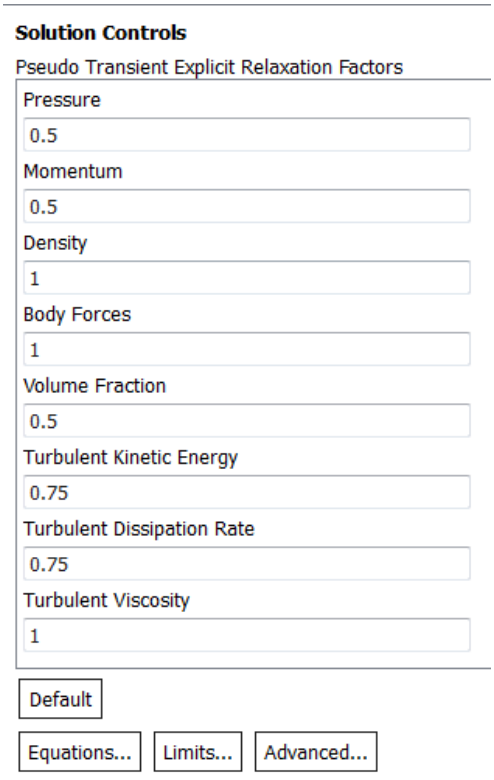

Figure A.14: Solving: Solution Controls details

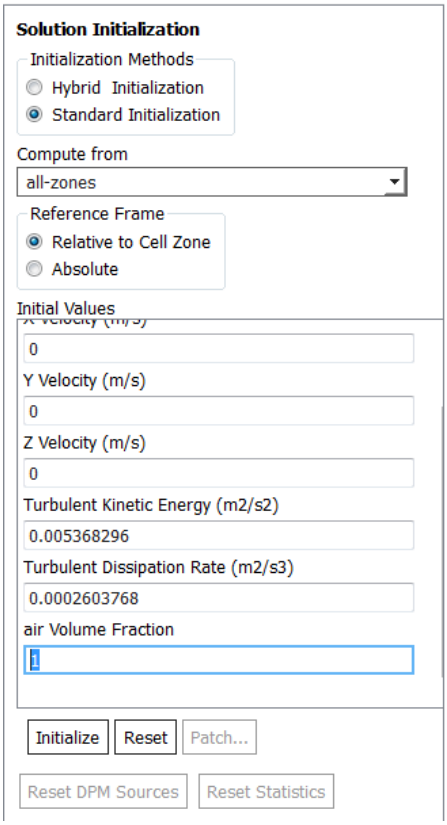

Figure A.15: Solving: Solution Initialisation details (i.e. geometry initially filled with air)

A.8 Shield's parameter along bed surfaces (final design)

Table A.10: Maximum sediment size transported along centreline of intake bed surface

Parameter	Equation	Value	Unit	Comments
Control point: p_2				**Location: downstream edge of reverse bottom curve**
Arc length width (b_2)		16.244	*m*	Measured from drawn geometry in CFD
Flow depth (y_2)		1.345	*m*	Scaled from Figure 4.3-2
Flow area (A_2)	$A_2 = y_2 \cdot b_2$	21.845	*m²*	Solved so $H_2 = H_1$
Wetted flow perimeter (P_2)	$P_2 = b_2 + 2 \cdot y_2$	18.934	*m*	
Flow velocity (V_2)	$V_2 = \frac{Q_e}{A_2}$	5.447	*m/s*	$Q_e = 119\ m^3/s$
Control point: p_3				**Location: start of conduit bed slope**
Surface length between p_2 and p_3 (L_{2-3})		12.270	*m*	Measured from drawn geometry in CFD
Conduit width (b_3)		6.000	*m*	$b_3 = B$

Flow depth (y_3)		2.793	*m*	Scaled from Figure 4.3-2
Flow area (A_3)	$A_3 = y_3 \cdot b_3$	16.759	*m²*	
Wetted flow perimeter (P_3)	$P_3 = b_3 + 2 \cdot y_3$	11.586	*m*	
Flow velocity (V_3)	$V_3 = \frac{Q_e}{A_3}$	7.101	*m/s*	
Average hydraulic radius (R_{avg})	$R_{avg} = \frac{(A_2 + A_3)}{(P_2 + P_3)}$	1.265	*m*	
Average flow velocity (V_{avg})	$V_{avg} = (V_2 + V_3)/2$	6.274	*m/s*	
Transition loss between p_2 and p_3 ($h_{L_{2-3}}$)	$h_{L_{2-3}} = \frac{k \cdot {V_{avg}}^2}{2 \cdot g}$	0.502	*m*	$k = 0.25$ for converging section (SANRAL, 2013)
Friction loss between p_2 and p_3 ($h_{f_{2-3}}$)	$h_{f_{2-3}} = \frac{{V_{avg}}^2 \cdot n^2 \cdot L_{2-3}}{(R_{avg})^{4/3}}$	0.090	*m*	$n = 0.016$
Energy slope between p_2 and p_3 (Sf_{2-3})	$Sf_{2-3} = \frac{\sum h_{L_{2-3}} + h_{f_{2-3}}}{L_{2-3}}$	0.048	*m/m*	
Average flow depth (y_{avg})	$y_{avg} = (y_2 + y_3)/2$	2.069	*m*	
Maximum sediment size between p_2 and p_3 ($d_{1_{2-3}}$)	$d_{1_{2-3}} = 11 \cdot y_{avg} \cdot Sf_{2-3}$	1.098	*m*	Along centreline of intake bed surface

Table A.11: Maximum sediment size transported along low-level outlet conduit

Parameter	Equation	Value	Unit	Comments
Control point: p_5				**Location: conduit outlet**
Conduit width (b_5)		6.000	*m*	$b_5 = B$
Flow depth (y_5)		1.212	*m*	Assumed normal flow; Solved so $Q = Q_e$
Flow area (A_5)	$A_5 = y_5 \cdot b_5$	7.274	*m²*	
Wetted flow perimeter (P_5)	$P_5 = b_5 + 2 \cdot y_5$	8.425	*m*	
Discharge (Q)	$Q = \frac{{A_5}^{5/3} \Phi^{0.5}}{n {P_5}^{2/3}}$	119	*m³/s*	Manning's Equation; $\Phi = 1/12$; $n = 0.016$
Flow velocity (V_5)	$V_5 = \frac{Q}{A_5}$	16.360	*m/s*	
Energy slope (Sf_5)		0.083	*m/m*	$Sf_5 = \Phi$ (normal flow)
Maximum sediment size at p_5 (d_{1_5})	$d_{1_5} = 11 \cdot y_5 \cdot Sf_5$	1.111	*m*	Inside low-level outlet conduit where normal flow occurs

Appendix B Physical model and results

B.1 Physical model setup

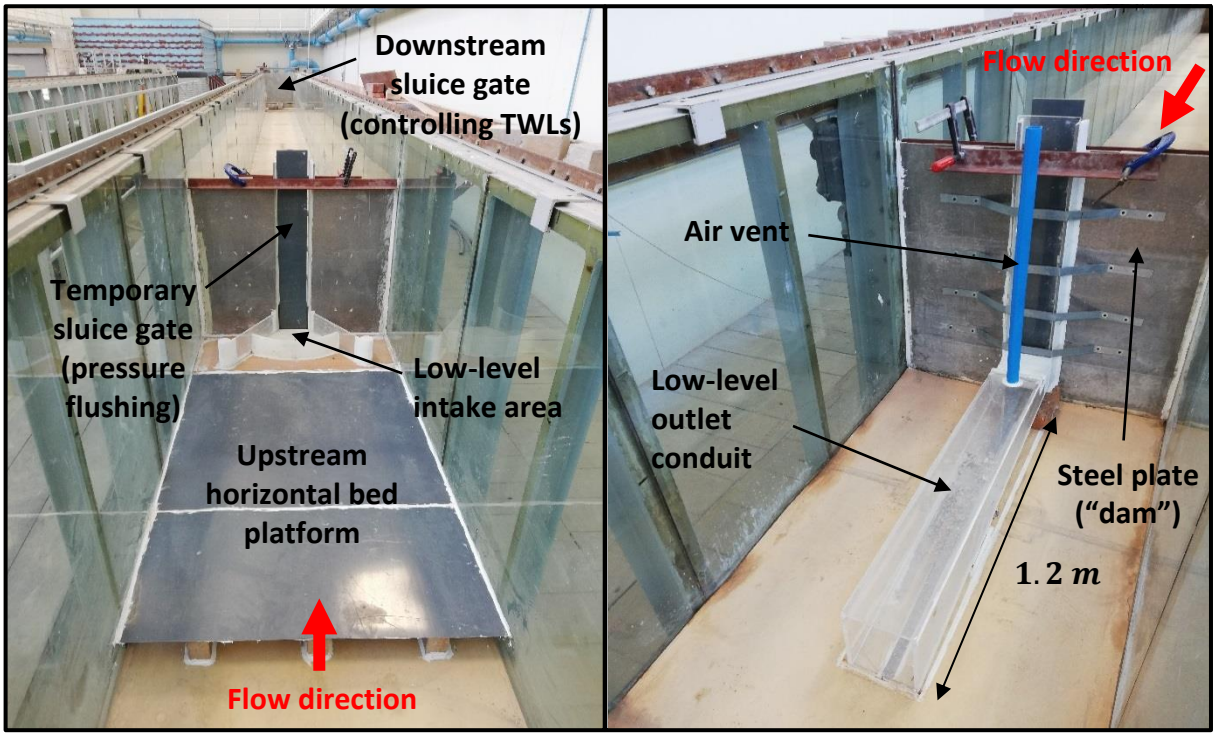

Figure B.1: Physical model setup in laboratory flume

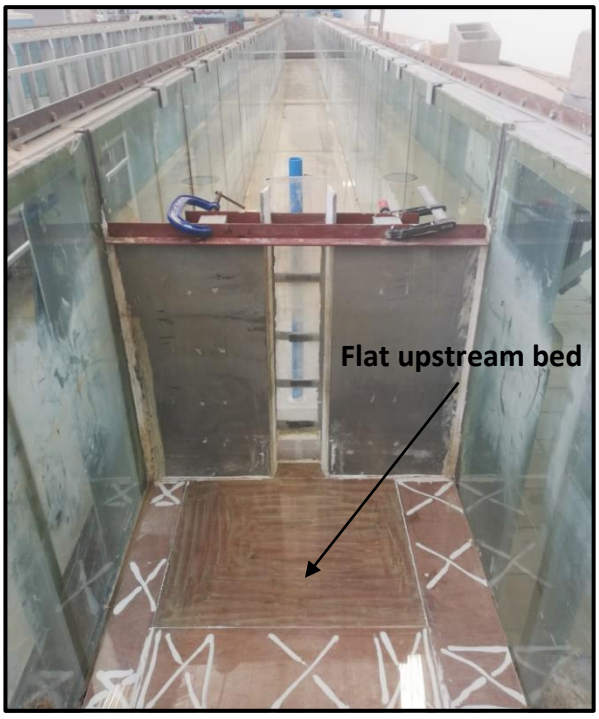

Figure B.2: Physical model setup without intake structure

B.2 Hydraulic model setup

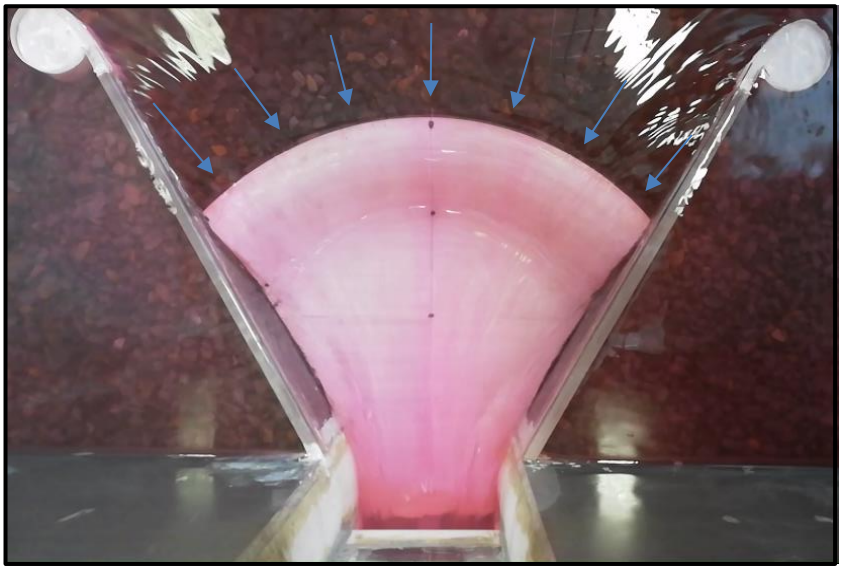

Figure B.3: Streamlines (dye) during free-flow flushing (Q =119 m³/s)

B.3 Physical sediment properties

Table B.1: Physical sediment properties of d_{50} = 13.2 mm sediment group

Test	Measured					Calculated			
	a (mm)	b (mm)	c (mm)	T (s)	V_{ss} (m/s)	S_p (Equation 2-2)	C_d (Equation 2-7)	d (mm)	V_{ss} (m/s) (Equation 2-4)
1	25.0	14.1	9.4	4.12	0.461	0.50	1.20	11.65	0.461
2	21.7	14.0	8.9	3.71	0.512	0.51	1.18	14.18	0.512
3	20.4	13.6	7.4	4.08	0.466	0.44	1.29	12.78	0.466
4	24.6	17.5	9.7	3.87	0.491	0.47	1.25	13.79	0.491
5	22.2	14.0	7.9	4.67	0.407	0.45	1.28	9.71	0.407
6	25.3	10.2	8.3	4.44	0.428	0.52	1.17	9.82	0.428
7	12.2	8.5	6.6	4.20	0.452	0.65	0.96	9.01	0.452
8	19.4	12.3	11.6	4.23	0.449	0.75	0.80	7.36	0.449
9	20.0	12.3	8.8	4.35	0.437	0.56	1.10	9.61	0.437
10	17.1	14.0	10.6	3.57	0.532	0.69	0.90	11.70	0.532
11	15.1	12.0	10.5	3.92	0.485	0.78	0.75	8.07	0.485
12	21.2	14.1	9.8	3.18	0.597	0.57	1.09	17.83	0.597
13	15.0	11.8	9.9	3.01	0.631	0.74	0.81	14.74	0.631
14	15.3	9.8	8.0	3.58	0.531	0.65	0.95	12.29	0.531
15	23.4	13.4	9.0	4.56	0.417	0.51	1.19	9.42	0.417
16	17.0	12.6	8.7	3.73	0.509	0.59	1.05	12.44	0.509
17	16.8	15.0	10.7	3.80	0.500	0.67	0.92	10.53	0.500
18	25.2	14.7	5.7	5.98	0.318	0.30	1.53	7.04	0.318
19	18.1	13.7	9.3	3.03	0.627	0.59	1.06	18.96	0.627
20	13.3	12.1	8.8	4.12	0.461	0.69	0.89	8.65	0.461
21	15.9	11.8	5.7	4.52	0.420	0.42	1.33	10.77	0.420

22	16.2	13.1	7.0	3.96	0.480	0.48	1.23	12.95	0.480
23	19.2	10.7	8.3	3.88	0.490	0.58	1.07	11.76	0.490
24	15.4	15.0	8.7	3.91	0.486	0.57	1.08	11.70	0.486
25	16.5	12.1	9.5	4.08	0.466	0.67	0.92	9.16	0.466
26	21.4	13.0	8.2	3.85	0.494	0.49	1.21	13.51	0.494
27	19.7	12.9	6.7	4.10	0.463	0.42	1.33	13.03	0.463
28	25.8	13.1	10.0	3.13	0.607	0.54	1.13	19.02	0.607
29	15.0	14.2	4.3	6.25	0.304	0.29	1.53	6.46	0.304
30	15.0	11.4	9.3	3.27	0.581	0.71	0.86	13.30	0.581
Avg	**18.9**	**12.9**	**8.6**	**4.04**	**0.483**	**0.56**	**1.10**	**11.71**	**0.483**

Table B.2: Physical sediment properties of d_{50} = 19 mm sediment group

Test	**Measured**					**Calculated**			
	a (mm)	b (mm)	c (mm)	T (s)	V_{ss} (m/s)	S_p (Equation 2-2)	C_d (Equation 2-7)	d (mm)	V_{ss} (m/s) (Equation 2-4)
1	35.6	26.4	9.5	3.73	0.509	0.31	1.50	17.71	0.509
2	35.7	23.0	13.4	3.17	0.599	0.47	1.25	20.41	0.599
3	43.0	24.3	18.5	2.90	0.655	0.57	1.08	21.12	0.655
4	37.6	27.0	14.7	3.37	0.564	0.46	1.26	18.20	0.564
5	52.0	20.0	12.0	3.58	0.531	0.37	1.40	17.96	0.531
6	38.4	33.8	11.6	3.76	0.505	0.32	1.48	17.21	0.505
7	35.4	25.6	15.0	3.19	0.596	0.50	1.20	19.36	0.596
8	47.4	22.7	19.8	3.06	0.621	0.60	1.03	18.09	0.621
9	37.8	22.7	11.5	3.45	0.551	0.39	1.37	18.88	0.551
10	38.0	34.0	10.7	3.71	0.512	0.30	1.52	18.14	0.512
11	38.8	22.0	9.0	4.48	0.424	0.31	1.51	12.30	0.424
12	43.0	25.8	22.0	3.06	0.621	0.66	0.94	16.50	0.621
13	32.0	30.0	15.1	3.39	0.560	0.49	1.22	17.40	0.560
14	44.0	22.7	19.0	3.64	0.522	0.60	1.04	12.84	0.522
15	31.8	26.8	13.0	3.48	0.546	0.45	1.29	17.42	0.546
16	51.4	22.0	19.0	3.67	0.518	0.57	1.10	13.33	0.518
17	34.3	34.1	6.0	4.63	0.410	0.18	1.72	13.14	0.410
18	47.5	21.3	15.0	3.68	0.516	0.47	1.25	15.07	0.516
19	39.0	27.5	11.2	4.10	0.463	0.34	1.45	14.16	0.463
20	33.8	23.7	16.5	3.48	0.546	0.58	1.07	14.44	0.546
21	43.3	23.4	17.0	3.46	0.549	0.53	1.15	15.68	0.549
22	35.7	32.0	14.6	3.07	0.619	0.43	1.31	22.75	0.619
23	40.0	22.5	12.3	3.96	0.480	0.41	1.34	14.04	0.480
24	40.4	24.7	13.9	3.15	0.603	0.44	1.30	21.40	0.603
25	39.6	30.2	9.4	5.24	0.363	0.27	1.57	9.34	0.363
26	46.0	26.6	19.1	3.66	0.519	0.55	1.13	13.78	0.519
27	33.0	31.5	20.0	3.17	0.599	0.62	1.01	16.43	0.599
28	41.0	19.0	13.0	3.68	0.516	0.47	1.25	15.18	0.516
29	36.9	25.7	12.4	3.97	0.479	0.40	1.36	14.09	0.479
30	49.3	25.8	9.5	4.85	0.392	0.27	1.57	10.96	0.392
Avg	**40.1**	**25.9**	**14.1**	**3.66**	**0.530**	**0.44**	**1.29**	**16.24**	**0.530**

Table B.3: Physical sediment properties of d_{50} = 37.5 mm sediment group

Test	Measured					Calculated			
	a (mm)	b (mm)	c (mm)	T (s)	V_{ss} (m/s)	S_p (Equation 2-2)	C_d (Equation 2-7)	d (mm)	V_{ss} (m/s) (Equation 2-4)
1	76.4	42.3	41.7	6.54	0.789	0.73	0.83	23.85	0.789
2	73.3	52.2	39.4	5.30	0.974	0.64	0.98	43.11	0.974
3	60.6	46.8	37.7	5.20	0.992	0.71	0.87	39.60	0.992
4	63.5	48.7	38.3	5.49	0.940	0.69	0.90	36.79	0.940
5	65.3	56.3	39.5	6.24	0.827	0.65	0.96	30.37	0.827
6	59.0	44.3	35.4	5.87	0.879	0.69	0.89	31.97	0.879
7	55.5	54.7	35.6	5.98	0.863	0.65	0.97	33.36	0.863
8	76.0	54.3	36.0	5.06	1.020	0.56	1.10	53.21	1.020
9	68.5	43.0	28.1	5.57	0.926	0.52	1.17	46.62	0.926
10	66.8	53.6	35.3	6.59	0.783	0.59	1.06	30.03	0.783
11	77.0	62.8	36.5	5.82	0.887	0.52	1.16	42.29	0.887
12	70.0	55.0	34.4	6.81	0.758	0.55	1.11	29.63	0.758
13	87.1	53.3	29.4	6.61	0.781	0.43	1.31	37.01	0.781
14	75.0	57.9	42.8	5.10	1.012	0.65	0.96	45.61	1.012
15	56.0	50.2	40.7	5.47	0.943	0.77	0.77	31.85	0.943
16	76.3	52.2	28.0	6.81	0.758	0.44	1.29	34.35	0.758
17	60.0	58.3	42.1	4.11	1.255	0.71	0.86	62.94	1.255
18	85.0	36.2	31.0	6.58	0.784	0.56	1.11	31.53	0.784
19	70.2	49.0	30.7	5.97	0.864	0.52	1.16	40.27	0.864
20	60.8	50.9	26.9	6.61	0.781	0.48	1.23	34.65	0.781
21	73.0	55.4	41.0	5.01	1.030	0.64	0.97	47.64	1.030
22	60.2	50.0	43.8	4.09	1.262	0.80	0.72	53.34	1.262
23	60.8	52.4	40.4	5.68	0.908	0.72	0.85	32.71	0.908
24	76.9	54.0	26.0	7.25	0.712	0.40	1.35	31.82	0.712
25	66.6	51.6	30.0	4.92	1.049	0.51	1.18	60.25	1.049
26	73.2	47.4	38.1	5.37	0.961	0.65	0.97	41.32	0.961
27	60.5	42.3	38.9	5.18	0.996	0.77	0.77	35.42	0.996
28	82.7	53.0	34.6	5.97	0.864	0.52	1.16	40.32	0.864
29	60.4	50.3	39.2	5.13	1.006	0.71	0.86	40.45	1.006
30	59.1	57.4	42.0	4.37	1.181	0.72	0.85	54.71	1.181
Avg	**68.5**	**51.2**	**36.1**	**5.69**	**0.926**	**0.62**	**1.01**	**39.90**	**0.926**

B.4 Sediment bed setup

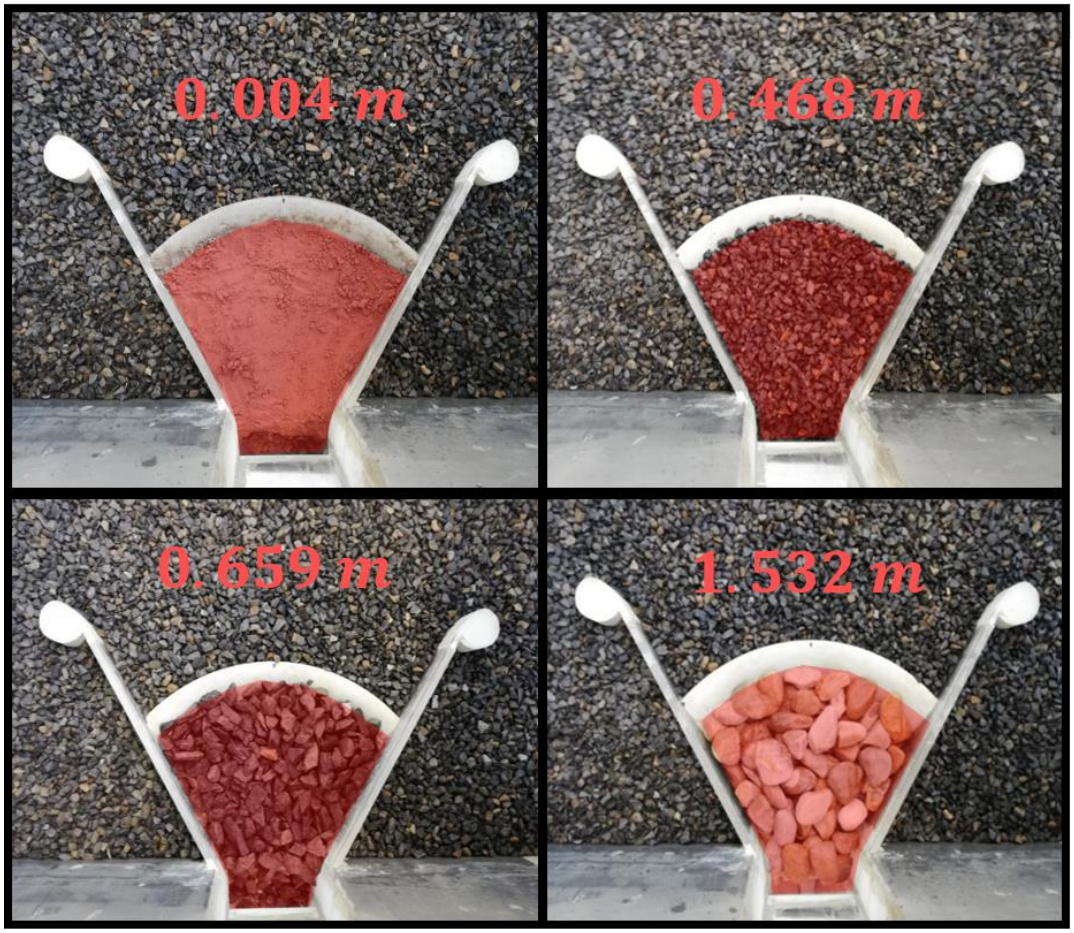

Figure B.4: ***Sediment depth 1*** **setup**

Figure B.5: ***Sediment depth 2*** **setup**

B.5 Sediment scour cones from pressure flushing at H_{u1} = 24.16 m (without intake structure)

Figure B.6: Scour cone of d_{eff} = 0.004 m *sediment depth 2* setup

Figure B.7: Scour cone of d_{eff} = 0.468 m *sediment depth 2* setup

Figure B.8: Scour cone of d_{eff} = 0.659 m *sediment depth 2* setup